# Thermodynamic and structural analysis of the interactions between Epstein-Barr virus transcription factors and the host targeting factor RBP-Jkappa.

**By Robert Simmons**

**Department of Biochemistry**

**School of Life Sciences**

**University of Sussex**

**Doctorate in Philosophy**

**2018**

# Acknowledgements

I would like to thank my Supervisor Michelle West and Co-supervisor Chris Prodromou for all their advice and help throughout the years, for having my back throughout numerous tedious negotiations and for having a lot of patience with me during my PhD. I would like to thank all the members of the West Lab, Sinclair Lab and Mancini Lab for making the lab and office an excellent place to work in, for offering lots of help and advice on the way and for being awesome SGM and Christmas partiers. I would also like to thank my family and friends for supporting me through the tougher stages of my thesis. I would also like to thank my housemates from Coldean lane for a fantastic year of my life and Coombe road for some of the finest wine drenched debates never to appear on television. I would also like to apologise to both houses for my lack of washing up and general cleanliness.

I would like, in particular, to thank Barak Naranjo for being a great council and friend outside of work for the long list of problems I created for myself and for creating the Coldean lane house, which was a magical place to live in. I would also like to thank Barak for inspiring me to write this acknowledgement, as without his warm and moving acknowledgement I would not have thanked all those that had made this journey possible.

Finally, I would like to thank Rajesh for his tenacity and advice to drive me to the finish line and I wish him the best in his future EBV endeavours. I would also like to thank my collaborators, Mark Roe for his help with the crystallography and structure determination, Mark Morgan, for the AKTA training, Matthew Day and Raquel Arribas for their help throughout the years and my other collaborators for their numerous negotiation workshops. I would also like to thank all those I worked with at the Charles Street Tap for being fabulous to work with and for getting my head settled ready for writing.

**I hereby declare that this thesis has not been and will not be, submitted in whole or in part to another University for the award of any other degree. I declare that all work in this thesis to be my own and any work that is not has been appropriately referenced:**

# Abstract

Epstein-Barr virus (EBV) asymptomatically infects >90% of the world population but is also associated with multiple malignancies. The EBV latent nuclear proteins EBNA2, 3A, 3B and 3C orchestrate changes in host gene transcription to drive B-cell immortalisation by hijacking cellular DNA-binding transcription factors. This project set out to obtain thermodynamic and structural information on host transcription factor RBP-Jkappa, the DNA-binding mediator of the Notch pathway, and its interactions with the EBNAs. EBNA2 activates transcription by binding RBP-Jkappa through the same WΦP motif found in Notch proteins. EBNA3 proteins bind RBP-Jkappa through a distinct motif (TΦGC) and compete with EBNA2 for binding, inhibiting EBNA2-mediated gene activation, but can also use RBP-Jkappa to bind DNA independently. Interestingly, EBNA3C also contains an adjacent WΦP motif (WTP) that can bind RBP-Jkappa *in vitro*. We used Isothermal Titration Calorimetry (ITC) to measure binding affinities of EBNA2 and EBNA3C peptides containing these motifs to RBP-Jkappa. We found that EBNA2 peptides bound RBPJ-kappa via its WWP motif with an affinity 10-fold less than the WLP motif of Notch 2. Surprisingly, we found that EBNA3 peptides containing TΦGC motifs did not bind to RBP-Jkappa *in vitro*. Phosphorylation of the threonine in this motif did not lead to any detectable binding. However, EBNA3C peptides containing both the TFGC and WTP motifs bound RBP-Jkappa with a similar affinity to EBNA2 peptides, but this interaction was entirely mediated by the WTP motif. We also demonstrated that the EBNA3C TFGC peptide could not compete with EBNA2 for RBP-Jkappa binding using a fluorescent polarisation binding assay. Interestingly, we found that an EBNA3A peptide bound weakly to RBP-Jkappa via a motif with similar physiochemistry to the Notch WTP motif (FKL) and not its TLFC motif. These data indicate that TΦGC motifs in EBNA3 proteins may only direct RBPJ-kappa binding in the context of other EBNA3C residues in a properly folded full-length protein or may mediate indirect binding.

# Contents

## List of Tables

## List of Figures

## Abbreviations

4-hydroxytamoxifen (4HT)
Acquired immune deficiency syndrome (AIDS)
Ankyrin (Ank)
B-cell lymphoma 2 (Bcl-2)
Bcl-2-like protein 11 (BIM)
Beta-trefoil domain (BTD)
Bovine Serum Albumin (BSA)
Burkitt's lyhphoma (BL)
C promoter (Cp)
Chroatin immunoprecipitation (ChIP)
Chromatin conformation capture (CCC)
C-Jun N-terminal kinase (JNK)
Conserved Region (CR)
Corepressors (CoR)
C-terminal activation region 1 transformation effector site 1 (CTAF-TES1)
C-terminal domain (CTD)
Deoxyribose nucleic acid (DNA)
Diffuse Large B Cell Lymphoma (DLBCL)
Dimethyl sulfoxide (DMSO)
EBV non-coding RNAs (EBERs)
EBNA2 N-terminal Domain (END)
Electrophoretic mobility shift assay (EMSA)
Epstein-Barr Nuclear Antigen (EBNA)
Epstein-Barr Nuclear Antigen Leader Protein (EBNA-LP)
Epstein-Barr Virus (EBV)
Ethylenediaminetetraacetic acid (EDTA)
Extracellular Signal-Regulated Kinase (ERK)
Fluorescent Polarisation (FP)
Gastric Carcinoma (GC)
Gel Sample Buffer (GSB)
Heat shock protein 70 (Hsp70)
Histone 3 Lysine 27 acetylation (H3K27ac)
Histone 3 lysine 4 monomethylation (H3K4me1)
Histone acetylase (HAT)
Histone Deacetylase (HDAC)
Hodgkin's lymphomas (HL)
Homology domain (HD)
Human immunodeficiency virus (HIV)
Human Simplex Virus (HSV)
Intracellular Notch (NotchIC)
Isopropyl β-D-1-thiogalactopyranoside (IPTG)
Isothermal titration calorimetry (ITC)
Kaposi's sarcoma-associated herpesvirus (KSHV)
Latent Membrane Proteins (LMP)
Lysogeny Broth (LB)

Marginal zone (MZ)
Maltose Binding protein (MBP)
Mitogen-activated protein kinase (MAPK)
Nasopharyngeal carcinoma (NPC)
Natural killer and T cells (NK/ T cells)
Neural precursor cell expressed developmentally down-regulated protein (NEDD)
N-teriminal domain (NTD)
Nuclear factor -kappa-B (NFκB)
Nuclear localisation sequence (NLS)
Nuclear magnetic resonance (NMR)
Optimal density (O.D)
Origin of complex (ORC)
Phosphate Buffer Saline (PBS)
Phosphatase and tensin homolog (PTEN)
Polymerase (pol)
Post Transplant Lymphoproliferative Disease (PTLD)
Phosphoinositide 3-kinase (PI3K)
Protein kinase B (AKT)
RBP-Jκ association molecule (RAM)
Receptor-interacting serine/threonine-protein kinase 1 (RIP1)
Recombination signal binding protein for immunoglobulin kappa J region (RBP-Jκ)
Retinoblastoma (Rb)
Runt-related transcription factor (RUNX)
Self association domain (SAD)
SKI-interacting protein (SKIP)
Super Optimal broth with Catabolite repression (SOC)
Su-Homology (SH)
SWItch/Sucrose Non-Fermentable (SWI/SNF)
Transactivational domain (TAD)
Transcription factor (TF)
Transcription factor II Human (TFIIH)
Transcription start sites (TSS)
Transforming growth factor beta (TGFβ)
Tumour necrosis factor receptor associated factors (TRAF)
Tumour necrosis factor receptor type 1-associated DEATH domain protein (TRADD)
W promoter (Wp)

# Chapter 1 : Introduction

## 1.1 : Epstein-Barr virus

### 1.1.1 : Discovery of Epstein-Barr virus

Anthony Epstein had originally worked on viruses which caused tumours to grow in animals. A chance attendance at a lecture being given by Denis Burkitt would set the discovery of the first cancer causing virus in humans in motion. Denis Burkitt identified tumours growing on children's jaws whilst serving as a doctor in Uganda after World War II. After searching for records of similar cases he identified that there was a geographical correlation between high incidences of Burkitts lymphoma and the altitude and microclimate of the homes of the patients (Burkitt, 1958, Burkitt, 1962). Denis Burkitt identified that, in the malaria belt of equatorial Africa, Burkitts lymphoma was the most common childhood cancer. Secondly, he identified that a higher number of cases of Burkitts lymphoma manifested in humid low lands compared to highlands which, had drier climates. He hypothesised that the Burkitts lymphoma was being transferred by an infectious agent being administered by mosquitos in a similar manner to malaria (Burkitt, 1962).

Upon learning this, Anthony Epstein applied and won a grant from the British Empire Cancer Campaign to go to East Africa to collect samples of Burkitts lymphoma to elucidate if there was an infectious agent. Initial attempts to identify a virus from the Burkitts lymphoma tissues samples were unsuccessful, most likely due to the tissue eliciting an immune response. Epstein hypothesised that by culturing Burkitts cells this could be avoided. They achieved this by accident when a sample of cells being flown from Uganda was delayed by fog. The following week Epstein observed a cloudy

substance had formed in the tissue fluid but inspection under a microscope revealed that cloudy fluid was proliferating lymphoblasts not bacterial contamination (Epstein, 2012). The cells (then referred to as EB (Epstein-Barr) cells) were cultured by Yvonne Barr which, Anthony Epstein and Bert Achong used to take the first images of Epstein-Barr viral capsids using Electron Microscopy in 1964 (Epstein *et al.*, 1964a, Epstein and Barr, 1964). The capsid's morphology and shape appeared to be that of a herpes virus but analysis with fluorescently tagged antibodies grown against known herpes viruses of the time, tested negative in the EB cell line suggesting the virus was novel. In addition to this, globulins, grown against EB cells, only bound to small proportion of EB cells (1-3%) but were found in over 90% of serum donations (from US donors) suggesting that a large proportion of the population had the virus (Epstein *et al.*, 1965, Henle *et al.*, 1969). Later studies would show that EBV predominantly exists as an episome in persistent infections explaining why so few of the lymphoblasts were shown to contain EBV (Babcock *et al.*, 1999). However, there was still scepticism that the EBV was causing cancers in humans and was suggested to be a passenger rather than a driver of metastasis. However, detection of EBV DNA in Nasopharyngeal carcinomas from south east Asia in 1970 and EBV being associated with Non-Hodgkins lymphoma and oral hairy leukoplakia in acquired immune deficiency syndrome (AIDS) patients in the subsequent decade built a strong case for EBV being a cancer causing virus (zur Hausen *et al.*, 1970, Greenspan *et al.*, 1985, Jones *et al.*, 1988). In addition to this the association of Kaposi's sarcoma in human immunodeficiency virus (HIV) patients with Kaposi's sarcoma-associated herpesvirus (KSHV) in 1994 and Human papilloma virus being proven to cause cervical cancer in 2002, demonstrated that

Anthony Epstein had been correct and viruses could cause cancers in humans (Bosch *et al.*, 2002, Gonçalves *et al.*, 2017).

The discovery of the link between infectious mononucleosis and EBV similarly relied on a fruitful accident. Anthony Epstein had sent the EB cells to the Henle laboratory in Philadelphia for analysis as British laboratories refused to collaborate on a project that insinuated a virus could cause human cancers. Their technician had donated lymphocytes for experiments that did not immortalise in culture (Levine 1985, H, 2005). However, one week later she fell ill with infectious mononucleosis, potentially from the EB cells, after which her lymphocytes immortalised in culture and she had also developed EBV-specific antibodies. Samples donated from Yale university from students before and after suffering from infectious mononucleosis were later used to confirm the link between EBV and infectious mononucleosis (Henle *et al.*, 1968). As EBV is spread by the exchange of saliva amongst adolescents and infectious mononucleosis manifests from an over reactive T cell response to an EBV infection, infectious mononucleosis gained the nickname 'the kissing disease' (Balfour *et al.*, 2013, Balfour *et al.*, 2015).

The decades of research into EBV has not only contributed vast amounts of information into EBV biology and potential pathways to human cancer development, but has also produced EBV immortalised B cell lines, which have proven invaluable to B cell biology and genomic studies (Pope *et al.*, 1968, Menezes *et al.*, 1975, Ben-Bassat *et al.*, 1977).

### 1.1.2 : EBV infection

EBV is spread to new hosts through the exchange of saliva (Niederman *et al.*, 1976). EBV is a gamma herpes virus that establishes a persistent infection in B cells (Epstein *et al.*, 1964a, Moghaddam *et al.*, 1997). There is debate as to whether the primary site of infection is in epithelial oropharyngeal cells or in circulating B cells in the oropharynx (Sixbey *et al.*, 1984, Allday and Crawford, 1988). The lytic model of infection starts when EBV enters the oropharyngeal tissues via interactions between EBV glycoprotein BMRF-2 and epithelial cell integrin 1 receptors (Xiao *et al.*, 2009). EBV, upon infecting the oropharynx, intiates the lytic programme of expression expressing 80 genes which manufacture new virus leading to shedding of EBV virus (Yao *et al.*, 1985, Farrell, 2001). However, to enter host B cells during infection EBV major envelope glyco-protein gp350, binds to B cell protein CD21 (Fingeroth *et al.*, 1984, Nemerow *et al.*, 1987). HLA class II molecules have also been shown to act as co-receptors via interactions with the EBV glycol-protein gp42 whilst EBV docks to B cells (Li *et al.*, 1997). Upon entry to B cells the EBV capsid disassembles releasing the EBV genome. EBV switches its linear genome to a circular genome expressing 9 latent genes and a number of untranslated mRNAs initially from the C promoter (Cp) or W promoter (Wp) and then from the LMP, EBER and BART promoters (Adams and Lindahl, 1975, Baer *et al.*, 1984, Farrell, 2001). This makes treatment of EBV diseases by the common antiviral drug aciclovir, which targets linear viral genome replication, not possible (Sixbey and Pagano, 1985).

Latency genes are expressed upon infection of naïve B cells and memory B cells circulating underneath the nasopharyngeal epithelium (Miyashita *et al.*, 1997, Babcock *et al.*, 1999)(Figure 1.1). During Latency III EBV expresses 6 Epstein-Barr Nuclear

Antigens (EBNA1, EBNA2, EBNA3A, EBNA3B, EBNA3C, EBNA-LP), 3 Latent Membrane Proteins (LMP1, LMP2A, LMP2B) and non-coding RNAs (EBERs) (Babcock *et al.*, 2000, Babcock and Thorley-Lawson, 2000)(Figure 1.1). *In vitro* only EBNA-LP, EBNA2, EBNA3A and EBNA3C are required to immortalise B cell lines. However, *in vivo* EBV latency III EBV transcription factors mediate B cell expression to promote B cell growth, mediate cell-cell contacts, drive B cell maturation and encourage immune evasion (Sinclair *et al.*, 1994, Stewart *et al.*, 2004, McClellan *et al.*, 2012). Latency III expression is thought to be brief as EBV viral proteins have been shown trigger immune responses from cytotoxic T cells. Cytotoxic T cells are thought to control the progress of EBV latency infections and prevent excessive outgrowth of EBV infected cells (Niedobitek *et al.*, 1997, MacArthur *et al.*, 2007)(Figure 1.1). Latency II expression (EBNA1, EBNA-LP, LMP1, LMP2A, LMP2B and EBERs) is thought to protect EBV infected B cells from germinal centre selection as LMP1 and LMP2 have been shown to mimic CD40 and B cell receptor (BCR) respectively cloaking the cells from autoreactive immune surveillance (Wang *et al.*, 1985, Gires *et al.*, 1997, Caldwell *et al.*, 1998)(Figure 1.1.). Following migration through the germinal centre EBV infected B cells migrate to B cell memory pool adopting minimalistic EBV expression programmes latency I (EBNA1 and EBERs) and latency 0 (EBERs) (Babcock *et al.*, 2000)(Figure 1.1). In addition to this B memory cells infected by EBV in the oropharynx have been suggested to migrate directly to the B cell memory pool (Babcock *et al.*, 1999). The EBV genome has been shown to persist as an episome in the nucleus of infected B cells in the B cell memory pool (Babcock *et al.*, 2000). It is suggested that EBV reactivates or partially reactivates lytic expression programmes in order to produce virus to infect new hosts however, the mechanism of this is not well understood (Tsurumi *et al.*, 2005)(Figure 1.1.).

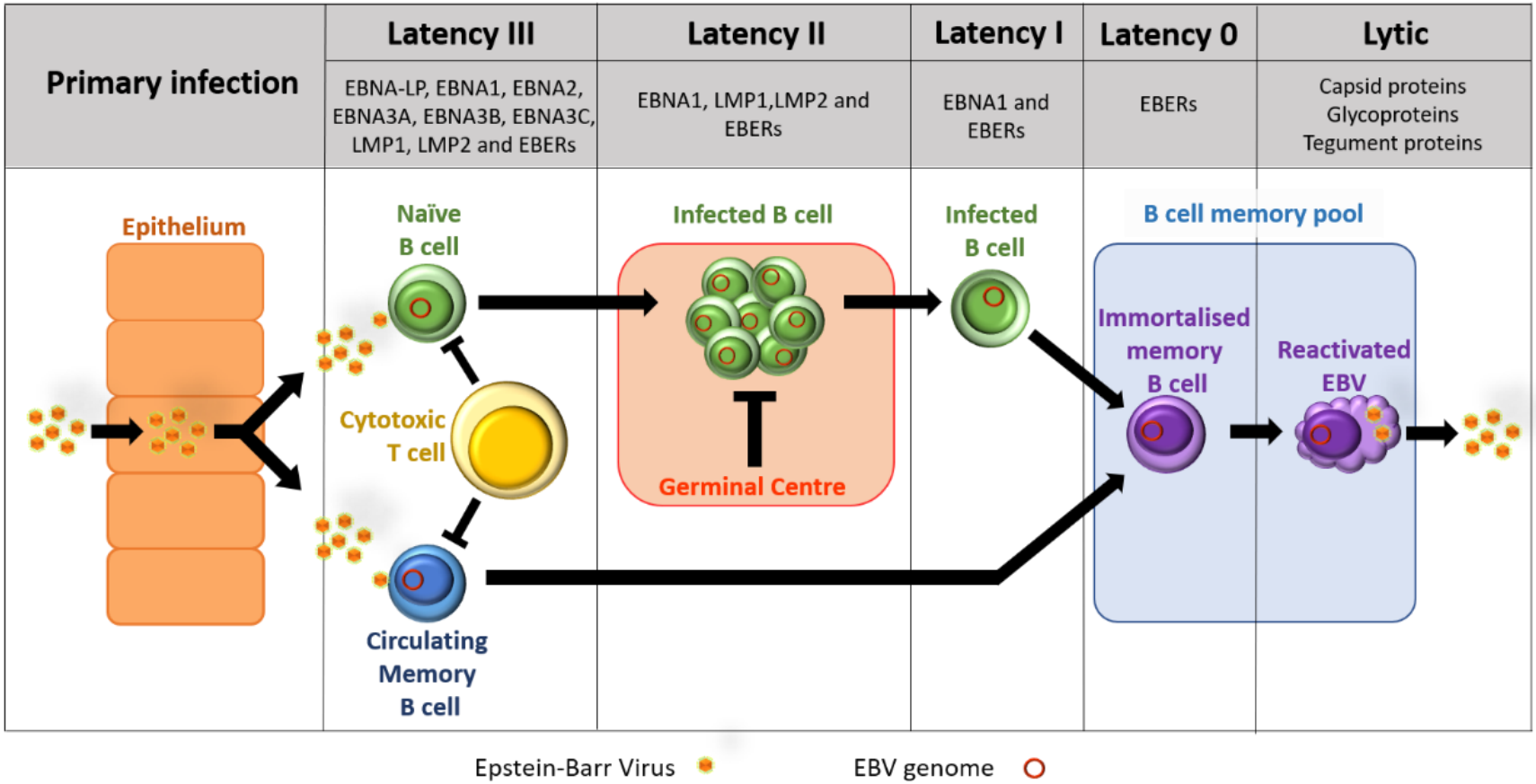


**Figure 1.1. Epstein-Barr viral infection and expression of Epstein-Barr viral proteins.** EBV upon infecting a person, through the exchange of saliva, passes through the epithelium of the nasopharynx to infect naïve B cells and memory B cells circulating below the epithelium and adopts a latency III pattern of expression. Cytoxic T cells elicit an EBV specfifc immune reponse to infected B cell. Infected Naïve cells pass through the germinal center whilst adopting a latency II pattern of expression then latency I pattern of expression. Both infected B cell types adopt latency 0 when they have immortalised a B cell in the B cell memeroy pool. EBV can be reactivated and adopt a lytic pattern of expression to produce more virus.

### 1.1.3 : EBNA1

EBNA1 was the first EBNA discovered and is essential for sustaining immortalisation in B cells (Reedman and Klein, 1973, Humme *et al.*, 2003, Altmann *et al.*, 2006). EBNA1 is required for the maintenance of the EBV genome through host cell division (Yates *et al.*, 1984, Yates and Guan, 1991). To do this, EBNA1 associates with the latent origin of replication as a dimer via 18bp palindromic sequences in DS element of the *oriP* during the S phase of the cell cycle (Rawlins *et al.*, 1985, Yates *et al.*, 1985, Jones *et al.*, 1989, Ambinder *et al.*, 1990, Shah *et al.*, 1992, Wu *et al.*, 1996). As EBNA1 possesses no helicase or DNA melting activity of its own, it recruits host DNA polymerase to facilitate the replication of the EBV genome (Frappier and O'Donnell, 1991, Schepers *et al.*, 2001). EBNA1 has been shown to recruit origin of complex (ORC) to the DS element to facilitate EBV DNA replication (Dhar *et al.*, 2001, Schepers *et al.*, 2001). During cell division EBNA1 mediates the even distribution of the EBV episome between the daughter cells by tethering the episome to host chromatin (Hodin *et al.*, 2013). EBNA1 has also been shown to activate the expression of Cp and LMP1 promoters via binding through the Fr element (Sugden and Warren, 1989, Gahn and Sugden, 1995). EBNA1 can also downregulate its own expression from the Q promoter (Nonkwelo *et al.*, 1996). Additionally, 903 EBNA1 binding sites on the host genome in B cells have been identified and approximately 7% of these sites were proximal to transcription start sites (TSS) (Lu *et al.*, 2010). However, the mechanism of how EBNA1 mediates transcription is not yet understood. EBNA1 has been shown to promote cell survival and immortalisation through its effects on host proteins such as USP70 where it competes with with p53 for USP70 binding (Humme *et al.*, 2003, Altmann and Hammerschmidt, 2005, Altmann *et al.*, 2006). EBNA1 is thought to prevent p53 binding

resulting in decreased levels of p53 which is suggested to prevent cell cycle arrest during infection (Holowaty *et al.*, 2003, Saridakis *et al.*, 2005). EBNA1 has also been shown to interfere with NFκB and TGFβ signalling (Wood *et al.*, 2007, Valentine *et al.*, 2010).

### 1.1.4 : LMPs

Latent membrane protein 1 (LMP1) expression is controlled by its bidirectional promoter, which expresses LMP1 and LMP2B in opposite directions (Laux *et al.*, 1994b). RBP-Jκ and PU.1 sites in the promoter allow EBNA2 and EBNA3C to mediate the expression of LMP1 and LMP2B (Allday *et al.*, 1993b, Allday and Farrell, 1994, Henkel *et al.*, 1994, Sjoblom *et al.*, 1995, Sjoblom *et al.*, 1998b). However, during an established infection, LMP1 co-ordinates multiple host signalling pathways to regulate its own expression (Sjoblom *et al.*, 1998a, Rowe *et al.*, 2014). LMP1 has been shown to mimic CD40 receptors which is suggested to prevent autoreactive immune responses destroying the EBV infected cell in the germinal centre (Uchida *et al.*, 1999). LMP1 has 6 membrane spanning domains which tether LMP1 to the cell membrane (Fennewald *et al.*, 1984). Upon associating with the cell membrane LMP1 clusters into aggregates, which intercalate into lipid rafts to provide a platform for signalling (Mann *et al.*, 1985, Gires *et al.*, 1997, Ardila-Osorio *et al.*, 1999, Higuchi *et al.*, 2001). The LMP1 C-terminal activation region 1 transformation effector site 1 (CTAF-TES1) is bound by the Tumour necrosis factor receptor associated factors (TRAF) 1,2,3 and 5 at a PXQXT motif which activates the non-canonical NFκB signalling pathway (Devergne *et al.*, 1996, Gires *et al.*, 1997, Devergne *et al.*, 1998). TRAF6 binds to the LMP1 CTAF-TES2 via TRADD or RIP1, which activates the canonical NFκB signalling pathway (Izumi and Kieff, 1997, Schultheiss *et al.*, 2001, Luftig *et al.*, 2003, Huye *et al.*, 2007). NFκB signalling promotes

cell survival of EBV infected cells during their journey through the germinal centre (Devergne *et al.*, 1998, Babcock *et al.*, 2000, Cahir-McFarland *et al.*, 2004). LMP1 is also shown to activate the PI3K/AKT and JNK signalling pathways which are thought to promote longevity of the EBV infected cell via telomerase activity after it has migrated through the germinal centre (Ding *et al.*, 2007, Shair *et al.*, 2007, Yang *et al.*, 2014).

Latent membrane protein 2 (LMP2) is expressed as 2 proteins LMP2A and LMP2B (Laux *et al.*, 1988, Rowe *et al.*, 1988, Laux *et al.*, 1989, Sample *et al.*, 1989, Rowe *et al.*, 1990). After primary infection, LMP2 is suggested to self-regulate its expression using host factors it activates such as Notch (Anderson and Longnecker, 2008a). LMP2 inserts into the cell membrane via its multiple hydrophobic α-helices and palmitoylation (Matskova *et al.*, 2001, Katzman and Longnecker, 2004). Like LMP1, LMP2 aggregates in the membrane (Matskova *et al.*, 2001). The N-terminal domains contain tyrosine residues, which are hyper-phosphorylated in order to bind to host proteins with SH3 domains (Longnecker *et al.*, 1991, Burkhardt *et al.*, 1992, Fruehling *et al.*, 1998). The N-terminal domain also contains proline rich regions which can bind neural precursor cell expressed developmentally down-regulated protein (NEDD) ubiquitinases which tag the LMP2A for degradation reglulating LMP2A activity (Ikeda *et al.*, 2003). Through these interactions with host proteins, LMP2 mimics B cell receptor (BCR) signalling by hijacking PI3K, Notch, Bcl2, ERK/MAPK and p27 signalling pathways to promote B cell growth, survival, maturation and migration during an EBV infection (Henderson *et al.*, 1991, Caldwell *et al.*, 1998, Fruehling *et al.*, 1998, Babcock *et al.*, 2000, Pegtel *et al.*, 2005, Anderson and Longnecker, 2008a, Anderson and Longnecker, 2008b, Shair *et al.*, 2012, Fish *et al.*, 2014).

### 1.1.5 : EBNA-LP

Epstein-Barr Nuclear Antigen Leader Protein (EBNA-LP) is expressed from the Wp during early infection and produces varying isoforms, which contain different numbers of the W1W2 repeats and Y1Y2 C-terminal repeats (Wang *et al.*, 1987b, Nitsche *et al.*, 1997). EBNA-LP, via its bipartite nuclear localisation sequence (NLS), predominantly localises in the nucleus (Peng *et al.*, 2000). EBNA-LP has been shown to co-activate expression of LMP1 with EBNA2 (Harada and Kieff, 1997a, Nitsche *et al.*, 1997, McCann *et al.*, 2001). However, the interaction between EBNA2 and EBNA-LP that facilitates co-activation is not fully understood. EBNA-LP has also been shown to interact with tumour suppressors Retinoblastoma (Rb), p53 and p14ARF (Inman and Farrell, 1995, Portal *et al.*, 2006). However, the physiological effects of these interactions with EBNA-LP have yet to be elucidated. EBNA-LP has also been shown to interact with HDAC4 and is suggested to activate gene expression using HDAC4 to facilitate epigenetic changes to the genes to promote gene expression (Portal *et al.*, 2006, Portal *et al.*, 2013).

### 1.1.6 : EBNA2 and EBNA3s

EBNA2 and EBNA3 family of EBV proteins are expressed during the latency programme III and regulate the expression of EBV latency genes for a short time frame in EBV infected tonsillar tissue (Thorley-Lawson and Babcock, 1999, Babcock *et al.*, 2000)(Figure 1.1). EBNA2 and EBNA3s also orchestrate host cell expression and are essential, with exception of EBNA3B, for sustaining immortalised B cells in culture (Tomkinson and Kieff, 1992, Tomkinson *et al.*, 1993). EBNA2 and EBNA3s cannot bind to DNA directly like EBNA1 and rely on host transcription factors to target them to viral and host regulatory elements (Ling *et al.*, 1994, Sample and Parker, 1994, Hsieh and

Hayward, 1995). RBP-Jκ, the effector of the Notch signalling pathway, was the first host transcription factor shown to act as a DNA adaptor to EBNA2. RBP-Jκ was also shown to be essential to recruiting EBNA2 to EBV Cp promoter to trans-activate the expression of the EBV LMP proteins (Abbot *et al.*, 1990, Wang *et al.*, 1990, Woisetschlaeger *et al.*, 1991, Randahl *et al.*, 1992, He and Pear, 2003a). The EBNA3 family were subsequently shown to require RBP-Jκ to regulate LMP2 expression and were also shown, using a CAT reporter assay, to inhibit EBNA2-transactivation (Le Roux *et al.*, 1994, Marshall and Sample, 1995).

Interactions between EBNA2, EBNA3s and RBP-Jκ have been shown to be essential for sustaining immortalised LCLs (Robertson *et al.*, 1996b, Maruo *et al.*, 2003, Maruo *et al.*, 2005, Maruo *et al.*, 2006, Lee *et al.*, 2009). Mutating the RBP-Jκ binding motif to alanine residues in EBNA3C, fused to a 4-hydroxytamoxifen (4HT)-dependent oestrogen receptor (EBNA3C-HT) allowing for conditional expression of EBNA3C, was shown to prevent EBNA3C repression of host genes in LCLs. In addition to this the EBNA3C RBP-Jκ mutant was also shown to be unable to sustain LCL growth and in reporter assays failed to silence EBNA2 transactivation of a reporter construct regulated by RBP-Jκ (Waltzer *et al.*, 1996, Lee *et al.*, 2009, Maruo *et al.*, 2009). Conversely a recent study showed that infecting primary $CD19^{+}$ cells with EBV expressing EBNA3C with a mutated RBP-Jκ binding motif established an immortalised cell line suggesting EBNA3-RBP-Jκ interactions being essential to sustaining B cell lines may be cell-type specific (Wang *et al.*, 2015, Kalchschmidt *et al.*, 2016). Electro-mobility-shift assays (EMSAs) showed that when EBNA3C was incubated with an EBNA2-RBP-Jκ-DNA complex the EBNA2 was displaced from RBP-Jκ, which also resulted in RBP-Jκ unbinding from the DNA (Waltzer *et al.*, 1996). EBNA2 and EBNA3 competing

for RBP-Jκ binding was confirmed when ChIP-re ChIP of RBP-Jκ controlled genes showed EBNA2 and EBNA3s bound RBP-Jκ independently (McClellan *et al.*, 2013b). However, genome wide ChIP-seq analysis of Mutu III and LCLs has confirmed that RBP-Jκ is not displaced from DNA as previously suggested as EBNA3s are shown to be enriched at RBP-Jκ consensus sites (McClellan *et al.*, 2013b, Wang *et al.*, 2015).

### 1.1.7 : EBNA2

Most studies of EBNA2 have identified EBNA2 as a transactivator of EBV and host gene expression. However there are a small number of cases, such as the host regulator of B cell diversity activation-induced cytidine deaminase (AID), where EBNA2 inhibits gene expression via mechanisms that are not yet understood (Tobollik *et al.*, 2006). EBNA2 is expressed earlier on during an EBV infection and is not identified to be expressed at the later stages of infection in hosts capable of eliciting a healthy cytotoxic T cell response (Babcock *et al.*, 2000, Kurth *et al.*, 2003). However, EBNA2 has been shown to be expressed in malignancies in immunocompromised transplant patients (Thomas *et al.*, 1990). Upon a primary EBV infection of B cells latent viral gene expression is directed from the W promoter (Wp) (Woisetschlaeger *et al.*, 1990, Grossman *et al.*, 1994b). EBNA2 is required to switch viral expression to C promoter (Cp) which allows expression of all the EBNA genes as a long primary transcript (Grossman *et al.*, 1994a). Immortalised B cell lines that do not express EBNA2 or had mutated EBNA2 enhancers upstream of the Cp were shown to continue to use Wp to direct expression (Yoo *et al.*, 1997, Yoo *et al.*, 2002). EBNA2 binding at the Cp has also been shown to be essential for promotor stalling of RNA polymerase II (PolII) at the Cp, allowing for effective pTEFb recruitment, via Brd4, for phosphorylation of serine 5 of PollII CTD (Jang *et al.*, 2005, Palermo *et al.*, 2011). EBNA2 induced PolII promoter stalling allows for efficient

transcription of the long Cp promotor transcript (Palermo *et al.*, 2011). BL cells lacking EBNA2 expression (Mutu I), were shown, using Chip-Seq, to have significant nucleosome assembly around the Cp promoter compared to Burkitts lymphoma cells (Mutu III) expressing EBNA2. This suggested the stalled PolII complex protects the Cp promoter from nucleosome assembly to aid transcription (Palermo *et al.*, 2011). EBNA2 also transactivates the expression of the viral LMP proteins, predominantly via RBP-Jκ binding. A combination of deletion analysis of reporter constructs of LMP1, LMP2A and LMP2B promoters and gel retardation assays have confirmed the presence of RBP-Jκ consensus sites in all LMP promoters (Abbot *et al.*, 1990, Sung *et al.*, 1991, Zimber-Strobl *et al.*, 1991, Ling *et al.*, 1993a, Zimber-Strobl *et al.*, 1993, Henkel *et al.*, 1994, Laux *et al.*, 1994b, Waltzer *et al.*, 1994, Zimber-Strobl *et al.*, 1994). However, RBP-Jκ binding at the LMP1 and LMP2B promoters is comparatively weak and it has been shown that EBNA2 requires PU.1 to be bound to facilitate effective transactivation of the LMP1 promoter (Laux *et al.*, 1994a, Laux *et al.*, 1994b, Johannsen *et al.*, 1995).

9 conserved regions (CR) were identified by comparative analysis of EBNA2 from EBV, baboon and rhesus lymphocryptovirus which searched for similarities in their sequences (Peng *et al.*, 2000)(Figure 1.2). EBNA2 nuclear localisation sequences (NLS) in CR7 and CR9 were identified when deletion of both of these regions was shown, using immunofluorescent microscopy, to ablate EBNA2 migration to the nucleus (Cohen *et al.*, 1991). A bacterially expressed polypeptide of EBNA2 CR6 was identified as being essential for RBP-Jκ interactions (Ling and Hayward, 1995). A competition binding assay using EMSA showed that a peptide of the EBNA2 CR6 WWP motif competed with EBNA2 for RBP-Jκ binding (Ling and Hayward, 1995)(Figure 1.2). This

revealed EBNA2 mimicked the Notch RAM domain WΦP RBP-Jκ binding motif, which is conserved across species in Notch, to interact with RBP-Jκ (Ling and Hayward, 1995, Johnson *et al.*, 2010). CR5 has also been shown to bind to a mediator of co-activator and co-repressor binding to RBP-Jκ called SKIP. Reporter assays showed that deletion of this domain could prevent EBNA2 binding to RBP-Jκ and disrupt EBNA2 transactivation (Sifang Zhou, 2000)(Figure 1.2). In addition to this EBNA2 can be phosphorylated by EBV kinase and cdc2/Cyclin B1 at serine 243 which leads to decreased activation of LMP1 in both cases (Cohen and Kieff, 1991a, Yue *et al.*, 2005, Yue *et al.*, 2006). CR1/2 and CR8 have been identified as N and C terminal TAD respectively (Cohen and Kieff, 1991b, Gordadze *et al.*, 2004)(Figure 1.2).

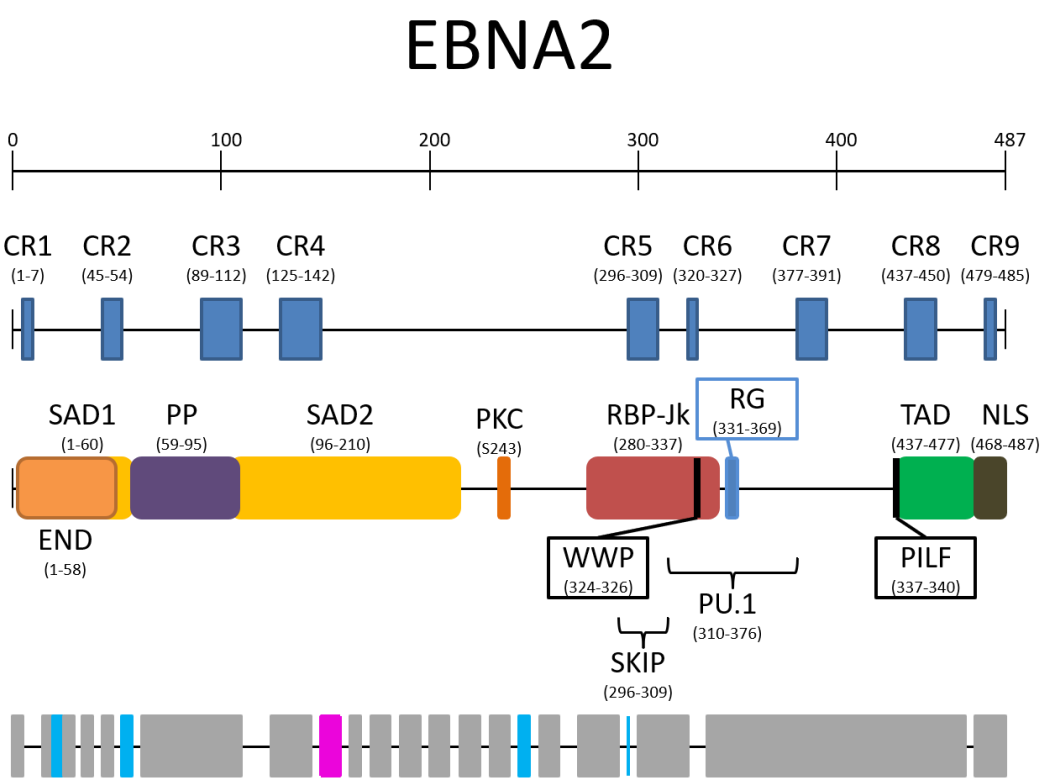


**Key:** Grey: Loop structures, Blue: α-Helices, Pink: β-Sheets.

**Figure 1.2. Domain map of EBNA2.** At the top is an amino acid ruler. Below the ruler is a map of the conserved regions (CR) between the type1 and type 2 EBNA2 (dark blue boxes) (Cancian *et al.*, 2011). Domain map shows the Self Association Domains (SAD) in yellow (Friberg *et al.*, 2015) which contains EBNA2 N-terminal Domain (END) in light orange, proline rich region (PP) in purple (Wu *et al.*, 1996), kinase phosphorylation site (PKC) in dark orange (Yue *et al.*, 2006), the RBP-Jκ binding region (RBP-Jκ) in red (Ling and Hayward, 1995), the WWP motif in black, an Arginine/ Glycine rich region(Voss *et al.*, 2001), the PILF motif has been shown to associate with PU.1 *in vivo* (Zimber-Strobl and Strobl, 2001), a Trans Activation Domain (TAD) in green and a Nuclear localisation sequence (NLS) in brown (Ling *et al.*, 1993b). Just below the domain the SKIP (Sifang Zhou, 2000) and another PU.1 binding region is highlighted (E Johannsen, 1995). At the bottom of the diagram is a map of the predicted secondary structure, the unstructured loops are shown in grey, the alpha helix regions are shown in blue and the beta sheet regions are shown in pink (Yenamandra *et al.*, 2009).

The EBNA2 C-terminal TAD that has been shown to have structural similarities to Human Simplex Virus (HSV) VP16 TAD. EBNA2 TAD (aa453-466) conjugated to Gal4 was shown to activate expression of CD23 and LMP1 in a reporter assay in Burkitts lymphoma (BL) cells (Cohen, 1992). The VP16 TAD (aa412-490) could be substituted with the EBNA2 TAD to transactivate expression in the same assay suggesting they had similar functions (Cohen, 1992). EBNA2 TAD and VP16 TAD have both been shown to interact with TFIIB and TAF4 which, open chromatin to facilitate gene expression (Tong *et al.*, 1995a, Tong *et al.*, 1995b, Tong *et al.*, 1995c, Wu *et al.*, 2000b). In addition to this NMR chemical shift perturbation studies showed that when the EBNA2 TAD binds to the plextrin homology domain of Tfb1/p62 subunit (Tfb1PH) of TFIIH this induces similar $H^1$ $N^{15}$ shifts to that seen when HSV V16 TAD and human p53 TAD interact with Tfb1PH (Chabot *et al.*, 2014). The EBNA2 TAD is predicted to be an intrinsically disordered protein, however NMR chemical shift perturbation and the NMR structure of the EBNA2 TAD bound to Tfb1PH showed that the EBNA2 TAD (aa448-471) folded into a 9 residue α-helix flanked by disordered regions, which bound in a shallow hydrophobic pocket on the surface of the Tfb1PH (Chabot *et al.*, 2014) (Figure 1.3A). The EBNA2 residues W458, I461 and F462 mimicked the ΦXXΦΦ motif used by p53 and VP16 to interact with TFIIH. However, this structure showed that EBNA2 presented these hydrophobic residues in a conformation, unique to that of p53 and VP16 (Chabot *et al.*, 2014).

Consistent with EBNA2s role as an activator of gene expression ChIP data shows EBNA2 binding coincides with the chromatin remodelling factor SWI/SNF (Wu *et al.*, 2000a). In EBNA2 negative cell lines SWI/SNF binding to EBNA2 target genes is not detected

suggesting EBNA2 indirectly recruits SWI/SNF. No data has shown that the SWI/SNF complex and EBNA2 directly interact however, EBNA2 has been shown to bind to the SWI/SNF co-activator and Histone Acetylase (HAT) p300 (Wang *et al.*, 2000, Wu *et al.*, 2000a). NMR chemical perturbation studies of the interactions between EBNA2 TAD (aa448-471) and the KIX domain of the CBP/p300 complex (residues 586-672) showed significant $H^1$ and $N^{15}$ shifts in the structure of EBNA2 when it was introduced to KIX suggesting the disordered EBNA2 TAD changes conformation upon binding to KIX potentially interacting with KIX in a similar manner as VP16 TAD and p53 TAD (Chabot *et al.*, 2014). Together this suggests EBNA2 recruits SWI/SNF via its co-activators to modify histone tails and promotes open chromatin conformations at regulatory elements to transactivate gene expression (Wu *et al.*, 2000a, Chabot *et al.*, 2014).

CR1/2 and CR3/4 were predicted to contain two EBNA2 self association domains (SAD1 aa1-60 and SAD2 aa101-214) (Harada and Kieff, 1997a)(Figure 1.2). Additionally, yeast two hybrid assays had shown EBNA2 residues 122-344 could interact with full length EBNA2 (Tsui and Schubach, 1994). Recombinant EBNA2 expressed in insect cells and EBNA2 expressed in EBV infected B cells had also been shown to assemble into a 440kDa polymer (Grässer *et al.*, 1991, Tsui and Schubach, 1994). Co-immunoprecipitations of truncations of EBNA2 and full length EBNA2 expressed in BJAB cells were analysed by western blot to identify regions 1-60 and 101-214 were essential for EBNA2 dimerisation (Harada and Kieff, 1997b). Due to EBNA2 binding sites on the *LMP2A* promoter being 11bp apart and multiple host transcription factor binding sites being identified in close proximity to the single EBNA2 binding site on the Cp promoter, it was suggested EBNA2 dimerised to bind multiple host transcription factors to mediate LMP regulatory elements (Sung *et al.*, 1991, Zimber-Strobl *et al.*,

1993, Zimber-Strobl *et al.*, 1994, Harada and Kieff, 1997b). The NMR structure of $EBNA2_{1-58}$ confirmed that it dimerised and folded into a structure containing 4 β-strands organised in an anti-parallel fashion and a short α-helix (Figure 1.3B)(Friberg *et al.*, 2015). The EBNA2 dimer fold was identified as a novel topology that had not been seen in the protein data bank (PDB) before, so was named the END (EBNA2 N-terminal Dimerisation) domain. The hydrophobic interface of the dimer stabilises the END domain through inter-monomer hydrophobic interactions between the leucine, tyrosine, and valine residues creating a hydrophobic core (Figure 1.3B). EliBL cell lines transfected with EBNA2 END domain mutants showed that L16D and I50D mutations strongly attenuated EBNA2 activation of LMP expression (Friberg *et al.*, 2015). RT-QPCR analysis of host targets CCL3 and CD23 in ELiBL cells that L16D and I50D mutations caused a significant loss in EBNA2 induced activation of the genes, demonstrating that the EBNA2 dimerisation plays a key role in EBV hijacking of host gene expression (Friberg *et al.*, 2015).

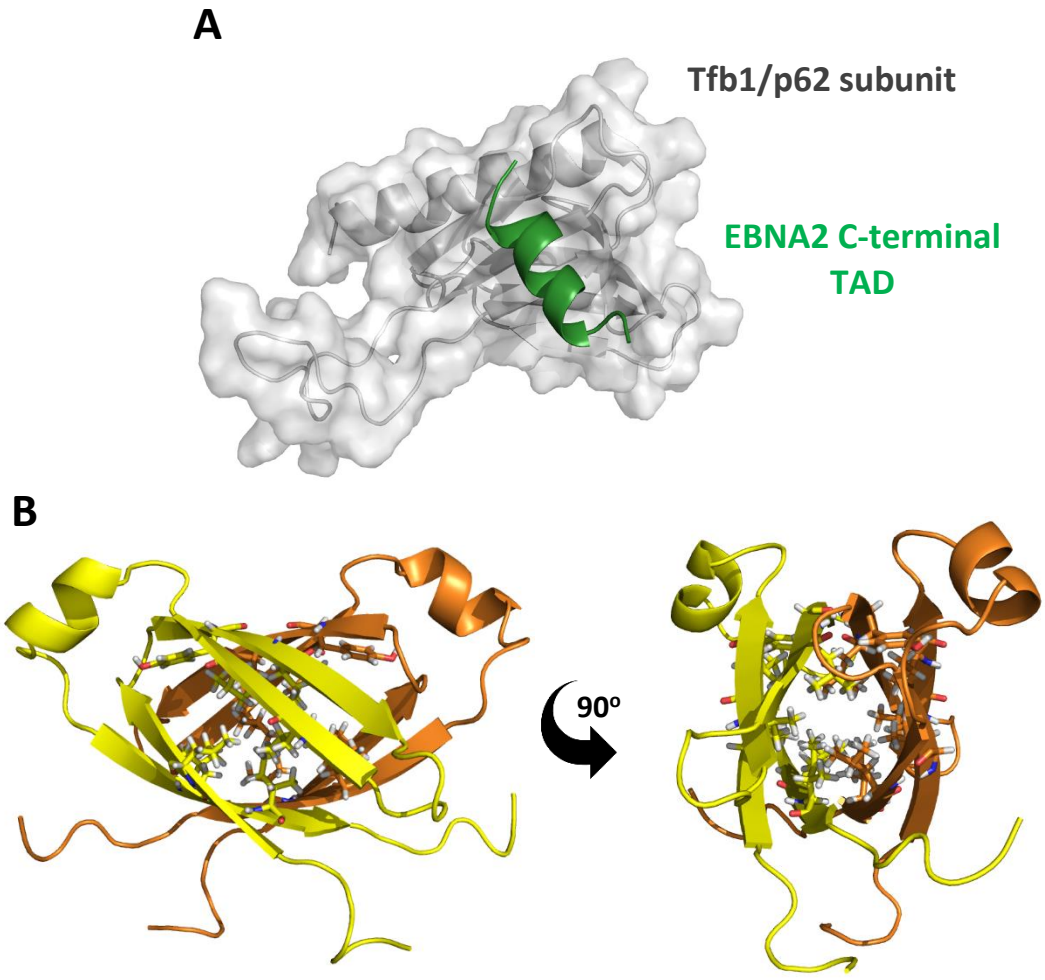


**Figure 1.3. NMR structures of EBNA2. A.** NMR structure of EBNA2$_{1\text{-}58}$ (in green) bound to Tfb1/p62 subunit of the host transcription factor TFIIH (in grey) (Chabot *et al.*, 2014). **B.** EBNA2 NTD transactivational domain dimerises. Structure has been rotated 90º to show hydrophobic core (hydrophodic residues have been shown as sticks) of NTD EBNA2 dimer. EBNA2 monomer have been coloured yellow and orange to distinguish them from each other (Friberg *et al.*, 2015).

Due to EBNA2 binding sites being identified in the EBV Cp, LMP1p and the promotor of CD23 and reporter assays confirming EBNA2 transactivated these genes it was originally thought EBNA2 mediated gene expression via promoters (Wang *et al.*, 1987a, Wang *et al.*, 1990, Wang *et al.*, 1991, Ling *et al.*, 1994, Rymo, 1995). Microarrays in EBV positive cell lines not only confirmed CD23 to be upregulated by EBNA2 but also identified key B cell growth genes *RUNX3* and *MYC* were also upregulated by EBNA2 (Maier *et al.*, 2006, Spender *et al.*, 2006, Zhao *et al.*, 2006). No EBNA2 binding sites were identified to transactivate at *RUNX3* or *MYC* promoters, however genome wide ChIP-Seq analysis of EBNA2 binding in BL cells (Mutu III) identified that 75% of EBNA2 binding was at distal regulatory elements (McClellan *et al.*, 2013b, Gunnell *et al.*, 2016, Wood *et al.*, 2016). For example, EBNA2 relies on interactions with RBP-Jκ to bind to the *RUNX3* -97kb super enhancer (SE) and to the -139kb and -250kb enhancers of *RUNX1* (Gunnell *et al.*, 2016). EBNA2 transactivation of RUNX3 leads to repression of *RUNX1* and its inhibitory effects on B cell growth (Spender *et al.*, 2005). Additionally, EBNA2 RBP-Jκ dependent binding at the -139kb and -250kb RUNX enhancers also resulted in decreased expression of RUNX1 (Gunnell *et al.*, 2016). However, Notch 1 has been shown in multiple cell systems to upregulate RUNX1 expression (Burns *et al.*, 2005, Nakagawa *et al.*, 2006, Meier-Stiegen *et al.*, 2010). This revealed EBNA2 bound distal enhancers, via interactions with RBP-Jκ, to down regulate RUNX1 expression and B cell growth inhibition, via a mechanism distinct from Notch to promote B cell growth during EBV infections (Gunnell *et al.*, 2016). EBNA2 was also shown not to bind at the *MYC* promoter (Wood *et al.*, 2016). However, in EREB cells with conditionally active EBNA2, increased EBNA2 binding was shown, using Capture HiC, at the -556, -428, -186/168 SE of the *MYC* locus whilst reduced EBNA2 binding was shown at the +456,

+570, +1.8/9 upstream SE of the *MYC* locus (Wood *et al.*, 2016). Chromatin conformation capture (CCC) was then used to confirm that the presence of EBNA2 induced downstream enhancer-promoter interactions. Therefore, EBNA2 binding at the *MYC* locus created a unique looping profile bringing downstream enhancers and the *MYC* promoter together to turn on MYC expression whilst silencing other MYC elements (Wood *et al.*, 2016).

Motif searching of ChIP-Seq data of EBNA2 binding peaks confirmed EBNA2 bound at RBP-Jκ (80% of EBNA2 binding sites in LCLs), PU.1, RUNX and EBF1 sites (McClellan *et al.*, 2013b, Wang *et al.*, 2015). EBF1 has more recently been shown to bind EBNA2 to drive the assembly of EBNA2-EBF1-RBP-Jκ complexes at co-occupied sites and even anchor EBNA2 to DNA at EBNA2 sites independent of RBP-Jκ, to activate the expression of host genes (Lu *et al.*, 2016, Glaser *et al.*, 2017). When the chromatin landscape of GM12878 LCLs was mapped to the EBNA2 peaks, the majority of the EBNA2 peaks were shown to have Histone 3 Lysine 27 acetylation (H3K27ac) and Histone 3 lysine 4 monomethylation (H3K4me1) indicative of active gene expression (McClellan *et al.*, 2013a). This confirmed the role of EBNA2 as a transcriptional activator and that EBNA2 utilised host factors to bind distal regulatory elements to mediate host gene expression.

### 1.1.8 : EBNA3 family

EBNA1, EBNA2 and LMP1 had already been identified however a 142kDa protein was also shown to react with EBV exposed human antisera (Hennessy *et al.*, 1985). The protein, dubbed EBNA3, was identified to be expressed from the BamHI E fragment of the rightward open reading frame (BERF1) of the EBV genome (Hennessy *et al.*, 1985, Hennessy *et al.*, 1986). The gene was cloned into a bacterial vector and expressed in rodent cells, however EBNA3 antisera was also shown to react with other incrementally larger proteins (Hennessy *et al.*, 1986). Subsequently, EBNA3C (155kDa) and EBNA3B (165kDa) were discovered forming the EBNA3 family of EBV transcription factors (Petti and Kieff, 1988, Petti *et al.*, 1988). EBNA3A, EBNA3B and EBNA3C genes are arranged in tandem on the EBV genome suggesting that they arose through gene duplication (Farrell, 2001). The EBNA3 family are expressed as a single alternately spliced transcript from the Cp (Allday *et al.*, 1989). The EBNA3 family of proteins do not share much amino acid sequence homology. However, analysis of the EBNA3s amino acid sequence revealed a region in the N-terminus of each EBNA3 with increased shared homology, called the homology domain (HD), which shared 23% to 28% sequence homology (Yenamandra *et al.*, 2009). However secondary structure predictions of the amino acid sequences of the EBNA3 HDs predicted 72% to 78% of their folding adopted similar conformations (Yenamandra *et al.*, 2009). However, full length EBNA3s overall are predicted to be disordered proteins (West, 2006, Yenamandra *et al.*, 2009). EBNA3A and EBNA3C were originally shown to be essential to sustain immortalised B cells. However, more recently an EBNA3A negative cell line has been established but has significantly attenuated growth (Tomkinson *et al.*, 1993, Hertle *et al.*, 2009). As previously discussed EBNA3s share many DNA binding sites with

EBNA2 to inhibit EBNA2 transactivation of host and EBV genes (Waltzer *et al.*, 1996, McClellan *et al.*, 2013b). However, they are shown to independently bind the host factor RBP-Jκ suggesting EBNA2 and EBNA3s compete for RBP-Jκ binding to antagonistically control gene expression (McClellan *et al.*, 2013a). RBP-Jκ binding has been mapped to each of the EBNA3 homology domains (Robertson *et al.*, 1996b). In addition to this, TΦGC and a WΦP motifs in the EBNA3C homology domain have been shown to be important for RBP-Jκ interactions (Lee *et al.*, 2009, Calderwood *et al.*, 2011).

Analysis of the EBNA3A amino acid sequence showed it contained two negatively charged clusters (aa16-60 and aa343-369), a glutamic acid and phenylamine rich region (aa271-289), a positively charged cluster (aa376-402) and a large proline rich region (aa417-794) which have been hypothesised to play roles in EBNA3A interactions with other proteins (Yenamandra *et al.*, 2009)(Figure 1.4A). The EBNA3A homology domain is predicted to fold into clusters of α-helices and β-sheets but no structural studies have confirmed this (Yenamandra *et al.*, 2009)(Figure 1.4A). EBNA3A has one NLS located at residues aa147-157 and another 5 which were predicted by computer models and confirmed using immunofluorescent microscopy (Le Roux *et al.*, 1993, Buck *et al.*, 2006)(Figure 1.4A). The C-terminal acidic region (841-944) has been shown to contain two CtBP-like binding motifs (ALDLS aa857-861 and VLDLS aa889-890) which are both necessary to bind to CtBP (Hickabottom *et al.*, 2002, Yenamandra *et al.*, 2009). Mutation of these motifs to alanine residues impaired the ability of EBNA3A to co-operatively immortalise and transform rat embryo fibroblasts with the oncogenic Ras protein suggesting EBNA3A-CtBP interactions can mediate repression of host genes (Hickabottom *et al.*, 2002). EBNA3A has also been shown to induce the

expression of and associate with Heat shock protein 70 (Hsp70) suggesting it exploits Hsp70 to aid its folding and improve its stability during an EBV infection (Young *et al.*, 2008). The EBNA3A N-terminal domain has been shown to be essential for interactions with RBP-Jκ (Robertson *et al.*, 1996b)(Figure 1.4A). In addition to this, when aa170-240 or aa300-286 were deleted or residues TLGC (aa198-202) were mutated to AAGA, EBNA3A was no longer able to silence EBNA2 transactivation of the Cp via RBP-Jκ binding in a reporter assay, or maintain the growth of LCLs grown in non-permissive conditions (Maruo *et al.*, 2005).

EBNA3B similarly has been predicted to contain 2 negatively charged regions (aa25-93 and aa355-378), a proline rich region (aa526-753) and a Sudo-homology domain (aa665-889) which have been predicted, but not confirmed, to be involved in protein-protein interactions (Yenamandra *et al.*, 2009)(Figure 1.4B). Additionally EBNA3B has been predicted to fold into α-helices and β-sheets with in its homology domain (Yenamandra *et al.*, 2009)(Figure 1.4B). NLS prediction models and confirmation via immunofluorescent microscopy identified EBNA3B had 2 functional NLS sequences (aa160-166 and aa867-873) (Burgess *et al.*, 2006)(Figure 1.4B). The N-terminal domain of EBNA3B (aa1-311) has also been shown to essential for binding RBP-Jκ (Robertson *et al.*, 1996b). EBNA3B is not required to maintain immortalised B cells but, despite this gene has not been selected against as EBV has evolved to persistently infect humans, suggesting that it has a vital role to play during an EBV infection (Chen *et al.*, 2005). When mice were infected with EBNA3B knockout EBV this caused highly proliferative B cell lymphomas to grow (White *et al.*, 2012). Furthermore, LCLs with EBNA3B deleted grow more robustly than LCLs expressing EBNA3B (White *et al.*, 2012). This suggests

that EBNA3B may play a role as a virally expressed tumour suppressor during EBV latency (White *et al.*, 2012). EBNA3B has been shown to play a role in recruiting T cells to EBV infected cells by promoting the expression of intracellular and cell surface proteins which has been suggested to prevent lymphoproliferation of B cells during an EBV infection (White *et al.*, 2012). However, T cells also aid immortalisation of B cells due to T cell binding activating pathways that promote B cell differentiation and germinal centre reactions (Nakayama *et al.*, 2002, White *et al.*, 2012).

Much like EBNA3A and EBNA3B, analysis of EBNA3C amino acid sequence has shown it contains a negative charge cluster (aa367-393) and a proline rich domain (Yenamandra *et al.*, 2009)(Figure 1.4C). However a glutamine/ proline rich region (aa724-826), which had a similar amino acid sequence to the TF Sp1, was able to activate gene expression in a CAT reporter assay when conjugated to Gal4 (Marshall and Sample, 1995)(Figure 1.4B). The EBNA3C homology domain has also been predicted to contain a basic leucine zipper (bZIP)(aa244-291) (West *et al.*, 2004). Circular dichroism and ultra-centrifugation analysis showed this region could fold into an α-helix however they did not observe the bZIP folding into homo or hetero dimer coil-coil structures characteristic of leucine zippers (West *et al.*, 2004).

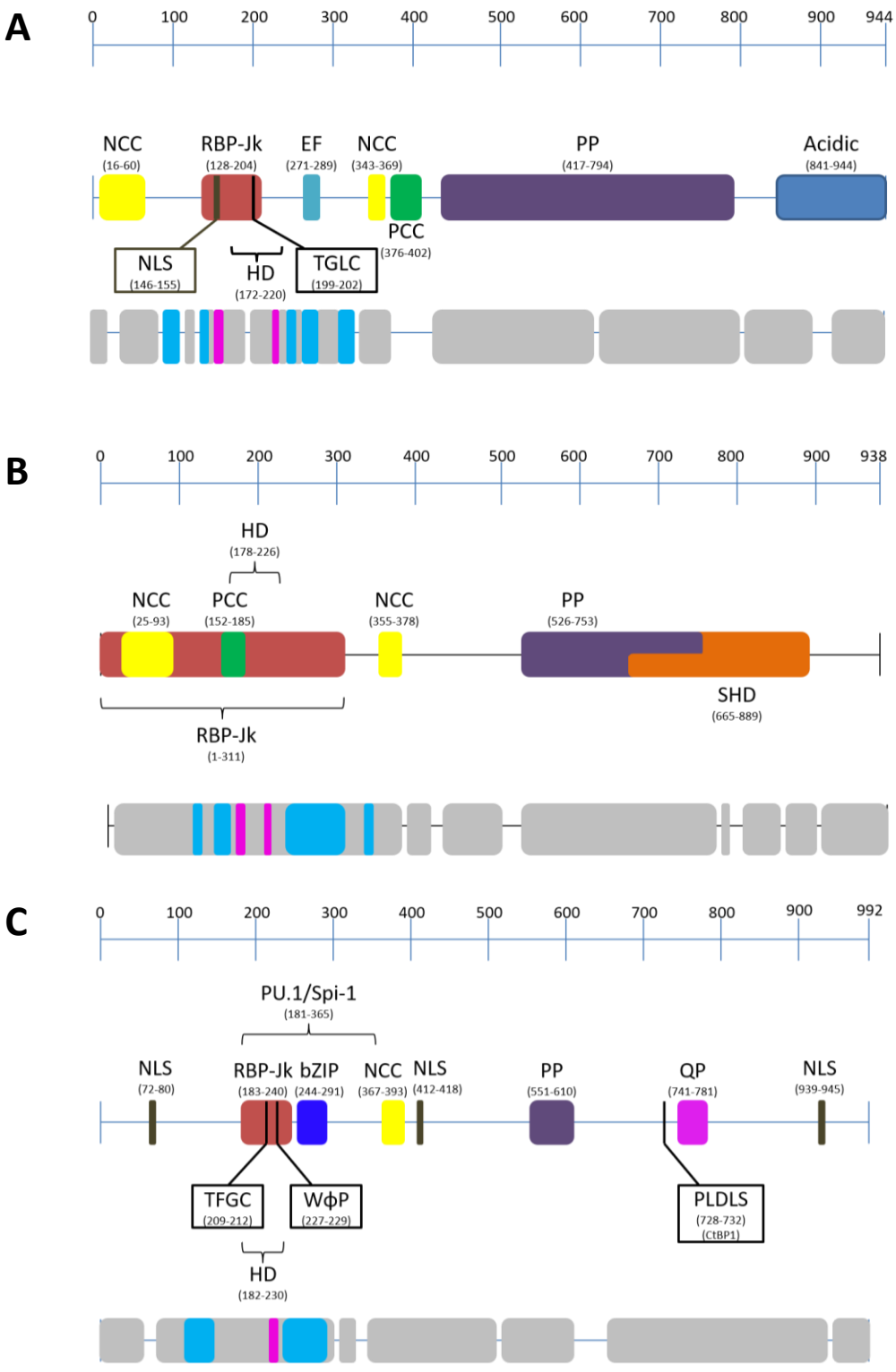


**Figure 1.4. Domain maps and folding predictions of the EBNA3 family of EBV TFs. A.** Shows a domain map of EBNA3A. **B** Shows a domain map for **EBNA3B. C.** Shows a domain map for EBNA3C. The B-zip region is shown in dark blue. The PU.1/ Spi-1 binding region has been highlighted above the domain map**.** The PLDLS motif, which binds to CtBP1, has also been highlighted. **The key for all the domains maps:** At the top is an amino acid ruler. The domain maps show Negative Charged Clusters(NCC) in yellow, RBP-Jk binding region (RBP-Jκ) in red, Glutamic acid and Phenylanine rich

regions (EF) in light blue, Positively Charged Clusters (PCC) in green, Proline rich regions (PP) in purple, Proline and Glutamine rich regions (PQ) in magenta, Sudo Homology Domains (SHD) in orange, Acidic regions in navy blue, the Nuclear Localisation sequence (NLS) is highlighted in brown and TΦGC motif is highlighted in black. Below the domain map is the predicted secondary structure map, the grey bars represent unstructured loops, the blue represents alpha helix regions and the pink represent regions of Beta-sheets. (Robertson *et al.*, 1996a, Waltzer *et al.*, 1996, Zhao *et al.*, 1996, Maruo *et al.*, 2003, West *et al.*, 2004, Maruo *et al.*, 2005, West, 2006, Maruo *et al.*, 2009, Yenamandra *et al.*, 2009, Calderwood *et al.*, 2011)

EBNA3C is the most studied of the EBNA3s and has been identified to interact with many host proteins. EBNA3C has been shown to bind to C-terminal binding protein (CtBP) via PLDLS motif used by Histone deactylases and co-repressors to interact with CtBP (Touitou *et al.*, 2001, Kuppuswamy *et al.*, 2008). EBNA3A and EBNA3C have also both been shown to epigenetically silence the expression of the cell cycle regulator p16 via CtBP (Maruo *et al.,* Skalska *et al.*, 2010b). In addition to this, EBNA3C has been shown to bind both isoforms of PU.1 *in vitro* and can co-activate the expression of LMP1 with EBNA2, via a PU.1 consensus site in the *LMP1* promotor (Zhao and Sample, 2000). The aa130-190 region of EBNA3C has been shown to bind to and stabilise the transcriptional activator c-Myc, promoting c-Myc recruitment to target genes (Bajaj *et al.*, 2008). This same region of EBNA3C is also shown to promote the degradation of retinoblastoma (RB) and p27 (Knight and Robertson, 2004, Knight *et al.*, 2005). Furthermore, EBNA3C has been shown to interact with and mediate the stability of p53, cyclin A and cyclin D1 (Knight and Robertson, 2004, Knight *et al.*, 2004, Yi *et al.*, 2009, Saha *et al.*, 2011). Together these interactions demonstrate how EBNA3C can target multiple control mechanisms of cell cycle via protein-protein interactions to promote B cell growth. EBNA3C has also been co-immunoprecipitated with Histone deacetylase (HDAC) 1 and 2 and treatment of EBV infected B cells with HDAC inhibitors results in expression of EBNA3C repressed genes such as *BIM* (Radkov *et al.*, 1999, Knight *et al.*, 2003, Paschos *et al.*, 2009). This suggests EBNA3C binds HDAC to silence Bim expression to promote cell survival during an EBV infection (Paschos *et al.*, 2009). EBNA3C homology domain has also been shown be essential to binding RBP-Jκ (Robertson *et al.*, 1996b). EBNA3C was originally shown to bind to RBP-Jκ via a TFGC motif, deletion of which ablated EBNA3C-RBP-Jκ interactions and EBNA3C inhibition of

EBNA2 transactivation (Maruo *et al.*, 2009). In addition to this LCLs expressing EBNA3C TFGC-AAAA mutant could not sustain immortalisation (Lee *et al.*, 2009, Maruo *et al.*, 2009).

Microarray analysis BL31 cells infected with strains of EBV with each of the EBNA3s knocked out revealed significant overlap in their mediation of host expression. 50% of the genes identified to have their expression mediated by EBNA3s were shown to be regulated by at least 2 of the EBNA3s (White *et al.*, 2010). Additionally out of the 1008 EBNA3 mediated host genes identified 22 were upregulated by all the EBNA3s and 34 were down regulated by all the EBNA3s. Whilst 30 novel genes targets were identified to be regulated by EBNA3A and EBNA3B the most common combination of EBNA3s was EBNA3B and EBNA3C which were shown to influence genes predominantly involved with haematopoiesis and B cell activation such as *ITGAL* and *RUNX1* (White *et al.*, 2010). All three EBNA3s were shown to be involved in regulating the expression of key B cell growth factors such as Notch2 and EBF1. Interestingly EBNA3B was shown to disproportionately affect the expression of genes involved with cell migration. H3K27me3, indicative of polycomb complex repression, was detected at genes repressed by EBNA3s. In EBNA3 knockout cells genes repressed by the EBNA3s were shown to not have H3K27me3. This suggested that together the EBNA3s could recruit polycomb complex to silence host gene expression involved with apoptosis, cell migration and B cell growth and maturation (White *et al.*, 2010). Multiple EBNA3s binding at genes was confirmed by ChIP-Seq analysis in Lymphoblastoid cell lines (LCLs) and BLs (McClellan *et al.*, 2013b, Wang *et al.*, 2015). Chip-Seq data from LCLs showed that 26% of EBNA3A sites were shared with EBNA3C, 21% of EBNA3B sites were shared with EBNA3A and 22% of EBNA3B sites were shared with EBNA3C. This confirmed that

the EBNA3s could collaborate to mediate host gene expression or mediate the same host genes to different degrees to fine tune host gene expression to facilitate B cell immortalisation (Wang *et al.*, 2015).

BCL2L11, also known as BIM, is a key pro-apoptotic factor which is targeted by EBNA3A and EBNA3C. Cancers often select for cells which have downregulated BIM expression, which permits indefinite cell proliferation (Paulin *et al.*, 1996, Pajic *et al.*, 2001). EBNA3A and EBNA3C were shown, using ChiP-Seq and CCC, to interfere with interactions between the long range enhancers (1,4 and 6) and the promoter of the *BCL2L11* locus downregulating its expression. EBNA3A and EBNA3C were shown to target the H3K27 methyltransferase (E2H2) to both the *BCL2L11* and *ACOXL* locus leading to H3K27me3 and silencing of the *BIM* locus (Paschos *et al.*, 2009, Skalska *et al.*, 2010b, Paschos *et al.*, 2012).

EBNA3A and EBNA3C have also been shown to repress the expression of the cyclin dependent kinase inhibitor p16 $^{INK4a}$ (Touitou *et al.*, 2001, Skalska *et al.*, 2010a, Maruo *et al.*, 2011). EBNA3C and EBNA3A bound CtBP was shown using ChIP-Seq to methylate the *p16$^{INK4a}$* chromatin and silence its expression (Skalska *et al.*, 2010a, Maruo *et al.*, 2011). EBNA3s may indirectly activate *p16$^{INK4a}$* by inhibiting CtBP2 expression suggesting the EBNA3s can delicately control p16$^{INK4a}$ induced senescence to promote cell growth whilst preventing tumorigenesis and detection by the immune system (Skalska *et al.*, 2010a, Maruo *et al.*, 2011).

EBNA3A and EBNA3C have also been shown to activate the expression of miR-221/222 to indirectly silence p57 expression. CCC revealed that EBNA3A and EBNA3C collaborated to loop long range enhancers to transactivate the expression of *miR*-

*221/222* (Bazot *et al.*, 2015). Increased expression of miR-221/222 leads to inhibition of $p57^{KIP2}$, a tumour suppressor involved with cell cycle regulation, likely contributing to B cell immortalisation during an EBV infection (Visone *et al.*, 2007, Bazot *et al.*, 2015).

## 1.2 : Epstein-Barr Virus associated cancers

Epstein-Barr virus was the first virus to be associated with causing cancer in humans when it was discovered to immortalise Burkitts lymphomas cells in 1964 (Epstein *et al.*, 1964b). Since then EBV has been shown cause multiple human cancers by hijacking host signally pathways to promote cell growth and cell survival leading to cancer development (Andersson, 2000).

### 1.2.1 : Burkitts lymphoma

Burkitts lymhphoma (BL) was dicovered by Denis Burkitt in 1958 whilst offering his services as a doctor in Uganda (Burkitt, 1962). Denis Burkitt discovered one of the three types of BL endemic BL (eBL) (Burkitt, 1962). Cases of eBL are predominantly found in Central Africa and in Papa New Guinea, accounting for 30-50% of childhood cancers in Central Africa. In addition to this, over 95% of cases of eBL are shown to be EBV positive (Parkin *et al.*, 1988, Hamilton-Dutoit *et al.*, 1993). Sporadic BL (sBl) occurs in the US and Europe accounting for 30-50% of childhood lymphomas however, only 10-15% of cases are EBV positive (Hamilton-Dutoit *et al.*, 1993, Morton *et al.*, 2006). 40% of Immunodeficiency associated BL (iBL) are EBV positive and coincide with HIV infections (Hamilton-Dutoit *et al.*, 1993, Guech-Ongey *et al.*, 2010). All BLs are shown to have *MYC* translocations which position the *MYC* gene proximal to powerful promoters in the Immunoglobin locus deregulating c-MYC expression (Magrath, 1990,

Brady *et al.*, 2007). BL are shown to have a latency I programme of latent expression (Gregory *et al.*, 1990). *In situ* hybridisation has confirmed the presence of EBERs which have been shown to protect cells from apoptosis and promote tumorigenicity in mouse models (Nanbo and Takada, 2002). EBNA1 has also been shown to competitively bind to USP7 ubiquitinase in the same pocket that p53 binds (Saridakis *et al.*, 2005). Ubiquitination of p53 by USP7 stabilises p53 allowing p53 to promote apoptosis (Brooks and Gu, 2011). It is therefore suggested that EBNA1 protects BLs with de-regulated MYC expression from apoptosis by destabilising p53 by blocking its binding to USP7 (Saridakis *et al.*, 2005).

### 1.2.2 : Hodgkin's lymphoma

Hodgkin's lymphomas (HL) produce growths in lymph nodes on the neck, arm or groin and are detected through the presence of Hodgkin's Reed Sternberg cells (Ansell, 2015). With early detection HL are effectively treated with chemotherapy (Armitage, 2010). HL develops from B cells after passage through the germinal centre (Kanzler *et al.*, 1996, Marafioti *et al.*, 2000). HLs are shown to lack B cell receptor (BCR) which is thought to manifest due to DNA damage or epigenetic silencing occurring in the immunoglobulin loci (Jox *et al.*, 1999, Ushmorov *et al.*, 2004). Approximately 50% of HLs are predicted to be infected with EBV and are shown to have an EBV latency II programme of expression (Schmitz *et al.*, 2009, World.Health.Organisation, 2014). EBV has been shown to rescue germinal centre B cells from apoptosis that lack functional immunoglobin (Bechtel *et al.*, 2005, Mancao *et al.*, 2005). LMP2A has also been shown to mimic BCR signalling and microarrays have shown LMP2A alter host gene expression to prevent apoptosis and promote B cell growth (Bechtel *et al.*, 2005, Mancao and Hammerschmidt, 2007). LMP1 is also shown to mimic CD40 expression activating NFκB

expression to promote cell growth and survival (Mosialos *et al.*, 1995, Devergne *et al.*, 1996, Gires *et al.*, 1997, Uchida *et al.*, 1999). This suggests EBV plays a role in HL pathogenesis by protecting HL lacking BCR signalling in the germinal centre from apoptosis (Mancao and Hammerschmidt, 2007).

### 1.2.3 : Post Transplant Lymphoproliferative Disease

During EBV primary infection the host immune system plays a key role in regulating EBV infection and preventing excessive proliferation of EBV infected B cells (Benninger-Doring *et al.*, 1999, Nikiforow *et al.*, 2001, Precopio *et al.*, 2003, Lee *et al.*, 2004). Cytotoxic T cells are the main effectors of regulating EBV infected cells and do so by recognising peptides of EBV proteins present by MHC class II molecules (Maini *et al.*, 2000, Gudgeon *et al.*, 2005, Hislop *et al.*, 2005, Landais *et al.*, 2005). Transplant patients receive immunosuppressants after surgery to prevent graft versus host disease. This results in transplant patients having very low T cell counts. In these conditions EBV infected cells, sometimes derived from donors, grow uncontrollably resulting in Post Transplant Lymphoproliferative Disease (PTLD) (Babcock *et al.*, 1999, Rasche *et al.*, 2014). EBV is shown to have a latency III programme of expression in PTLD patient samples suggesting the EBNAs and LMPs, without an effective cytotoxic T cell response drive excessive growth in B cells (Murray *et al.*, 1992, Tomkinson *et al.*, 1993, Benninger-Doring *et al.*, 1999, Lee *et al.*, 1999, Portis and Longnecker, 2004, Jha *et al.*, 2013). However, EBV-specific T cells grown from patient samples have proven effective at treating PTLD (Heslop *et al.*, 2010, Uhlin *et al.*, 2010). In addition to this anti-CD20 antibodies (Rituximab) infusions, which tag B cells for degradation, have also been shown to be effective at treating PTLD (Stuhler *et al.*, 2006, McIver *et al.*, 2010).

### 1.2.4 : Diffuse large B cell lymphoma

EBV positive Diffuse Large B Cell Lymphoma (DLBCL) is a cancer that is predominantly associated with immunocompetent patients over the age of 50 and is associated with worse outcomes when compared to EBV negative DLBCL (Morton *et al.*, 2006, Park *et al.*, 2007, Castillo *et al.*, 2011). Caucasians (less than 5% EBV positive) have been shown to be the least affected group whilst cases of EBV DLBCL are most prominent in Asia (8.9% EBV positive) and South America (14.9% EBV positive) (Park *et al.*, 2007, Beltran *et al.*, 2011, Ok *et al.*, 2013). It is suggested that ageing causes the make up of T cell population in the immune system to change resulting in reduced Cytotoxic T cell activity making patients more susceptible to EBV positive DLBCL (Aw *et al.*, 2007, Lefebvre *et al.*, 2012). However, more recent studies have reported similar percentages of EBV positive DLBCL cases in people under the age of 50 (Cohen *et al.*, 2014, Hong *et al.*, 2015). EBV positive DLBCL have been shown to adopt both latency II and III programmes of expression (Oyama *et al.*, 2007, Castillo *et al.*, 2011, Nguyen-Van *et al.*, 2011). EBV positive DLBCL cells also have been shown to have increased levels of NFκB and JAK/STAT implicating a role for LMP proteins in DLBCL pathogenesis (Shair *et al.*, 2007, Montes-Moreno *et al.*, 2012, Ok *et al.*, 2014). Additionally, increased CD30 expression and the expression of the EBERs are used as markers of EBV positive DLBCL (Ok *et al.*, 2014).

### 1.2.5 : Nasopharyngeal carcinomas

EBV was detected in Nasopharyngeal carcinoma (NPC) tissues in 1970 (Henle *et al.*, 1970, zur Hausen *et al.*, 1970). Further analysis revealed that EBV expressed a latency II pattern of expression in NPC (Young *et al.*, 1988, Brooks *et al.*, 1992). NPC are most prominent in South East Asia and EBV detection in NPCs is shown to increase in specific

geographical locations (Wang and He, 2016). Because of this and the large chromatin deletion and methylation events detected in NPCs, it is suggested that hereditary factors and high carcinogenic diets, such as salted fish, increase susceptibility to EBV associated NPC carcinogenesis (Huang *et al.*, 1978, Huang *et al.*, 1989, Waghray *et al.*, 1992, Lo *et al.*, 1996, Lo *et al.*, 2001, Chan *et al.*, 2002, Yu and Yuan, 2002). LMP2 has been detected in the majority of EBV positive NPCs and has been shown to regulate STAT and NFκB in NPC cell lines (Brooks *et al.*, 1992, Heussinger *et al.*, 2004, Stewart *et al.*, 2004). Additionally, microarray analysis reveals NPCs to have deregulated NFκB signalling as a result of up regulation of multiple components of the NFκB signalling pathway (Shi *et al.*, 2006). Also, methylation of p16 likely contributes to cell cycle deregulation to promote NPC carcinogenesis (Huang *et al.*, 1989, Chan *et al.*, 2002).

### 1.14 Gastric Carcinoma

EBV positive Gastric Carcinoma (GC) accounts for 10% of GC cases worldwide and due to GC being the second most prominent cause of death by cancer, EBV positive GC is suggested to be the most common EBV associated cancer (Shibata and Weiss, 1992, Tokunaga *et al.*, 1993, Boysen and Friborg, 2013). The countries with the highest proportion of GC, which are EBV positive GC, are the United States and Germany and EBV positive GC occurs more often in males. Much like NPC it has been suggested that environmental and genetic factors potentially increase the risk of EBV positive GC (Akiba *et al.*, 2008, Camargo *et al.*, 2011). Due to EBV GC being an epithelial carcinoma it is debated how EBV infects these tissues. Alternative mechanisms involving EBV glycoprotein gHgL interacting with epithelial integrins to enter cells have been suggested, but the precise mechanism remains unknown (Chesnokova *et al.*, 2009).

EBV carcinomas have been shown to have a latency I programme of expression in cells (Oh *et al.*, 2004). The mechanism to how EBV triggers carcinogenesis is not known, however EBERs have been suggested to protect EBV positive GC from apoptosis (Nanbo *et al.*, 2005).

### 1.2.6 : Natural Killer cell and T cell lymphomas

Detection of EBERs in Natural killer and T cells (NK/T cells) samples from tonsillar tissue from IM patients has suggested that during a primary EBV infection EBV is able to infect NK/T cells (Anagnostopoulos *et al.*, 1995, Trempat *et al.*, 2002, Hudnall *et al.*, 2005). The mechanism of EBV infection of NK/T cells is not known, however it is suggested that infection occurs when NK/T cells are eliciting a cytotoxic T cell response to EBV infected B cells (Tabiasco *et al.*, 2003). Latency II expression programmes have been detected in Extra-nodal NK cell lymphomas (ENKL) and EBER *in situ* hybridisation identified the presence of EBV in Nodal Peripheral T cell lymphomas from immunocompetent patients (PTCLs) (Kanemitsu *et al.*, 2012, Kato *et al.*, 2012). Despite EBV infected cell lines of NK/T lymphomas being established little is understood about how EBV latency expression influences NK/T cell lymphomas (Imai *et al.*, 1996, Tsuchiyama *et al.*, 1998).

## 1.3 : RBP-Jκ and the Notch signalling pathway

RBP-Jκ, the effector TF of the notch signalling pathway, was the first host TF shown to facilitate EBV TF binding DNA (Waltzer *et al.*, 1994). RBP-Jκ has since been shown to be essential for EBNA2 transactivation of expression with 70% of EBNA2 binding sites in LCLs being shared with RBP-Jκ. The EBNA3s are suggested to compete for RBP-Jκ binding to silence EBNA2 transactivation allowing EBV to control host expression to establish a persistent infection (McClellan *et al.*, 2013b, Wang *et al.*, 2015).

### 1.3.1 : Introduction of the Notch signalling Pathway

The Notch signalling pathway is conserved across metazoans and plays key roles in development and cell fate determination steps across a plethora of cell types. Delta-like are cell surface transmembrane ligands, the deletion of which results in early embryonic death in mouse models due to their essential role in activating Notch signalling pathways during development (Gale *et al.*, 2004, Jung *et al.*, 2011). When the delta-like ligand binds to the Notch receptor at the cell membrane an intracellular section of Notch (NotchIC) is cleaved by a protease and released into the cytoplasm (Santos *et al.*, 2007). NotchIC consists of a chain of Ankyrin (Ank) repeats and a RBP-Jκ association molecule (RAM) domain which associate with RBP-Jκ (Nam *et al.*, 2006). There is also a C-terminal PEST domain which is ubiquitinated tagging the protein for proteosomal degradation ensuring Notch signalling is tightly regulated (Oberg *et al.*, 2001). Here NotchIC is cleaved by more proteases (ADAM protease and γ-secretase) and is then transported to the nucleus (Schroeter *et al.*, 1998, Andersson *et al.*, 2011). Whilst in the nucleus NotchIC interacts with two populations of RBP-Jκ, static and dynamic RBP-Jκ (Castel *et al.*, 2013). Static RBP-Jκ is permanently associated with the

DNA and transcription is silenced by its association with corepressors (CoR) and histone-deacetylases (HDACs). CoR and HDACs are displaced from the fixed RBP-Jκ by NotchIC which associates with RBP-Jκ via its WΦP motif located in the RAM domain (Figure 1.5). Once the WΦP motif has tethered Notch to RBP-Jκ the Ank repeats of Notch can bind to RBP-Jκ and provide a platform for TFs like Mastermind (Figure 1.5) and Histone acetyltranferase such as p300 to bind to RBP-Jκ and together form the Notch complex (Figure 1.5) (Nam *et al.*, 2006). When NotchIC binds to dynamic RBP-Jκ in the nucleoplasm NotchIC recruits RBP-Jκ to consensus sites to activate RBP-Jκ mediated genes (Castel *et al.*, 2013). Upon Notch binding to the dynamic RBP-Jκ TFs and HDACs are recruited to facilitate Notch complex assembly and the activation of RBP-Jκ mediated genes (Figure 1.5). The WΦP motif is highly conserved across species and mutation of the threonine residue to serine negates Notch-RBP-Jκ binding and silences the Notch signalling pathway (Figure 1.5) (Baron, 2003, Johnson *et al.*, 2010). Notch signalling is thought to be mediated by the PEST domain in Notch being tagged by ubiquitin ligases labelling Notch for proteosomal degradation. Corepressors such as SHARP are also known to interfere with Notch signalling by recruiting HDAC to RBP-Jκ binding sites to silence Notch induced gene activation (Oswald *et al.*, 2002, Oswald *et al.*, 2005). Notch signalling activates the expression of number genes in different cell types however the HES-1 family of genes, which expression is involved with proliferation, maturation and growth, are targeted by Notch across a plethora of cell types (Jarriault *et al.*, 1995, Castel *et al.*, 2013). RBP-Jκ binds to DNA via the RBP-Jκ consensus site GTGGGA (HES-1 site) (Friedmann and Kovall, 2010). Notch signalling can be deregulated in cancers of the lung, breast, pancreus, central nervous system and in T-cell leukaemia (Nam *et al.*, 2002, Andersson *et al.*, 2011, Aster, 2014).

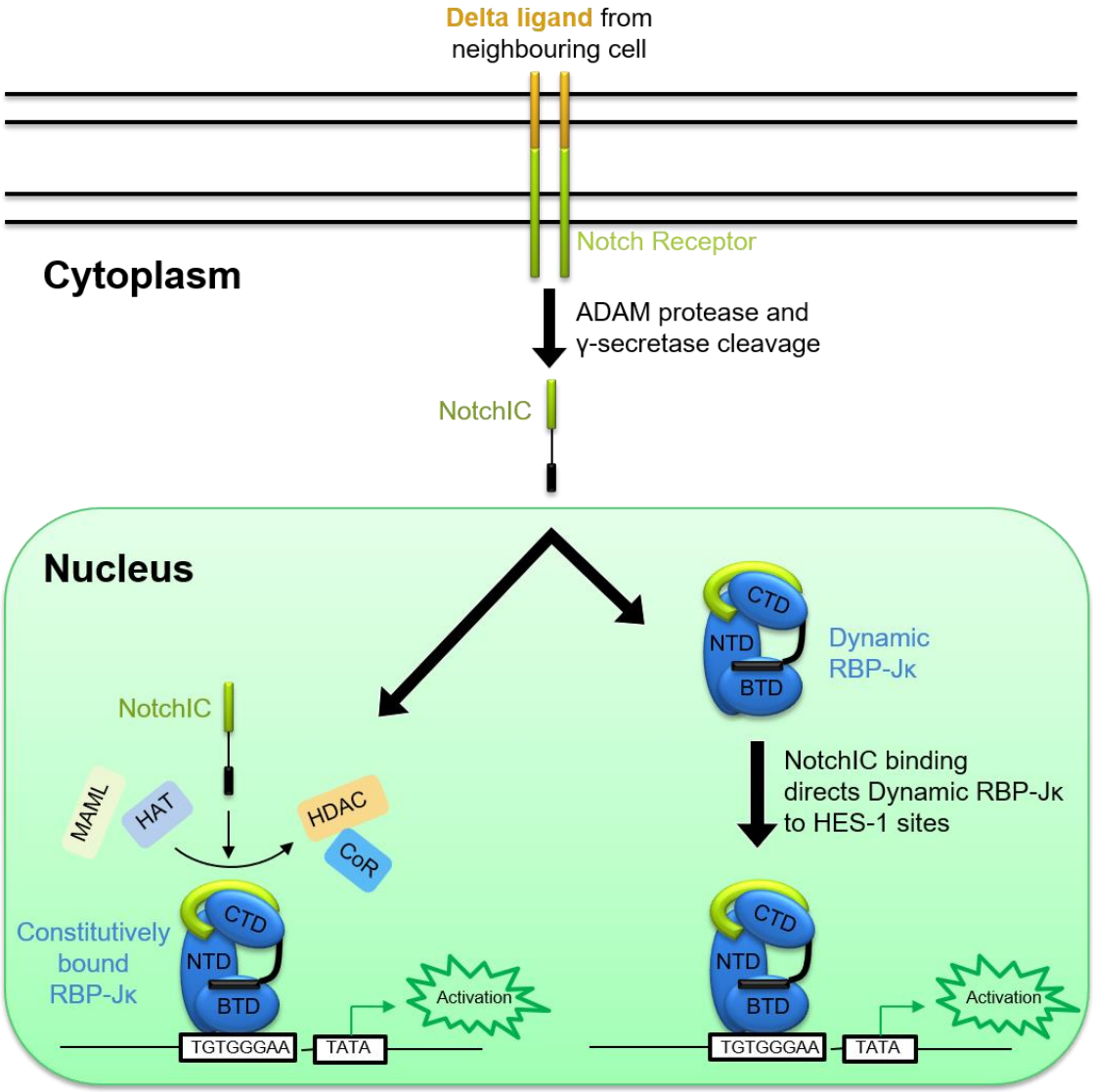


**Figure 1.5. Model of the Notch signalling pathway.** Notch receptor is bound by a Delta ligand presented by neighbouring cells. This causes the Intracellular domain of Notch (NothchIC) to be cleaved from the receptor where it undergoes further modification in the cytoplasm before being allowed to be shipped to the nucleus. When in the nucleus Notch interacts with Static RBP-Jκ which is permanently associated with the DNA or Dynamic RBP-Jκ which is not bound to DNA. NotchIC displaces Histone deacetylases (HDAC) and co-repressors (CoR) off of the Static RBP-Jκ to provide a platform for transcription factors such as MAML and Histone acetylates (HAT) to be recruited to activate gene expression. Dynamic RBP-Jκ is recruited to genes upon NotchIC binding, changing the cells chromatin landscape to promote differentiation or a particular developmental path.

### 1.3.2 : Variation of Notch signalling outcomes

Despite the Notch signalling pathway having few steps the Notch signalling pathway is able to elicit a diverse number of outcomes in a large number of cells types (Baron, 2003, Bigas *et al.*, 2010, Andersson *et al.*, 2011). The ability of Notch to recruit TFs, enhancers and HAT to create cell specific transcriptional landscapes, is thought to be the source of the Notch signalling pathways diverse outcomes over different cell types (Oswald *et al.*, 2001, Visel *et al.*, 2009). For example, Runt-related-TF (RUNX) enhancer has been shown in B cells to be enriched around RBP-Jκ sites and is suggested to open the DNA exposing HES-1 sites for Notch complex assembly and gene activation (Ito *et al.*, 2015, Gunnell *et al.*, 2016). In contrast Ikaros, a zinc finger protein, has been shown to block enhancer binding and Notch1 activation of *MYC* genes in T-cells (Ong *et al.*, 2006, Geimer Le Lay *et al.*, 2014). Transcription factors can also indirectly influence Notch signalling, for example Notch induced oestrogen receptor (ESR1) expression can be silenced by BCL6 preventing MAML recruitment or by recruiting HDAC to epigenetically silence expression (Gyory and Minarovits, 2005, Kitagawa, 2016). Proteins also directly interact with RBP-Jκ to promote Notch induced gene activation such as Ski-interacting protein (SKIP) or interfere with Notch complex assembly such as BEN-SOLO protein has been shown to do (Sifang Zhou, 2000, Vasquez-Del Carpio *et al.*, 2011, Dai *et al.*, 2013). Notch expression levels, post-translational modifications and metalloprotease availability have also been shown to influence different Notch signalling outcomes in certain cell types (Zolkiewska, 2008, Fortini, 2009).

### 1.3.3 : Notch Signalling in B cells

Notch 1 has been shown to be expressed at different levels throughout B cell development, whilst Notch 2 is expressed in late pre-B cells and is essential for

marginal zone (MZ) B cell development (Hsieh *et al.*, 1997, He and Pear, 2003b, Kuroda *et al.*, 2003, Saito *et al.*, 2003, Santos *et al.*, 2007). Notch signalling is involved in two cell fate determining steps during B cell development and maturation. During lymphopoiesis Notch 1 signalling has been shown to determine whether B cell progenitor cells specialise into B cells or T cells in mice (Ciofani and Zúñiga-Pflücker, 2005). Notch 1 signalling in mice is activated when delta ligand from a neighbouring B cell progenitor cell binds to the notch receptor activating genes to promote the cell to specialise into a T cell. It is hypothesised this ensures that an equal number of T cells and B cells are produced in the marrow providing balance to the immune system (Besseyrias *et al.*, 2007). Hes-1 expression has been shown to be high in immature B cells but reduces significantly in mature B cells, which is why it is not thought that EBV competes or interacts with Notch during an EBV infection (Bertrand *et al.*, 2000, Saito *et al.*, 2003). It must be noted that HES-1 expression is not only activated by the Notch pathway, so does not directly correlate to Notch signalling. Although much of the research into Notch signalling in B cells has been done in mice, no murine B cell malignancies have been shown to result from oncogenic Notch signalling (Zweidler-McKay *et al.*, 2005). However increased Notch 2 expression has been shown to occur in B-cell chronic lymphocytic leukaemia and Notch 1 expression has been shown to be higher in malignant B cells from Hodgkin's lymphoma patients (Hubmann *et al.*, 2002, Jundt *et al.*, 2002). Notch signalling and EBV hijacking of host RBP-Jκ are mutually exclusive. They lead to different outcomes for B cells *in vivo* and are not shown to compete with each other for RBP-Jκ binding (Zimber-Strobl and Strobl, 2001, Rowe *et al.*, 2014). Notch 1 has been shown to mimic the ability of EBNA2 to activate CD21 and down regulate Igμ transcription in Burkitts lymphoma cell infected with EBV with

EBNA2 knocked out. However, Notch 1 does not mimic EBNA activation of CD23 and LMP1 and can only transiently sustain proliferation if LMP1 is artificially activated in these cells lines (Strobl *et al.*, 2000, Höfelmayr *et al.*, 2001).

### 1.3.4 : Introduction to RBP-Jκ

The Notch signalling pathway and the transcription factor suppressor of hairless (SuH) were discovered in *D. melanogaster* and is conserved across metazoans (*C.elegans* (Lag-1 or CSL), mouse (CSL) and humans (RBP-Jκ or CBF1)) (Bailey and Posakony, 1995)(Figure 1.6). Four isoforms of RBP-Jκ are expressed in humans and there is little variation between their amino acid sequences with the exception of the N and C termini of each isoform. RBP-Jκ variant 1 is the largest isoform with significant extensions of the N and C termini and is the second most expressed isoform in B cells (Amakawa R, 1992, Kenia G. Krauer, 1999). RBP-Jκ variant 2 is the smallest isoform and is the dominantly expressed isoform of RBP-Jκ in B cells. RBP-Jκ variants 3 and 4 are not expressed in B cells but have significant roles in Notch signalling in a plethora of different cell types (Kenia G. Krauer, 1999). The differences between the N and C termini of the different isoforms of RBP-Jκ are thought to contribute to the ability of relatively small number of RBP-Jκ and Notch isoforms to produce such a large number of developmental and cell signalling out comes (Espinosa, 2012). RBP-Jκ has three domains in its structure, the N-terminal domain (NTD), the beta trefoil domain (BTD) and the C-terminal domain (CTD) (Choi *et al.*, 2012). The BTD and NTD bind the DNA RBP-Jκ consensus site (GTGGGA) but have also been shown to bind to RBP-Jκ sites that have some sequence variation with a weak affinity (Friedmann and Kovall, 2010). NotchIC RAM domain initially associates via its WΦP motif to the BTD, this causes conformational changes to RBP-Jκ that promote the NotchIC Ank binding to RBP-Jκ

CTD. MAML then binds to the Notch ANK repeats and RBP-Jκ NTD to form an active Notch transcription complex, which activates RBP-Jκ, mediated genes such as *MYC*, *CD21* and *Igμ* which drive cell proliferation (He and Pear, 2003b, Johnson *et al.*, 2010, Vasquez-Del Carpio *et al.*, 2011, Choi *et al.*, 2012). Proteins such as SKIP have also been shown to be key in the assembly of an active NotchIC-DNA complex as previously described (Sifang Zhou, 2000). There are two populations of RBP-Jκ present in the nucleus, dynamic and static, and their ability to bind DNA is influenced by epigenetic factors anchoring them into closed chromatin structures or Notch binding recruiting them to target genes. Notch has been shown by Chromatin Immunoprecipitation Sequencing (ChIP-Seq) to promote unique RBP-Jκ binding profiles in cells with constitutively activated Notch signalling when compared to cells with Notch signalling turned off. There was also a sub population of RBP-Jκ which DNA binding was not affected by Notch signalling status called static RBP-Jκ (Castel *et al.*, 2013).

### 1.3.5 : The structure of the human Notch complex

The structure of the human notch complex was determined in 2012 (Choi *et al.*, 2012) (Figure 1.6). The complex contained aa8-435 of RBP-Jκ removing the N and C termini of RBP-Jκ and preserving the highly conserved core of RBP-Jκ. Notch was assembled using 2 different domains, the Ank-repeats and a peptide of the RAM domain. This was shown to improve the resolution of the RAM domain (Choi *et al.*, 2012). When the Ank and RAM domains of Notch were co-crystallised as one protein, in the structure of RBP-Jκ-HES-1-site, the resolution of the RAM domain was poor and was thought to have been compromised by the disordered amino acid chain linker between the Notch RAM and Ank domains (Nam *et al.*, 2006). The RAM domain WΦP RBP-Jκ binding motif is shown to slot into a hydrophobic pocket on the surface of the BTD (Nam *et al.*,

2006). Interestingly, the presence of a proline residue immediately after the WΦP RBP-Jκ binding motif appears to influence the direction in which the RAM domain binds to BTD (Borggrefe and Oswald, 2016). The Lin-12 RAM domain, which has a proline residue after the WΦP motif, in the structure of the *C.elegans* CSL-Lin12-DNA complex was shown to bind in a linear fashion to the BTD. However, the structure of the human Notch transcription complex shows that the RAM domain, which contains a glycine residue after the WΦP motif, is shown to kink after the WΦP motif (Wilson and Kovall, 2006, Choi *et al.*, 2012)(Figure 1.6). The biological implications of this difference are not known and this difference could be an artefact of crystal packing. Furthermore, a thermodynamic study of the RAM-CSL interaction showed that these residues play a less essential role in RAM-CSL interactions (Johnson *et al.*, 2010). The Notch complex has also been shown to dimerise when two opposing RBP-Jκ binding sites within 16bp of each other are present on the DNA (Arnett *et al.*, 2010). The structure of the Notch complex dimer showed that salt bridges form between Notch complexes, which are thought to stabilise the dimer complex (Arnett *et al.*, 2010).

The cross species conservation of interactions between RBP-Jκ, the RBP-Jκ DNA binding site and Notch are demonstrated in a comparison between x-ray crystal structures of the mouse, *C.elegans* and human Notch complex and the *Drosophila* suppresser of Hairless complex (Friedmann *et al.*, 2008, Choi *et al.*, 2012, Yuan *et al.*, 2012)(Figure 1.6). These structures show that, the overall structure of RBP-Jκ involves interactions between domains that are located far away from each other in the amino acid sequence. This had made expressing truncations of the different RBP-Jκ domains in previous studies challenging, preventing the determination of where RBP-Jκ interacting proteins bind to RBP-Jκ (Johnson *et al.*, 2010, Calderwood *et al.*, 2011, Kurth *et al.*,

2011). This has also made determining where the EBNA3 TΦGC motif interacts with RBP-Jκ challenging (Calderwood *et al.*, 2011).

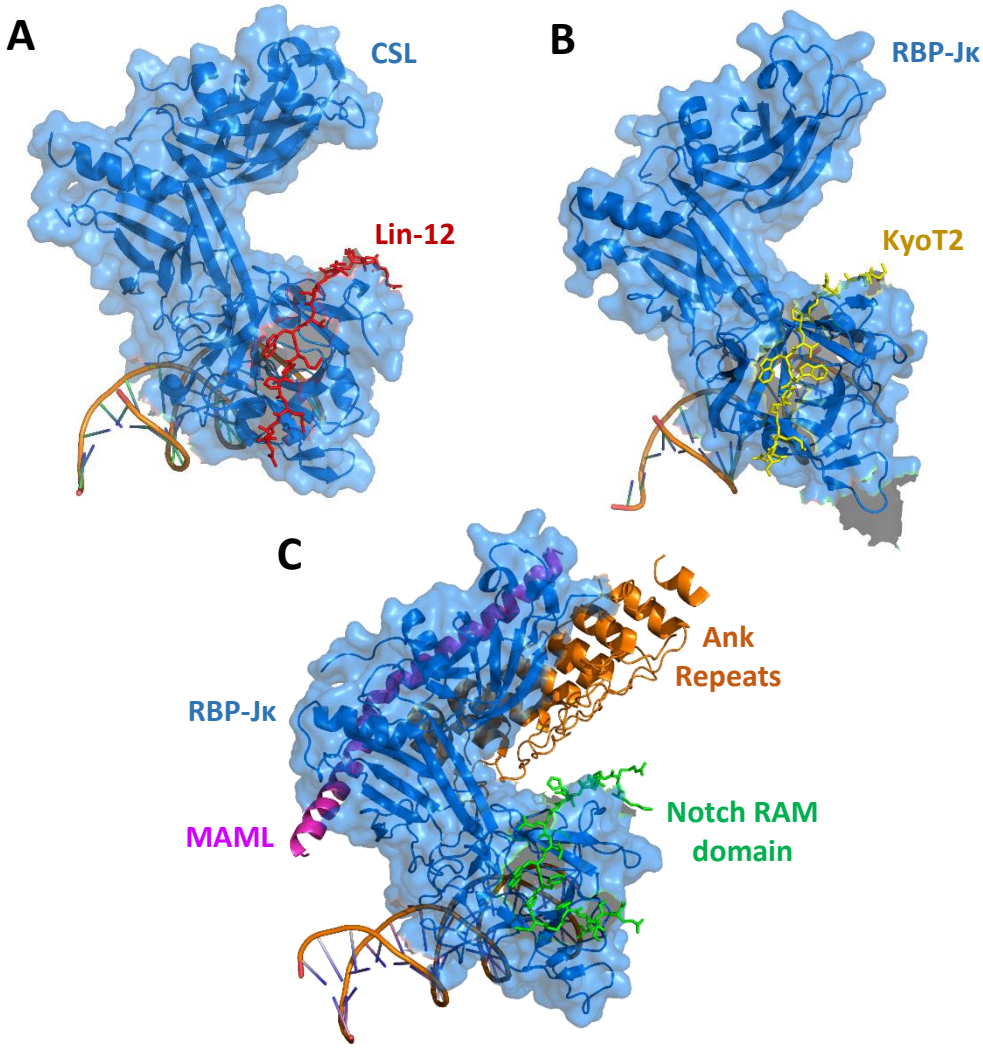


**D**

| | |
|---|---|
| EBNA3A | ATLGCTGGRRCHVTFSAGTFKLPRCTPGDRQW |
| EBNA3B | ATLGCDEGTRHATTYSAGIVQIPRISDQNQKI |
| EBNA3C | ATFGCQNAARTLNTFSATVWTPPHAGPREQER |
| EBNA2 | PPPGVINDQQLHHLPSGPPWWPPISDPPQPSK |
| Hs Notch2 | FIILLGVIMAKRKRKHGSLWLPEGFTLRRDAS |
| Ce Notch | LGALPGNRTRKRRMINASVWMPPMENEEKNRK |
| Mm Notch | FVGCGVLLSRKRRRQHGQLWFPEGFKVSEASK |
| Mm KyoT2 | RKNRSLAAPRGPGLVKAPVWWPMKDNPGTTTA |

**Figure 1.6. Structures of the human Notch complex and its mouse and worm homologues. A**. X-ray crystal structure C.elegans CSL (RBP-Jκ homologue)(shown in blue) bound to DNA with Lin-12 RAM domain bound (Notch homologue)(shown in red)(Friedmann and Kovall, 2010). **B.** X-ray crystal structure of Mouse RBP-Jκ (shown in blue) bound to DNA with Notch signalling inhibitor KyoT2 (shown in yellow) bound (Collins *et al.*, 2014). **C.** X=ray crystal structure of the Human Notch complex. RBP-Jκ, MAML, Notch ANK repeats and Notch RAM domain shown in blue, pink, orange and green respectively (Choi *et al.*, 2012). **D.** Table of aligned amino acid sequences of RBP-Jk binding motifs of EBV and human transcription factors.

### 1.3.6 : EBNA interactions with RBP-Jκ

The host transcription factor RBP-Jκ has been implicated in targeting the EBNAs to DNA since it was shown to recruit EBNA2 to the LMP1 promoters of the EBV genome (Wang *et al.*, 1987, Allday *et al.*, 1993, Zimber-Strobl *et al.*, 1993). RBP-Jκ has been shown to bind to EBNA2 and the EBNA3 family HD using pull downs from EBV infected B cells (Johannsen *et al.*, 1996, Waltzer *et al.*, 1996, Calderwood *et al.*, 2011). Pull-downs, using RBP-Jκ as bait, of truncations of the EBNAs identified $EBNA2_{280\text{-}337}$, $EBNA3A_{172\text{-}220}$, $EBNA3B_{1\text{-}311}$ and $EBNA3C_{183\text{-}240}$ as RBP-Jκ binding regions (Waltzer *et al.*, 1996). EBNA3s were initially thought to bind RBP-Jκ exclusively via TFGC/TLGC (TΦGC) motif as $EBNA3C_{TFGC\text{-}AAAA}$ mutants did not pull down RBP-Jκ and were not able to sustain growth in EBNA3C negative LCLs (Zhao *et al.*, 1996, Kenia G. Krauer, 1999, Klaus Peter Fuchs1, 2001, Maruo *et al.*, 2009). Later scanning alanine mutations were used to show how EBNA2 bound to RBP-Jκ via WWP motif suggesting EBNA2 mimicked Notch to bind RBP-Jκ (Klaus Peter Fuchs, 2001, Zimber-Strobl and Strobl, 2001). However a WTP motif was identified 14aa away from the TFGC and was shown to be essential for EBNA3CHD-RBP-Jκ interactions when the EBNA3C HD was expressed in *E.coli* however was shown to be dispensable for EBNA3CHD-RBP-Jκ interactions when the EBNA3C HD was expressed in mammalian cells (Calderwood *et al.*, 2011). Mutation of RBP-Jκ residues L326 and Q333 were shown to knockout EBNA2 binding in a yeast two hybrid mutagenesis screen of RBP-Jκ (Klaus Peter Fuchs, 2001). Later an EBNA2 peptide containing the WΦP motif was shown to interact with a truncation of the RBP-Jκ BTD using ITC (Johnson *et al.*, 2010). This confirmed that EBNA2 bound to the RBP-Jκ BTD by mimicking Notch. Mapping where the EBNA3s bind to RBP-Jκ has been more challenging. Even though the WΦP motif has been shown to bind the BTD of RBP-Jκ,

the binding site of the TΦGC motif has been more challenging to locate (Calderwood *et al.*, 2011). Although EBNA3C was pulled down with a truncation of the RBP-Jκ NTD there is debate whether the NTD expressed was functional (Calderwood *et al.*, 2011). As previously described the NTD relies on β-sheets in the CTD to stabilise the hydrophobic core of RBP-Jκ (Choi *et al.*, 2012). Therefore, independently expressing NTD has proven challenging for groups studying homologues of RBP-Jκ, leading many to question the validity of their own data when they were unable to show proteins of interest binding to the NTD (Friedmann *et al.*, 2008, Maier *et al.*, 2011).

## 1.4 : Aims

Microarrays of EBNA knockout cell lines have shown that EBNA2 and the EBNA3 family hijack the expression of host genes involved with cell survival, apoptosis, cell growth and immune evasion to establish a latent EBV infection (Maier *et al.*, 2006, Zhao *et al.*, 2006, White *et al.*, 2010). Additionally, ChIP-Seq analysis has revealed that the EBNAs control host expression predominantly from distal promoters and has identified the host transcription factor RBP-Jκ to be an essential adaptor for the EBNAs to interact with the host genome (McClellan *et al.*, 2013a, Wang *et al.*, 2015). Chip re-Chip experiments have also shown that EBNA2 and the EBNA3s independently occupy shared binding sites suggesting they compete for RBP-Jκ binding (McClellan *et al.*, 2013b). A combination of pull downs, yeast 2-hybrid assays and reporter assays have identified the EBNA2 WFP, EBNA3 family TΦGC and the EBNA3C WTP motifs play key roles in EBNA-RBP-Jκ interactions (Ling and Hayward, 1995, Lee *et al.*, 2009, Calderwood *et al.*, 2011). However, the mechanism to how the EBNAs hijack host expression via RBP-Jκ is still not fully understood. Understanding the mechanism to how the EBNAs exploit RBP-Jκ to immortalise B cells and establish persistent EBV infection could improve our understanding to how cells lose control of essential pathways and develop into cancers. Additionally, understanding the mechanism of how EBNAs hijack host gene expression could lead to the discovery of potential therapeutic targets in order to treat EBV associated cancers.

Therefore, we aim to use structural biology approaches to obtain three dimensional structures of the EBNAs bound to RBP-Jκ to study how the EBNAs interact with RBP-Jκ. We also aim to use biophysical techniques to examine the role and contribution of the

EBNA RBP-Jκ binding motifs to improve the understanding of the mechanism to how EBV TFs hijack RBP-Jκ to promote the establishment of persistent EBV infections and EBV associated cancers.

# Chapter 2: Methods

## 2.1: Molecular biology

### *2.1.1 : Restriction Enzyme Digests*

Buffer selection and DNA concentrations were based on manufacturer's recommendations. Digests were incubated at 37°C for 2 hours then stored at 4°C. Restriction digests were analysed using a 1% agarose gel and stained with simply red stain. Uncut DNA and single restriction digests were run on the agarose gel in parallel to double restriction digests where appropriate.

### *2.1.2 : Polymerase chain reaction (PCR)*

Buffer selection, polymerase and nucleotides used in the PCRs were based on manufacturer's recommendations. The primers were designed using serial cloner software and ordered from Thermofisher. The annealing temperature was calculated using the NEB Tm calculator (https://www.neb.com/tools-and-resources/interactive-tools/tm-calculator). PCRs were carried out using a G-Storm thermal cycler and stored at 4°C upon completion. The PCR products were run on a 1% agarose gel and vectors with no polymerase were run in parallel with the PCRs as negative controls. PCR products that were to be used for cloning were purified using the QUIAGEN QIA-prep Gel extraction Miniprep kits.

### *2.1.3 : DNA Sequencing*

All DNA sequencing was completed by the Eurofins MWG operon automated sequencing service. 1000ng of DNA was added to 20ng of sequencing primer and made up to 18µL with ultrapure water. The barcode was noted and sent for sequencing in the post.

*2.1.4 : Agarose gel electrophoresis*

Agarose powder was melted in boiling ultrapure water, after cooling simply gel red was added and then the mixture was poured into a cast. DNA samples were mixed with Orange DNA Loading Dye then loaded into wells and ran at 95V for 50 minutes (Biorad power pack). 1kb ladder was ran in parallel to estimate the size of the DNA products loaded. Bands were analysed on a Licor machine.

*2.1.4 : Small scale plasmid DNA preparation*

1µg of plasmid was used to transform 100µL of competent DH5α *E.coli* cells. Plasmid was mixed with DH5α *E.coli* cells and incubated on ice for 15 minutes, then heat shocked for 45 seconds at 42$^{o}$C and returned to the ice for 5 minutes. 250µL of LB was added to the transformed cells and they were then grown in a 37$^{o}$C shaking incubator at 225rpm for an hour. The cells were plated on agar, containing an appropriate selective antibiotic for the vector, then cultured at 37$^{o}$C overnight. Colonies were then picked and grown in LB containing selective antibiotic overnight. Cells were pelleted at 4000rpm in a Sorvall™ ST 8 Small Benchtop Centrifuge, the medium was removed and the plasmid was extracted and purified using QIAGEN QIA-prep Miniprep kits according to manufacturers recommendations.

*2.1.5 : Ligation*

Buffer selection, polymerase and nucleotides used in the PCRs were based on manufacturer's recommendations. The amount of insert to add to the ligation reaction was calculated using the formula below and takes into account the molar ratio of insert to vector, the insert length, the vector length and the mass of the vector.

$$\boldsymbol{Insert\ mass\ (ng) = Molar\ ratio \times \left[\frac{Insert\ length\ in\ bp}{Vector\ length\ in\ bp}\right] \times Vector\ mass\ in\ ng}$$

Ligation reactions were incubated in ice water overnight. The following day the ligation was transformed into competent DH5α *E.coli* and plated onto agar containing an appropriate antibiotic. Colonies were grown in selective LB overnight. Cells were pelleted at 4000rpm (Ch 500062PP rotor, VWR microstar 17 centrifuge), the medium was removed and the plasmid was extracted and purified using QIAGEN QIA-prep Miniprep kits according to manufacturers recommendations. Diagnostic restriction digests were carried out and successful ligations were sent off for sequencing.

*2.1.6 : Competent Bacteria*

DH5α or Rosetta pLysS De3 *E.coli* cells from -80$^{o}$C stock were streaked onto agar plates and incubated at 37$^{o}$C overnight. chloroquine was added to plates and Lysogeny broth (LB) was used to grow Rosetta pLysS De3 *E.coli* cells. A single colony was picked and used to inoculate 10ml of LB which grown up overnight at 37$^{o}$C in a shaking incubator. 1ml of the overnight culture was used to inoculate 200ml of LB which was grown to an OD of 0.4. The *E.coli* is rapidly cooled on ice, then pelleted at 4000rpm (J-LITE JLA 8.1000 Fixed Angle rotor, Avanti J-26XP centrifuge). Pellets were resuspended in 66mls of BufferI (Appendix 3), incubated on ice for 15 minutes then pelleted at 4000rpm for 12 minutes at 4$^{o}$C (J-LITE JLA 8.1000 Fixed Angle rotor, Avanti J-26XP centrifuge). Next the pellet was resuspended in 8mls of BufferII (Appendix 3) and incubated on ice for 20 minutes. Cell were then aliquoted into sterile Eppendorf tubes, flash frozen in liquid nitrogen and stored at -80$^{o}$C.

*2.1.7 : Cloning*

*2.1.7.1 : Cloning of pFastBac vectors to express C-terminally His-tagged RBP-Jκ$_{8-435}$.*

cDNA of C-terminally His-tagged RBP-Jκ$_{8-435}$ was amplified, using PCR, from the pET28B.JK.8-435 vector (Appendix 2) which was produced by a summer student in Michelle West's Group. Forward and reverse primers ('RBP-Jκ 8-435 Forward SmaI' and 'RBP-Jκ 8-435 Reverse XbaI')(Appendix 1) were designed to add SmaI and XbaI restriction sites respectively to the cDNA of C-terminally His-tagged RBP-Jκ$_{8-435}$ cDNA of C-terminally His-tagged RBP-Jκ$_{8-435}$ and pFastBac.CP.17.2 vector (Figure 2.1)(Appendix 2) was digested with SmaI and XbaI restriction enzymes and ligated together with a 1:3 vector to insert ratio. This strategy simultaneously removed the N-terminal His-tag from the p10 multiple cloning site (MCS) whilst inserting the C-terminally His-tagged RBP-Jκ$_{8-435}$ cDNA. Diagnostic restriction digests of the ligation products were carried out to determine whether the cDNA of C-terminally His-tagged RBP-Jκ$_{8-435}$ had been correctly inserted into the p10 MCS of the empty pFastBac.CP.17.2 vector. SmaI and XbaI single restriction digests of pFastBac.CP.17.2 were run as controls. Successful clones were sent for sequencing at Eurofins for verification.

*2.1.7.2 : Cloning of pFastBac co-expression vectors to co-express EBNA2$_{272-333}$ and RBP-Jκ$_{8-435}$ or RBP-Jκ variant 2*

cDNA of the EBNA2$_{272-333}$ fragment was amplified, using PCR, from the pF.CP17.272 vector produced by a masters student from Dr Christomous Prodromou group. Primers 'EBNA2 fragment Forward NheI, XbaI' and 'EBNA2 fragment Reverse BamHI' were designed to add XbaI and BamHI restriction sites to the EBNA2$_{272-333}$ cDNA (Appendix 1). EBNA2$_{272-333}$ cDNA, pF.JK.8-435 vector and pF.JK.V2 vector were cut with XbaI and BamHI restriction enzymes and ligated together with a 1:3 vector to insert ratio.

Diagnostic restriction digests of the ligation products were run to determine whether $EBNA2_{272-333}$ cDNA had been correctly inserted into the polyhed MCS of the pF.JK.8-435 vector and pF.JK.V2 vectors. Successful clones were sent for sequencing at Eurofins for verification. pF.JK.8-435.272 and pF.JK.V2.272 vectors were made into recombinant baculovirus by the processes discussed in chapter 2.2.1.

*2.1.7.3 : Cloning of pFastBac co-expression vectors to co-express full length EBNA2 and RBP-Jκ$_{8-435}$ or RBP-Jκ variant 1 or 2*

EBNA2 cDNA was amplified, using PCR, from the pF.CP17.EB2 vector (appendix 2) produced by a masters student from Dr Christomous Prodromou group. Primers 'EBNA2FL Reverse SalI' and 'EBNA2FL Forward NheI, XbaI' (appendix 1) were designed to add XbaI and SalI restriction sites to the EBNA2 cDNA. EBNA2 cDNA, pF.JK.8-435 vector, pF.JK.V1 and pF.JK.V2 vector were cut with XbaI and SalI restriction enzymes and ligated together with a 1:3 vector to insert ratio. Diagnostic restriction digests of the ligation products were run to determine whether EBNA2 cDNA had been correctly inserted into the polyhed MCS of the pF.JK.8-435 vector and pF.JK.V2 vectors. Successful clones were sent for sequencing at Eurofins for verification. pF.JK.8-435.EB2 vector was made into recombinant baculovirus by the processes discussed in chapter 2.2.1.

*2.1.7.4 : Cloning of pFastBac vectors to express His-tagged EBNA3C$_{100-356}$ or EBNA3C$_{100-413}$*

$EBNA3C_{100-356}$ and $EBNA3C_{100-413}$ cDNA was amplified, using PCR, from the pcDNA.EBNA3C vector provided to us by Dr A Bell from the University of Birmingham (appendix 2). Forward and reverse primers (3CHD p10 Forward HindIII, 3CHD.1 p10

Reverse NheI and 3CHD.2 p10 Reverse NheI (appendix 1)) were designed to add XbaI and SalI restriction sites respectively to the EBNA3C$_{100-356}$ and EBNA3C$_{100-413}$ cDNA. EBNA3C$_{100-356}$ cDNA, EBNA3C$_{100-413}$ cDNA and pFastBac.CP.17.2 vector were cut with NheI and HindIII restriction enzymes and ligated together with a 1:3 vector to insert ratio. Diagnostic restriction digests of the ligation products were run to determine whether the EBNA3C$_{100-356}$ and EBNA3C$_{100-413}$ cDNA had been correctly inserted into the p10 MCS of the empty pFastBac.CP.17.2 vector. Successful clones were sent for sequencing at Eurofins for verification. pF.EB3C.HD1 and pF.EB3C.HD2 vectors were made into recombinant baculovirus by the processes discussed in chapter 2.2.1.

*2.1.7.5 : Cloning of pFastBac co-expression vectors to co-express EBNA3C$_{100-356}$ or EBNA3C$_{100-413}$ with RBP-Jκ$_{8-435}$*

EBNA3C$_{100-356}$ and EBNA3C$_{100-413}$ cDNA was amplified, using PCR, from the pcDNA.EBNA3C vector provided to us by Dr A. Bell from the University of Birmingham (Appendix 2). Forward and reverse primers (3CHD polyhed Forward XbaI, 3CHD.1 polyhed Reverse BamHI, 3CHD.2 polyhed Reverse BamHI (Appendix 1)) were designed to add XbaI and BamHI restriction sites respectively to the EBNA3C$_{100-356}$ and EBNA3C$_{100-413}$ cDNA. EBNA3C$_{100-356}$ cDNA, EBNA3C$_{100-413}$ cDNA and pF.JK.8-435 vector were cut with XbaI and BamHI restriction enzymes and ligated together with a 1:3 vector to insert ratio. Diagnostic restriction digests of the ligation products were run to determine whether EBNA3C$_{100-356}$ and EBNA3C$_{100-413}$ cDNA had been correctly inserted into the polyhed MCS of the pF.JK.8-435 vector. Successful clones were sent for sequencing at Eurofins for verification. pF.JK.8-435. EB3C.HD1 and pF.JK.8-435. EB3C.HD2 vectors were made into recombinant baculovirus by the processes discussed in chapter 2.2.1.

*2.1.7.6 : Plasmid Maps*

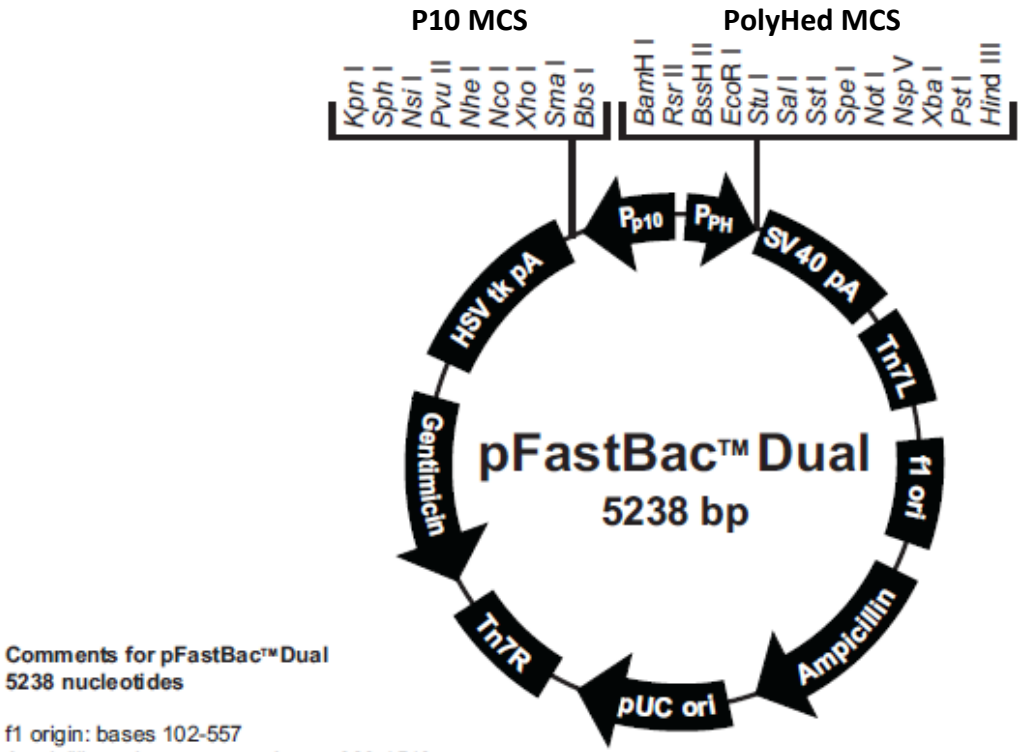


**Comments for pFastBac™ Dual**
**5238 nucleotides**

f1 origin: bases 102-557
Ampicillin resistance gene: bases 689-1549
pUC origin: bases 1694-2367
Tn7R: bases 2611-2835
Gentamicin resistance gene: bases 2902-3435 (complementary strand)
HSV tk polyadenylation signal: bases 3992-4274 (complementary strand)
Multiple cloning site: bases 4274-4337 (complementary strand)
p10 promoter ($P_{p10}$): bases 4338-4459 (complementary strand)
Polyhedrin promoter ($P_{PH}$): bases 4478-4606
Multiple cloning site: bases 4606-4704
SV40 polyadenylation signal: bases 4722-4962
Tn7L: bases 4991-5156

**Figure 2.1. pFastBacDual plasmid map from the Invitrogen Bac-to-Bac manual.**
PFCP17.2 has been engineered from a pFastBacDual vector to contain a cleavable N-terminal 6x His-tag in multiple cloning site (MCS) controlled by the p10 promoter (p10 MCS) and a N-terminal Cleavable StrepII-Tag in the MCS controlled by the polyhedron promoter (polyhed MCS).

| pET-28a(+) sequence landmarks | |
|---|---|
| T7 promoter | 370-386 |
| T7 transcription start | 369 |
| His•Tag coding sequence | 270-287 |
| T7•Tag coding sequence | 207-239 |
| Multiple cloning sites (*Bam*H I - *Xho* I) | 158-203 |
| His•Tag coding sequence | 140-157 |
| T7 terminator | 26-72 |
| *lacI* coding sequence | 773-1852 |
| pBR322 origin | 3286 |
| Kan coding sequence | 3995-4807 |
| f1 origin | 4903-5358 |

The maps for pET-28b(+) and pET-28c(+) are the same as pET-28a(+) (shown) with the following exceptions: pET-28b(+) is a 5368bp plasmid; subtract 1bp from each site beyond *Bam*H I at 198. pET-28c(+) is a 5367bp plasmid; subtract 2bp from each site beyond *Bam*H I at 198.

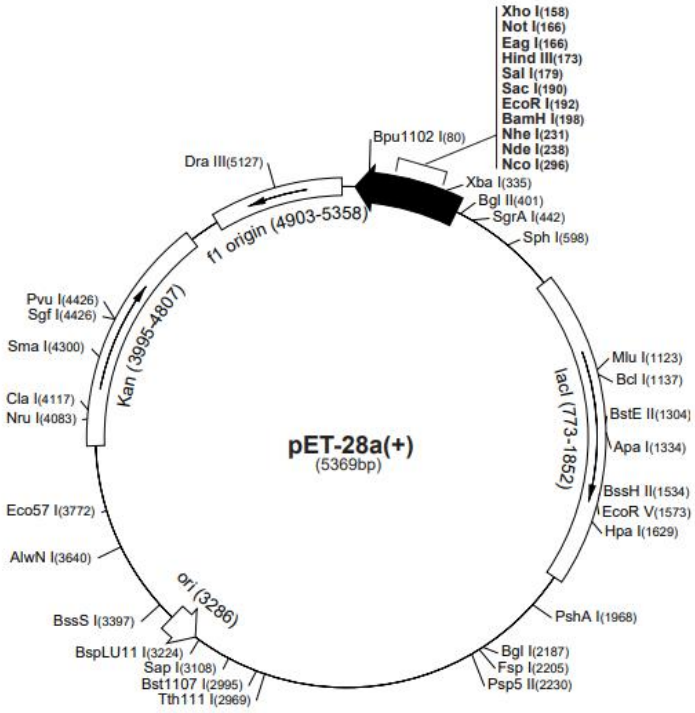


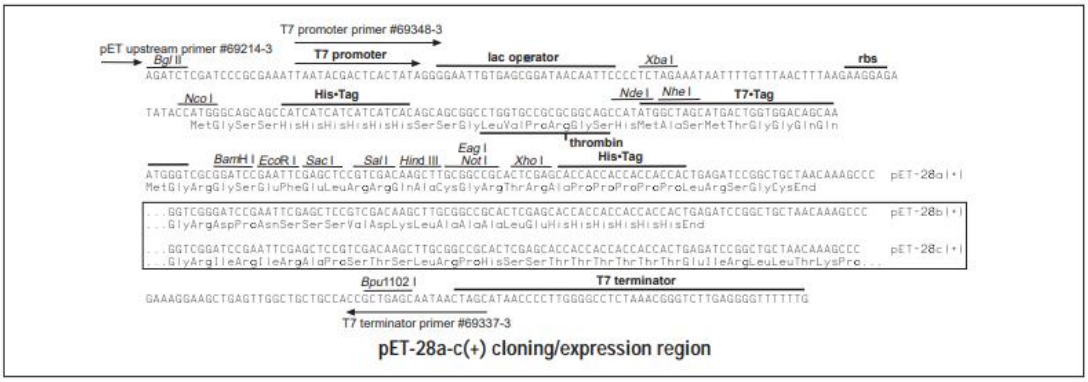


**Figure 2.2. pET28b plasmid map from the Novagen pET28a-c manual.**

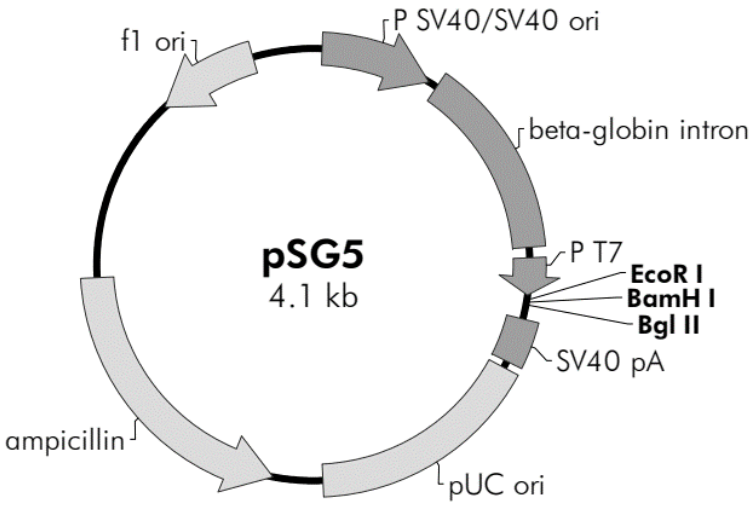


| Feature | Nucleotide Position |
|---|---|
| SV40 promoter and SV40 origin of replication | 28–366 |
| β-globin intron | 395–967 |
| T7 promoter | 1022–1040 |
| EcoR I | 1043 |
| BamH I | 1049 |
| Bgl II | 1055 |
| SV40 polyA signal | 1069–1202 |
| pUC origin of replication | 1342–2009 |
| ampicillin resistance (*bla*) ORF | 2160–3017 |
| f1 origin of ss-DNA replication | 3587–3893 |

**Figure 2.3. pSG5 plasmid map from the Agilent Technology pSG5 manual.**

*2.1.8 : Sodium dodecyl sulphate polyacrylamide gel electrophoresis (SDS-PAGE)*

Protein samples and cell pellets were mixed in a 1:1 ratio with Gel Sample Buffer (GSB) and boiled on a heating block for 2 and 10 minutes respectively. Boiled cell lysates were spun down at 12500 rpm (Ch 500062PP rotor, VWR microstar 17 centrifuge) to prevent cell debris being loaded onto the gel. Samples were loaded onto 10% or 4-12% Tris-Bis pre-cast Novex SDS-PAGE gels and run in MOPS buffer for 50 mins at 200V using a Biorad volt pack. Seeblue® plus2 pre-stained protein standard was ran alongside samples. Gels were stained using Simply blue stain microwaved with the gel for 10-20 seconds.

*2.1.9 : Western blotting*

Cell pellets were lysed in GSB buffer, boiled, spun at 13,000 x g (Ch 500062PP rotor, VWR microstar 17 centrifuge) for 2 minutes, then ran on a 10% or 4-12% Bis-Tris SDS-PAGE gel with a SeeBlue™ Plus2 Pre-stained Protein Standard. The protein was transferred onto a nitrocellulose membrane at 75V for 90 minutes using a Biorad power pack. Ponceu stain was used to verify the transfer had been successful then was washed off the membrane with water then PBS buffer. The membrane was then blocked in 2% powdered milk dissolved in PBS Tween, washed with PBS, then probed with primary anti-body. After the primary antibody was bound the membrane was washed in PBS tween and incubated with secondary antibody conjugated to a Horseraddish-peroxidase (HRP). After a final wash to remove any unbound secondary antibody the membrane was stained with ECL. The chemiluminescence emitted by the bands was measured on a Licor machine. Appropriate positive and negative controls were ran along side the samples.

*2.1.10 : Electrophoretic mobility shift assay (EMSA) to test whether the C-terminally His-tagged RBP-Jκ$_{8-435}$ expressed in insect cells was functional*

Single stranded oligonucleotides encompassing the RBP-Jκ consensus site were dissolved in ultrapure water at 100mg/ml, mixed together, then denatured in a 95$^{o}$C heating block. They were then slowly annealed by gradually decreasing the temperatureby leaving the heat block to cool down overnight. 3.3µM of RBP-Jκ consensus site (AAACACGCC**GTGGGA**AAAAAT) or RBP-Jκ consensus mutant (AAACACGCCGTGGCTAAAAAT) was mixed with EMSA stock buffer (5 x Buffer: 50mM Tris pH7.5, 5mM MgCl, 2.5mM EDTA, 2.5mM DTT, 250mM NaCl, 0.25µg/µl PolydIdC, 20% glycerol) then incubated with increasing concentrations of C-terminally His-tagged RBP-Jκ$_{8-435}$ expressed in insect cells for 30 minutes at room temperature. Each sample was then loaded onto a 6% Nupage DNA retardation gel in 0.5xTBE buffer and separated for 50 minutes at 100V. The gel was stained with Gel Safe Red, then bands were visualised on the Licor machine.

*2.1.11 : Site directed mutagenesis of the EBNA3C RBP-Jκ binding motifs.*

The Q5 site directed mutagenesis kit from NEB was used to mutate EBNA3C cDNA, in a pSG5 vector, TΦGC RBP-Jκ binding motif to alanines and the tryptophan in the WΦP motif to serine. AFGC, TAGC and AAGC mutants were probing how RBP-Jκ-EBNA3C interactions were affected when compared to TFGC-AAAA EBNA3C mutants. We also intended to see, by probing the western blots with antibodies with specificity to other host TFs known to bind EBNA3C, how these mutants affected other EBNA3C-host protein interactions. The EBNA3C STP mutant was made to confirm whether it ablates EBNA3C-RBP-Jκ interactions (Calderwood *et al.*, 2011). Primers with the desired mutated sequences were designed to amplify the entire vector in opposite directions

from the sequence that was to be mutated shown in chapter 2.1.7. Q5 fidelity mix contained a high fidelity polymerase and buffers designed to aid with the amplification of the entire vector. The PCR products were incubated with a kinase, ligase, DpnI mix (KLD mix) which simultaneously phosphorylated the ends of the linear PCR products and ligated the linear PCR products back into circular vectors whilst the DpnI digested the methylated DNA of the original vector. The mutated vectors were transformed into NEB DH5α competent *E.coli* by heat shock at 42$^{o}$C for 30 seconds, grown up in Super Optimal broth with Catabolite repression (SOC) media for 1 hour, then plated onto ampicillin agar which were incubated at 37$^{o}$C overnight. Colonies were picked, grown in LB with ampicillin at 37$^{o}$C then the DNA was extracted using a QIAGEN QIA-prep Miniprep kit. Each of the mutant vectors was then sent for sequencing at Eurofins to verify whether the DNA had been successfully mutated.

*2.1.12 : Large scale plasmid preparation*

Re-streaked colonies of each of the pSG5 vectors containing wild type EBNA3C and EBNA3C with mutated RBP-Jκ binding motifs were picked and grown up in 50ml over a day. The 50ml culture were then used to grow 400ml cultures of each vector in LB with ampicillin overnight. Each of the cultures were pelleted at 4000rpm (TX-100 rotor, Thermo heraeus multifuge x3r centrifuge), resuspended in SolI (Appendix 3), lysed in SolII (Appendix 3), then the pH was neutralised with SolIII (Appendix 3) to prevent damaging the vector. The cell debris was separated from the solution by spinning the mixture down at 4000rpm (TX-100 rotor, Thermo heraeus multifuge x3r centrifuge) and filtering it through cheese cloth into fresh falcon tubes. Isopropanol was added to solution to precipitate the DNA which was pelleted at 4000rpm (TX-100 rotor, Thermo heraeus multifuge x3r centrifuge). The DNA pellet was resuspended in ultrapure water

and the RNA was precipitated with 5M $NH_4$ acetate. The RNA was pelleted at 4000rpm (TX-100 rotor, Thermo heraeus multifuge x3r centrifuge) and the DNA supernatant was pipetted into fresh falcon tubes. 100% ethanol was added to the DNA supernatant and samples were incubated at -20$^{o}$C to precipitate the DNA. The DNA was pelleted at 4000rpm (TX-100 rotor, Thermo heraeus multifuge x3r centrifuge), resuspended in 4ml of water and $CsCl_2$ was dissolved in the DNA solution. Ethidium Bromide was added to the CsCl-DNA solution in excess then this mixture was pipetted into Beckmann optiseal centrifuge tubes and ultra-centrifuged at 50,000 RPM overnight at room temperature (VTi 65.2 Vertical-Tube Rotor, Proteome Lab XL-A/XL-I centrifuge). This produced a density gradient which separated the linear chromosomal DNA from the desired circular plasmid DNA. The band of plasmid DNA was extracted from the ultracentrifuge tube using a syringe. Ethidium bromide was removed by adding the mixture to CsCl saturated butanol. The DNA entered the aqueous phase whilst the ethidium bromide remained in the organic butanol phase. The DNA was pelleted at 4000rpm (TX-100 rotor, Thermo heraeus multifuge x3r centrifuge) and left at room temperture to dry. The DNA pellet was resuspended in as little ultrapure water as possible to keep the DNA concentrated.

*2.1.13.1 : Quantification of C-terminally His-tagged RBP-Jκ$_{8-435}$ expressed in 100ml of E.coli bound to $Co^{2+}$-beads.*

The talon beads ($Co^{2+}$ beads) were blocked with 5% BSA dissolved in PBS buffer overnight at 4$^{o}$C. Pellets of 100ml preparations of *E.coli* expressing C-terminally His-tagged RBP-Jκ$_{8-435}$ were thawed, lysed in buffer A (50mM Tris pH8.8, 500mM NaCl, 0.5mM TCEP, 10mM imidazole) + nuclease + lysozyme and sonicated 10 sec on, 10 sec off for 2 minutes at 35% using a Vibra-Cell VC 750 sonicator (Sonics). The cell debris

was separated from the lysate by centrifuging the sample at 13,500rpm (Ch 500062PP rotor, VWR microstar 17 centrifuge). The lysate was then incubated with blocked talon beads for an hour on a rolling shaker. The beads were then washed twice with buffer A. Known quantities of Bovine Serum Albumin were boiled in Gel Sample Buffer (GSB)(Appendix 3) and 30µL of RBP-Jκ$_{8\text{-}435}$ bound to talon beads boiled in GSB were run on a Bis-Tris SDS-PAGE gel alongside a SeeBlue™ Plus2 Pre-stained Protein Standard. The gel was run in MOPS buffer for 50 minutes at 200V after which it was stained with Coomassie. The band intensities from the Coomassie were measured on the Licor machine and it was estimated that there was 0.44µg RBP-Jκ$_{8\text{-}435}$ on the 30µL sample of talon beads. The formula below was used to calculate how much RBP-Jκ$_{8\text{-}435}$ bound to 100µL talon beads from a 100ml *E.coli* prep.

$$\frac{\sim 0.44\mu g \times \frac{100\mu L\ (total\ beads)}{30\mu L\ sample}}{49.5kDa} = \sim 30\mu M\ protein\ bound\ to\ 100\mu L\ of\ beads$$

*2.1.13.2 : Pull down assay using RBP-Jκ$_{8\text{-}435}$.*

The talon beads were blocked with 5% BSA dissolved in PBS buffer overnight at 4$^{o}$C. 100ml preps *E.coli* expressing C-terminally His-tagged RBP-Jκ$_{8\text{-}435}$ were pelleted at 1100rpm (TX-100 rotor, Thermo heraeus multifuge x3r centrifuge) and frozen. The pellets were thawed, lysed in buffer A + nuclease + lysozyme and sonicated 10 sec on, 10 sec off for 2 minutes at 35% using a Vibra-Cell VC 750 sonicator (Sonics). The cell debris was separated from the lysate by centrifuging the sample at 13,500rpm (Ch 500062PP rotor, VWR microstar 17 centrifuge). The lysate was then incubated with

blocked talon beads for an hour on a rolling shaker. The beads were then washed twice with buffer A.

The DG75 pellets were resuspended in lysis buffer PD (50mM Tris pH7.5, 150mM NaCl, 20mM $MgCl_2$, 1% NP-40, 0.5% Na Deoxycholate) and sonicated five times 10 seconds on 10 seconds off at 35% using a Vibra-Cell VC 750 sonicator (Sonics). The cells were spun at 13,500 rpm (Ch 500062PP rotor, VWR microstar 17 centrifuge) to separate the cell debris from the lysate. Next, the DG75 cell lysate was incubated with RBP-J$\kappa_{8\text{-}435}$ bound to the cobalt beads (talon beads) at 4$^{o}$C for 1 hour, then washed with buffer PD (Appendix 3) for 10 minutes, then washed with Phosphate Buffer Saline (PBS) for 10 minutes and then the beads were boiled in GSB for western blot analysis. Unfortunately, due to time constraints we were unable to reduce the significant amounts of background binding of EBNA3C and the EBNA3C mutants to the talon beads.

## 2.2: Expression, purification and analysis of postranslational modifications.

### *2.2.1: Introduction to insect cell expression system*

Insect cells as an expression system offer protein crystallographers better folding machinery than *E.coli* cells and post translational modifications with fewer of the difficulties associated with mammalian cell protein expression systems. To utilise insect cells as an expression system a recombinant baculovirus containing the genes encoding for the protein of interest must be produced in order to infect the insect cells and express the protein of interest. To produce a RBP-Jκ expressing recombinant baculovirus RBP-Jκ cDNA regions were cloned into a pFastBac vector. Competent MAX Efficiency DH10Bac™ cells contain helper vectors that facilitate the transposition of

genes from the pFastBac vector into the Bacmid. The recombinant bacmids were transfected into SF9 insect cells using Cellfectin to produce P1 stocks of RBP-Jκ expressing recombinant baculovirus. Passage 1 (P1) stocks were grown up into P2 then P3 baculoviral stocks which could be used for large scale infections of insect cells to overexpress RBP-Jκ.

*2.2.1.1 : Transposition and Bacmid generation*

Vectors were transformed into a Bacmid in specialised MAX Efficiency DH10Bac™ competent *E.coli* by heatshock. MAX Efficiency DH10Bac™ competent *E.coli* contain helper vectors which express transposition proteins which facilitate the site specific transposition of the DNA between the mini Tn7 elements in the pFastBac vector into the mini-Tn7*att* site in the bacmid. The transformed MAX Efficiency DH10Bac™ cells were supplemented with 500µL SOC media, grown for 4 hours at 37$^{o}$C then plated. After 48 hours incubating at 37$^{o}$C in X-gal agar plates with Gentamicin, Tetracyclin and Kanamycin, we used blue-white selection of colonies to verify if the pFastBac vectors had been successfully transposed into the bacmid. White colonies were re-streaked to verify if they were true white colonies and then picked to be grown up in order to extract the bacmid from the cells. The bacmids were purified from the cells via ethanol precipitation and diagnostic PCRs were ran using pUC/ M13 primers, which amplify across the bacmid transposition sites, to see if the vector had been successfully transposed. Due to the large size of the co-expression vectors the Phusion polymerase did not have the fidelity to extend across the entire transposed region of the recombinant bacmids. We therefore amplified across the cDNA and the most proximal transposition site to validate whether the transposition of each co-expression vector had been successful.

*2.2.1.2 : Transfection of Sf9 insect cells and generation of Baculovirus P1, P2 and P3 stocks*

A monolayer of insect cells were transfected with the bacmid containing the desired genes to be expressed. 200µl SF900II medium, 8µl Cellfectin and 2µg of bacmid were mixed to make the transfection medium. After a 5 hour incubation of the bacmid and transfection mixture with the insect cell monolayer the transfection mixture was replaced with SF900II media containing 100U/ml penicillin/streptomycin (pen/strep) and incubated at 28$^{o}$C for 5 to 6 days. Successfully transfected insect cells producing recombinant baculovirus would appear swollen and the insect cell nuclei would be dense and swollen. The media containing the P1 baculovirus was pipetted into cryotubes. After the P1 stock was harvested the cells in the well were dissolved in SDS buffer and boiled for western blot analysis of protein expression. P2 baculovirus stocks were generated by infecting 50ml of SF9 cells in SF900II medium + pen/strep with 1ml of the P1 stock. When cell viability dropped to 70% indicating successful infection the insect cells were pelleted at 1000xg (TX-100 rotor, Thermo heraeus multifuge x3r centrifuge). The baculovirus containing media was mixed with 2% FCS and stored at 4$^{o}$C for up to a year. This process was repeated again with P2 stock to make P3 stocks with a high enough viral titre for large scale insect cell preps.

*2.2.1.3 : Viral plaque assay used to calculate titre of baculovirus.*

Viral plaque assays were used to determine of the titre of virus in P3 stocks. 3 plates containing monolayers of insect cells were prepared and infected with $10^{-5}$, $10^{-6}$ and $10^{-7}$ serially diluted P3 baculovirus. The insect cell monolayers were covered in agarose mixed with SF900II media . These cells were incubated for 4 days at 27$^{o}$C. As the virus replicates, lyses and infects neighbouring cells the plaques of lysed cells created can be

visualised with neutral red staining in plaque forming units (pfu). By counting the number of plaques, the titre of virus can be calculated using the dilution factor of the virus and the volume of inoculum used using the formula below.

$$\boldsymbol{Titre\ of\ Virus}\ (\boldsymbol{pfu/ml}) = \frac{\boldsymbol{The\ number\ of\ plaques\ counted} \times \boldsymbol{Dilution\ factor}}{\boldsymbol{ml\ of\ innoculum\ used}}$$

*2.2.1.4 : Insect Cell infection and Protein expression*

Insect cells at 2 x $10^7$cells/ml were infected with baculovirus overexpressing the protein of interest. Insect cells were counted by mixing 10µl cells with at a 1:1 ratio with trypan blue, loading them onto Countess® Cell Counting Chamber Slides and using the Countess® Automated Cell Counter to count the cells and estimate cell viability. To establish the optimal infection time for protein expression a 200ml small scale infection of insect cells was initially carried out. In order to calculate the amount of baculovirus to use the viral titre, cell density, cell volume and the multiplicity of infection (MOI) were taken into account (shown in the formula below).

$$\boldsymbol{Volume\ of\ baculovirus\ required}\ (\boldsymbol{mL})$$

$$= \frac{\boldsymbol{MOI} \times \boldsymbol{culture\ cell\ count}\ (\boldsymbol{cells\ per\ ml}) \times \boldsymbol{culture\ volume}(\boldsymbol{mL})}{\boldsymbol{viral\ titre}}$$

We infected the insect cells with a MOI of two which meant for every insect cell there would be two virions. Insect cells expressing C-terminally His-tagged RBP-J$\kappa_{8\text{-}435}$ and N-terminally His-tagged EBNA3C$_{100\text{-}356}$ were harvested 2 days after infection as we measured a drop in yield by day 3 of the prep.

### *2.2.2 : Insect cell expression and purification of RBP-Jκ*

*2.2.2.1 : Analysis of expression of C-terminally His-tagged RBP-Jκ8-435 and N-terminally His-tagged RBP-Jκ variant in insect cells.*

50ml of Sf9 cells were infected with baculovirus at an MOI of 2 and were incubated at 27$^{o}$C for three days. Each day 1ml of cells was taken, spun down at 1000 x g (TX-100 rotor, Thermo heraeus multifuge x3r centrifuge) for 8 minutes, washed with PBS and then frozen. On the third day all the cell pellets were lysed in GSB buffer, boiled for analysis on Coomassie gels and western blots. His-tagged ZTA from Prof Allison Sinclair's group was run as a positive control.

*2.2.2.2 : Nickel bead pulldown of C-terminally His-tagged RBP-Jκ$_{8-435}$ expressed in insect cells.*

50ml of Sf9 cells were infected with baculovirus at an MOI of 2 and are incubated at 27$^{o}$C for three days. After 3 days the cells were pelleted and lysed in 1ml of lysis buffer (50mM Tris pH8.8, 500mM NaCl, 5mM β-mercaptoethanol) with a dounce homogeniser (on ice) and spun at 13,000 x g (Ch 500062PP rotor, VWR microstar 17 centrifuge) for 20 minutes at 4$^{o}$C. The beads were primed with lysis buffer spun at 13,000rpm (Ch 500062PP rotor, VWR microstar 17 centrifuge) for 1 minute then the lysis buffer was removed. The lysate was incubated with the beads on a windmill rotator for 60 minutes at 4$^{o}$C. The beads were spun down at 5000 x g (Ch 500062PP rotor, VWR microstar 17 centrifuge) for 30 seconds. The lysate was removed and stored at -20$^{o}$C for future analysis. Beads were washed twice in buffer (50mM Tris pH8.8, 500mM NaCl, 5mM β-mercaptoethanol). After each wash step the beads were spun down and the wash buffer was removed. The wash step was repeated twice to ensure high purity. Next, elution buffer (50mM Tris pH8.8, 500mM NaCl, 5mM β-

mercaptoethanol, 200mM imidazole) was added to the beads and mixed for 20 minutes as described previously. The beads pelleted at 5000 x g (Ch 500062PP rotor, VWR microstar 17 centrifuge) for 30seconds and the eluate was removed and stored on ice. To determine if any protein remained bound to the beads they were incubated in 2 x GSB for 5 minutes at 95$^{o}$C. The samples taken at each step of the $Ni^{2+}$ bead pull down were mixed with GSB buffer at 1:1 ratio and boiled for SDS-PAGE and western blot analysis.

*2.2.2.3 : Quantification of C-terminally His-tagged RBP-Jκ$_{8-435}$ expressed in 45ml of insect cells*

Known quantities of Bovine Serum Albumin (BSA) and 5µL of RBP-Jκ$_{8-435}$ eluate from the $Ni^{2+}$ bead pull down were boiled in GSB and run on a Bis-Tris SDS-PAGE gel. The formula below was used to estimate how much RBP-Jκ$_{8-435}$ could be purified from a 6L prep.

$$\sim 0.5\mu g \times \frac{50\mu L\ (total\ eluate)}{5\mu L\ sample} \times \frac{6000mL\ (large\ scale\ prep)}{50mL\ (small\ scale\ prep)}$$

$$= \sim 0.6mg\ estimated\ yeild$$

*2.2.2.4 : Initial large scale expression of C-terminally His-Tagged RBP-Jκ$_{8-435}$ in 3L of insect cells*

The buffers used were based on the buffers used to purify C-terminally His-tagged RBP-Jκ$_{8-435}$ in the structure of the Notch transripction complex (Wilson and Kovall, 2006). We substituted the reducing agent β-mercaptoethanol (βME) for Tris(2-carboxyethyl)phosphine hydrochloride (TCEP) as βME is known to oxidise during Isothermal titration calorimetry (ITC) binding assays which generates artefacts when collecting data. P3 stock (amounts of which varied on baculovirus yield) of

recombinant baculovirus expressing C-terminally His-Tagged RBP-Jκ$_{8-435}$ was used at an MOI of 2 to infect 3L of Sf9 insect cells in SF900II media +Pen/Strep. C-terminally His-Tagged RBP-Jκ$_{8-435}$ was expressed in Sf9 insect cells for two days then pelleted at 1000 x g for ten minutes in a Beckman Avanti J-20 High Capacity Centrifuge. The pellet was frozen, thawed, then lysed in buffer A (50mM Tris pH8.8, 500mM NaCl, 0.5mM TCEP) with a dounce homogeniser (10 plunges). Nuclease was added to digest the DNA released and the lysate was filtered through a 50 µm syringe filter to make the lysate less viscous. After this the lysate was spun at 20,000 x g for 40 minutes to pellet the cell debris in a Beckman Avanti J-20 High Capacity Centrifuge. The lysate was loaded onto a His Trap FF column (GE life sciences) and eluted in with a gradient of buffer B (50mM Tris pH8.8, 500mM NaCl, 0.5mM TCEP, 1M imidazole). The eluates were pooled and passed through a desalt 26/10 column GE life sciences) primed with buffer C (20mM Tris pH8.8, 100mM NaCl, 0.5mM TCEP) in order reduce the salt concentration and remove the imidazole from the buffer. The pooled eluates were loaded onto a MonoQ 5/50 (GE life sciences) and eluted with a gradient of high salt buffer D (20mM Tris pH8.8, 500mM NaCl, 0.5mM TCEP). The protein was then concentrated in a protein concentrator (Millipore 30kDa filter) to 10mg/ml. For crystallisation trials the protein was further purified using a S200 10/30 size exclusion column primed with buffer C (20mM Tris pH8.8, 100mM NaCl, 0.5mM TCEP). Eluates from the size exclusion step were concentrated with a Millipore 30kDa filter concentrator to ~7mg/ml and flash frozen in liquid nitrogen. At each step 10µL of eluates were mixed with 10µL of GSB and boiled for analysis by SDS-PAGE.

*2.2.2.5 : Optimised large Scale expression of C-terminally His-Tagged RBP-Jκ$_{8-435}$ in 5L of insect cells*

A P3 stock of recombinant baculovirus expressing C-terminally His-Tagged RBP-Jκ$_{8-435}$ was used to infect 5L of Sf9 insect cells in SF900II media with Pen/Strep antibiotics. C-terminally His-Tagged RBP-Jκ$_{8-435}$ was expressed in Sf9 insect cells for two days then spun into a pellet at 1000 x g (JA-20 rotor, Avanti J-26XP centrifuge) for ten minutes. The pellet was frozen, thawed, then lysed in buffer A with a dounce homogeniser (15 to 20 plunges). Nuclease was added to digest the DNA released and the lysate was filtered through a 50 µm syringe filter to make the lysate less viscous. The lysate was then pelleted at 20,000 x g for 40 minutes (JA-20 rotor, Avanti J-26XP centrifuge). The lysate was loaded onto a $Co^{2+}$ column (5ml Talon column (GE life sciences)) and eluted with a gradient of buffer B (50mM Tris pH8.8, 500mM NaCl, 0.5mM TCEP, 1M imidazole). We used $Co^{2+}$ column instead of a $Ni^{2+}$ columns, as $Co^{2+}$ columns bind more specifically to His-tagged proteins, reducing the amount of impurities which are eluted with the protein of interest improving the purity of the sample. The eluates were pooled and passed through a desalt 26/10 column (GE life sciences) primed with buffer C (20mM Tris pH8.8, 100mM NaCl, 0.5mM TCEP) in order to reduce the salt concentration and remove the imidazole from the buffer. The sample was then loaded onto a MonoQ 5/50 (GE life sciences) and eluted with a gradient of high salt buffer D (20mM Tris pH8.8, 500mM NaCl, 0.5mM TCEP). The protein was then concentrated in a protein concentrator (Millipore 30kDa filter) at 3500rpm (TX-100 rotor, Thermo heraeus multifuge x3r centrifuge) to 10mg/ml. For crystallisation trials the protein was incubated with RBP-Jκ consensus site DNA (TTACT**GTGGGA**AAGA) for 30 mins on ice at 1:1.2 (RBP-Jκ:DNA) ratio and loaded on to S200 10/30 size exclusion column primed

with buffer C (20mM Tris pH8.8, 100mM NaCl, 0.5mM TCEP). Eluates from the size exclusion step were concentrated with a Millipore 30kDa filter concentrator to ~8-10mg/ml. At each step 10µL of eluates were mixed with 10µL of GSB and boiled for SDS-PAGE analysis.

*2.2.2.6 : Size exclusion column assay to test the effects of DNA and peptide binding to the conformation of C-terminally His-Tagged RBP-Jκ$_{8-435}$*

The RBP-Jκ used in these assays was initially prepared for Isothermal titration calorimetry (ITC). C-terminally His-tagged RBP-Jκ was therefore expressed in insect cells and purified through to the anion exchange step where it was concentrated to ~8mg/ml in a protein concentrator (Millipore 30kDa filter) at 3500rpm (TX-100 rotor, Thermo heraeus multifuge x3r centrifuge), dialysed into ITC buffer (20mM Tris pH8.8, 100mM NaCl, 0.5mM TCEP, 0.5mM EDTA) and diluted to 37.8µM. RBP-Jκ$_{8-435}$ was incubated with EBNA2.26aa peptide (see appendix 4) and or RBP-Jκ$_{8-435}$ consensus site DNA (TTACT**GTGGGA**AAGA) for hour on ice then each assay was passed through S200 10/30 size exclusion column primed with buffer C (20mM Tris pH8.8, 100mM NaCl, 0.5mM TCEP). 10µL from each well of each assay was mixed with 10µL of GSB and boiled for SDS-PAGE anlysis. The chromatograms from each assay were overlaid using unicorn software.

***2.2.3 : Phosphorylation of RBP-Jκ expressd in insect cells.***

*2.2.3.1 : λ-phosphatase dephosphorylation assay*

C-terminally His-tagged RBP-Jκ$_{8-435}$ was expressed in insect cells, purified on a $Co^{2+}$ column and desalted on the desalt 26/10 column. The RBP-Jκ$_{8-435}$ was concentrated to 1.4mg/ml giving a concentration of 29µM. 50µL of RBP-Jκ$_{8-435}$ was incubated for 30

minutes on ice with 10mM $MgCl_2$ and 3µL (100 units) of λ-phosphatase (NEB) or buffer C (20mM Tris pH8.8, 100mM NaCl, 0.5mM TCEP) as a negative control. The RBP-Jκ$_{8-435}$ incubated with or without λ-phosphatase was loaded onto a MonoQ 5/50 and eluted with a gradient of high salt buffer D (20mM Tris pH8.8, 500mM NaCl, 0.5mM TCEP).

*2.2.3.2 : In-gel trypsin digests of RBP-Jκ$_{8-435}$ expressed in insect cells.*

During the anion exchange purification process RBP-Jκ$_{8-435}$ expressed in insect cells eluted in 2 peaks (peak 1 and peak 2). To investigate why, 10µL of peak one and peak two of the eluates of the anion exchange purification step were mixed with 10µL of GSB, boiled then run on a 10% Bis-Tris SDS-PAGE gel in MOPS. The gel was stained with Coomassie and the 49kDa bands represent RBP-Jκ$_{8-435}$ were cut out of the gel with a scalpel. The cut-out bands were destained with destain buffer (50% MeCN, 25 mM $NH_4HCO_3$) , then dehydrated in a speedvac, reduced with DTT, alkylated with iodoacetamide solution (50 mM iodoacetamide, 25 mM $NH_4HCO_3$) in the dark and dehydrated once more before being soaked in a trypsin solution (12.5 ng/ul trypsin, 25 mM $NH_4HCO_3$) overnight. The peptides from each sample were separated from the remaining undigested protein using reversed phase separation facilitated by adding formic acid. The peptides were stored in 0.1% TFA at -20$^{o}$C prior to mass spectroscopy analysis.

*2.2.3.3 : Collection and of Mass spectroscopy data analysis.*

Peptides were loaded on to the LTQ-Oribitrap XL (University of Sussex) via a nanoLC column in order to separate the peptides by size before being ionized. The peptides were ionised with an electrospray (2.2-3.0 kV) creating an aerosol of charged peptides. These gaseous charged peptides were injected in packets into the orbitrap at a tangent

to the inner electrode. The voltage of the inner electrode was ramped up till the charged peptides established an orbit around the inner electrode. Once the analyte was loaded and orbiting the field was ramped down and became static. This allowed the peptides to separate in to different rings of orbit around the inner electrode based on their mass to charge ratio. The current generated by the charged peptide oscillating around the inner electrode was detected by the outer electrode and sensors attached to outer electrode simultaneously calculated the mass of multiple peptides based on their different mass to charge ratio dependent oscillations. A BSA standard was injected initially to calibrate the LTQ-Oribitrap XL then the peptides from the peak 1 and peak 2 in-gel digests were injected. The raw mass spectra for each charged peptide detected was loaded in to Mascot software which verified both peaks contained Human RBP-Jκ. Mascot software was next used to fit amino sequences into the masses of the peptides detected in the LTQ-Oribitrap XL. We set the mascot software parameters to search for peptide sequences from human RBP-Jκ and set the software to search for peptides sequences with phosphorylated residues. Sequence coverage and statistics on detected peptides were calculated by the Mascot software.

*2.3.3.4 : Using Cuckoo workshop Group-based prediction software to verify predicted phosphorylation sites of RBP-Jκ$_{8-435}$ expressed in insect cells and identify potential kinase candidates.*

We used an online tool to verify whether the peptides corresponding to phosophorylated-peptides sizes by mass spectroscopy were indeed predicted to contain phosphorylated residues.The cuckoo workshop had developed an online tool for predicting phosphorylation. The tool works by comparing the inputted sequence with a matrix of known phosphorylation sites and kinome databases then scores the

residues likelihood of being phosphorylated (Xue *et al.*, 2008). To reduce false positives the tool scans the residues upstream and downstream of the threonine, serine or tyrosine residue in the suspected kinase binding motif to determine whether the folding of the region is ordered or disordered (Xue *et al.*, 2008). If the protein around the motif is disordered they hypothesised that this would reduce the likelihood the suspected kinase site would be able to interact with kinases adding another level of selection (Xue *et al.*, 2008). The software also predicts the false positive rate for each inputted sequence therefore providing a guide for the phosphorylation prediction algorithm to how many kinase sites to disregard(Xue *et al.*, 2008). Finally the program also organises the kinases in the kinome database by hierarchy therefore making the predictions more biologically relevant (Xue *et al.*, 2008).

### *2.2.4 : E.coli expression and purification of RBP-Jκ*

#### *2.2.4.1 : Small scale 1L E.coli expression and purification of C-terminally His-tagged RBP-Jκ$_{8-435}$*

Competent Rosetta plys De3 were transformed with pET28B.JK.8-435 by heat shock for 45 sec at 45$^{o}$C, and then briefly recovered in Lysogeny broth (LB) with no antibiotics at 37$^{o}$C, diluted in LB then plated onto chloroquine/ kanamycin (chl/kan) agar plates and incubated over night at 37$^{o}$C. Colonies were selected, grown in 50ml of LB (chl/kan) media grown overnight and used to inoculate 1L of LB (chl/kan) media at an Optimal density (O.D) of 0.07. Some of the 50ml inoculant was used to produce glycerol stocks which were stored at -80$^{o}$C. The 1L culture was grown to an O.D of 0.8, then rapidly cooled on ice prior to induction with 0.5mM of Isopropyl β-D-1-thiogalactopyranoside (IPTG) overnight in a shaking incubator at 18 $^{o}$C. The cells were then pelleted at 4000rpm for 20 minutes in a 4000rpm (J-LITE JLA 8.1000 Fixed Angle rotor, Avanti J-

26XP centrifuge). The cells were then lysed in buffer A (50mM Tris pH8.8, 500mM NaCl, 0.5mM TCEP) + DNAase (25 units) + 1ml of lysozyme and sonicated 10s on, 10s off for 10min at 30% using a Vibra-Cell VC 750 sonicator (Sonics). The lysate was spun at 20,000rpm for 1 hour to separate the cell debris from the lysate (JA-20 rotor, Avanti J-26XP centrifuge).

The lysate was loaded onto a $Co^{2+}$ column (5ml Talon FF column (GE Life Sciences)), washed and eluted with a gradient of imidazole buffer B (50mM Tris pH8.8, 500mM NaCl, 0.5mM TCEP, 1M imidazole). We continued using $Co^{2+}$ columns for the initial purification step as $Co^{2+}$ columns bind to His-tags more specifically than $Ni^{2+}$ columns reducing the number of impurities in the eluates. The eluates from the $Co^{2+}$ column purification step were then loaded onto a desalt 26/10 column (GE Life Sciences) calibrated in buffer C (20mM Tris pH8.8, 100mM NaCl, 0.5mM TCEP) to reduce the [NaCl] to 100mM and remove the imidazole. The desalted sample was loaded onto a 5ml HitrapQ column (GE Life Sciences) and eluted with an increasing gradient of high salt buffer D (20mM Tris pH8.8, 500mM NaCl, 0.5mM TCEP). Finally, the eluates from the anion exchange step were concentrated to 250µL, incubated with DNA (TTACT**GTGGGA**AAGA) on ice with a 1:1.5 protein to DNA ratio and loaded on to a S200 10/30 size exclusion column (GE Life Sciences) equilibrated in buffer C. 10µL samples of eluates from each step were mixed with equal amounts of GSB, boiled and run on 10% Bis-Tris SDS-PAGE gel in MOPS at 200V for 50 mins then stained with Coomassie for anlysis. The chromatograms from each purification step were produced on unicorn software.

*2.2.4.2 : Large scale E.coli expression and optimised purification of C-terminally His-tagged RBP-Jκ$_{8-435}$*

Glycerol stocks of Rosetta plys De3 transformed with pET28B.JK.8-435 were inoculated in 150ml of LB (chl/kan) media overnight which was used to inoculate 4L of LB (chl/kan) media at an O.D of 0.07. The 4L culture was grown to an O.D of 0.8, rapidly cooled on ice ready for the cells to be induced with 0.5mM of Isopropyl β-D-1-thiogalactopyranoside (IPTG overnight in a rotating incubator at 18 $^{o}$C. The cells were then pelleted at 4000rpm for 20 minutes (J-LITE JLA 8.1000 Fixed Angle rotor, Avanti J-26XP centrifuge). The cells were then lysed with buffer A (50mM Tris pH8.8, 500mM NaCl, 0.5mM TCEP, 10mM imidazole) + DNAase (50units) + lysozyme and sonicated 60s on, 30s off for 15min at 35% using a Vibra-Cell VC 750 sonicator (Sonics). The lysate was spun at 20,000rpm for 1 hour to separate the cell debris from the lysate (JA-20 rotor, Avanti J-26XP centrifuge).

The lysate was loaded onto a $Co^{2+}$ Column (5ml Talon FF column (GE Life Sciences)), washed and eluted with a gradient of imidazole buffer B. The eluates from the $Co^{2+}$ column purification step were then loaded onto a desalt 26/10 column (GE Life Sciences) calibrated in buffer C to reduce the concentration of NaCl to 100mM and remove the imidazole. The desalted sample was loaded onto a 5ml HitrapQ column (GE Life Sciences) and eluted with an increasing gradient of high salt buffer D. The gradient was stopped when [NaCl] 150mM until all the RBP-Jκ$_{8-435}$ had eluted. Finally, the eluates from the anion exchange step were concentrated to 250µL, incubated with double stranded oligonucleotide (TTACT**GTGGGA**AAGA) on ice with a 1:1.5 protein to DNA ratio and loaded on to a S200 10/30 size exclusion column (GE Life Sciences) equilibrated in buffer C. 10µL samples of eluates from each step were mixed with

equal amounts of GSB and boiled or SDS-PAGE analysis. The chromatograms from each purification step were produced on unicorn software.

### *2.2.5 : Expression of full length EBNA2 and EBNA3C homology domain*

*2.2.5.1 : Analysis of small scale infection of recombinant baculovirus expressing full length EBNA2*

A P2 stock of recombinant baculovirus expressing full length EBNA2 had been produced by a masters student from Dr Christomous Prodromou group but not tested for expression. We grew up a P3 stock of the baculovirus and infected 100ml of insect cells at an MOI of 2. Insect cells were incubated at 27$^{o}$C in SF9 medium with pen/strep antibiotics. Samples of cells were taken each day after infection, pelleted and lysed in GSB buffer for SDS-PAGE and western blot analysis.

*2.2.5.2 : Purification of N-terminally His-tagged EBNA3C$_{100-356}$ expressed in insect cells.*

A P3 stock of recombinant baculovirus expressing N-terminally His-tagged EBNA3C$_{100-356}$ was used to infect 3L if Sf9 insect cells in SF900II media with Pen/Strep antibiotics. N-terminally His-tagged EBNA3C$_{100-356}$ was expressed in Sf9 insect cells for two days then spun into a pellet at 1000 x g for ten minutes (J-LITE JLA 8.1000 Fixed Angle rotor, Avanti J-26XP centrifuge). The pellet was frozen, thawed, then lysed in buffer A (50mM Tris pH8.0, 500mM NaCl, 0.5mM TCEP, 20mM imidazole, 5% glycerol) with a dounce homogeniser (15 plunges). Nuclease was added to digest the DNA released and the lysate was filtered through a 50 µm syringe filter to make the lysate less viscous. After this the lysate was spun at 20,000 x g for 40 minutes (JA-20 rotor, Avanti J-26XP centrifuge) to pellet the cell debris. The lysate was loaded onto a 5ml Talon (GE life sciences) and eluted with a gradient of buffer B (50mM Tris pH8.0, 500mM NaCl,

0.5mM TCEP, 1M imidazole, 5% glycerol). The eluates were then concentrated in a protein concentrator (Millipore 10kDa filter) at 3500rpm (TX-100 rotor, Thermo heraeus multifuge x3r centrifuge) to 250µL. This concentrated protein was loaded on to S200 10/30 size exclusion column primed with buffer C. Eluates from the size exclusion step were concentrated with a Millipore 10kDa filter concentrator to ~0.5mg/ml, flash frozen in liquid nitrogen and stored at -80$^{o}$C. At each step 10µL of eluates were mixed with 10µL of GSB, boiled and run on 4-12% Bis-Tris SDS-PAGE gels in MOPS buffer at 200V for 50mins alongside a SeeBlue™ Plus2 Pre-stained Protein Standard. These gels were then stained with Coomassie for analysis.

## 2.3 : Thermodynamic techniques

### *2.3.1 Introduction to Isothermal Titration Calorimetry*

Isothermal titration calorimetry (ITC) is used to measure the enthalpy (ΔH), stoichiometry (N) and entropy (ΔS) of the interactions between two biomolecules (Freyer and Lewis, 2008). In the reaction cell the ligand is titrated on to the receptor which causes a release of heat as the two molecules interact. The change in temperature is detected between the reaction cell and the control cell and the MicroCal ITC200 heats the control cell till the cells are at equal temperatures. The energy the machine uses to correct the temperatures between the two cells is registered as a heat peak which is integrated to quantify the energy released by the ligand and receptor binding. The ligand is titrated into the reaction cell till the receptors are saturated with ligand generating a binding curve. The binding curve is fitted to a non-linear regression curve which allows the gradient and the midpoint of the curve to calculated. The midpoint of the curve represents the point where the [ligand], [receptor] and [complex] is equal therefore the stoichiometry (N) of the

interaction can be calculated. The gradient of the curve is used to calculate $k_{association}$ ($k_a$) which can be used to calculate $k_{disassociation}$ ($k_d$) which quantifies the affinity of the interaction between the ligand and receptor. Enthalpy (ΔH) is calculated from the largest heat peak as this represents the maximal energy released from the ligand and receptor interacting. As the interaction occurs in water changes in entropy (ΔS), due to conformational changes to the proteins caused by the interaction, can be calculated. The error is calculated from the sum of the deviations between model fitted curve and the integrated heat peak data collected. Finally, the enthalpy (ΔH) and entropy (ΔS) can be used to calculate Gibbs free energy (ΔG) which confirms whether the interaction occurs spontaneously. When designing ITC experiments there must be enough of the ligand and receptor to generate measurable heat peaks. Additionally it is imperative that the buffer the ligand and receptor are in are the same buffer as differences will generate heat peaks and create artefacts in the ITC data (Freyer and Lewis, 2008).

*2.3.2 : Isothermal Titration Calorimetry analysis of RBP-Jκ interacting with peptides.*

RBP-J$\kappa_{8-435}$ was then thawed on ice then dialysed into ITC dialysis buffer (Buffer C + 1mM EDTA) overnight at 4$^{o}$C. The peptides (Appendix 4) arrived in powder form, were measured on a precision microbalance and dissolved in DMSO. The peptide DMSO stock was used to make 600µM solution of peptide in buffer ITC (20mM Tris pH8.8, 100mM NaCl, 0.5mM TCEP, 0.5mM EDTA, 2% DMSO). DMSO was added to the buffers with peptide or RBP-J$\kappa_{8-435}$ dissolved in so they both contained 2% DMSO. Dr Chrisostomos Prodromou consulted us about the design of our ITC and recommended we used between 30-60µM of RBP-J$\kappa_{8-435}$ to ensure that the heat peaks generated, by what we predicted to be a relatively weak interaction, were large enough to be

accurately measured. Due to the low predicted yield of a 5L prep of C-terminally His-tagged RBP-Jκ$_{8-435}$ expressed in insect cells we calculated that we would only produce enough material per preparation to have a maximum of concentration 37.8µM RBP-Jκ$_{8-435}$ in each ITC binding assay. 37.8µM of RBP-Jκ$_{8-435}$ was loaded into the sample cell then 30 injections of 600µM of peptide dissolved in buffer ITC were titrated onto RBP-Jκ$_{8-435}$. To be able to measure the interactions between the EBNA3A.33aa or EBNA3B.33a peptides and RBP-Jκ we reduced the number of injections to 20 whilst increasing the volume of peptide we injected to increase the size of the heat peaks in order to make the weak binding curves more accurate. Heat peaks were measured using MicroCal ITC200 (Malvern analytical) at 30$^{o}$C. Curves were fitted to the heat peaks and the $k_d$, stoichiometry and entropy of each interaction was calculated using origin 5.0 Software.

*2.3.3.1 : Fluorescent polarisation binding assay of the RBP-Jκ$_{8-435}$-EBNA2.28aa.FP interaction*

The EBNA2.26aa peptide was ordered from Peptide Synthetics with a fluorescein tag. Two glycine residues were added to the N-terminus of the protein to facilitate the chemistry required to conjugate the fluorescein tag to the peptide. 28µM of C-terminally His-tagged RBP-Jκ$_{8-435}$ (expressed in insect cells) was serially diluted over 12 wells (in triplicate) containing 100nM EBNA2.28aa.FP-RBP-Jκ$_{8-435}$ and buffer FP (buffer C + 2%DMSO + 0.5%IPEGAL). Samples were incubated at 4$^{o}$C for 30 minutes then the percentage of polarised emissions (i.e the percentage EBNA2.28aa.FP bound to RBP-J) was measured using the BMG Lab-tech Polarstar omega. As the EBNA2.28aa.FP binds to C-terminally His-tagged RBP-Jκ$_{8-435}$ (expressed in insect cells) the emissions for the fluorescein tag become polarised allowing us to measure the proportion of the

EBNA2.28aa.FP in the wells that is bound to RBP-Jκ$_{8-435}$. When 50% of the emissions from the EBNA2.28aa.FP peptide are polarised half of the EBNA2.28aa.FP in the well is bound to RBP-Jκ$_{8-435}$ which means that there is an equilibrium of free EBNA2.28aa.FP and EBNA2.28aa.FP bound to RBP-Jκ$_{8-435}$. Therefore, the $k_d$ of the interaction can be calculated as the concentration of the receptor. From this we calculated the $k_d$ of the EBNA2.28aa.FP-RBP-Jκ$_{8-435}$ interaction.

*2.3.3.2 : Fluorescent polarisation competition binding assays*

10µM of unlabelled competitor peptides were dissolved in buffer FP (Buffer ITC + 0.05% IPEGAL) then serially diluted across a 96 well plate in triplicate. 1mM RBP-Jκ$_{8-435}$ was incubated with 1mM EBNA2.28aa.FP and added to all the wells. These plates were left to incubate at 4$^{o}$C for 30 minutes then the percentage of polarised emissions (i.e the percentage EBNA2.28aa.FP still bound to RBP-Jκ$_{8-435}$) was measured using the BMG Lab-tech Polarstar omega.

*2.3.4 : Introduction to a novel Biosensor called SwitchSense*

SwitchSense is a biosensor system which can monitor binding of proteins to DNA, protein-protein interactions and measure conformational changes in proteins. Switchsense utilises a DNA nanolever bound to a gold chip to tether proteins to the chip as opposed to antibodies or gold chips coated in reagents that chemically immobilise proteins. The DNA nanolever is made of two parts, the DNA switch is a single stranded piece of DNA covalently bound to the gold chip and has a fluorophore attached to the end (Figure 2.4A). The other half of the DNA nanolever can be synthesised to contain a consensus site for a transcription factor we wanted to study or premade DNA switches capable of binding to His-tags could be ordered. The

designed half of the nanolever is annealed to the DNA switch (Figure 2.4A) before starting binding assays. Depending on the experiment alternating or direct current was passed through the chip and due to the DNA's negative charge the nanolever is attracted or repelled from the gold chip. In order to measure the movement of the DNA nanolever an extremely sensitive light sensor measures the fluorescence emitted from the fluorophore attached the DNA nanolever. When the DNA nanolever is attracted to the gold chip with a positive charge the fluorophores emissions are quenched by the gold plate enabling the machine to measure whether the nanolever is in an up-right or horizontal position (Figure 2.4B). The rate at which the switch recovers from the horizontal position has is termed the dynamic response and this can be measure for an individual recovery or multiple recoveries in real time as samples are injected and passed over the chip.

When a protein binds to the consensus site that has been designed into the nanolever this causes the dynamic response to slow as the protein increases the hydrodynamic friction or drag of the nanolever. This decrease in the dynamic response of the nanolever can be measured in real time to generate binding and disassociation curves which can be used to calculate $k_d$s of protein-DNA interactions. In addition to this the dynamic response can also be altered when the conformation of the protein changes due to more open conformations increasing the hydrodynamic friction and more tightly packed conformations decreasing hydrodynamic friction. Therefore, the SwitchSense Biosensors can also measure the effect of drug-binding, peptide binding and protein interactions on the conformation of the protein of interest.

The Switchsense biosensor is extremely robust and can tolerate a large range of buffers and reagents, even cell lysates, that other biophysical machines cannot. The most significant benefit of the switchsense biosensor for our project was that the machine can measure binding interactions of proteins even when only fM quantities of material are available potentially allowing us to study the EBV transcription factors despite the fact we maybe only express them in very low quantities.

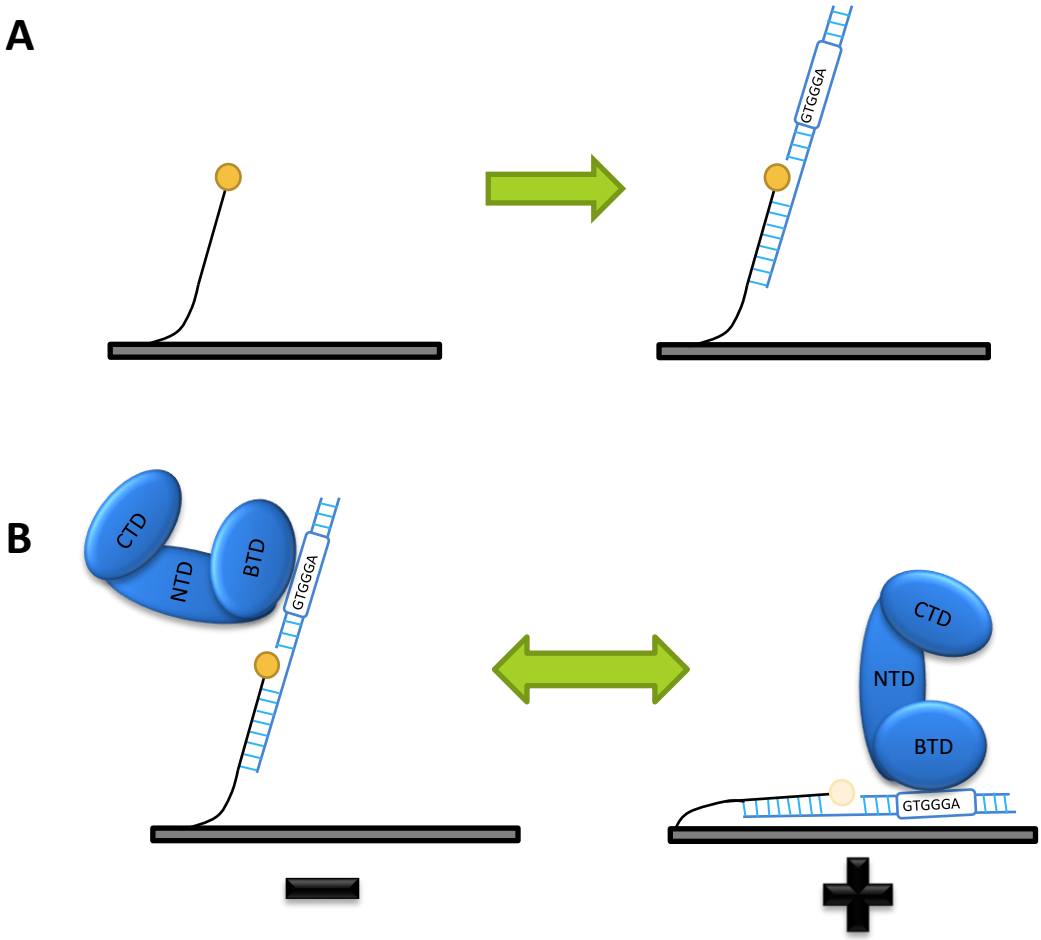


**Figure 2.5. Introduction to SwitchSense Bioassay. A.** This diagram shows the DNA containing the RBP-Jk consensus site (GTGGGA) being annealed to the Switch (in black). The fluorescent tag on the switch is shown in orange. **B.** In this diagram on the left the RBP-Jk (shown in blue) has been bound to the switch. There is a negative current passing through the chip. On the right hand side a positive current is passing through the chip. This attracts the DNA switch to the chip. When the switch is proximal to the gold chip the fluorophore on the switch is quenched by the gold chip. This allows the machine to detect when switch is up-right or attracted to the chip. The machine measures the dynamic response (i.e the DNA recovering from the position in the right of the diagram to the position on the left) which changes whether something is bound to the chip. These measurements can then be used to calculate the thermodynamics of an interaction between the switch and protein.

*2.3.4.1 : SwitchSense assay; Optimising RBP-Jκ binding to RBP-Jκ consensus nanolever and control nanolever.*

C-terminally His-tagged RBP-$\kappa_{8-435}$ was purified as described in chapter 2.2.2.5 up to the anion exchange step and flash frozen. RBP-$\kappa_{8-435}$ was thawed on ice and diluted into a 1µM stock with SwitchSense buffer (20mM Tris pH8.8, 50mM NaCl, 0.5mM TCEP, 2%DMSO). RBP-J$\kappa_{8-435}$ was diluted with SwitchSense buffer into 100nM and 10nM aliquots to test the optimal amount to bind to the RBP-J$\kappa_{8-435}$ consensus nanolever (5' AAA CAC GCC **GTG GGA** AAA AAT ATC AGC GTT CGA TGC TTC CGA CTA ATC AGC CAT ATC AGC TTA CGA CTA 3') and control nanolever, which was later found to contain a RBP-Jκ non-consensus site (5' **GTG TGA A**CC CTC CAA CAA AGG TAG CAT TTG CCA GCT CTC GTG ATG CAG 3'). RBP-Jκ consensus nanolever and control nanolever were annealed to the switches by injecting them onto the switches in triplicate. The machine heated the chip to ~80$^{o}$C then gradually cooled allowing the nanolevers to anneal to the switches. 10nM, 100nM and 1µM concentrations of RBP-J$\kappa_{8-435}$ were injected onto the RBP-Jκ consensus nanolever and RBP-Jκ non-consensus nanolever in triplicated. The Biosensor Switchsense measured the dynamic response in real time. The machine automatically combines the data from the three repeats to produce the binding and disassociation curves. Due to time constraints of the free trial we were unable to wait for RBP-J$\kappa_{8-435}$ to completely disassociate from the nanolever so the $k_{off}$ was estimated from the small disassociation curve generated by giving RBP-J$\kappa_{8-435}$ 40 minutes to disassociate. Switchanalysis software was used to produce the curves and calculate $k_{on}$, $k_{off}$ and $k_d$ from this data with the help of the technicians from Dynamic Biosensors.

*2.3.4.2 : SwitchSense assay to determine the effects Notch2 and EBNA peptides have on RBP-Jκ-DNA binding.*

RBP-$\kappa_{8-435}$ was thawed on ice and diluted into a 100nM stock with SwitchSense buffer. DMSO stocks of each of the peptides were dissolved in Buffer SwitchSense. 100nM of RBP-$\kappa_{8-435}$ was incubated with 100nM of each of the peptides for 30 minutes on ice. Each of the RBP-$\kappa_{8-435}$-peptide complexes were injected in triplicate on to chips with RBP-Jκ consensus nanolever or RBP-Jκ non-consensus nanolever bound. The Biosensor SwitchSense measured the dynamic response in real time as the RBP-$\kappa_{8-435}$-peptide complexes bound to the switch and was also able to measure a single movement of the nanolever. Switch analysis software was used to produce the curves from this data with the help of the technicians from Dynamic Biosensors.

*2.3.4.3 : Switchsense was used to determine the effect of DMSO on the conformation of RBP-$\kappa_{8-435}$*

RBP-$\kappa_{8-435}$ was thawed on ice and diluted into a 100nM stock with Buffer SwitchSense with and without 2% DMSO. RBP-$\kappa_{8-435}$ with and without 2% DMSO was injected in triplicate on to chips with RBP-Jκ consensus nanolevers bound. The Biosensor SwitchSense measured the dynamic response in real time as the RBP-$\kappa_{8-435}$ bound to the nanolevers. The machine automatically combined the data from the three repeats to produce the binding and disassociation curves. Switchanalysis software was used to produce the curves from this data with the help of the technicians from Dynamic Biosensors.

## 2.4 : Cell culture

### *2.4.1 : DG75 cell culture*

DG75 cells were chosen to overexpress EBNA3C and the EBNA3C mutants for the pull down as they were B cells (i.e the cells EBV immortalises during latency) with an EBV-negative background (to prevent EBNAs interfering with EBNA3C-RBP-Jκ interactions). DG75 cells were grown up in RPMI 1640 Medium with penicillin and streptomycin added at 37$^{o}$C. Cells were split 1 in 10 every three days to sustain the cell line.

### *2.4.2 : Cell counting*

DG75 cells were counted by mixing 10µl cells with at a 1:1 ratio with trypan blue, loading them onto Countess® Cell Counting Chamber Slides and using the Countess® Automated Cell Counter to count the cells and estimate cell viability.

### *2.4.3 : Electroporation of plasmids into B cells*

DG75 Cells were diluted 1 in 3 with fresh media the day before electroporation to ensure the cells would be in a growth phase for the electroporation. Cells were pelleted at 1300 rpm for 10 miuntes (TX-100 rotor, Thermo heraeus multifuge x3r centrifuge) and resuspended at 2 x $10^{7}$ cells/ml in serum-free media and aliquoted into 1 million cell aliquots into electroporation cuvettes. The cells were then incubated with 20µg of each of the vectors on ice for ten minutes then electroporated with a BioRad Gene Pulser II at 260V and 950 µF. The cells were then left to recover in serum free media at 37$^{o}$C for 30 minutes after which they were transferred to conditioned media cell culture flasks and incubated at 37$^{o}$C for 48 hours. After this the cells were pelleted at 1300rpm (Ch 500062PP rotor, VWR microstar 17 centrifuge), washed in PBS and then flash frozen in liquid nitrogen for storage at -80$^{o}$C. Some cells were kept aside for

western blot analysis to test whether they expressing the EBNA3C mutants. BL31 cells infected with EBV or MutuIII whole cell lysates were ran in parallel as EBNA3C positive controls.

## 2.5 : Crystallisation trials and structural biology

### *2.5.1 : Broad screen crystallisation trials of RBP-Jκ$_{8-435}$-DNA-EBNA2.26aa or RBP-Jκ$_{8-435}$-DNA-EBNA3C.33aa expressed in insect cells*

RBP-Jκ$_{8-435}$ was expressed in insect cells, purified with a $Co^{2+}$ column step, an anion exchange step, incubated with DNA (TTACT**GTGGGA**AAGA) and then passed through a size exclusion column. The DNA contained a RBP-Jκ consensus site and had a 2bp overhang. The RBP-Jκ$_{8-435}$-DNA complex was then concentrated to ~8mg/ml using Vivaspin 20 MWCO 30000 concentrator spun at 4000rpm (TX-100 rotor, Thermo heraeus multifuge x3r centrifuge). Concentrated RBP-Jκ$_{8-435}$-DNA complex was incubated with the EBNA2.26aa or EBNA3C.33aa peptide at a 1:1.5 ratio. The complex was loaded onto 98 well sitting drop plates at 4$^{o}$C or at room temperature with broad crystal screening conditions JCSG+, PacT, Proplex (molecular dimensions) and Natrix (Hampton research) using an Art Robins Phoenix robot. 200nL of complex was mixed with 200nL of crystallisation condition in each sitting droplet. The crystallisation plates were left at 4$^{o}$C or 20$^{o}$C to grow crystals. The plates were scored 7 days after being set up and images of crystals were taken using a leica microscope camera system and processed in leica imaging software.

### *2.5.2 : Resolution of crystal structure*

The crystal produced in Proplex C2 condition was fished then cryoprotected by incrementally increasing the percentage of PEG4000 to 30% and then flash freezed in

liquid nitrogen. The crystal was exposed to X-rays on the IO2 beamline at the Diamond Light Source where a full data set with a resolution of 3.6Å was acquired. Dr Mark Roe processed the scatter data. Initially Diamond XIA2 software was used to reduce the scatter data (Winter, 2010). Next Phaser software from the CCP4 package was used for the molecular replacement (McCoy *et al.*, 2007, Winn *et al.*, 2011). The phase data of the RBP-Jκ$_{8-435}$ and DNA (PDB: 3V79) from Choi et al's 2012 structure of the Notch 1 transcription complex was used for molecular replacement (Choi *et al.*, 2012). The initial refinements were completed in refmac software and the phenix suite was used for completion (Vagin *et al.*, 2004, Adams *et al.*, 2010). The image of the structure was taken in Pymol software (*The PyMOL Molecular Graphics System, Version 1.2r3pre, Schrödinger, LLC,* DeLano). Data processing statistics were produced by XIA2 software and the refinement statistics were calculated by the phenix suite (Adams *et al.*, 2010, Winter, 2010).

*2.5.3 : Modelling the EBNA2 peptide onto the crystal structure of RBP-Jκ$_{8-435}$ bound to RBP-Jκ consensus site.*

Wincoot software was used to mutate each of the residues of the RAM domain in the structure of the Notch1 transcription complex (Choi *et al.*, 2012) to residues of EBNA2, aligned by the WΦP motif (Emsley *et al.*, 2010). Rotamers of each of the EBNA2 residues were tested by eye to ensure that there were no steric clashes with the RBP-Jκ electron density. Our structure of RBP-Jκ$_{8-435}$ bound to RBP-Jκ consensus site and the structure of the Notch1 transcription complex with EBNA2 modelled onto the structure were over laid onto each other in pymol. The Notch1, RAM domain, RBP-Jκ, Mastermind and DNA from the structure of the Notch 1 complex (Choi *et al.*, 2012) were hidden leaving the structure of RBP-Jκ$_{8-435}$ bound to DNA with the EBNA2 peptide

modelled onto it. The same process was repeated to model EBNA2, EBNA3A, EBNA3B and EBNA3C onto the structure of the Notch1 transcription complex (Choi *et al.*, 2012) and the structure of CSL (Lag-1) bound to DNA with Lin-12 RAM peptide (PDB: 3BRD) (Friedmann *et al.*, 2008). The models were edited and imaged in pymol (*The PyMOL Molecular Graphics System, Version 1.2r3pre, Schrödinger, LLC,* DeLano).

*2.5.4 : Broad screen crystallisation trials of the RBP-Jκ$_{8-435}$-DNA-EBNA2.14aa complex expressed in E.coli cells*

RBP-Jκ$_{8-435}$ was expressed in *E.coli*, purified with a $Co^{2+}$ column step, an anion exchange step, incubated with DNA (TTACT**GTGGGA**AAGA) and then passed through a size exclusion column. The DNA contained a RBP-Jκ consensus site and had a 2bp overhang. The RBP-Jκ$_{8-435}$-DNA complex was then concentrated to ~10mg/ml using Vivaspin 20 MWCO 30000 concentrator spun at 4000rpm (TX-100 rotor, Thermo heraeus multifuge x3r centrifuge). Concentrated RBP-Jκ$_{8-435}$-DNA complex was incubated with the EBNA2.14aa 1:4 protein to peptide ratio. The complex was loaded onto 96 well sitting drop plates at room temperature with broad crystal screening conditions JCSG+, PacT, Proplex (molecular dimensions) and Natrix (Hampton research) using an Art Robins Phoenix robot. 200nL of complex was mixed with 200nL of crystallisation condition in each sitting droplet. The crystal trials were left in a 20$^{o}$C incubator to grow crystals. The plates were checked for crystals daily for the first 7 days then weekly after this. Images of crystals were taken using a leica microscope camera system and processed in leica imaging software.

*2.5.5 : Production of deepwell blocks of optimisation conditions and set up of optimisation plate crystal trials of RBP-Jκ$_{8-435}$-DNA-EBNA2.14aa complex expressed in E.coli cells.*

The crystal conditions designed in optimisation plates 1 and 2, Natrix conditions, published conditions and the PEG screens were manually pipetted into 2ml 96 well deep well blocks and stored at 4$^{o}$C. The crystallisation conditions were manually pipetted from the deep well blocks into buffer wells in 48 well sitting drop plates then Douglas Instruments Oryx8 robot was used to load 200nL of crystallisation buffer and 200nL of complex onto the sitting drop wells. The plates were sealed and incubated at 20$^{o}$C then checked for crystals everyday for the first 7 days then weekly after this. Images of crystals were taken using a leica microscope camera system and processed in leica imaging software.

*2.5.6 : Production of crystal seed for crystallisation trials*

The Seed Bead kit from Hampton research was used to generate seed stocks of crystals grown in optimisation plate 1 C2 and Natrix G10. Crystals were pipetted in to the Eppendorf tubes with the seed bead and the crystallisation buffer from the wells and was vortexed and put on ice three times. The seed stock was serially diluted with more crystallisation buffer then flash frozen in liquid nitrogen. Seeded crystallisation trials were set up in 48 well sitting drop plates with the Douglas Instruments Oryx8 robot which was used to load 180nL of crystallisation buffer, 200nL of protein complex and 20nL of seed stock onto the sitting drop wells. The plates were sealed and incubated at 20$^{o}$C then checked for crystals everyday for the first 7 days then weekly after this. Images of crystals were taken using a leica microscope camera system and processed in leica imaging software.

*2.5.7 : Proplex A8, Proplex A8 PEG400 and PacT E7 additive screens to crystallise RBP-Jκ$_{8-435}$-DNA-EBNA2.14aa complex expressed in E.coli cells.*

Proplex A8, Proplex A8 PEG400 or PacT E7 was pipetted into 96 deep well blocks so that they could be mixed with molecular dimension additive screen and loaded with RBP-Jκ$_{8-435}$-DNA-EBNA2.14aa complex expressed in *E.coli* cells into 96 well hanging drop plates. 200nL of additive screen mixed with crystallisation buffer was loaded with 200nL of Jκ$_{8-435}$-DNA-EBNA2.14aa complex at 2.5mg/ml, 5mg/ml or 20mg/ml using the Art Robins Phoenix robot. The plates were sealed and incubated at 20$^{o}$C then checked for crystals everyday for the first 7 days then weekly after this.

# Chapter 3 : Results chapter

## Chapter 3.1 : Optimisation of the purification of RBP-Jκ expressed in SF9 insect cells and *E.coli*

We intitially attempted to express RBP-Jκ variant 2 as this was the isoform of RBP-Jκ predominantly expressed in B-cells and would therefore be the most likely RBP-Jκ isoform to interact with EBV transcription factors (Masashi Kawaichi, 1991, Amakawa R, 1992, Kenia G. Krauer, 1999). We also used a C-terminally His-tagged RBP-Jκ$_{8-435}$ as this had previously been used to purify and crystallise human RBP-Jκ (Wilson and Kovall, 2006).

EBNA2, EBNA3A, EBNA3B and EBNA3C have been shown to bind to RBP-Jκ and interactions between EBNA2, EBNA3A or EBNA3C and RBP-Jκ have been shown to be essential to sustaining EBV immortalised cell lines (Waltzer *et al.*, 1996, Zhao *et al.*, 1996, Zhao *et al.*, 2011). EBNA2 and EBNA3s binding to the human genome is facilitated by RBP-Jκ and it is clear that RBP-Jκ plays a key role in enabling EBV TFs to manipulate host gene expression (McClellan *et al.*, 2013a, Kalchschmidt *et al.*, 2016, Lu *et al.*, 2016).

EBNA2 has been shown to activate genes through EBNA2 binding and this activation is inhibited by EBNA3A, EBNA3B and EBNA3C (Ling and Hayward, 1995, Johannsen *et al.*, 1996, Robertson *et al.*, 1996a, Waltzer *et al.*, 1996, Calderwood *et al.*, 2011). EBNA2 and EBNA3s binding to RBP-Jκ is mutually exclusive and they bind competitively to human genome sites (McClellan *et al.*, 2013a). However, there is no molecular information to explain how EBNA2 and EBNA3C antagonistically hijack and control

RBP-Jκ gene expression. We aimed to express and purify RBP-Jκ to study the thermodynamics and nature of the EBNA-RBP-Jκ interactions and to attempt obtain structural information on the EBNA domain RBP-Jκ complexes.

### 3.1.1.1 : Producing recombinant baculovirus to express RBP-Jκ variant 2 and RBP-Jκ$_{8-435}$ in Sf9 insect cells

We used PCR to amplify C-terminally His-tagged RBP-Jκ$_{8-435}$ cDNA from a bacterial vector (pET28b.JK.8-435) produced by a summer student in Michelle West's laboratory (Figure 3.1A). We digested the RBP-Jκ$_{8-435}$ PCR product and the the destination baculovirus expression vector (pFastBac.CP.17.2) (Figure 3.1B). The pFastBac17.2 vector was a pFastBac co-expression vector that had been engineered in the laboratory by Dr Christomous Prodromou group to contain two multiple cloning sites (MCS), p10 MCS containing a N-terminal His-tag and polyhed MCS which contained a cleavable N-terminal Strep-II tag (Figure 2.1). P10 and polyhed referred to the promoters of each of the MCS. The restriction sites that were chosen to ligate the C-terminally His-tagged RBP-Jκ$_{8-435}$ cDNA into the pFastBac17.2 vector would remove the N-terminal His tag from the p10 MCS so that RBP-Jκ$_{8-435}$ would only be expressed with a C-terminal His-tag. Once the C-terminally His-tagged RBP-Jκ$_{8-435}$ cDNA had been ligated into the pFastBac17.2 vector a diagnostic restriction digest was undertaken to identify successful plasmid clones (Figure 3.1C). Clones C.1 and C.3 produced products with sizes close to the predicted size of the insert (1311bp) (Figure 3.1C). However, sequencing showed that only C3 contained the C-terminally His-tagged RBP-Jk$_{8-435}$ cDNA correctly inserted into the pFastBac17.2 vector. This plasmid was termed pF.JK.8-435.

RBP-Jk variant 2 had already been cloned into pFastBac.CP.17.2 by a Masters student from Dr Christomous Prodromou group (pF.JK.V2). However, a different cloning strategy to the pF.JK.8-435 vector was used which meant the RBP-Jκ variant 2 would be expressed with an N-terminal His-tag.

The vectors containing N-terminally His-tagged RBP-Jκ variant 2 and C-terminally His-tagged RBP-Jκ$_{8-435}$ were transposed into bacmids that would be used to generate recombinant baculovirus. The plasmids were initially transformed into MAX efficiency DH10Bac$^{Tm}$ *E.coli*. These cells not only contained the destination bacmid but also helper vectors that facilitated the transposition of the pFastBac vectors into the bacmid (Chapter 2.2.1). Successful transpositions were identified by blue-white screening as the bacmid contained a gene expressing LacZ peptide. These colonies were restreaked and a diagnostic PCR was performed, which amplified the bacmid DNA across both the translocation sites (Figure 3.2). All the bacmids tested gave PCR products of the correct predicted size, 4099bp and 3965bp for RBP-Jκ variant 2 and RBP-Jκ$_{8-435}$ respectively (with the exception of pF.JK.8-435 C1)(Figure 3.2).

Next the bacmids containing N-terminally His-tagged RBP-Jκ variant 2 and C-terminally His-tagged RBP-Jκ$_{8-435}$ were transfected into Sf9 insect cells to produce recombinant baculovirus. After the transfection the media containing the P1 recombinant baculovirus was extracted and the Sf9 insect cells were analysed for RBP-Jκ expression by western blot (Figure 3.3). Both N-terminally His-tagged RBP-Jκ variant 2 (JK.V2)(54kDa) and C-terminally His-tagged RBP-Jκ$_{8-435}$ (JK.8-435)(49kDa) were expressed, however RBP-Jκ variant 2 had much lower levels of expression compared to RBP-Jκ$_{8-435}$ (Figure 3.3).

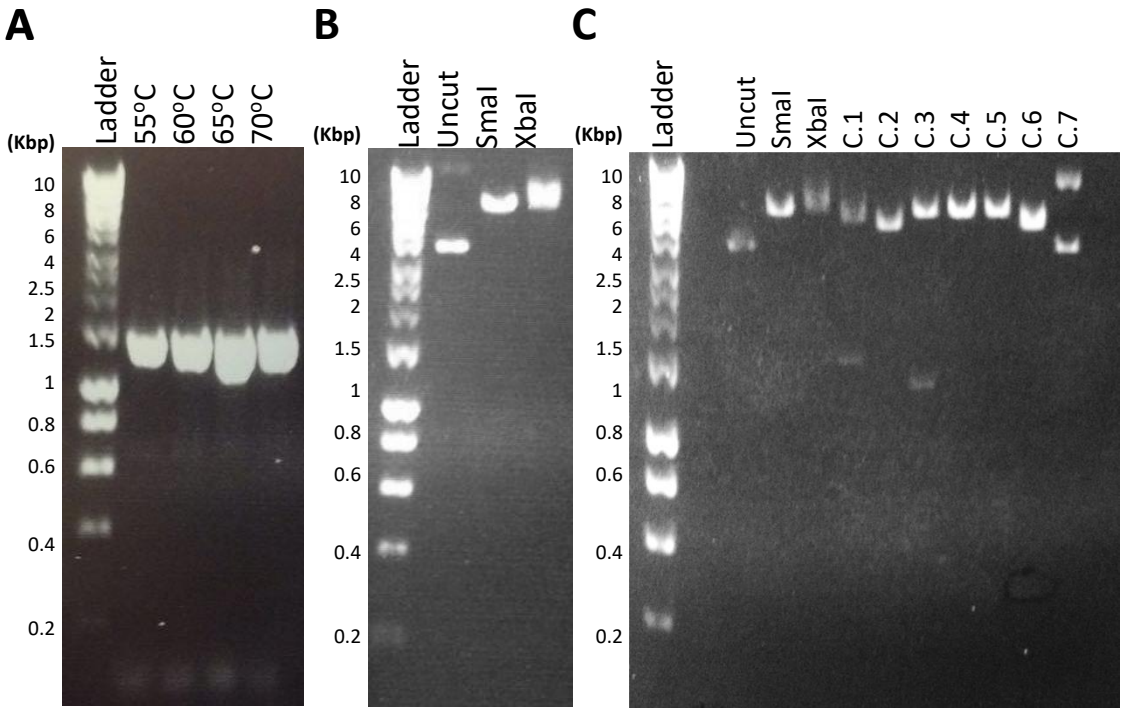


**Figure 3.1. Diagnostic Gels for cloning C-terminally His-tagged RBP-Jk$_{8-435}$ from a pET28b vector into a pFastBac vector. A.** 1% Agarose Gel showing PCR of cDNA encoding C-terminally His-tagged RBP-Jk$_{8-435}$ (1311bp expected size) from pET28b.JK.8-435. The temperatures indicate the temperature used during the annealing step. **B.** 1% agarose gel showing restriction digests of the pFastBac17.2 vector. **C.** Diagnostic restriction digests of different clones following ligation of the RBP-Jk$_{8-435}$ PCR product and pFastBac17.2. Clones 1 and 3 produced products with sizes proximal to the predicted size of the insert and were sent for sequencing. Clone 3 was concluded to be the correct product.

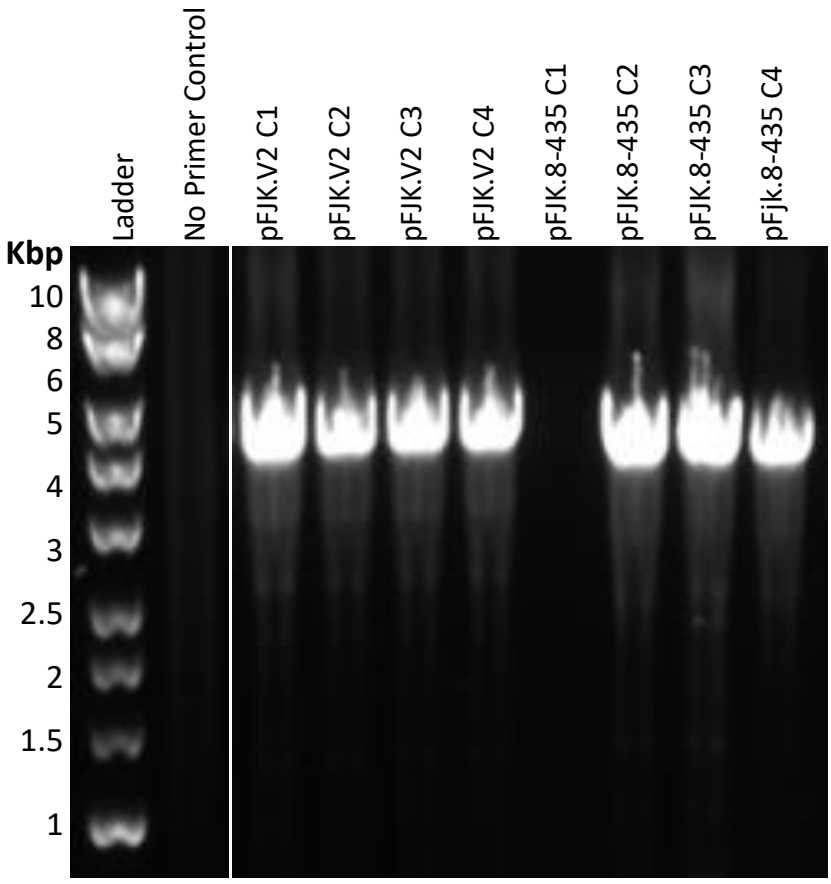


**Figure 3.2. Diagnostic PCR showing successful translocation of pFastBac vectors containing N-terminally His-tagged RBP-Jk variant 2 and C-terminally His-tagged RBP-Jk$_{8\text{-}435}$ into bacmids.** The pFastBac Vectors containing N-terminally His-tagged RBP-Jk variant 2 and C-terminally His-tagged RBP-Jk$_{8\text{-}435}$ were transposed into bacmids ready to produce recombinant baculovirus. Diagnostic PCRs amplified entire transposed region in the bacmid using pUC M13 primers and were run on 1% agarose gel with a 1Kb ladder. Expected band sizes for transposed RBP-Jk variant 2 and RBP-Jk$_{8\text{-}435}$ were 4099bp and 3965bp respectively.

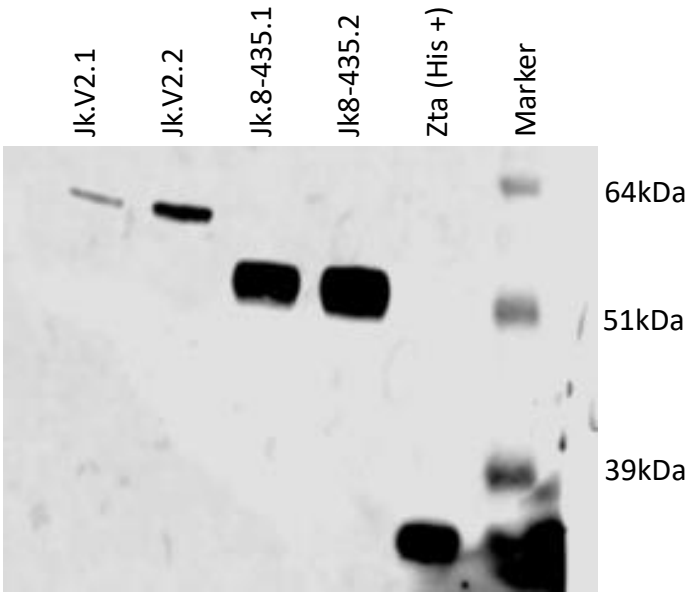


**Figure 3.3. Western blot analysis of Sf9 insect cells infected with of N-terminally His-tagged RBP-Jk variant 2 or C-terminally His-tagged RBP-Jk$_{8-435}$ P1 baculovirus.** Bacmids containing pFJK.V2 or pFJK.8-435 were transfected into Sf9 insect cells and cell lysates were prepared after 72 hours. Samples were ran on a 10% Tris-SDS gel and probed with an anti-His antibody. Purified His-tagged Epstein-Barr virus ZTA protein was used as a positive control. Expected band sizes for N-terminally His-tagged RBP-Jk variant 2 and C-terminally His-tagged RBP-Jk$_{8-435}$ were 54kDa and 49kDa respectively.

### 3.1.1.2 : Ability to pull down RBP-Jκ with nickel beads is dependent on which terminal the His-tag is attached to.

Initially we calculated the optimal time to harvest the insect cells post transfection by infecting them with recombinant baculovirus expressing N-terminally His-tagged RBP-Jκ variant 2 or C-terminally His-tagged RBP-Jκ$_{8-435}$ and taking samples each day for western blot analysis (Figure 3.4). It is important to harvest infected cells before cell viability drops below 90% to avoid losing significant amounts of protein yield. C-terminally His-tagged RBP-Jκ$_{8-435}$ reached peak expression by day 2 and by day 3 the insect cells appear to begin lysing significantly reducing the protein yield (Figure 3.4). N-terminally His-tagged RBP-Jκ variant 2 also reached peak yield by day 2 (Figure 3.4).

We next used nickel beads to attempt to purify N-terminally His-tagged RBP-Jκ variant 2 and C-terminally His-tagged RBP-Jκ$_{8-435}$ from a small scale insect cell infection. Although, on a stained gel, the RBP-Jκ V2 was visible in cell lysates, it did not bind to nickel beads (Figure 3.5). This was evident on western botting with anti-his antibody (Figure 3.4).

In contrast, C-terminally His-tagged RBP-Jκ$_{8-435}$ successfully bound to the nickel beads and could be eluted with imidazole (Figure 3.6). This was confirmed by western blotting (Figure 3.4). To estimate the concentration of RBP-Jκ$_{8-435}$ we ran eluate from the nickel bead pull down of C-terminally His-tagged RBP-Jκ$_{8-435}$ against known concentrations of bovine serum albumin (BSA) on an SDS-PAGE gel (Figure 3.7). We estimated that the yield from a 6L preperation would be approximately 0.6mg of protein.

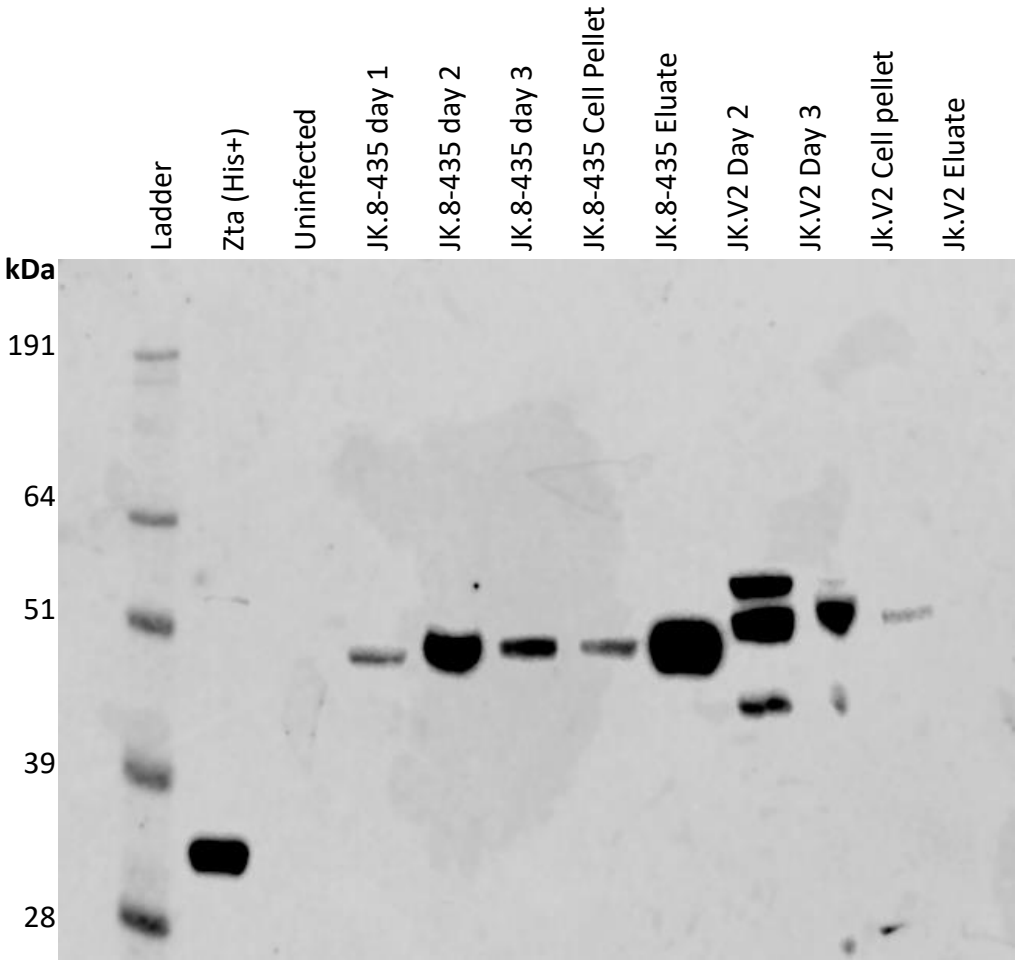


**Figure 3.4. Western blot analysis of a small scale grow up of Sf9 insect cells infected with N-terminally His-tagged RBP-Jk variant 2 or C-terminally His-tagged RBP-Jk$_{8-435}$ P3 baculovirus.** The sf9 cells were and incubated at 27$^{o}$C in rotating incubator. Samples were taken from the grow up 1, 2 and 3 days after infection, run on a 10% Bis-Tris SDS gel then probed with an anti-His antibody. The Sf9 insect cells were lysed after 3 days of expression and bound to Ni-beads, washed, then eluted proteins using imidazol and ran on a SDS-PAGE gel and probed for with anti-his anti-body. Purified His-tagged Epstein-Barr virus ZTA protein was used as a positive control. Expected sizes for N-terminally His-tagged RBP-Jk variant 2 and C-terminally His-tagged RBP-Jk$_{8-435}$ were 54kDa and 49kDa respectively.

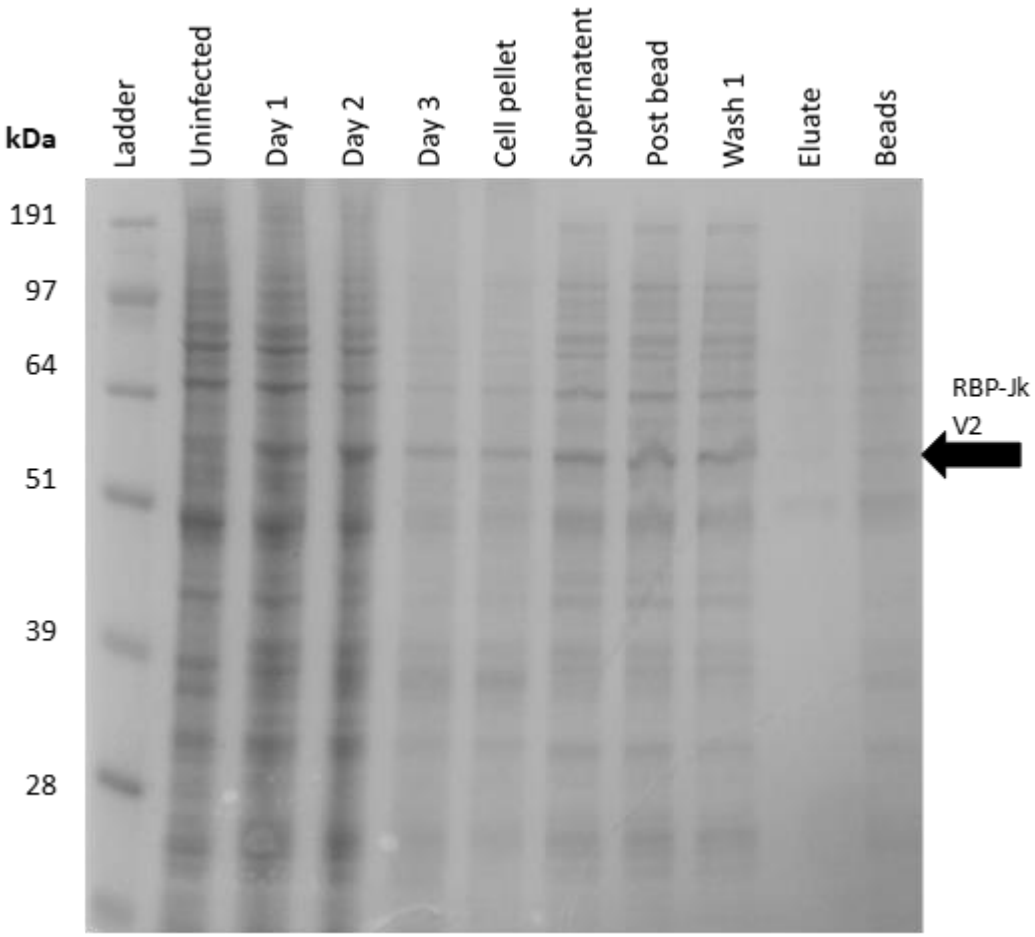


**Figure 3.5. Nickel bead pull down of RBP-JK variant 2 expressed in Sf9 insect cells.** Sf9 cells were infected with N-terminally His-tagged RBP-Jk Variant 2 baculovirus (JK.V2) and incubated at 27$^{o}$C in shaking incubator for 3 days. Samples were taken each day, then spun down and harvested. Cells were dounce homogenised and the lysate was separated from the pellet and incubated on Ni-beads. Ni-beads were washed in buffer A then incubated in the elution buffer B. Samples from each step were boiled in GSB and run on a 10% Bis-Tris SDS gel then stained using Coomassie Blue. Expected band size for N-terminally His-tagged RBP-Jk variant 2 is 54kDa.

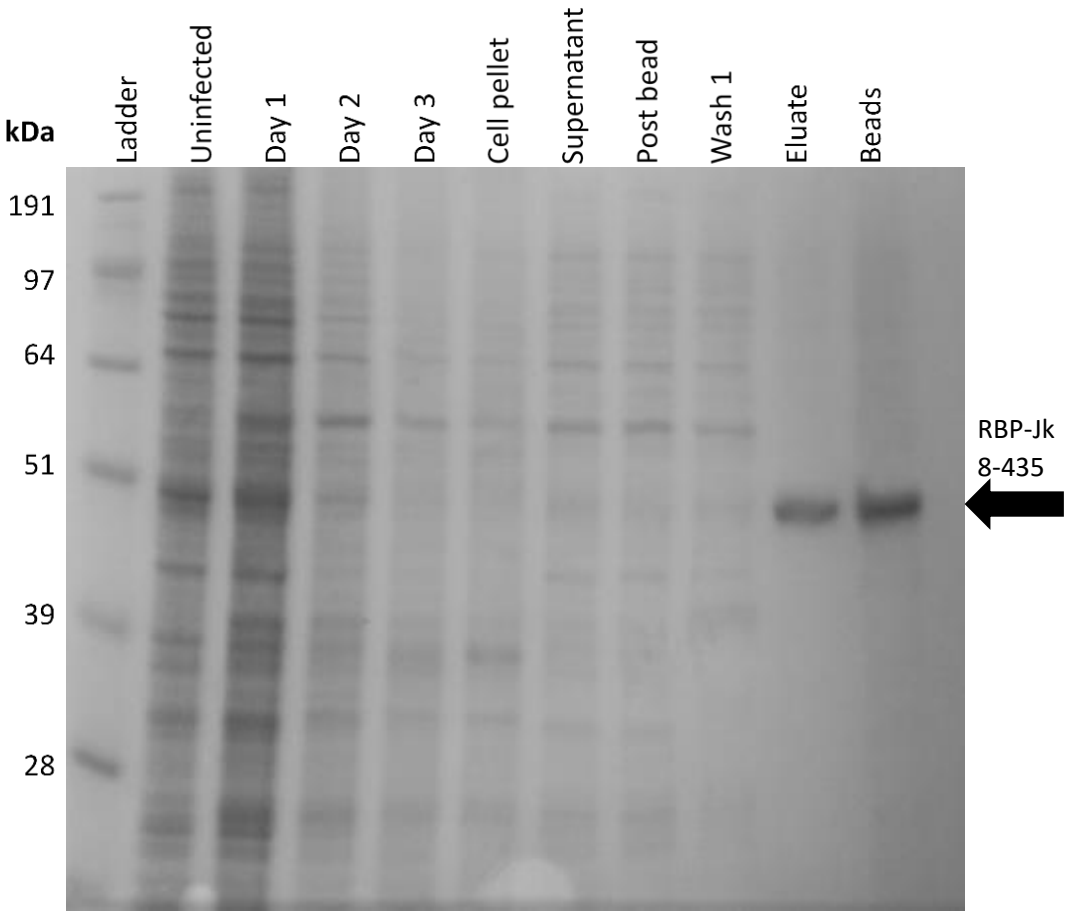


**Figure 3.6. Nickel bead pull down of RBP-Jk$_{8-435}$ expressed in Sf9 insect cells.** Sf9 cells were infected with C-terminally His-tagged RBP-Jk$_{8-435}$ baculovirus (JK.8-435) and incubated at 27$^{o}$C in shaking incubator for 3 days. Samples were taken each day, then spun down and harvested. Cells were dounce homogenised and the lysate was separated from the pellet and incubated on Ni-beads. Ni-beads were washed in buffer A then incubated in the elution buffer B. Samples from each step were boiled in GSB and run on a 10% Bis-Tris SDS gel then stained using Coomassie Blue. Expected band size for C-terminally His-tagged RBP-Jk$_{8-435}$ is 49kDa.

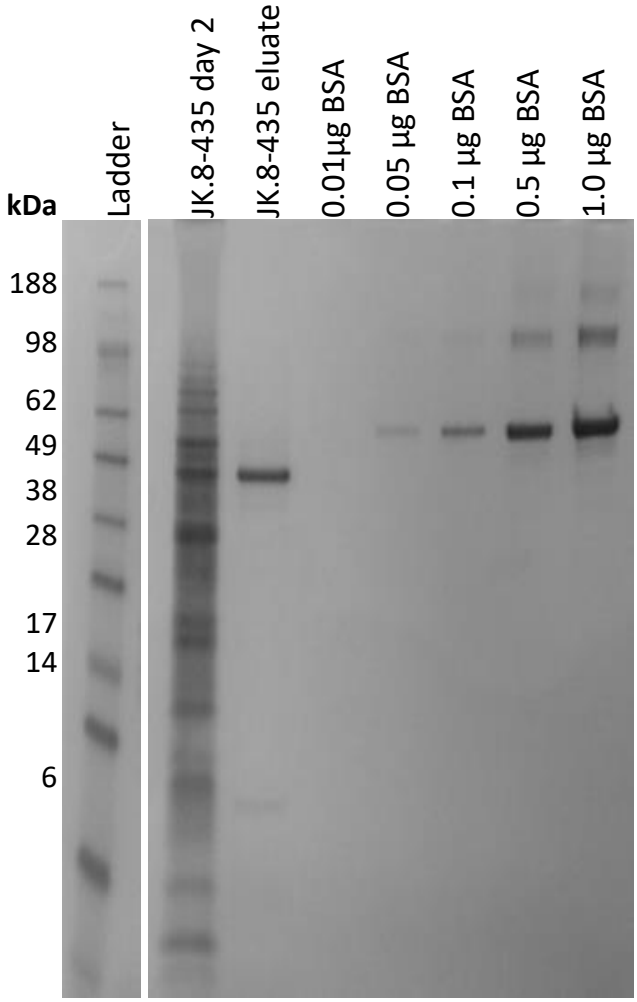


**Figure 3.7. Quantification of RBP-Jk$_{8-435}$ levels expressed in Sf9 cells.** 5µL from 50µL eluate of RBP-Jκ$_{8-435}$ was analysed. BSA standard were loaded to estimate the concentration of RBP-Jκ$_{8-435}$. Samples were boiled in GSB and run on a 10% Bis-Tris SDS gel then stained using Coomassie Blue. Expected band size for C-terminally His-tagged RBP-Jk$_{8-435}$ is 49kDa.

### 3.1.1.3 : Initial Purification of C-terminally His-tagged RBP-Jκ$_{8-435}$ expressed in Sf9 insect cells.

We scaled up the insect cell culture from a 45ml culture (Figure 3.7) to a 3L culture in order to optimise the large scale purification of C-terminally His-tagged RBP-Jκ$_{8-435}$. RBP-Jκ$_{8-435}$ was purified from the lysate using a 1ml $Ni^{2+}$ HistrapFF column and was eluted using an increasing concentration of imidazole (Figure 3.8A). The chromatogram clearly shows the elution peak of C-terminally His-tagged RBP-Jκ$_{8-435}$ as the concentration of imidazole is increased (Figure 3.8B). There were also a large amount of impurities shown binding and eluting from the Histrap column (Figure 3.8A).

The next step in the purification was to pass the eluates from the $Ni^{2+}$ step through a 26/10 desalt column to reduce the salt concentration from 500Mm to 100mM. This was carried out to ensure that the C-terminally His-tagged RBP-Jκ$_{8-435}$ had a net positive charge and would be able to bind to the MonoQ 5/50 anion exchange column.

C-terminally His-tagged RBP-Jκ$_{8-435}$ was eluted from MonoQ 5/50 anion exchange column as an increasing concentration of NaCl was passed though the column (Figure 3.9). A marked reduction in impurities was seen after this step but C-terminally His-tagged RBP-Jκ$_{8-435}$ required further purification for crystal trials (Figure 3.9A). The chromatogram of the MonoQ purification step showed that C-terminally His-tagged RBP-Jκ$_{8-435}$ was eluted in two peaks (Figure 3.9A and B). This could have been due to post translational modifications, such as phosphorylation, that could have occurred whilst C-terminally His-tagged RBP-Jκ$_{8-435}$ was being expressed in the Sf9 insect cells. Because we wanted a homogenous population of C-terminally His-tagged RBP-Jκ$_{8-435}$

for our crystallisation trials, we only pooled the eluates from the larger peak for the size exclusion step.

In order increase the purity of C-terminally His-tagged RBP-Jκ$_{8-435}$ we passed the eluates from the anion exchange step through a S200 10/30 size exclusion column (Figure 3.10). The broad elution peak produced was quite wide which could indicate the presence of multiple conformations of protein.

To determine whether the purified RBP-Jκ$_{8-435}$ we produced was functional we carried an electrophoretic mobility shift assay (EMSA) to test whether RBP-Jκ$_{8-435}$ expressed could bind specifically to the RBP-Jκ DNA consensus site (Figure 3.11). When increasing amounts of C-terminally His-tagged RBP-Jκ$_{8-435}$ was incubated with an excess of DNA containing a RBP-Jκ consensus site a shift indicative of RBP-Jκ binding was observed (Figure 3.11). However, when the RBP-Jκ consensus site was mutated from GTGGGA to GTGGCT no visible band shift was detectable (Figure 3.11) The C-terminally His-tagged RBP-Jκ$_{8-435}$ produced was therefore able to specifically bind to its cognate site *in vitro* (Figure 3.11).

At the end of the purification process we had obtained approximately 100µL of 8mg/ml of relatively pure C-terminally His-tagged RBP-Jκ$_{8-435}$, a total yield of approximately 0.8mg of protein. We therefore sought to increase the yield of RBP-Jκ$_{8-435}$ to provide enough protein for biophysical and crystallisation studies.

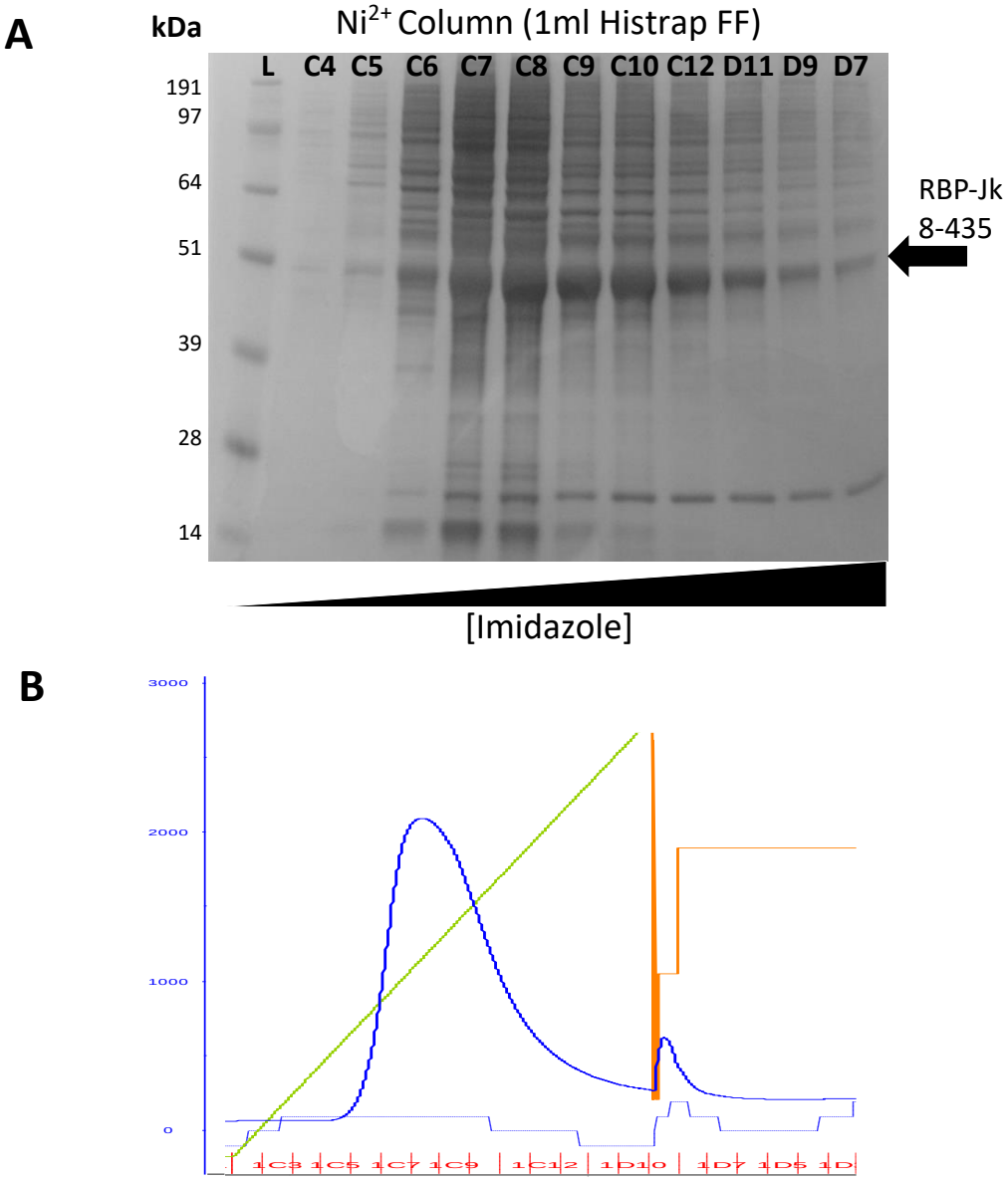


**Figure 3.8. Analysis of $Ni^{2+}$ column (1ml HisTrap FF) purification step of His tagged RBP-$Jk_{8-435}$ expressed in 3 litres of Sf9 cells. A.** Coomassie stained gel showing elution fractions from $Co^{2+}$ column (1ml HisTrap FF) as an increasing concentration of imidazole was passed through. 10µL from each 1ml fraction was mixed with 10µl GSB buffer and boiled for anlysis. **B.** Chromatogram from the Histrap step produced in Unicorn software. Shown is protein (blue), concentration of buffer B/ [imidazole] (green), flow rate (orange) and [salt] (in brown). The jump of flow in the middle was due to the column over pressurising and the AKTA pausing. Fractions C5 to D7 were pooled for further purification.

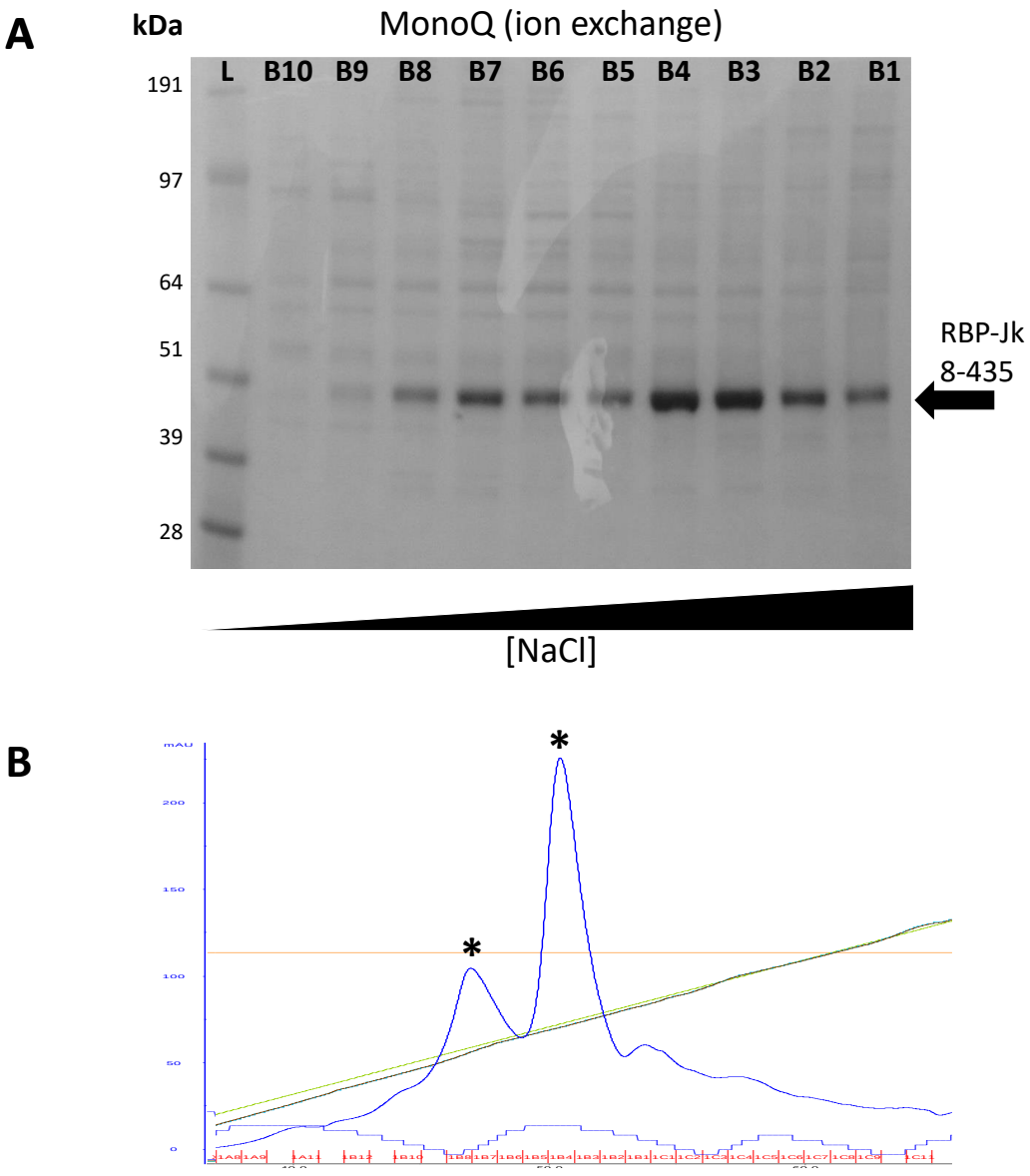


**Figure 3.9. MonoQ column purification of C-terminally His-tagged RBP-Jk$_{8-435}$. A.** Coomassie stained gel showing fractions from the MonoQ 10/50 column from GE healthcare as an increasing [NaCl] is passed through. 10µL from each 1ml of eluent was mixed with 10µl GSB buffer, boiled and loaded onto the 4-12% Bis-Tris SDS page gel where it was run MOPS buffer. **B**. Chromatogram showing eluates from monoQ. Shown is protein (blue), concentration of buffer D/ [NaCl] (green), flow rate (orange) and [salt] (in brown). Peaks containing RBP-Jκ have been marked with an astrix. Fraction B5 to B1 were pooled for further purification.

**A**

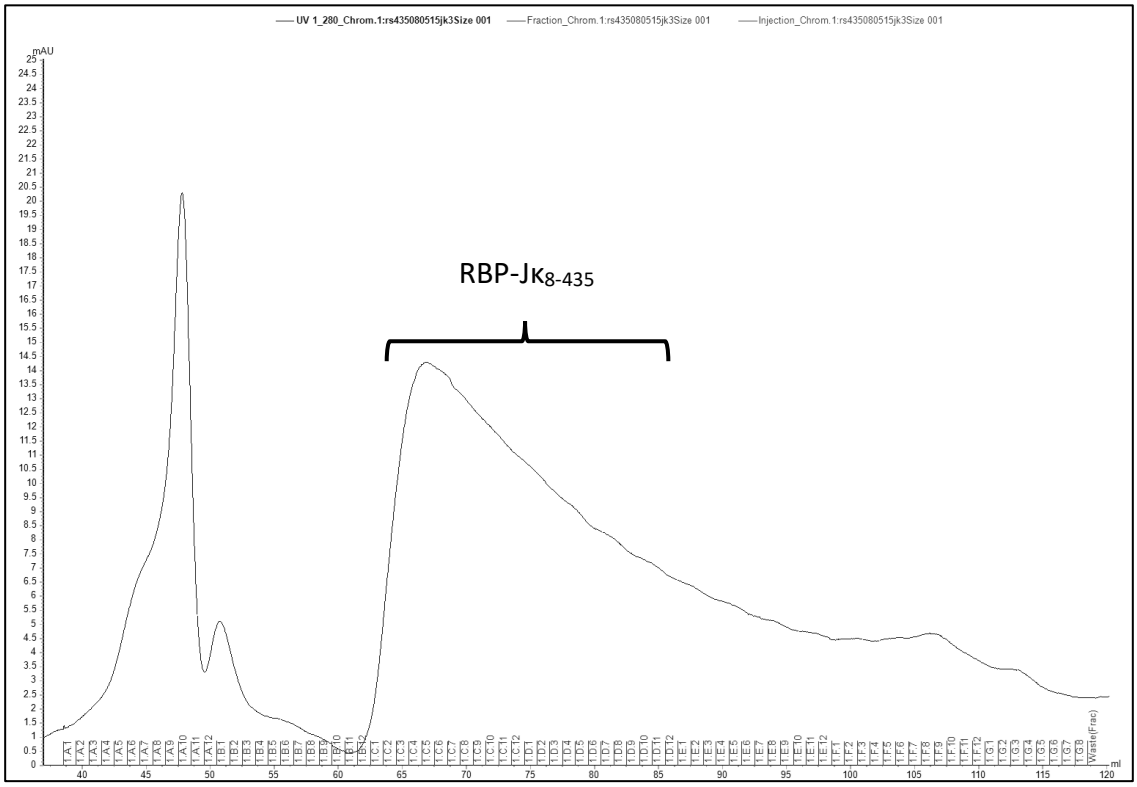


**B**

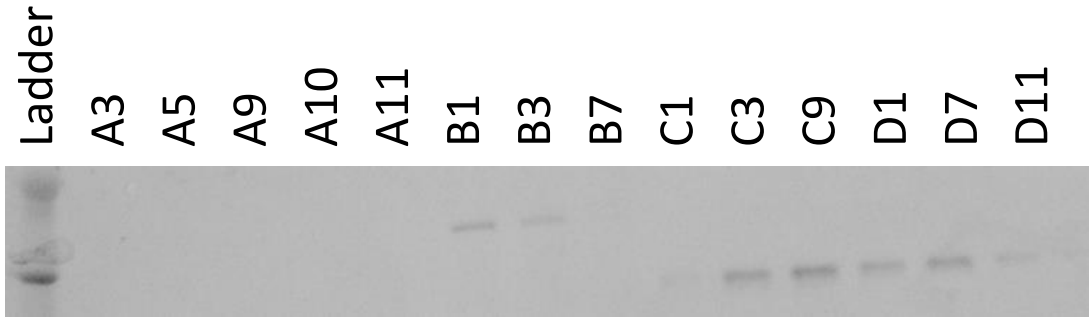


**Figure 3.10. Size exclusion purification step of C-terminally His-tagged RBP-Jk$_{8-435}$ expressed in sf9 cells. A.** Chro,atogram of size exclusion step. **B.** RBP-Jk$_{8-435}$ was passed through a Superdex S200 10/30 from GE healthcare calibrated in Buffer C. Coomassie stained gel of samples of each fraction. Bands in B1 to B3 are impurities and bands in C1 to D11 are RBP-Jk$_{8-435}$ and were used for crystallisation.

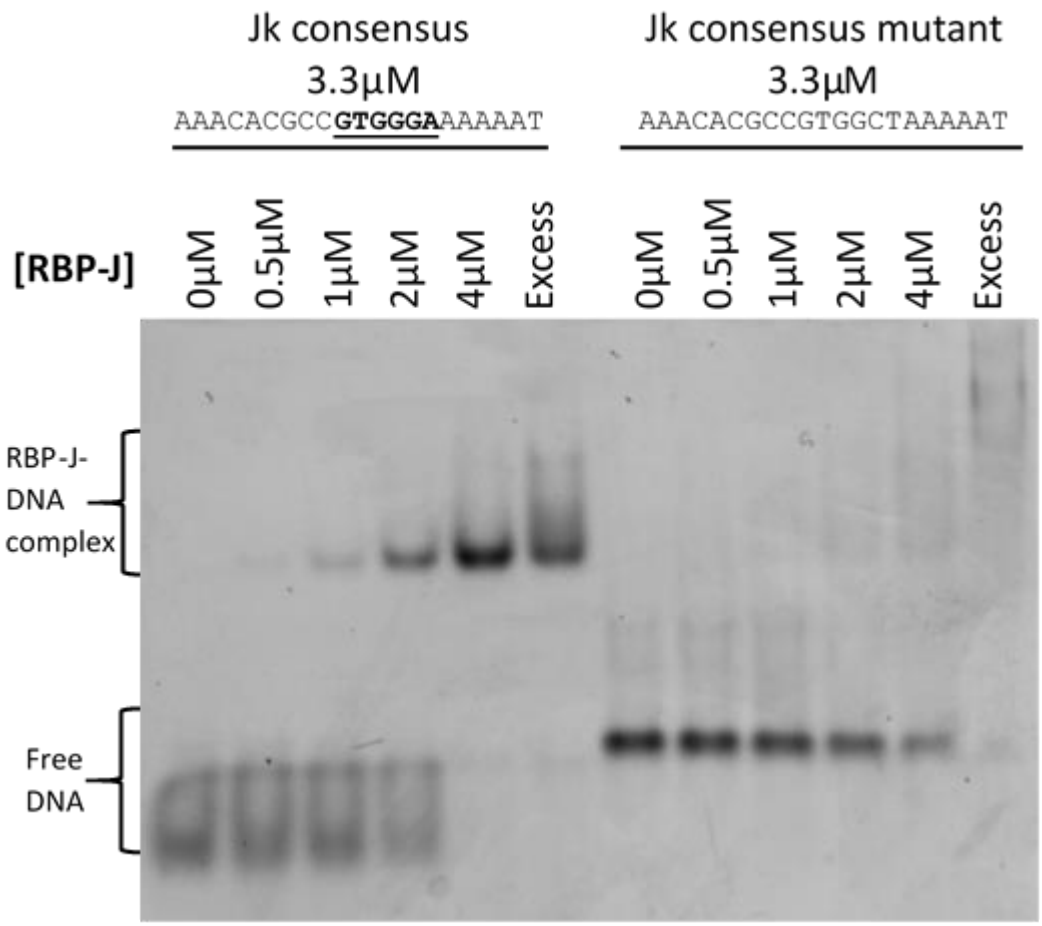


**Figure 3.11. Electro mobility shift assay of RBP-Jk$_{8-435}$ binding to DNA.** Double stranded oligonucleotides containing RBP-Jk consensus site or a mutant site were incubated with increasing amounts of C-terminally His-tagged RBP-Jk$_{8-435}$ then run on a 6% DNA retardation gel in 0.5x TBE buffer. Gels were stained using Gel Safe Red and bands were visualised on a Licor machine.

### 3.1.1.4 : Optimisation of the Purification of C-terminally His-tagged RBP-Jκ$_{8-435}$ expressed in Sf9 insect cells.

By increasing the number of plunges we dounced homogenised the lysate and increasing the 3L prep to a 5L prep we increased the yield to approximately 2mgs, however we found that the predominant factor dictating protein yield was the quality of the recombinant baculovirus used to infect the insect cells. We were however able to make some improvements to the purification method to optimise the yield and purity.

To reduce the background binding of impurities in the first purification step we switched from a $Ni^{2+}$ column (1ml Histrap FF) to a $Co^{2+}$ column (5ml Talon). Not only would the larger column potentially bind more C-terminally His-tagged RBP-Jκ$_{8-435}$ but whilst $Co^{2+}$ beads do not bind His-tagged proteins as tightly, they do bind more specifically to His-tagged proteins. $Co^{2+}$ ions co-ordinate their bonds in the same orientation as $Ni^{2+}$ which allows them to bind to His-tags. However, the net charge of the atom is weaker which does mean that $Co^{2+}$ ions have a weaker interaction with His-tags however this also significantly reduces binding to impurities improving the purity of the eluates. We also increased the volume of buffer used in the wash step from 20ml of buffer to 100ml to help remove the impurities.

The eluates from the $Co^{2+}$ column purification step contained significantly less background binding of impurities compared to the $Ni^{2+}$ column purification step (Figure 3.12A and 3.8A). We also increased the volume of the wash step in the MonoQ purification step from 5ml to 10ml, which allowed us to produce a pure enough sample

of C-terminally His-tagged RBP-Jκ$_{8-435}$ (Figure 3.12B) so that we could pool eluates directly from this step for Isothermal titration calorimetry (ITC) analysis.

To improve the homogeneity of the C-terminally His-tagged RBP-Jκ$_{8-435}$ for further purification we incubated the RBP-Jκ consensus site DNA (TTACT**GTGGGA**AAGA) before the size exclusion step so that any DNA that did not bind to RBP-Jκ$_{8-435}$ would be separated in the column. We also found that by incubating the RBP-Jκ consensus site DNA with C-terminally His-tagged RBP-Jκ$_{8-435}$ the elution peak from the size exclusion step was significantly sharpened indicating that DNA binding drove the RBP-Jκ sample into a single conformation (Figure 3.12C and 3.13). We also tested the effect of incubating a peptide of EBNA2 containing the RBP-Jκ motif (EBNA2.26aa) to see if this improved the homogeneity of C-terminally His-tagged RBP-Jκ$_{8-435}$ (Figure 3.13). The peptide had little effect on sharpening the elution peak of C-terminally His-tagged RBP-Jκ$_{8-435}$ (Figure 3.13). We therefore decided to incubate C-terminally His-tagged RBP-Jκ$_{8-435}$ with only the RBP-Jκ consensus site DNA before the size exclusion step.

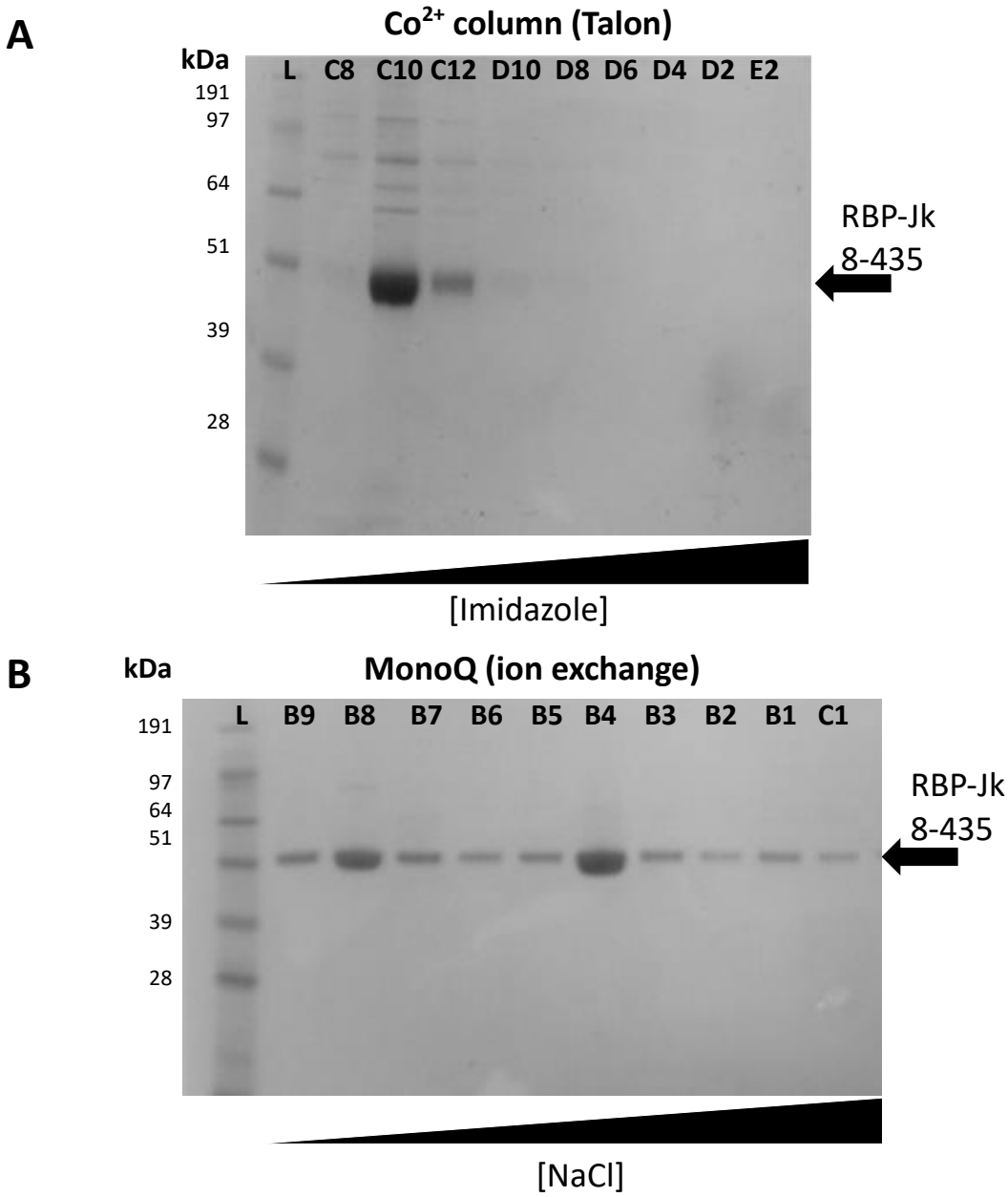


**Figure 3.12. Results of optimisation of purification of C-terminally his-tagged RBP-Jk$_{8-435}$ A.** Coomassie stained gel of $Co^{2+}$ column (TalonFF 5ml) Step. 10µL from each fraction was taken as an increasing [imidazole] was passed through the $Co^{2+}$ column. Well C8 to D10 were pooled for ion exchange purification step. **B** Coomassie stained gel of MonoQ 10/50 step as an increasing gradient of [NaCl] was passed through. B6 to C1 were pooled for further puriciation or use in thermodynamic experiments.

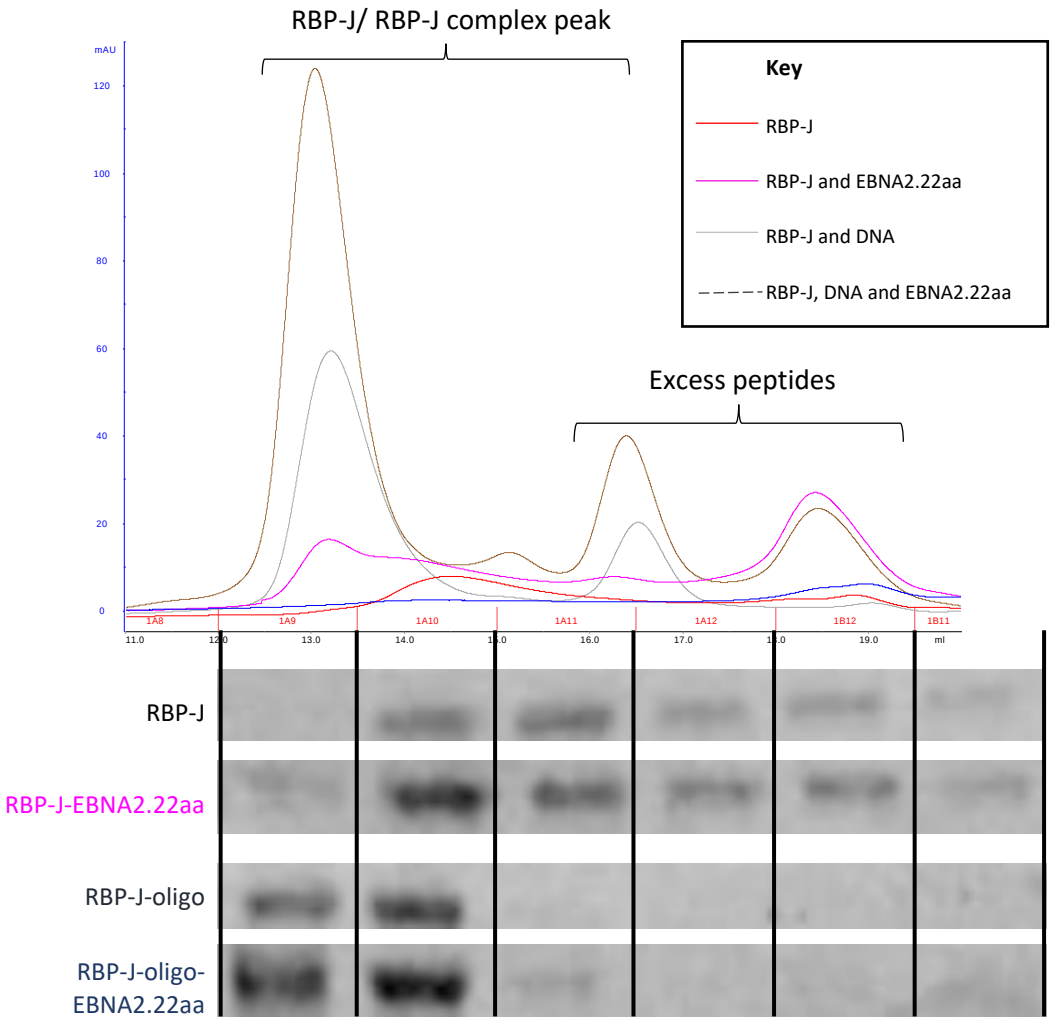


**Figure 3.13. Size exclusion step when C-terminally His-tagged RBP-Jk$_{8-435}$ is incubated with DNA and/or peptide before passing through the column.** RBP-Jk$_{8-435}$ was incubated with DNA and/or peptide with a ratio of 1:1.5 for 1 hour on ice and concentrated in a Viva spin MW30000 then injected into the Superdex 200 10/30 on an AKTA purifier. Above is the chromatogram from each run. Below is a Coomassie stained of each fraction from each run where 10µL from each fraction was mixed with 10µl GSB buffer, boiled and loaded onto the 4-12% Tris SDS page gel where it was run in MOPS buffer.

### 3.1.1.5 : Investigation into the post translational modifications of C-terminally His-tagged RBP-Jκ$_{8-435}$ expressed in insect cells.

As identified by the chromatogram of the MonoQ purification step of C-terminally His-tagged RBP-Jκ$_{8-435}$ eluted in two peaks (Figure 3.12B). Therefore, we investigated whether these peaks contained C-terminally His-tagged RBP-Jκ$_{8-435}$ with post translational modifications. Anion exchange columns separate protein by charge therefore we predicted that the most likely posttranslational modification that was causing RBP-Jκ$_{8-435}$ to be eluted in two peaks was phosphorylation.

If RBP-Jκ$_{8-435}$ was being phosphorylated in the insect cells we predicted that the most likely peak to contain phosphorylated RBP-Jκ$_{8-435}$ would be peak 1 (Figure 3.14) as phosphorylated residues have a negative charge which can cause the pI of the protein to increase significantly particularly when in buffers with a pH of 7 or more (Zhu *et al.*, 2005). An increased in pI would cause the electrostatic interaction between the protein and the anion exchange media to be weaker than that of the same protein with a lower pI. Therefore, a phosphorylated protein would elute off of the anion exchange medium at a lower concentration of salt.

To test this hypothesis we incubated eluates of C-terminally His-tagged RBP-Jκ$_{8-435}$ from the $Co^{2+}$ column purification step, after desalting, with λ-phosphatase (Figure 3.14). We found that peak 1 disappeared when C-terminally His-tagged RBP-Jκ$_{8-435}$ was incubated with λ-phosphatase consistent with phosphorylated forms of RBP-Jκ being in this peak (Figure 3.14).

To confirm whether C-terminally His-tagged RBP-Jκ$_{8-435}$ is phosphorylated in peak 1 we cut out a bands from a Coomassie stained gel from peak 1 and peak 2 of the MonoQ

purification step and performed trypsin digest to enable mass spectrometry to be carried out.

To determine whether the peptides, identified from either peak by mass spectroscopy, contained phosphorylated residues we set the Mascot Software to prioritise the identification of peptides containing phosphorylated residues (Figure 3.15). This revealed that the C-terminally His-tagged RBP-J$\kappa_{8-435}$ in peak 1 was potentially phosphorylated on residues Y66, S70, S394 or S405. The mass spectroscopy data for peak 2 did not detect phosphorylated peptide (Figure 3.16). Due to the good coverage of the data (49% for peak 1 and 31% for peak 2) and the search parameters being stringently set (peptide tol ±0.1Da) it is likely that peak 1 contained phosphorylated forms of RBP-J$\kappa_{8-435}$.

To confirm our findings, we ran the peptides predicted by mass spectroscopy to contain phosphorylated residues though Cuckoo's online Post Translation Preditction (PTM) tool (Figure 3.17). The PTM tool confirmed that residues Y66, S70, S394 or S405 were predicted to be phosphosites and suggested potential kinases that could phosphorylate these residues (Figure 3.17).

The RBP-Jκ residues Y66, S70, S394 or S405 that were predicted to be phosphorylated were highlighted on the crystal structure of the Notch1 transcription complex (Choi *et al.*, 2012) (Figure 3.18). All these residues are on the surface of RBP-Jκ and therefore potentially accessible to kinases (Figure 3.18).

Using the online line tool Phosphosite.org, a database that records published phosphorylation sites of proteins, none of these phosphorylation sites have been identified before on RBP-Jκ. We therefore decided to pool eluates from peak 2 for

further purification even though this lowered our overall yield. This was to ensure our C-terminally His-tagged RBP-Jκ$_{8-435}$ was as homogenous as possible for crystallisation trials, as peak 1 was likely to contain mixture of phosphorylated forms of RBP-Jκ$_{8-435}$.

However, after concluding a series of experiments using RBP-Jκ$_{8-435}$ expressed in insect cells, it became apparent that low yields and the length of time and resources necessary to generate new virus and grow up insect cells was restricting progress on the project. We therefore decided to attempt to produce RBP-Jκ$_{8-435}$ in *E.coli* cells.

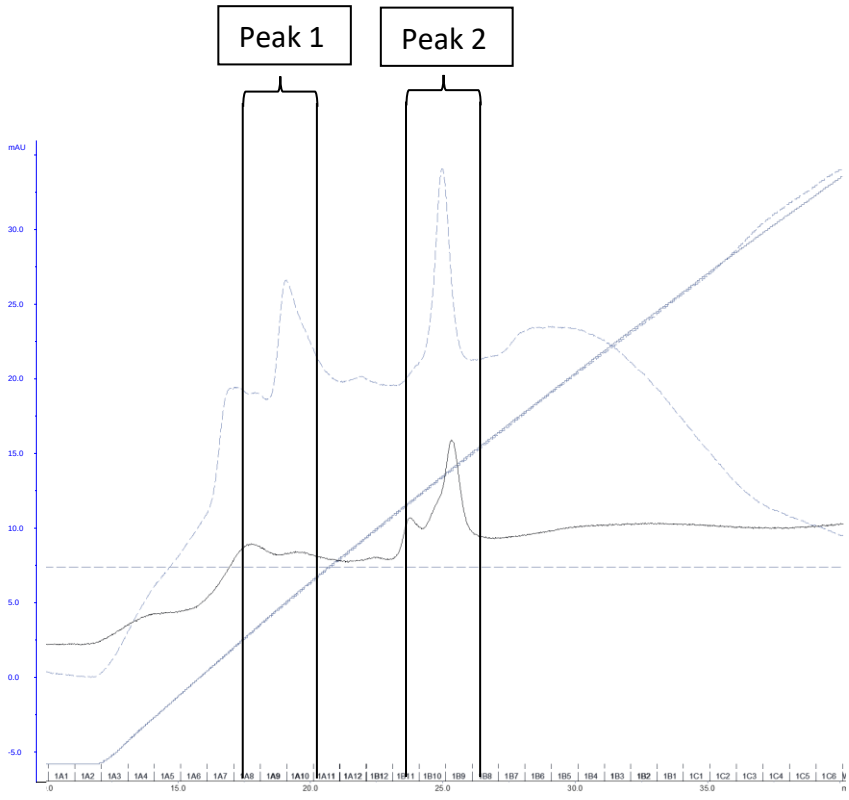


**Figure 3.14. A chromatogram showing the effect of λ-phosphatase on C-terminally His tagged RBP-Jk$_{8-435}$ purification properties.** Purified RBP-Jk$_{8-435}$ was incubated with λ-phosphatase at 4$^{o}$C for 2 hours then analysed by running it through a monoQ 5/50 shown in black. The dashed blue line represents RBP-Jk$_{8-435}$ control.

**A**

Nominal mass ($M_r$): **56343**; Calculated pI value: **6.80**
NCBI BLAST search of Q06330|SUH_HUMAN against nr
Taxonomy: Homo sapiens
Fixed modifications: Carbamidomethyl (C)
Variable modifications: Phospho (ST),Phospho (Y)
Cleavage by Trypsin: cuts C-term side of KR unless next residue is P
Sequence Coverage: **49%**

Matched peptides **Bold Red**, Phosphorylated peptides **Highlighted in yellow**, Not in construct **Highlighted in grey**

```
    1 MDHTEGSPAE EPPAHAPSPG KFGERPPPKR LTREAMRNYL KERGDQTVLI
   51 LHAKVAQKSY GNEKRFFCPP PCVYLMGSGW KKKKEQMERD GCSEQESQPC
  101 AFIGIGNSDQ EMQQLNLEGK NYCTAKTLYI SDSDKRKHFM LSVKMFYGNS
  151 DDIGVFLSKR IKVISKPSKK KQSLKNADLC IASGTKVALF NRLRSQTVST
  201 RYLHVEGGNF HASSQQWGAF FIHLLDDDES EGEEFTVRDG YIHYGQTVKL
  251 VCSVTGMALP RLIIRKVDKQ TALLDADDPV SQLHKCAFYL KDTERMYLCL
  301 SQERIIQFQA TPCPKEPNKE MINDGASWTI ISTDKAEYTF YEGMGPVLAP
  351 VTPVPVVESL QLNGGGDVAM LELTGQNFTP NLRVWFGDVE AETMYRCGES
  401 MLCVVPDISA FREGWRWVRQ PVQVPVTLVR NDGIIYSTSL TFTYTPEPGP
  451 RPHCSAAGAI LRANSSQVPP NESNTNSEGS YTNASTNSTS VTSSTATVVS
  501
```

**B**

| Start-End | Observed m/z | Mr(expt) | Mr(calc) | ΔMr | Sequence | Ion Score links | Phosphorylation? |
|---|---|---|---|---|---|---|---|
| 44 - 54 | 597.8451 | 1193.6757 | 1193.6768 | -0.001 | R.GDQTVLILHAK.V | (Ions score 55) | |
| 59 - 64 | 349.1612 | 696.3079 | 696.3078 | 0.0000 | K.SYGNEK.R | (Ions score 10) | |
| 66 - 81 | 649.2960 | 1944.8662 | 1944.8725 | -0.0063 | R.FFCPPPCVYLMGSGWK.K | (Ions score 22) | |
| 66 - 81 | 1053.4852 | 2104.9559 | 2104.8052 | 0.1507 | R.FFCPPPCVYLMGSGWK.K | (Ions score 13) | Phospho (ST); Phospho (Y) |
| 85 - 89 | 346.6552 | 691.2959 | 691.2959 | -0.0000 | K.EQMER.D | (Ions score 14) | |
| 121 - 126 | 378.6707 | 755.3269 | 755.3272 | -0.0003 | K.NYCTAK.T | (Ions score 25) | |
| 127 - 135 | 521.2585 | 1040.5024 | 1040.5026 | -0.0002 | K.TLYISDSDK.R | (Ions score 31) | |
| 138 - 144 | 431.2359 | 860.4572 | 860.4578 | -0.0006 | K.HFMLSVK.M | (Ions score 16) | |
| 145 - 159 | 564.9353 | 1691.7841 | 1691.7865 | -0.0024 | K.MFYGNSDDIGVFLSK.R | (Ions score 32) | |
| 163 - 169 | 379.7419 | 757.4692 | 757.4698 | -0.0006 | K.VISKPSK.K | (Ions score 23) | |
| 176 - 186 | 575.2819 | 1148.5492 | 1148.5496 | -0.0004 | K.NADLCIASGTK.V | (Ions score 46) | |
| 187 - 192 | 360.2135 | 718.4125 | 718.4126 | -0.0001 | K.VALFNR.L | (Ions score 39) | |
| 195 - 201 | 389.7061 | 777.3977 | 777.3981 | -0.0003 | R.SQTVSTR.Y | (Ions score 22) | |
| 239 - 249 | 640.8167 | 1279.6189 | 1279.6197 | -0.0008 | R.DGYIHYGQTVK.L | (Ions score 30) | |
| 250 - 261 | 652.3455 | 1302.6765 | 1302.6788 | -0.0023 | K.LVCSVTGMALPR.L | (Ions score 29) | |
| 270 - 285 | 584.3036 | 1749.8889 | 1749.8897 | -0.0008 | K.QTALLDADDPVSQLHK.C | (Ions score 49) | |
| 286 - 291 | 401.2017 | 800.3888 | 800.3891 | -0.0003 | K.CAFYLK.D | (Ions score 32) | |
| 296 - 304 | 600.2805 | 1198.5465 | 1198.5474 | -0.0010 | R.MYLCLSQER.I | (Ions score 50) | |
| 305 - 315 | 651.8472 | 1301.6799 | 1301.6802 | -0.0003 | R.IIQFQATPCPK.E | (Ions score 85) | |
| 384 - 396 | 801.8656 | 1601.7166 | 1601.7184 | -0.0018 | R.VWFGDVEAETMYR.C | (Ions score 57) | |
| 397 - 412 | 920.9073 | 1839.8001 | 1839.8318 | -0.0316 | R.CGESMLCVVPDISAFR.E | (Ions score 46) | |
| 397 - 412 | 960.8503 | 1919.6861 | 1919.7981 | -0.1120 | R.CGESMLCVVPDISAFR.E | (Ions score 3) | Phospho (ST) |
| 420 - 430 | 618.3769 | 1234.7393 | 1234.7398 | -0.0004 | R.QPVQVPVTLVR.N | (Ions score 47) | |

**Figure 3.15. Mass Spectroscopy results of the 1st peak from RBP-Jk$_{8-435}$ MonoQ purification step.** Purified RBP-Jk$_{8-435}$ was passed through a MonoQ 5/50. The two peaks were run on a 10% Tris-HCL SDS page where the RBP-Jk$_{8-435}$ bands were cut out using a scalpel for in-gel-digestion with trypsin. Digested JK.8-435 was loaded on to the mass spec LTQ-OrbitrapXL where they ran against a BSA standard. **A.** Table contains information and statistics generated by the Mascot Software used to identify RBP-Jk$_{8-435}$ showing whether peptides contain phosphorylated residues. **B.** A table containing a summary of the peptides identified from the peak data generated by 1st peak from the MonoQ step. Start-end column lists the aa number of the peptide, observed m/z is the peptide mass over charge measured, Mr expt mass expected, Mr calc is calculated mass of predicted peptide, ΔMr is the difference between these calculations, Sequence shows the sequence of the peptide, Ion score links to RAW data and phosphorylation column describes peptide phosphorylation.

**A**

Nominal mass ($M_r$): **56343**; Calculated pI value: **6.80**
NCBI BLAST search of Q06330|SUH_HUMAN against nr
Taxonomy: Homo sapiens

Fixed modifications: Carbamidomethyl (C)
Variable modifications: Phospho (ST),Phospho (Y)
Cleavage by Trypsin: cuts C-term side of KR unless next residue is P
Sequence Coverage: **31%**

Matched peptides **Bold Red**, Phosphorylated peptides **Highlighted in yellow**, Not in construct **Highlighted in grey**

```
1 MDHTEGSPAE EPPAHAPSPG KFGERPPPKR LTREAMRNYL KERGDQTVLI
51 LHAKVAQKSY GNEKRFFCPP PCVYLMGSGW KKKKEQMERD GCSEQESQPC
101 AFIGIGNSDQ EMQQLNLEGK NYCTAKTLYI SDSDKRKHFM LSVKMFYGNS
151 DDIGVFLSKR IKVISKPSKK KQSLKNADLC IASGTKVALF NRLRSQTVST
201 RYLHVEGGNF HASSQQWGAF FIHLLDDDES EGEEFTVRDG YIHYGQTVKL
251 VCSVTGMALP RLIIRKVDKQ TALLDADDPV SQLHKCAFYL KDTERMYLCL
301 SQERIIQFQA TPCPKEPNKE MINDGASWTI ISTDKAEYTF YEGMGPVLAP
351 VTPVPVVESL QLNGGGDVAM LELTGQNFTP NLRVWFGDVE AETMYRCGES
401 MLCVVPDISA FREGWRWVRQ PVQVPVTLVR NDGIIYSTSL TFTYTPEPGP
451 RPHCSAAGAI LRANSSQVPP NESNTNSEGS YTNASTNSTS VTSSTATVVS
501
```

**B**

| Start-End | Observed m/z | Mr(expt) | Mr(calc) | ΔMr | Sequence | Ion Score links | Phosphorylation? |
|---|---|---|---|---|---|---|---|
| 44 - 54 | 597.8452 | 1193.6759 | 1193.6768 | -0.0010 | R.GDQTVLILHAK.V | (Ions score 36) | |
| 85 - 89 | 346.6553 | 691.2960 | 691.2959 | 0.0001 | K.EQMER.D | (Ions score 9) | |
| 121 - 126 | 378.6708 | 755.3269 | 755.3272 | -0.0003 | K.NYCTAK.T | (Ions score 12) | |
| 138 - 144 | 431.2358 | 860.4570 | 860.4578 | -0.0008 | K.HFMLSVK.M | (Ions score 27) | |
| 145 - 159 | 846.9002 | 1691.7859 | 1691.7865 | -0.0006 | K.MFYGNSDDIGVFLSK.R | (Ions score 52) | |
| 163 - 169 | 379.7420 | 757.4695 | 757.4698 | -0.0003 | K.VISKPSK.K | (Ions score 30) | |
| 176 - 186 | 575.2814 | 1148.5482 | 1148.5496 | -0.0014 | K.NADLCIASGTK.V | (Ions score 42) | |
| 187 - 192 | 360.2136 | 718.4127 | 718.4126 | 0.0001 | K.VALFNR.L | (Ions score 31) | |
| 195 - 201 | 389.7062 | 777.3979 | 777.3981 | -0.0002 | R.SQTVSTR.Y | (Ions score 21) | |
| 239 - 249 | 640.8165 | 1279.6185 | 1279.6197 | -0.0012 | R.DGYIHYGQTVK.L | (Ions score 38) | |
| 250 - 261 | 652.3460 | 1302.6775 | 1302.6788 | -0.0014 | K.LVCSVTGMALPR.L | (Ions score 85) | |
| 270 - 285 | 584.3038 | 1749.8895 | 1749.8897 | -0.0002 | K.QTALLDADDPVSQLHK.C | (Ions score 56) | |
| 296 - 304 | 600.2806 | 1198.5467 | 1198.5474 | -0.0007 | R.MYLCLSQER.I | (Ions score 60) | |
| 305 - 315 | 651.8470 | 1301.6795 | 1301.6802 | -0.0006 | R.IIQFQATPCPK.E | (Ions score 89) | |
| 384 - 396 | 801.8664 | 1601.7182 | 1601.7184 | -0.0002 | R.VWFGDVEAETMYR.C | (Ions score 84) | |
| 420 - 430 | 618.3771 | 1234.7396 | 1234.7398 | -0.0002 | R.QPVQVPVTLVR.N | (Ions score 38) | |

**Figure 3.16. Mass Spectroscopy results of 2nd peak from RBP-Jk$_{8-435}$ MonoQ purification step.** Purified RBP-Jk$_{8-435}$ was passed through a MonoQ 5/50. The two peaks were run on a 10% Tris-HCL SDS page where the RBP-Jk$_{8-435}$ bands were cut out using a scalpel for in-gel-digestion with trypsin. Digested RBP-Jk$_{8-435}$ was loaded on to the mass spec LTQ-OrbitrapXL where they ran against a BSA standard. **A.** Table contains information and statistics generated by the Mascot Software used to identify RBP-Jk$_{8-435}$ showing whether peptides contain phosphorylated residues. **B.** A table containing a summary of the peptides identified from the peak data generated from the 2nd peak in the MonoQ step. Start-end column lists the aa number of the peptide, observed m/z is the peptide mass over charge measured, Mr expt mass expected, Mr calc is calculated mass of predicted peptide, ΔMr is the difference between these calculations, Sequence shows the sequence of the peptide, Ion score links to RAW data and phosphorylation column describes peptide phosphorylation.

**FFCPPPCVYLMGSGWK**

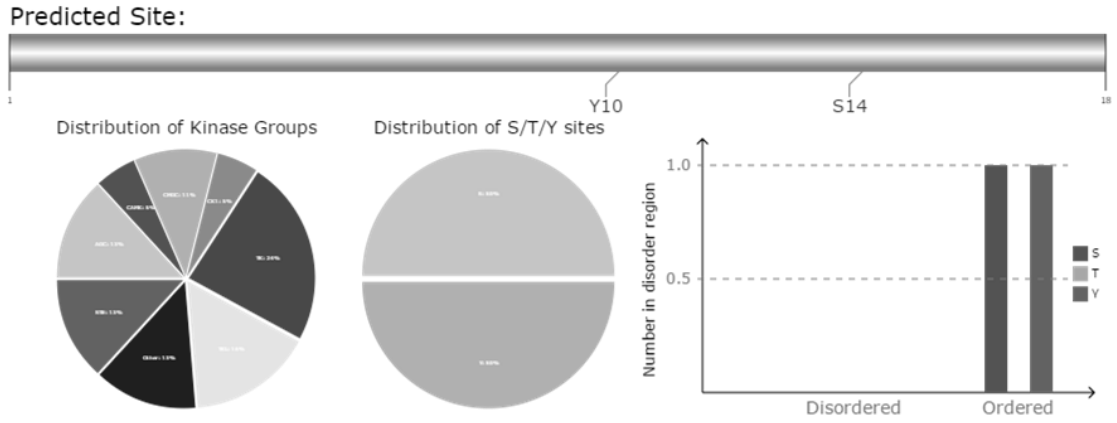


**RCGESMLCVVPDISAFR**

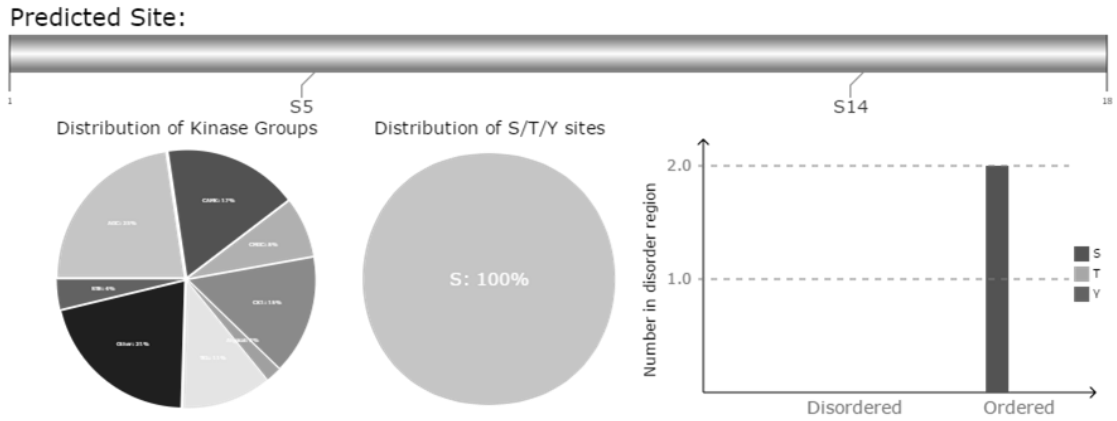


**Figure 3.17. Verification of phosphorylation sites using The Cuckoo workshop Group-based prediction software.** The peptides that were predicted to be phosphorylated by the Mascot software were inputted into the Cuckoo Post Translation Prediction (PTM) software (http://gps.biocuckoo.org/online.php). Both peptides were predicted to contain phosphorylatable residues by the software. It also identified that these residues were ordered.

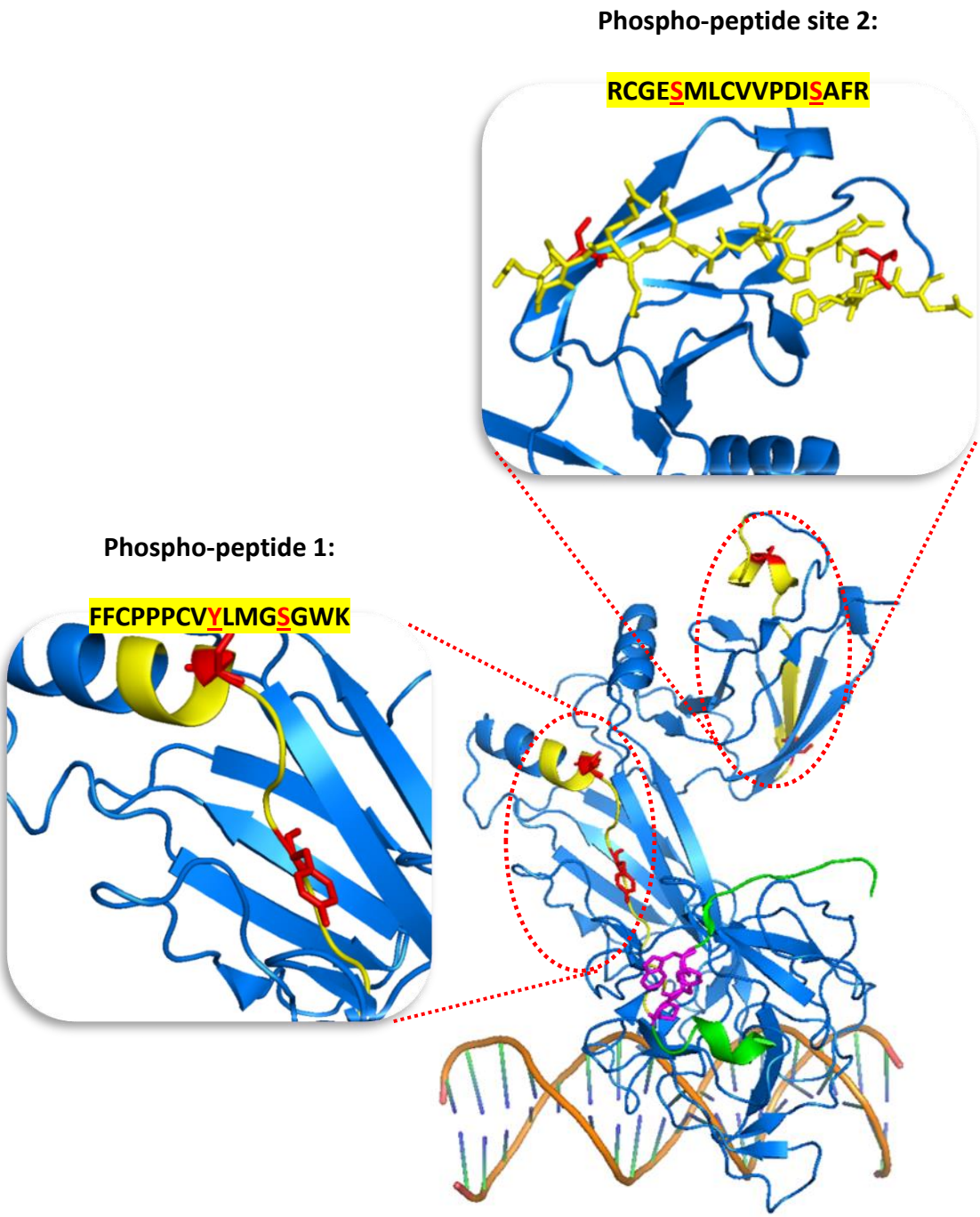


**Figure 3.18. Potential phosphorylation sites highlighted on the structure of RBP-Jκ to visualise kinase accessibility.** Peptides sequences were aligned to the structure of Notch1 transcription complex (3V79) in pymol (RBP-Jκ in blue, RAM molecule in green and WTP Notch binding motif is highlighted in pink)(Choi *et al.*, 2012). Entire peptide sequence identified in the mass spectrometry was highlighted in yellow whilst the residues predicted to phosphorylated were highlighted in red. Zoomed in view shows that the serine and tyrosine residues are on the surface and accessible to kinases.

### 3.1.2.1 : Initial Purification of C-terminally His-tagged RBP-Jκ$_{8-435}$ expressed in 1L Rosetta *E.coli* cells.

We transformed a pET28b.JK.8-435, produced by a summer student in Michelle West's group, containing cDNA to express C-terminally His-tagged RBP-Jκ$_{8-435}$ into *E.coli* Rosetta pLys cells. Cells were harvested and sonicated in buffer A (Appendix 3), then the lysate was loaded onto a $Co^{2+}$ column (5ml Talon FF) and RBP-Jκ$_{8-435}$ was eluted with an increasing concentration of imidazole (Appendix 3) (Figure 3.19A). We chose to continue using $Co^{2+}$ column (5ml Talon FF) for the initial purification step of C-terminally His-tagged RBP-Jκ$_{8-435}$ as the $Co^{2+}$ binds to His-tagged proteins more specifically which reduces background binding. Initially, we found that RBP-Jκ was eluted with many impurities (Figure 3.19A). The eluates from the $Co^{2+}$ column purification step were desalted in a 26/10 desalt column to lower the concentration of sodium chloride from 500mM to 100mM to ensure that the C-terminally His-tagged RBP-Jκ$_{8-435}$ would bind to the anion exchange column.

We changed the anion exchange column from a MonoQ 5/50 column to a 5ml HitrapQ FF column. This was because the Hitrap Q FF column media (45-165µm bead size) is less tightly packed compared to MonoQ 5/50 columns (10 µm bead size) which meant we could use faster flow rates and complete this purification step faster. Also, it was recommended in the MonoQ 5/50 manual not to load more than 10ml of sample per purification, which meant after the desalt step we often had to concentrate the sample to ensure we could load all the sample at once which added a significant amount of time to the purification process. Conversely the HitrapQ FF columns did not have a limit to how much sample could be loaded onto the column. C-terminally His-

tagged RBP-Jκ$_{8-435}$ was eluted from the HitrapQ column with a salt gradient, however there was still a significant amount of impurities present (Figure 3.20A).

The eluates were pooled, concentrated to 250µL, incubated with RBP-Jκ consensus site DNA (TTACT**GTGGGA**AAGA) and loaded onto an S200 10/300 size exclusion column (Figure 3.21). C-terminally His-tagged RBP-Jκ$_{8-435}$ was eluted from the column with fewer impurities, however require further purification (Figure 3.21). The overall yield of C-terminally His-tagged RBP-Jκ$_{8-435}$ expressed in 1L of Rosetta *E.coli* cells was approximately 100µL of RBP-Jκ$_{8-435}$ at 8mg/ml for a yield of ~0.8mg. This was a significant increase in yield per litre of cells used compared to insect cells which required approximately 3L of media to produce a similar quantity of C-terminally His-tagged RBP-Jκ$_{8-435}$.

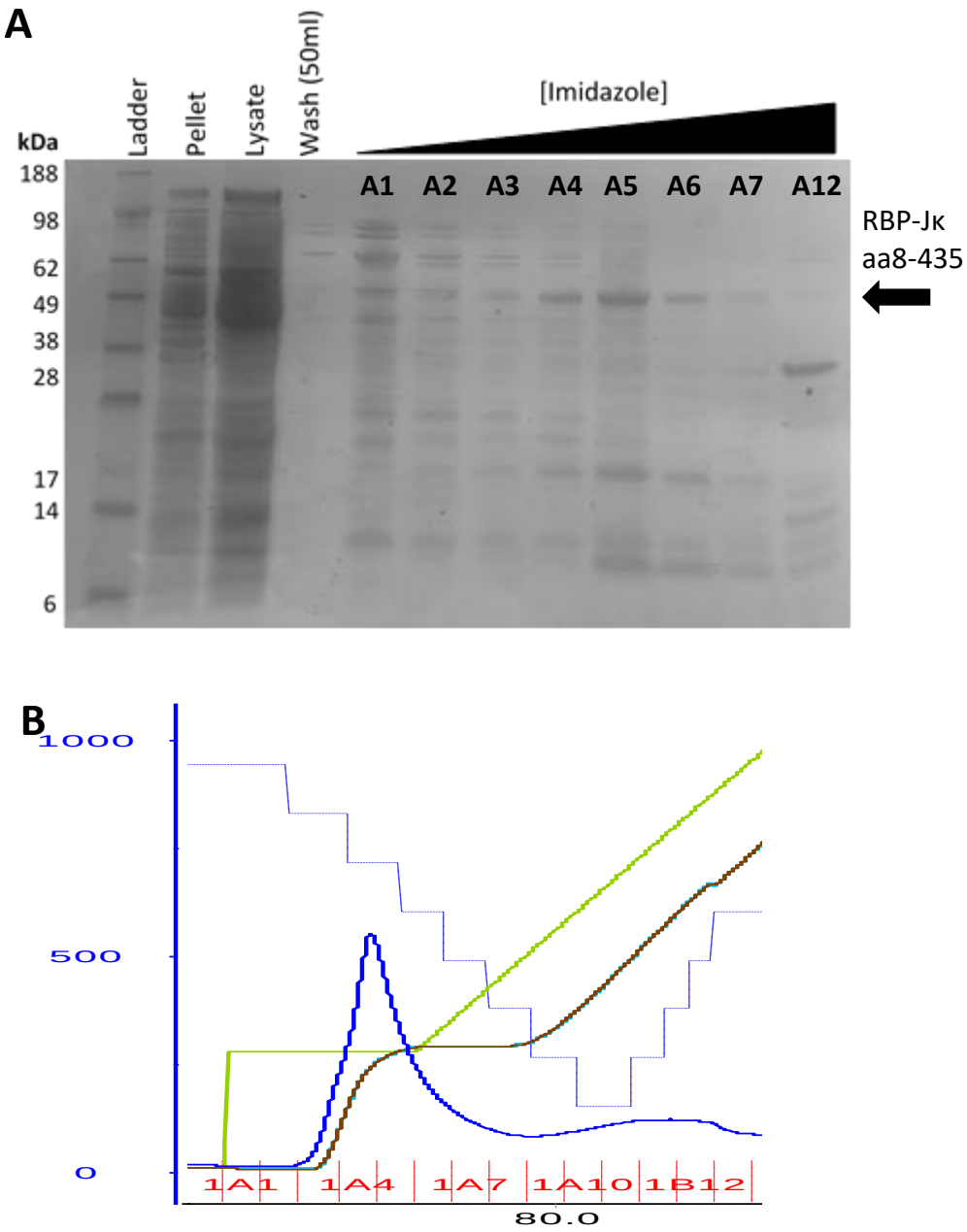


**Figure 3.19. Analysis of $Co^{2+}$ column (Talon) purification step of His tagged RBP-Jκ$_{8-435}$ expressed in 1 litre of *E.coli* Rosetta cells. A.** Coomassie stained showing pellet, lysate and elution fractions from $Co^{2+}$ column (5ml Talon FF) as an increasing concentration of imidazole was passed through. 10µL from each fraction was mixed with 10µl GSB buffer, boiled and loaded onto the 10% Tris SDS page gel where it was run in MOPS buffer. **B.** Chromatogram from the Talon step produced in Unicorn software. Shown is protein (blue), concentration of buffer B/ [imidazole] (green), flow rate (orange) and [salt] (in brown). Wells A2 to A7 were pooled for further purification.

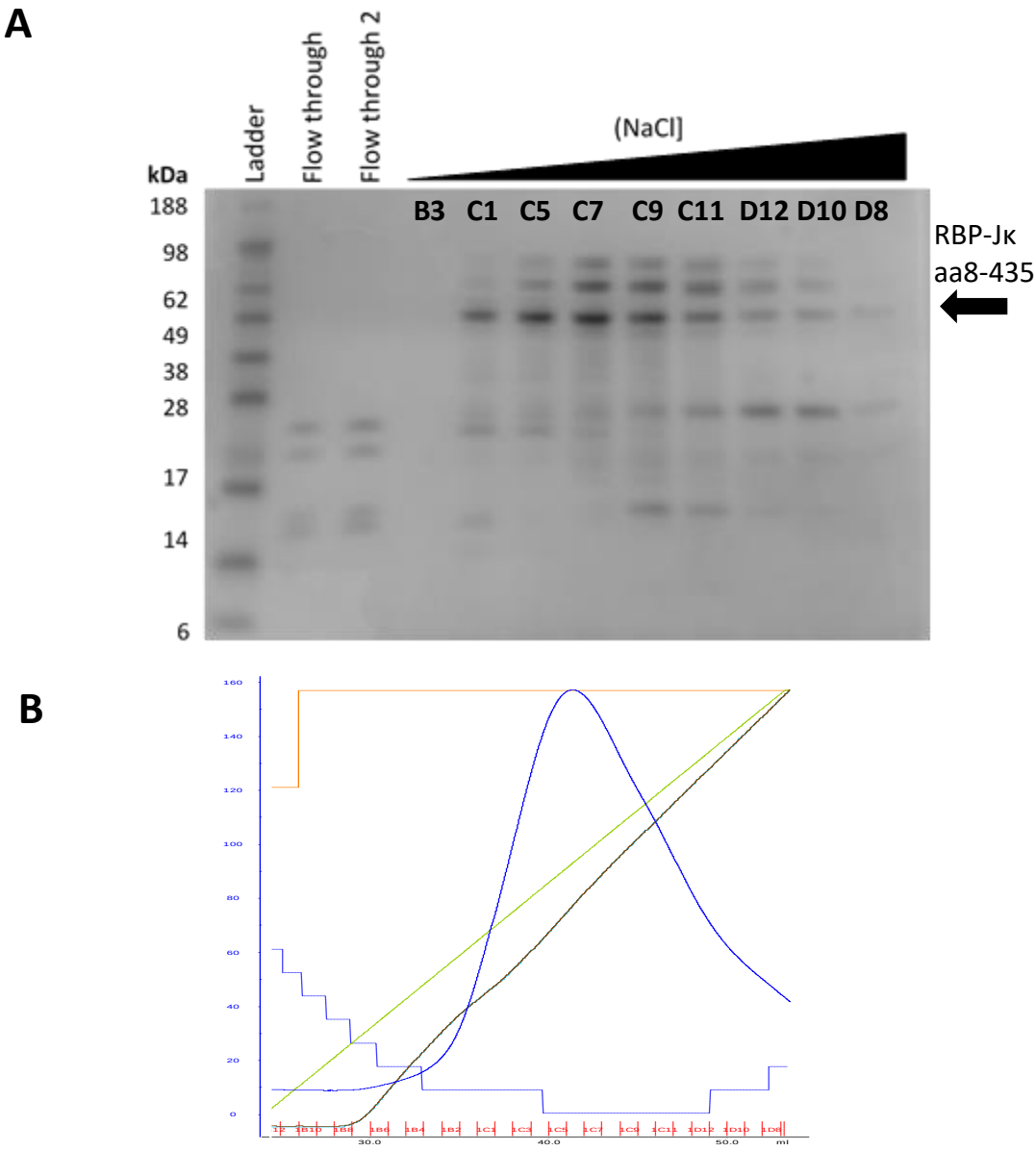


**Figure 3.20. Analysis of HitrapQ purification step of C-terminally His-tagged RBP-Jκ$_{8-435}$ expressed in 1 litre of *E.coli* cells. A.** Coomassie stained gel showing fractions from the 5ml HitrapQ FF column from GE healthcare as an increasing [NaCl] is passed through. Each fraction was mixed with GSB buffer, boiled and loaded onto the 10% Tris SDS page gel where it was run in MOPS buffer. **B**. Chromatogram showing HitrapQ purification step. Shown is [protein (blue), concentration of buffer D/ [NaCl] (green), flow rate (orange) and [salt] (in brown). Wells C1 to D10 were pooled for further purification.

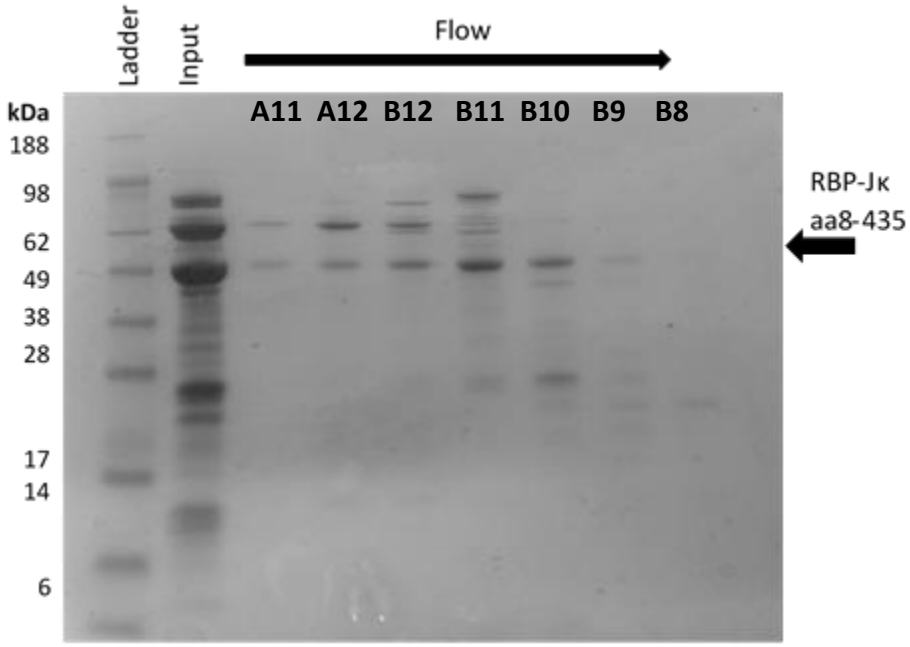


**Figure 3.21. Analysis of Size exclusion step for C-terminally His-tagged RBP-Jκ$_{8-435}$ expressed in 1 litre of *E.coli* cells**. Fractions were pooled, concentrated, incubated with DNA and injected into a size exclusion column primed in low salt Buffer C. Shown is the input and different fractions taken as RBP-Jκ$_{8-435}$ passed through the S200 10/300 size exclusion column. Samples were mixed with GSB, boiled and run on a 10% Tris-HCL SDS-PAGE gel in MOPS buffer. Wells A12 to B9 were pooled and used for crystallisation screens. Chromatogram not shown as air bubbles in the system made the chromatogram difficult to interpret.

### 3.1.2.2 : Optimisation of the Purification of C-terminally His-tagged RBP-Jκ$_{8-435}$ expressed in Rosetta *E.coli* cells.

To reduce the amount of contaminant binding to the $Co^{2+}$ column during the first step in the purification process we introduced 10mM of imidazole. To increase the yield of C-terminally His-tagged RBP-Jκ$_{8-435}$ we also increased the grow up from 1L to 4L. To ensure the *E.coli* cells were lysed properly we increased the time we sonicated the cell pellet. These changes improved to the amount to C-terminally His-tagged RBP-Jκ$_{8-435}$ that bound to the $Co^{2+}$ column and reduced contaminant binding (Figure 3.22A). However, some C-terminally His-tagged RBP-Jκ$_{8-435}$ was lost during the wash step (Figure 3.22A). Based on the chromatogram of the first HitrapQFF purification step performed, shown (Figure 3.20B) we calculated that C-terminally His-tagged RBP-Jκ$_{8-435}$ eluted at approximately 150mM NaCl. We therefore programmed the AKTA to increase the salt gradient until 150mM NaCl was running through the column then paused the gradient until the elution peak returned to zero. This ensured that impurities that eluted at higher or lower salt concentrations to C-terminally His-tagged RBP-Jκ$_{8-435}$ were not eluted with RBP-Jκ$_{8-435}$ further increasing the purity of the sample shown in (Figure 3.22B).

Finally the eluates from the HistrapQ FF step were pooled, concentrated to 250µL, incubated with RBP-Jκ consensus site DNA (TTACT**GTGGGA**AAGA) and loaded onto an S200 10/300 size exclusion column. The eluates from the size exclusion step were pure enough for crystallisation trials and with these optimisations we had greatly improved the purity and the overall yield from 0.8mg to 4mg of C-terminally His-tagged RBP-Jκ$_{8-435}$ (Figure 3.22C). We could produce this yield consistently, which enabled us to

conduct more crystallisation trials with fresh material than we could with the C-terminally His-tagged RBP-J$\kappa_{8-435}$ produced in insect cells.

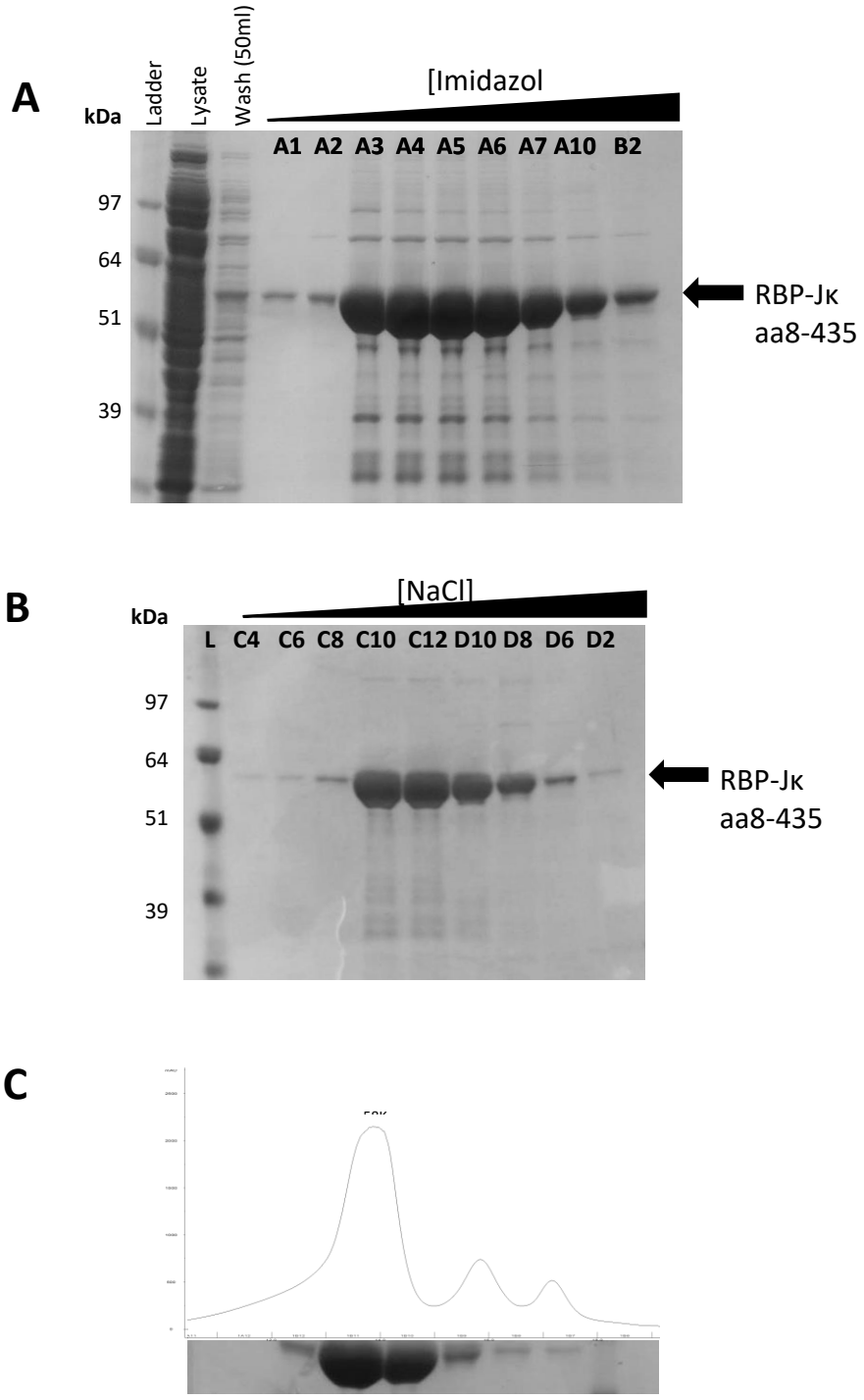


**Figure 3.22. Analysis of optimised steps of the purification of C-terminally His-tagged RBP-Jκ$_{8-435}$ expressed in *E.coli*. A.** Coomassie stained gel showing pellet, lysate and elution fractions from $Co^{2+}$ column (5ml Talon FF) as an increasing concentration of imidazole was passed through. Wells A3 to A10 were pooled for anion exchange. **B.** Coomassie stained gel showing fractions from the 5ml HitrapQ FF column as an increasing [NaCl] is passed through. Wells C8 to D6 were pooled for size exclusion. **C.** Shown are fractions taken as RBP-Jk$_{8-435}$ passed through the S200 10/300 size exclusion column. The chromatogram has been aligned to the Coomassie stained gel. The black line represents the protein concentration. B12 to B9 were used for crystallisation trials.

### 3.1.3.1 : Expression and purification of RBP-Jκ conclusion.

We initially expressed RBP-Jκ in insect cells as a PhD student from Munich had shown that the EBNA-RBP-Jκ interactions could be impacted by whether a eukaryotic or prokaryotic expression host had been used to produce RBP-Jκ (Robertson *et al.*, 1996a, Calderwood *et al.*, 2011). We produced a recombinant baculovirus that expressed C-terminally His-tagged RBP-Jκ$_{8-435}$ well in insect cells, which bound efficiently to $Ni^{2+}$ beads (Figures 3.1 to 3.6). We showed that RBP-Jκ$_{8-435}$ expressed in insect cells bound specifically to DNA containing RBP-Jκ consensus site using EMSA, which confirmed RBP-Jκ$_{8-435}$ functionality (Figure 3.7). We also produced a recombinant baculovirus that expressed N-terminally His-tagged RBP-Jκ variant 2 (V2) that did not express as well as C-terminally His-tagged RBP-Jκ$_{8-435}$ and did not bind to $Ni^{2+}$ beads (Figures 3.1 to 3.6). We therefore did not continue to optimise expression and purification of RBP-Jκ V2.

We developed a purification process for RBP-Jκ$_{8-435}$ expressed in insect cells (Figure 3.8 to 3.10). RBP-Jκ$_{8-435}$ eluted off the size exclusion column in a broad peak suggesting it was adopting multiple confirmations (Figure 3.10). Binding RBP-Jκ$_{8-435}$ to DNA, containing a RBP-Jκ consensus site, before the size exclusion step sharpened the elution peak suggesting DNA binding drove conformational changes to RBP-Jκ$_{8-435}$, which homogenised RBP-Jκ$_{8-435}$ folding in the sample (Figure 3.13). The same effect was not observed when RBP-Jκ$_{8-435}$ was pre-incubated with EBNA2 peptide before the size exclusion step (Figure 3.13). We also observed that RBP-Jκ$_{8-435}$ underwent post-translational modification during expression in insect cells. Incubating RBP-Jκ$_{8-435}$ with λ-phosphatase prior to the monoQ purification step identified one of the monoQ elution peaks contained phosphorylated RBP-Jκ$_{8-435}$ (Figure 3.14). Mass spectroscopy analysis of this peak identified that residues Y66, S70, S394 or S405 of RBP-Jκ$_{8-435}$ were

phosphorylated (Figure 3.15 and 3.16). Additionally, we verified these residues were accessible to kinases (Figure 3.18) and phosphorylatable using Cuckoo workshop Group-based prediction software (Figure 3.17).

After scaling up the preparation of RBP-Jκ$_{8-435}$ to 5L we increased the yield of protein from ~0.8mg to ~2mg and optimising the purification of process we produced RBP-Jκ$_{8-435}$ that was pure enough for crystallisation trials (Figures 3.8 to 3.12). From a 5L preparation we could even produce up to 4mg of RBP-Jκ$_{8-435}$ however, this was highly dependent on the quality of the P3 recombinant baculovirus produced, which fluctuated considerably.

Due to inconsistent yields of RBP-Jκ$_{8-435}$ in insect cells and the time consuming process affecting progress we switched production of RBP-Jκ$_{8-435}$ to *E.coli.* We transformed Rosetta *E.coli* with a bacterial expression vector (pET28b.JK.8-435) to produce C-terminally His-tagged RBP-Jκ$_{8-435}$ (Figure 3.19). Initially we encountered lower yields (0.8 mg/L of culture) and impurities in the purified RBP-Jκ$_{8-435}$ (Figures 3.19 to 3.21). By improving the lysis step, adding 10mM imidazole to the lysis buffer, increasing the length of washes during purification and scaling up the culture to 4L we consistently produced yields 4mg of RBP-Jκ$_{8-435}$ (Figure 3.22). As we were able to consistently produce high purity RBP-Jκ$_{8-435}$ we were able to complete larger numbers of crystallisation trials and finish our thermodynamic studies of EBNA-RBP-Jκ interactions.

## Chapter 3.2 : Thermodynamic studies into the interactions between Epstein-Barr Viral transcription factors and RBP-Jκ

After successfully expressing and purifying C-terminally His-tagged RBP-Jκ$_{8-435}$, in insect cells and *E.coli*, we had the material we needed to start investigating how EBNA2 and the EBNA3 family of transcription factors hijack RBP-Jκ mediated viral and cellular transcription. Previous work in our laboratory and others (unpublished observations) had found that expression of full length EBNA2 and EBNA3s is problematic due to issues with instability and insolubility of recombinant proteins. Instability *in vitro* was likely due to EBNA2 and the EBNA3 family being predicted to be predominantly disordered (Yenamandra *et al.*, 2009, Friberg *et al.*, 2015). EBNA2 and the EBNA3 family also rely on multiple host transcription factors for their activity which may confer stability *in vivo* (Maruo *et al.*, 2005, Young *et al.*, 2008, Lee *et al.*, 2009, Chabot *et al.*, 2014). Therefore, we decided to initially investigate interactions between peptides of EBNA2 and the EBNA3 family, which contained the WΦP and TΦGC RBP-Jκ binding motifs, with RBP-Jκ (Ling and Hayward, 1995, Calderwood *et al.*, 2011). EBNA2 mimics the Notch RAM domain WΦP motif to interact with RBP-Jκ and mutation of this motif has been shown to silence EBNA2 activation of host genes (Ling and Hayward, 1995, Johnson *et al.*, 2010). It has been suggested that the EBNA3 family TΦGC RBP-Jκ binding motif, located in the N-terminal homology domain of the EBNA3s, binds to the NTD of RBP-Jκ. Mutation of the EBNA3 TΦGC motif to alanines ablates RBP-Jκ binding and decreases EBNA3C mediation of host gene expression (Maruo *et al* 2009, Calderwood *et al* 2011).

### 3.2.1.1 : Isothermal titration calorimetry (ITC) binding assays to study the interactions between RBP-Jκ and the EBNAs

Initially we used ITC to measure the interaction between C-terminally His-tagged RBP-$J\kappa_{8-435}$ expressed in insect cells and a 14 amino acid peptide of $EBNA2_{314-327}$ which contained the WΦP RBP-Jκ binding motif (EBNA2.14aa) which was provided by Dr Chrisostomos Prodromou's group. Initially C-terminally His-tagged RBP-$J\kappa_{8-435}$ expressed in insect cells was pooled from the MonoQ purification step, concentrated to ~8mg/ml then dialysed in buffer C + 1mM Ethylenediaminetetraacetic acid (EDTA) overnight. 1mM EDTA was added to protect the protein from degradation during dialysis. Based on previously published affinity of the binding between EBNA2 and RBP-Jκ ($k_D$ = 4.6μM)(Johnson *et al.*, 2010) we calculate that 30μM to 60μM RBP-Jκ would be optimal for ITC experiments. Due to low yields of RBP-Jκ being predicted to be produced by insect cells (Figure 3.7) we calculated we could use a maximum 37.8μM of RBP-Jκ for each ITC experiment.

The EBNA2 and EBNA3C peptides ordered contained predominantly hydrophobic residues, therefore we predicted that they would likely have low solubility in the ITC buffer. Consequently, we decided to initially dissolve the EBNA2.14aa peptide powder directly into dimethyl sulfoxide (DMSO) and then diluted it into ITC buffer (Appendix 3). For each injection to produce a measurable heat peak we needed to use at least 10 times the amount of ligand (peptide) to substrate (RBP-Jκ). But we needed to keep the overall concentration of DMSO in the buffer below 0.5% as any more would likely disrupt RBP-$J\kappa_{8-435}$ folding. We calculated that the maximum amount of ligand we could dissolve in injection solution, before the final percentage of DMSO was greater than 0.5%, was 600μM of peptide.

0.5% DMSO was added to RBP-Jκ$_{8-435}$ solution to ensure that both the substrate and ligand buffers were the same to prevent heat peaks being generated during the binding assay, that would overwhelm the heat peaks generated by the RBP-Jκ$_{8-435}$-EBNA2.14aa interaction. We chose to titrate the peptide with 28 injections to ensure that the binding curve contained sufficient data points for reliable curve fitting.

The ITC analysis of the RBP-Jκ$_{8-435}$-EBNA2.14aa interaction measured a $k_d$ of 1.35 ± 0.07 μM revealing that the interaction was relatively weak as predicted (Figure 3.23). The stoichiometry of the interaction was calculated to be 1:1 which confirmed that the WΦP RBP-Jκ binding motif was directing EBNA2.14aa peptide interactions with the BTD of RBP-Jκ$_{8-435}$ (Figure 3.23).

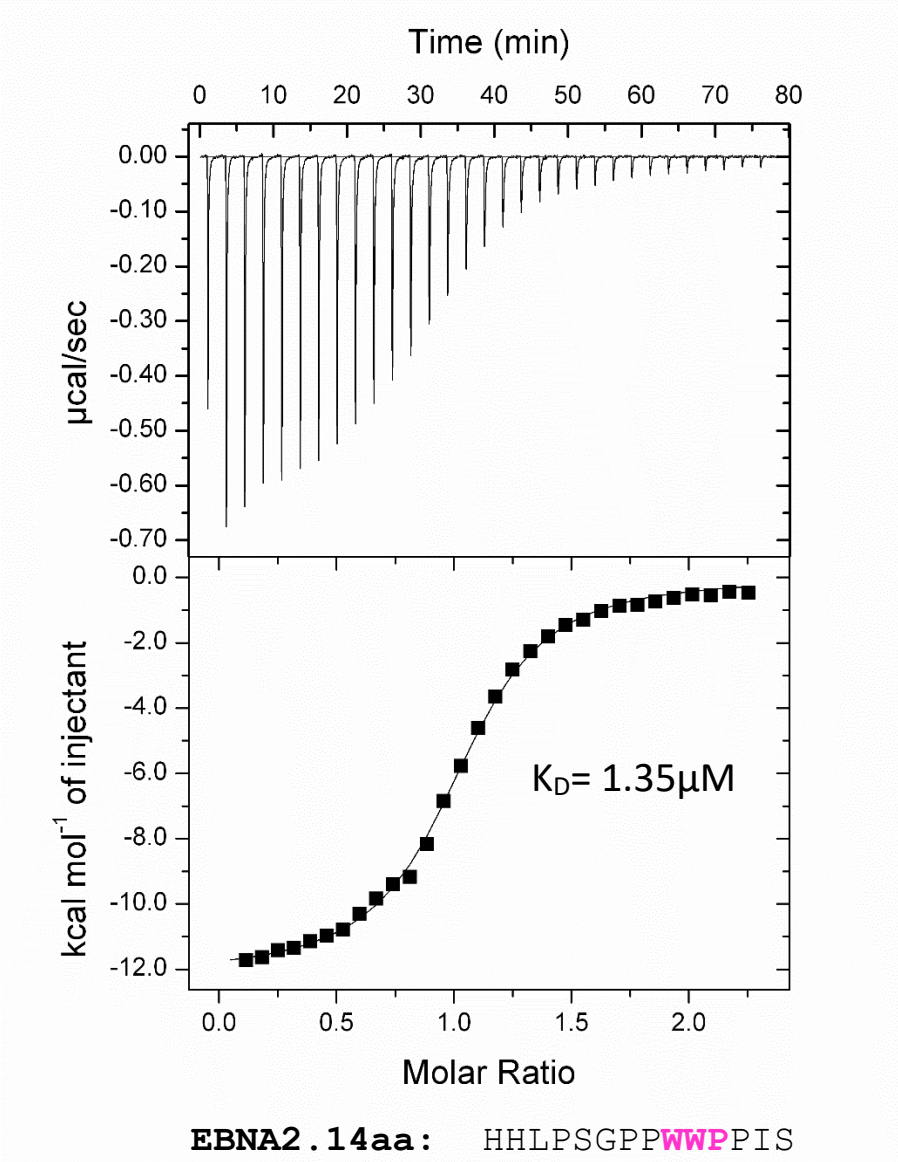


**Figure 3.23. Isothermal Titration Calorimetry analysis of the interaction between C-terminally His-tagged RBP-Jκ$_{8-435}$ expressed in Sf9 insect cells and an EBNA2 peptide containing Notch binding motif.** Heat peaks and integrated fitted heat peaks are shown for the interaction between RBP-Jκ$_{8-435}$ and EBNA2.14aa peptide in low salt buffer C + 1mM EDTA + 0.5% DMSO. The $K_d$ is shown next to the integrated fitted heat peaks. The WΦP Notch binding motif is highlighted in pink in the amino acid sequence for the EBNA2 peptide.

### 3.2.1.2 : EBNA2-RBP-Jκ$_{8-435}$ interactions are weaker then Notch 2-RBP-Jκ$_{8-435}$ Interactions.

We next determined the binding affinity of Notch with RBP-Jκ to compare to binding affinity of EBNA2. Notch 2 has been shown to be expressed in mice mature B cells and promote Marginal Zone B cell lineage development so we used a peptide of human Notch 2 for our analysis (Saito *et al,* 2003). The Notch 2$_{1700-1725}$ peptide (Notch2.26aa) was designed so that the WΦP RBP-Jκ binding motif (Figure 3.24) was in the centre of the peptide and to include residues of the RAM domain previously identified as important to the Notch-RBP-Jκ interactions (Johnson *et al.*, 2010)(Appendix 4). A new EBNA2$_{312-337}$ peptide of the same length (EBNA2.26aa) peptide was designed containing a central WΦP RBP-Jκ binding motif was used to enable a better comparison of binding of the Notch2.26aa peptide (Figure 3.24)(Appendix 4)(Johnson *et al.*, 2010).

We found that the Notch2.26aa peptide bound to RBP-Jκ$_{8-435}$ with a $k_d$ of 0.16μM whereas the EBNA2.26aa peptide bound to RBP-Jκ$_{8-435}$ an order of magnitude weaker with a $k_d$ of 3.9μM (Figure 3.24). Although both peptides contained the WΦP RBP-Jκ binding motif, the presence of a leucine instead of a tryptophan in the Φ position or differences in surrounding residues resulted in a weaker interaction.

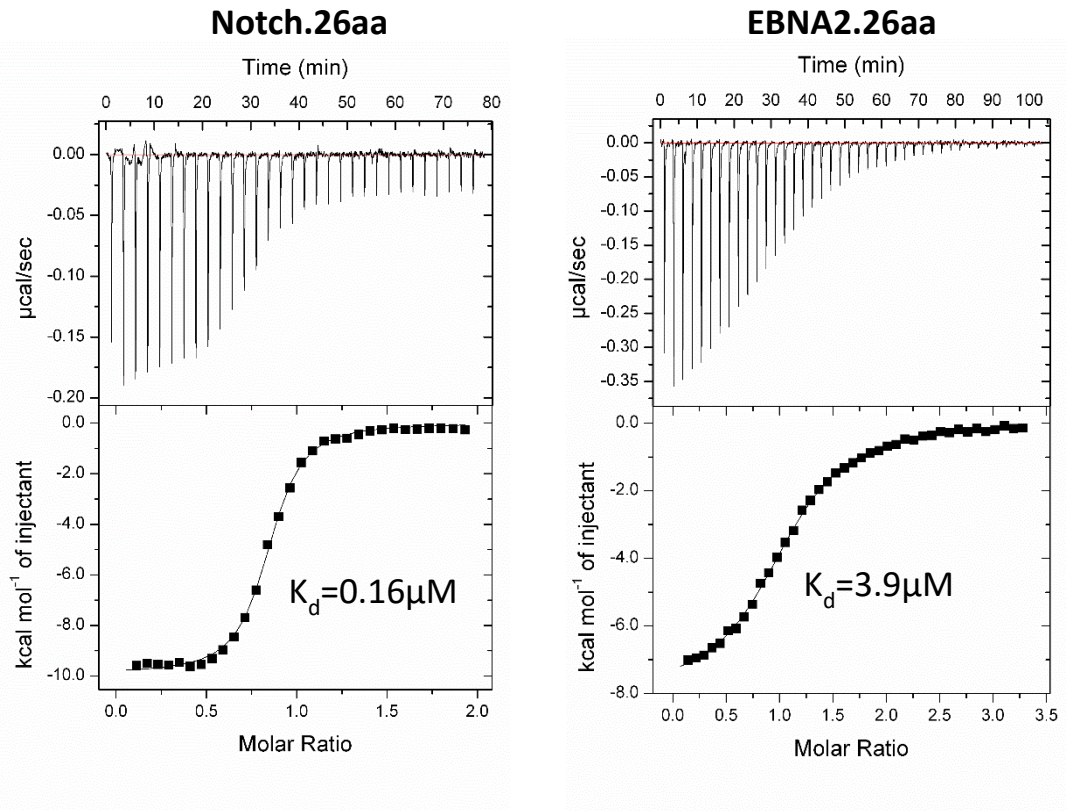


**Figure 3.24. Isothermal Titration Calorimetry analysis of the interaction between C-terminally His-tagged RBP-Jκ$_{8-435}$ expressed in insect cells and Notch peptide (Notch.26aa) or EBNA2 peptide (EBNA2.26aa) containing WΦP Notch binding motif.** Heat peaks and integrated fitted heat peaks are shown for the interaction between RBP-Jk$_{8-435}$ and Notch.22aa or EBNA2.14aa. The $K_d$ is shown next to the integrated fitted heat peaks. The WΦP Notch binding motif is highlighted in pink in the amino acid sequences of the peptide.

### 3.2.1.3 : Peptides of EBNA3A, EBNA3B and EBNA3C containing the TΦGC RBP-Jκ binding motif do not bind to RBP-Jκ$_{8-435}$ *in vitro*.

The TΦGC RBP-Jκ binding motif in EBNA3 proteins is found in the conserved homology domain of EBNA3A, EBNA3B and EBNA3C and its been shown that when this motif is mutated to four alanine residues EBNA3s no longer binds to RBP-Jκ (Robertson *et al.*, 1996a, Zhao *et al.*, 1996, Calderwood *et al.*, 2011).

14 amino acid peptides of EBNA3A$_{194-207}$, EBNA3B$_{201-214}$ and EBNA3C$_{204-217}$ were designed to contain the TΦGC RBP-Jκ binding motif at the centre of the peptide (EBNA3A.14aa, EBNA3B.14aa and EBNA3C.14aa respectively)(Appendix 4). However, we found that none of the EBNA3 family peptides with the TΦGC RBP-Jκ binding motif bound to RBP-Jκ$_{8-435}$ (Figure 3.25). It therefore appears that this motif is not able to direct RBP-Jκ in the context of a peptide sequence *in vitro*. This is in contrast to the WΦP directed RBP-Jκ binding.

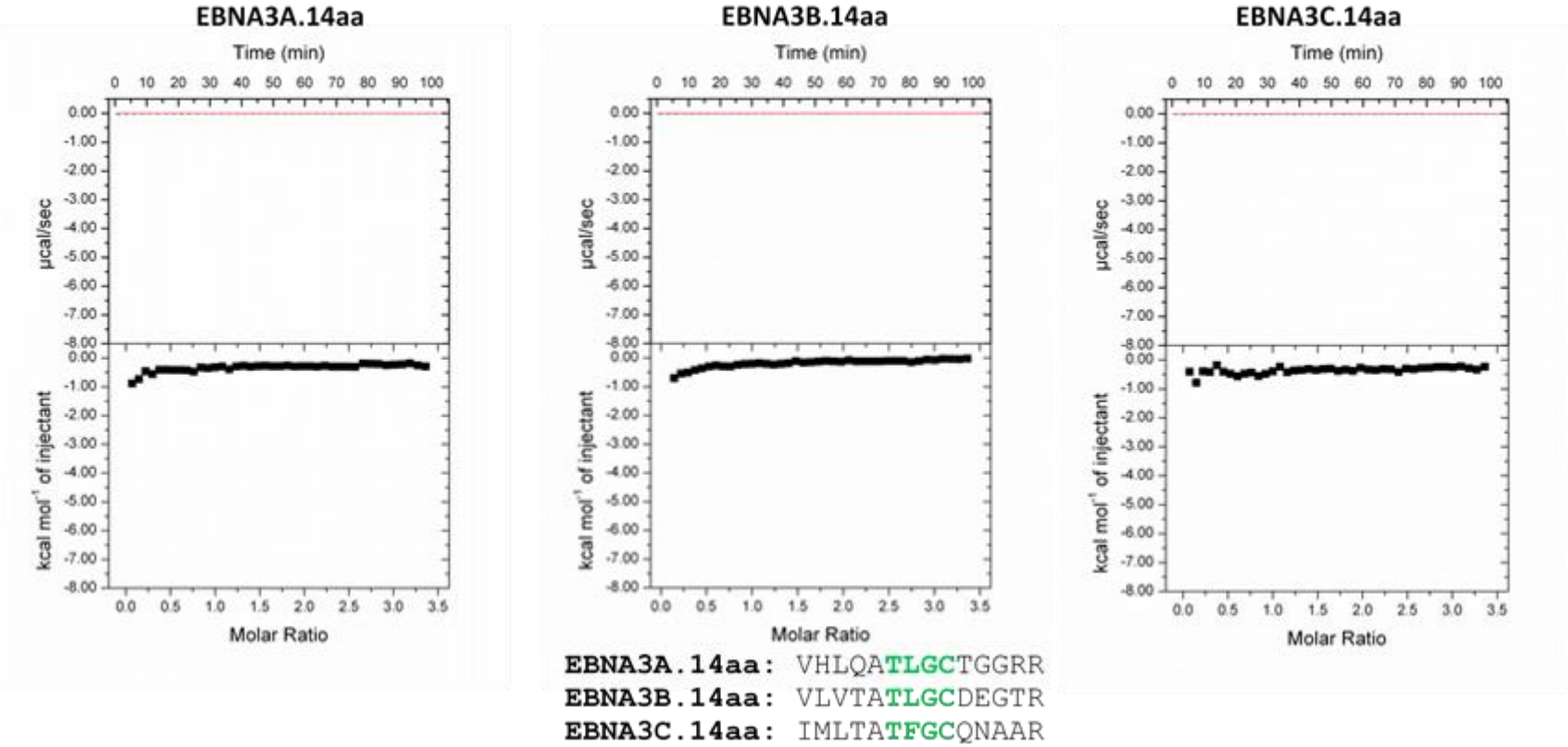


**Figure 3.25. Isothermal Titration Calorimetry analysis of the interaction between C-terminally His-tagged RBP-Jκ$_{8-435}$ expressed in insect cells and 14aa peptides of the EBNA3 family containing the TΦGC motif.** Heat peaks and integrated fitted heat peaks are shown for the interaction between RBP-Jk$_{8-435}$ and each of the 14aa EBNA3 peptides. The TΦGC RBP-Jk binding motif is highlighted in green in the amino acid sequences of each of the peptides.

### 3.2.1.4 : EBNA3C peptides bind RBP-Jκ through the WΦP RBP-Jκ binding motif

Previous studies identified an additional potential RBP-Jκ binding motif in EBNA3C that also resembles the WΦP RBP-Jκ binding motif (WTP)(Calderwood *et al.*, 2011). We sought to confirm this interaction using ITC. The WTP motif is located 15 amino acids c-terminal to the TFGC motif. We therefore investigated their binding affinities using a longer 33 amino acid EBNA3C$_{207\text{-}239}$ peptide (EBNA3C.33aa) containing both motifs and measured the impact of mutating either motif in this context. To do this we designed three 33 amino acid peptides of EBNA3C$_{207\text{-}239}$ that contained wild type EBNA3C (EBNA3C.33aa), the TΦGC RBP-Jκ binding motif mutated to alanines (EBNA3C.mTFGC.33aa) or the WΦP RBP-Jκ binding motif mutated to alanines (EBNA3C.mWTP.33aa) (Appendix 4).

The wild type EBNA3C peptide (EBNA3C.33aa) bound to RBP-Jκ$_{8\text{-}435}$ with a $k_d$ of 1.05μM (Figure 3.26) which was slightly stronger than the EBNA2.26aa-RBP-Jκ$_{8\text{-}435}$ interaction ($k_d$ of 3.9μM)(Figure 3.26) but similar to the EBNA2.14aa peptide affinity (Figure 3.23). Reapeats of these experiments confirmed these differences were small and may not be significant (Figure 3.30).

When the TΦGC RBP-Jκ binding motif was mutated to alanines there was no effect on the affinity of binding ($k_d$ of 1.57μM)(Figure 3.26) consistent with our previous observation that the TΦGC motif does not contribute to RBP-Jκ binding *in vitro*. These data indicate that RBP-Jκ binding of EBNA3C peptide is directed by the WTP motif. To confirm this, we mutated the WTP motif to alanines which abolished EBNA3C peptide binding to RBP-Jκ.

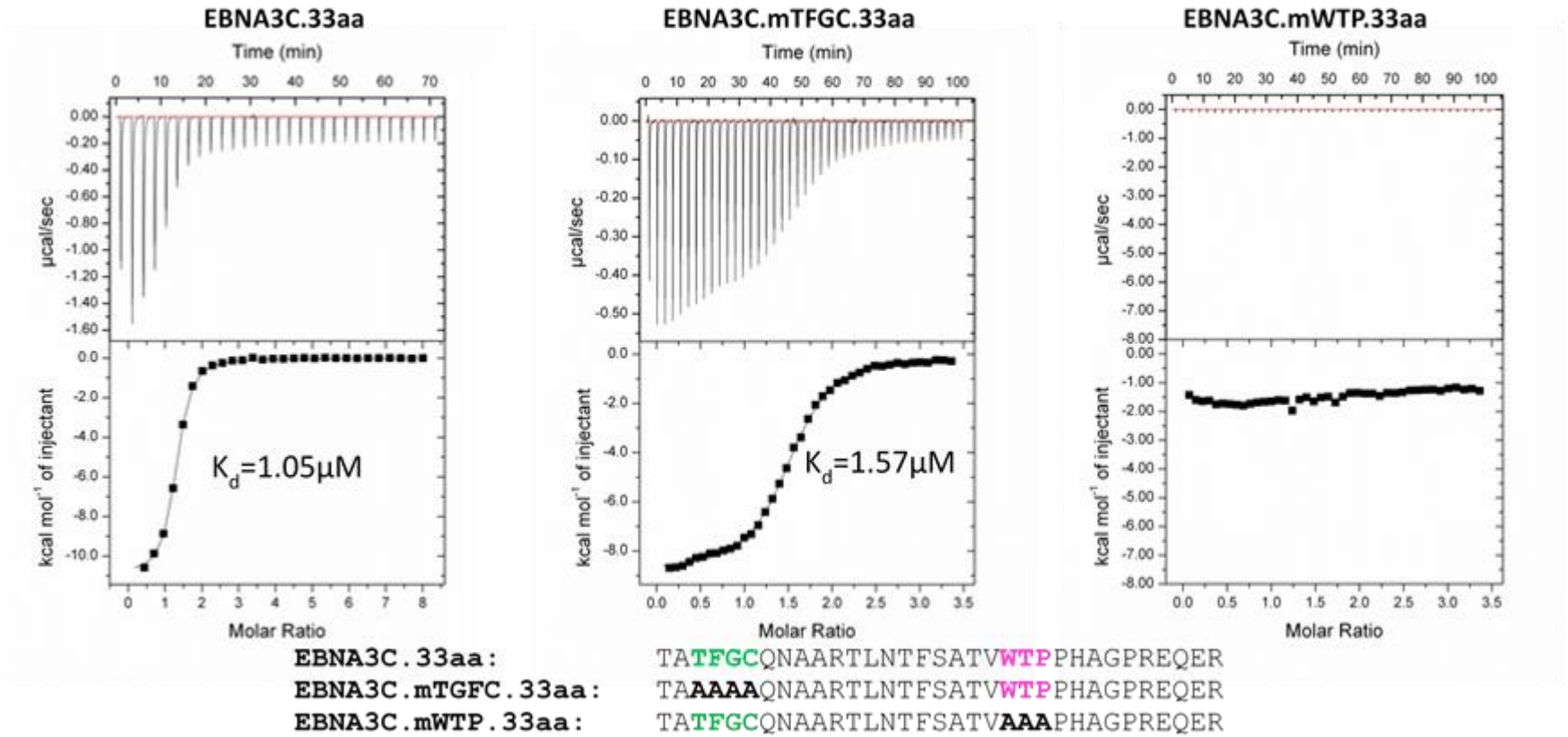


**Figure 3.26. Isothermal Titration Calorimetry analysis of the interaction between C-terminally His-tagged RBP-Jκ$_{8-435}$ expressed in insect cells and 33aa peptides of the EBNA3 family with knock outs of the TΦGC motif or WΦP Notch binding motif.** Heat peaks, the integrated fitted heat peaks and the $K_d$ are shown for the interactions between RBP-Jk$_{8-435}$ and each of the 33aa EBNA3. The TΦGC RBP-Jk binding motif and the WΦP Notch binding motif have been highlighted in green and pink respectively.

### 3.2.1.5 : Testing the binding of RBP-Jκ$_{8-435}$ expressed in *E.coli*

Due to time constraints and the unpredictable yields of RBP-Jκ$_{8-435}$ expressed in insect cells we we moved to RBP-Jκ$_{8-435}$ expressed in *E.coli.* In order to test whether the *E.coli* generated RBP-Jκ$_{8-435}$ bound effectively to EBNA peptides we undertook an ITC binding assay using the EBNA2.14aa peptide (Figure 3.27). We found that RBP-Jκ$_{8-435}$ expressed in *E.coli* bound to EBNA2.14aa with a $k_d$ of 1.67μM which was comparable to affinity between EBNA2.14aa peptide and RBP-Jκ$_{8-435}$ expressed in insect cells (Figure 3.27 and 3.30).

### 3.2.1.6 : Phosphorylating the threonine residue in the TΦGC RBP-Jκ binding motif does not affect RBP-Jκ binding

EBNA3C has been shown to be phosphorylated in EBV infected cell lines although which residues are phosphorylated and how this impacts EBNA3C function is unknown (Sample and Parker, 1994, West, 2006). We therefore tested whether phosphorylating the threonine in the TΦGC RBP-Jκ binding motif led to detectable RBP-Jκ binding. ITC was carried out using a 14 amino acid peptide of EBNA3C$_{204-217}$ with the threonine of the TΦGC RBP-Jκ binding motif phosphorylated (EBNA3C.P.14aa)(Figure 3.28)(Appendix 4). We detected no binding between RBP-Jκ$_{8-435}$ (expressed in *E.coli*) and the EBNA3C.P.14aa indicting that phosphorylation of this motif does not affect its ability to bind RBP-Jκ (Figure 3.28).

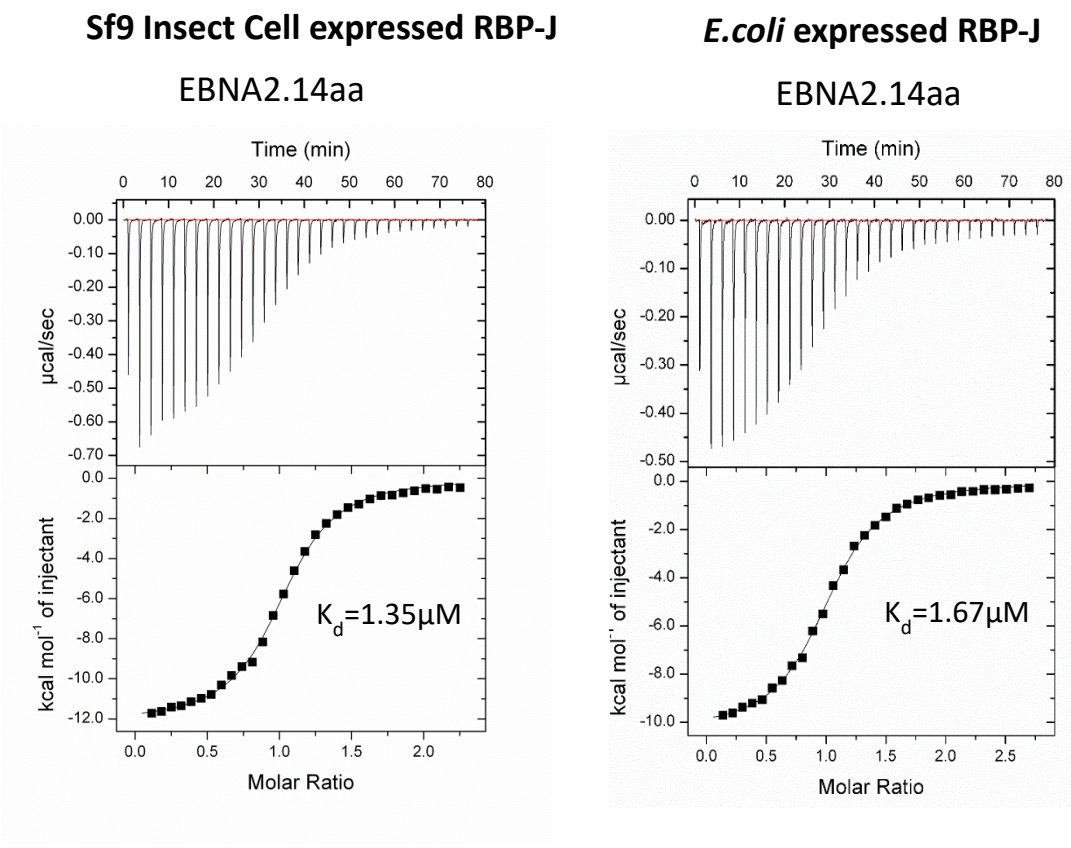


**Figure 3.27. Isothermal Titration Calorimetry of the interaction between C-terminally His-tagged RBP-Jk$_{8-435}$ expressed in Sf9 insect cells or Rosetta cells with a 14aa peptide of EBNA2 containing the WΦP Notch binding motif.** Heat peaks, the integrated fitted heat peaks and the $K_d$s are shown for the interactions between RBP-Jk$_{8-435}$ expressed in Sf9 or Rosetta cells with the EBNA2.14aa peptide in low salt buffer C + 1mM EDTA + 0.5% DMSO. The WΦP Notch binding motif has been highlighted in pink.

## EBNA3C.phos.14aa

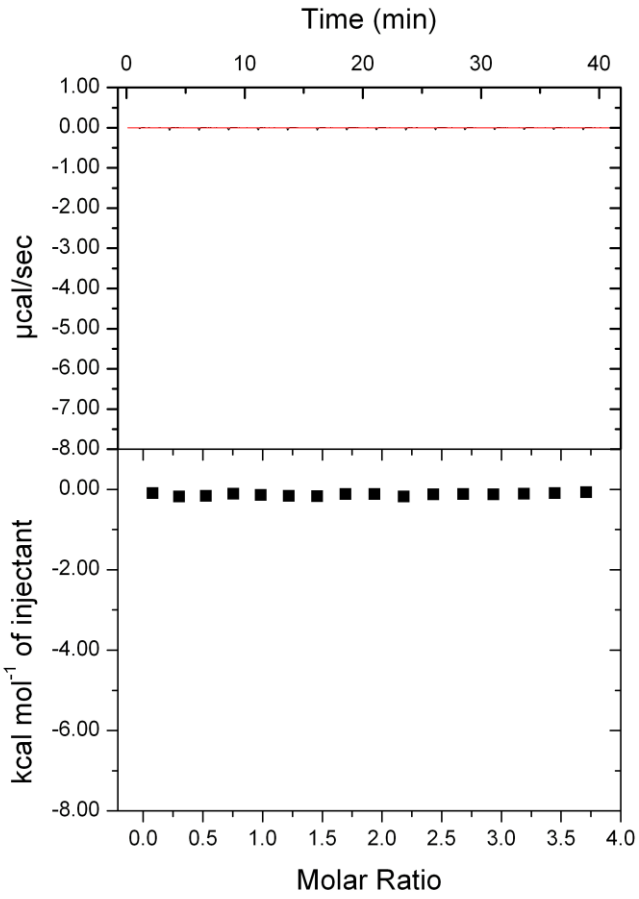


**EBNA3C.14aa:** IMLTA**T(P)FGC**QNAAR

**Figure 3.28. Isothermal Titration Calorimetry analysis of the interaction between C-terminally His-tagged RBP-Jk$_{8-435}$ expressed in *E.coli* cells and 14aa peptide of EBNA3C containing a phosphorylated TΦGC motif WΦP Notch binding motif.** Heat peaks and the integrated fitted heat peaks are shown for the interaction between RBP-Jk$_{8-435}$ and the EBNA3C.14aa.phos peptide in low salt buffer C + 1mM EDTA + 0.5% DMSO. The TΦGC RBP-Jk binding motif has been highlighted in green.

### 3.2.1.7 : Do residues in EBNA3A and EBNA3B that mimic the physiochemical properties of the WΦP RBP-Jκ binding motif facilitate binding to RBP-Jκ.

Although EBNA3A and EBNA3B do not contain a WΦP RBP-Jκ binding motif they do have residues with similar chemistry to WΦP RBP-Jκ binding motif that align with the WΦP RBP-Jκ binding motif of EBNA3C. The tryptophan in the WΦP RBP-Jκ binding motif has a large hydrophobic aromatic side chain like the phenylamine residue found in the same position on EBNA3A and is hydrophobic like the valine in the same position on EBNA3B. The middle residue in the WΦP RBP-Jκ binding motif is not highly conserved in Notch and thermodynamically contributes the least to RBP-Jκ binding (Johnson *et al.,* 2010) which may allow substitution of the lysine and glutamine residues that EBNA3A and EBNA3B have in this position respectively. Neither EBNA3A or EBNA3B have a proline in the third position of the EBNA3C WΦP RBP-Jκ binding motif they do have similarly hydrophobic residues leucine (EBNA3A) and isoleucine (EBNA3B) in the same position. We therefore tested whether 33 amino acid peptides of $EBNA3A_{197-239}$ and $EBNA3B_{205-237}$ that aligned to the EBNA3C.33aa peptide displayed any detectable RBP-Jκ binding by ITC (Appendix 4).

We found that the EBNA3A.33aa peptide produced a very weak binding curve when titrated onto RBP-$J\kappa_{8-435}$ (expressed in *E.coli*)(Figure 3.29). The calculated $k_d$ of the RBP-Jκ-EBNA3A.33aa interaction was 329 μM (Figure 3.29). In order to measure the weak RBP-$J\kappa_{8-435}$- EBNA3A.33aa interaction we had to reduce the number of injections and increase the volume of peptide titrated each time in order increase the size of the binding peaks to produce a binding curve. EBNA3B.33aa did not have any significant RBP-$J\kappa_{8-435}$ (expressed in *E.coli*) binding (Figure 3.29). Whether this weak binding is physiologically relevant remains to be tested.

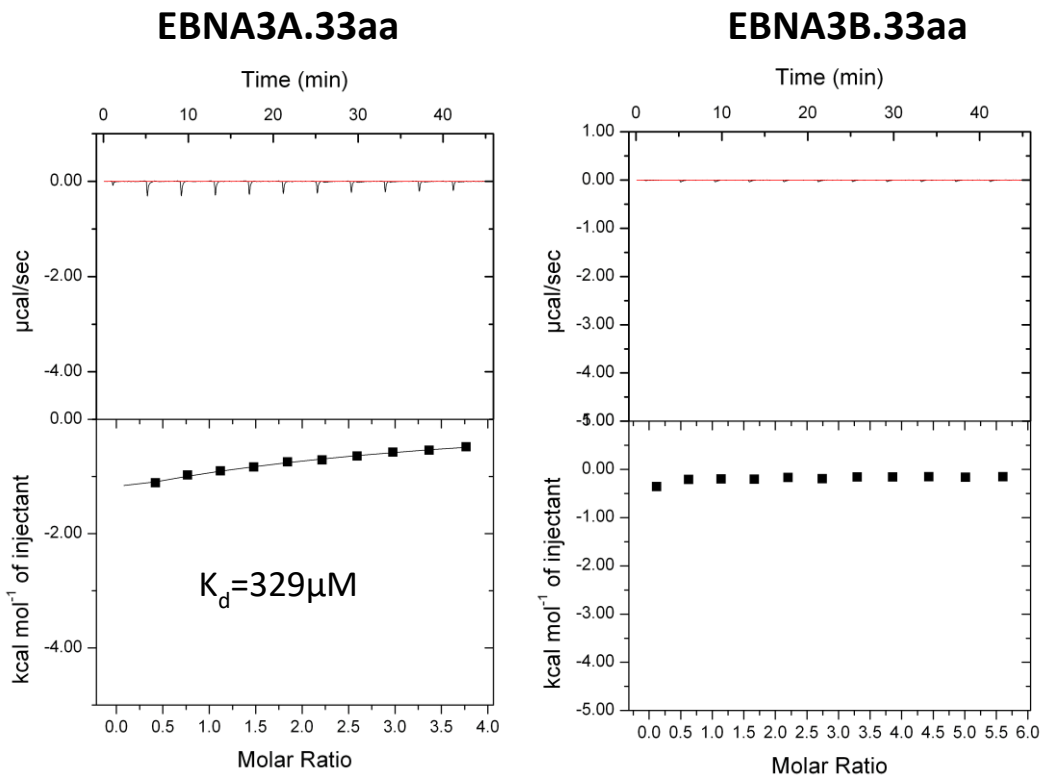


**EBNA3A.33aa:** QA**TLGC**TGGRRCHVTFSAGT**FKL**PRCTPGDRQW
**EBNA3B.33aa:** TA**TLGC**DEGTRHATTYSAGI**VQI**PRISDQNQKI
**EBNA3C.33aa:** TA**TFGC**QNAARTLNTFSATV**WTP**PHAGPREQER

**Figure 3.29. Isothermal Titration Calorimetry analysis of the interaction between C-terminally His-tagged RBP-Jκ$_{8-435}$ expressed in *E.coli* cells and 33aa peptides of the EBNA3A and EBNA3B family containing the TΦGC motif.** Heat peaks, the integrated fitted heat peaks and the $K_d$ are shown for the interaction between RBP-Jk$_{8-435}$ and each of the 33aa EBNA3. The TΦGC RBP-Jκ binding motif and the WΦP Notch binding motif have been highlighted in green and pink respectively. Hydrophobic residues that may mimic the WΦP Notch binding motif are highlighted red.

| Ligand | WØP | TØGC | $K_d$ (µM) | N | ΔS (Cal/mol/degree) | ΔH (kCal/mol) | ΔG (kCal/mol) |
|---|---|---|---|---|---|---|---|
| Notch2.26aa | ✓ | | 0.16 ± 0.01 | 0.83 | -1.63 | -9.9± 0.05 | -9.42 ± 0.06 |
| Notch2.26aa (R) | ✓ | | 0.27 ± 0.02 | 0.71 | -16.1 | -14± 0.11 | -9.12 ± 0.07 |
| EBNA2.14aa (Insect) | ✓ | | 1.35 ± 0.07 | 1.02 | -13.2 | -12.1 ± 0.07 | -8.09 ± 0.04 |
| EBNA2.14aa (*E.coli*) | ✓ | | 1.67 ± 0.06 | 1.02 | -7.66 | -10.33 ± 0.06 | -8.00 ± 0.05 |
| EBNA2.26aa | ✓ | | 3.9 ± 0.11 | 1.06 | -1.46 | -7.9 ± 0.06 | -7.50 ± 0.07 |
| EBNA2.26aa (R) | ✓ | | 4.7 ± 0.2 | 0.96 | -4.02 | -8.6 ± 0.09 | -7.38 ± 0.08 |
| EBNA3A.14aa | | ✓ | - | - | - | - | - |
| EBNA3B.14aa | | ✓ | - | - | - | - | - |
| EBNA3C.14aa | | ✓ | - | - | - | - | - |
| EBNA3C.Phos.14aa | | ✓ | - | - | - | - | - |
| EBNA3A.33aa | ~ | ✓ | 329 ± 17.8 | 1.00 | -21.5 | -11.3 ± 0.45 | -0.63 ± 0.02 |
| EBNA3A.33aa (R) | | ✓ | 251 ± 23.2 | 1.00 | -3.69 | -6.1 ± 0.39 | -4.9 ± 0.3 |
| EBNA3B.33aa | | ✓ | - | - | - | - | - |
| EBNA3C.33aa | ✓ | ✓ | 1.05 ± 0.09 | 1.19 | -9.85 | -11.2 ± 0.1 | -8.29 ± 0.08 |
| EBNA3C.33aa (R) | ✓ | ✓ | 1.23 ± 0.05 | 1.21 | -9.00 | -10.9 ± 0.06 | -8.17 ± 0.04 |
| EBNA3C.33aa.mTFGC | ✓ | | 1.57 ± 0.05 | 1.50 | -2.70 | -8.7 ± 0.03 | -8.05 ± 0.15 |
| EBNA3C.33aa.mWTP | | ✓ | - | - | - | - | - |
| EBNA3C.33aa.mTFGC.mWTP | | | - | - | - | - | - |
| EBNA3C.33aa (DNA) | ✓ | ✓ | 0.72 ± 0.02 | 1.01 | -7.10 | -10.6 ± 0.03 | -10.38 ± 0.19 |
| *Notch consensus 24aa* | ✓ | | *0.072 ± 0.004* | - | *−10.1* | *−19.8 ± 0.5* | *-9.93 ± 0.02* |
| *EBNA2 27aa* | ✓ | | *4.6 ± 1.3* | - | *−2.80* | *−10.2 ± 3.1* | *-7.33 ± 0.18* |

**Figure 3.30. Table containing summary of all interactions studied with Isothermal Titration Calorimetry.** The motifs that peptides contained is indicated by ticks. In italics is data from a previous study paper for comparison (Johnson *et al.*, 2010). (R) represents repeats.

### 3.2.2.1 : Fluorescent polarisation competition assay to measure whether EBNA3C WΦP RBP-Jκ binding motif can compete with EBNA2 for RBP-Jκ binding.

We next wanted to determine whether the WΦP RBP-Jκ binding motifs on EBNA2 EBNA3C competed for RBP-Jκ binding. To do this we designed a 28 amino acid fluorescein tagged EBNA2 peptide containing the WΦP RBP-Jκ binding motif (EBNA2.28aa.FP)(Appendix 4). Two Glycine residues were added to the EBNA2.26aa peptide sequence in order to facilitate the chemistry needed to covalently bind the fluorescein tag to the EBNA2.28aa.FP peptide.

Initial experiments tested the binding of the EBNA2.28aa.FP peptide to RBP-$J\kappa_{8-435}$ (expressed in insect cells) using FP. EBNA2.28aa.FP peptide was added to wells containing serially diluted RBP-$J\kappa_{8-435}$ to measure the EBNA2.28aa.FP-RBP-$J\kappa_{8-435}$ interaction. We found that the peptide bound efficiently with a $k_d$ of 0.39μM (Figure 3.31). Although this was lower than the $k_d$ measured by ITC for the EBNA2.26aa-RBP-$J\kappa_{8-435}$ interaction it is acknowledged that FP has an increased sensitivity compared to ITC.

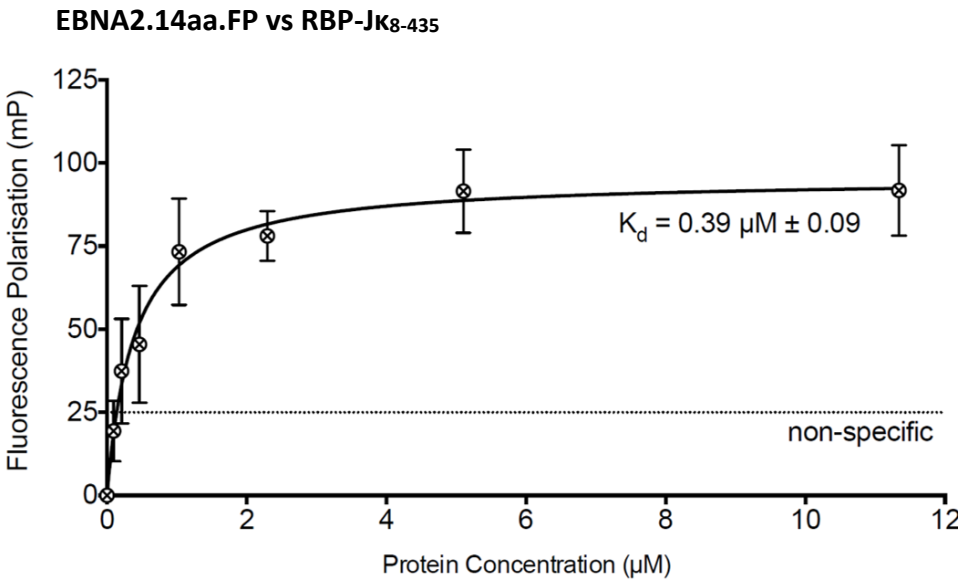


**Figure 3.31. Fluorescent polarisation end point assay of N-terminally Fluorescein-tagged EBNA2 peptide vs C-terminally His-tagged RBP-Jκ$_{8-435}$ expressed in insect cells.** An excess of EBNA2.26aa.FP was added to wells containing serially diluted RBP-Jκ$_{8-435}$ and the amount of EBNA2.26aa.FP bound to RBP-Jκ$_{8-435}$ was measured in each well in order to estimate the $K_d$ of the interaction. This $K_d$ could then be used to calculate the [RBP-Jκ$_{8-435}$] and [EBNA2.26aa.FP] needed for the fluorescent polarisation competition assays.

### 3.2.2.2 : The EBNA3C WΦP RBP-Jκ binding motif and not the TΦGC motif competes with EBNA2 for RBP-Jκ binding.

We serially diluted 10μM of competitor peptide based on the $k_d$s calculated from our ITC data. Unlabelled EBNA2.26aa peptide was serially diluted over EBNA2.28aa.FP-RBP-J$\kappa_{8-435}$ complex and competed off EBNA2.28aa.FP peptide from RBP-Jκ (Figure 3.32). The EBNA2.26aa only competed off 50% of the EBNA2.28aa.FP peptide from the EBNA2.28aa.FP-RBP-J$\kappa_{8-435}$ complex as they likely established an equilibrium due to having similar affinities for RBP-Jκ. This served as a control for competitive binding of unlabelled peptides.

We also investigated the ability of the Notch2.26aa peptide to compete off the EBNA2.28aa.FP peptide from the EBNA2.28aa.FP-RBP-J$\kappa_{8-435}$ complex (Figure 3.32). Consistent with the higher affinity of Notch2 peptide binding to RBP-Jκ, this peptide was able to compete off all the EBNA2.28aa.FP peptide from the EBNA2.28aa.FP-RBP-J$\kappa_{8-435}$ complex (Figure 3.32).

We next tested if the EBNA3C 33aa peptide were able to compete off the EBNA2 peptide (EBNA2.28aa.FP) from RBP-J$\kappa_{8-435}$. We found that both the wild type EBNA3C (EBNA3C.33aa) and EBNA3C with the TΦGC RBP-Jκ binding motif mutated to alanines (EBNA3C.mTFGC.33aa) were able to compete for EBNA2.28aa.FP binding to a similar extent as the unlabelled EBNA2.26aa peptide (Figure 3.33).

We next tested whether EBNA3C with the WΦP RBP-Jκ binding motif (EBNA3C.33aa.mWTP) or both the RBP-Jκ binding motifs mutated to alanines (EBNA3C.33a.mTFGC.mWTP) were able to compete EBNA2.28aa.FP off of RBP-J$\kappa_{8-435}$. We showed that when the WΦP RBP-Jκ binding motif is mutated to alanines the ability

of the EBNA3C peptides to disrupt the interactions between EBNA2.28aa.FP-RBP-Jκ$_{8-435}$ was abolished (Figure 3.34). We obtained similar results for the double mutant EBNA3C peptide EBNA3C.33a.mTFGC.mWTP (Figure 3.34).

The competition binding assay had shown that the TΦGC RBP-Jκ binding motif does not contribute to EBNA3Cs ability to compete with EBNA2 for RBP-Jκ binding, in the context of the peptide, contrary to a previous yeast-2-hybrid screen (Zhao *et al.*, 1996)(Figure 3.33 and 3.34). Instead they showed that the WΦP RBP-Jκ binding motif was essential for EBNA3C to compete with EBNA2 for RBP-Jκ binding in the context of the peptides. To validate the roles of WΦP and TΦGC RBP-Jκ binding motifs in EBV hijacking of RBP-Jκ mediated genes shown in our ITC data *in vivo* cell assays needed to be done to determine if these observations were artefacts of the peptides.

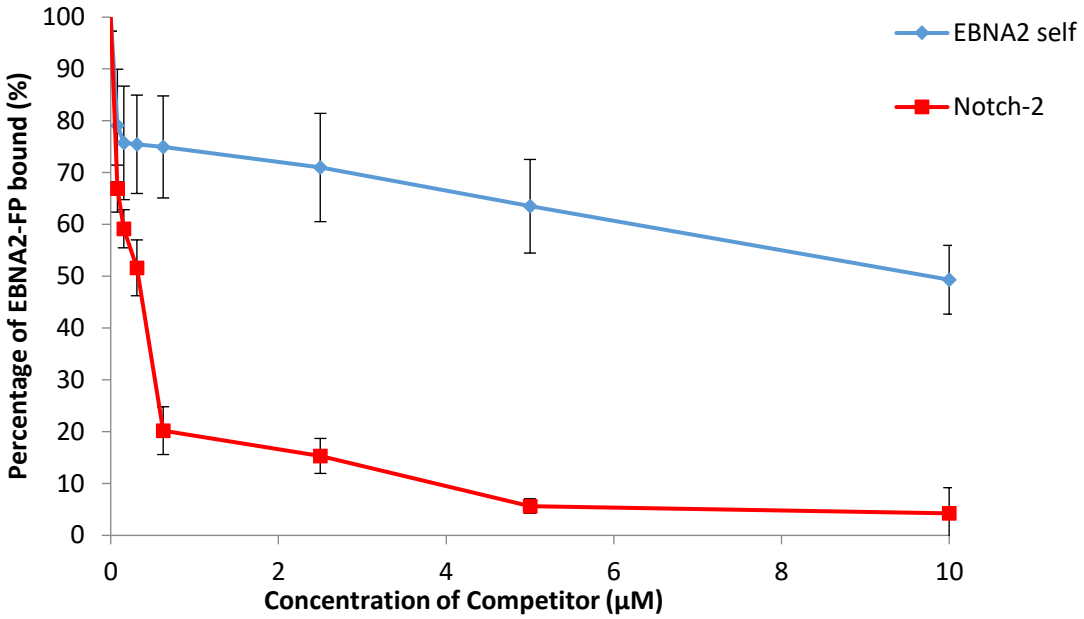


**EBNA2.26aa.FP** FP-GGQQLHHLPSGPPWWPPICDPPQPSKTQ
**EBNA2.26aa:** QQLHHLPSGPPWWPPICDPPQPSKTQ
**Notch2.26aa:** MAKRKRKHGSLWLPEGFTLRRDASNH

**Figure 3.32. Fluorescent polarisation competition binding assay between EBNA2.26aa.FP-RBP-J$_{8-435}$ complex expressed in insect cells and EBNA2.26aa or Notch.26aa peptides.** EBNA2.26aa.FP-RBP-J$_{8-435}$ complex was added to wells containing serially diluted competitor peptide. A control competition assay was run in parallel using an EBNA2.26aa peptide which did not have a fluoroscein tag. The flourescein tag and the WΦP RBP-Jk binding motif are highlighted in orange and pink respectively in the peptide sequences below. The bars show the standard deviation for each concentration of competitor peptide which was done in triplicate.

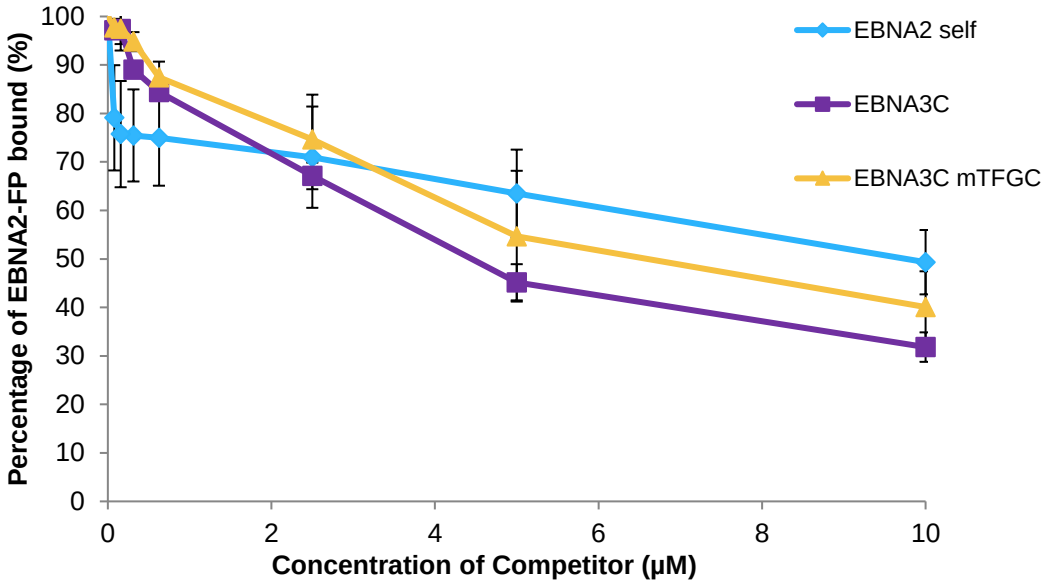


**EBNA2.26aa.FP** FP-GGQQLHHLPSGPPWWPPICDPPQPSKTQ
**EBNA2.26aa:** QQLHHLPSGPPWWPPICDPPQPSKTQ
**EBNA3C.33aa:** TATFGCQNAARTLNTFSATVWTPPHAGPREQER
**EBNA3C.mTGFC.33aa:** TAAAAAQNAARTLNTFSATVWTPPHAGPREQER

**Figure 3.33. Fluorescent polarisation competition binding assay between EBNA2.26aa.FP-RBP-$J_{8-435}$ complex expressed in insect cells and EBNA2.26aa, EBNA3C.33.aa or EBNA3C.33aa.mTFGC peptides.** EBNA2.26aa.FP-RBP-$J_{8-435}$ complex was added to wells containing serially diluted competitor peptide. A control competition assay was run in parallel using an EBNA2.26aa peptide which did not have a fluoroscein tag. The flourescein tag, the WΦP RBP-Jk binding motif and the TΦFC motif are highlighted in orange, pink and green respectively in the peptide sequences below. The bars show the standard deviation for each concentration of competitor peptide, which was done in triplicate.

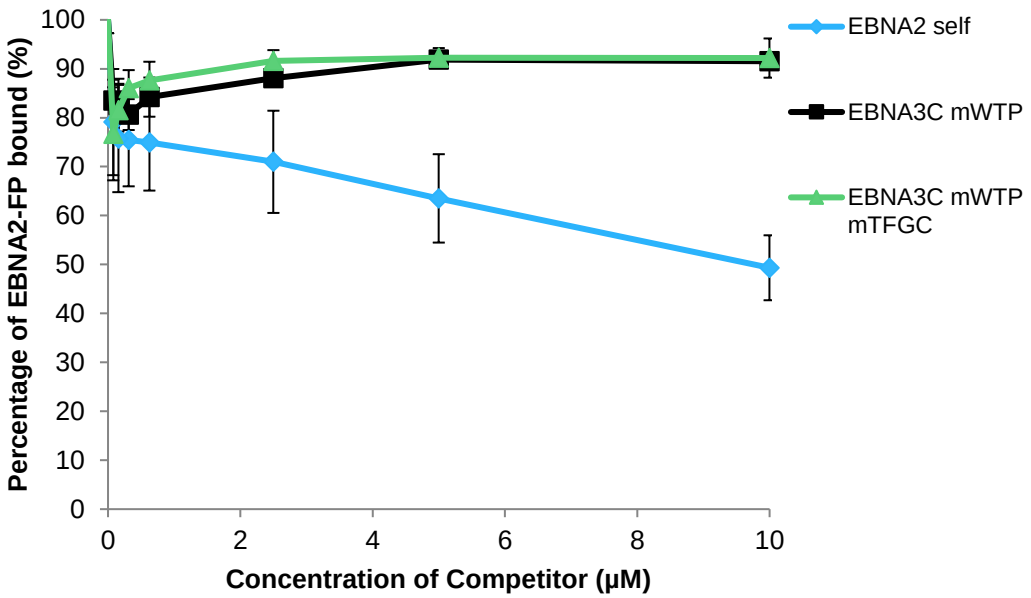


**EBNA2.26aa.FP** FP-GGQQLHHLPSGPPWWPPICDPPQPSKTQ
**EBNA2.26aa:** QQLHHLPSGPPWWPPICDPPQPSKTQ
**EBNA3C.mWTP.33aa:** TATFGCQNAARTLNTFSATVAAAPHAGPREQER
**EBNA3C.mTFGC.mWTP.33aa:** TAAAAAQNAARTLNTFSATVAAAPHAGPREQER

**Figure 3.34. Fluorescent polarisation competition binding assay between EBNA2.26aa.FP-RBP-J$_{8-435}$ complex expressed in insect cells and EBNA2.26aa or EBNA3C peptides with the WΦP motif mutated to alanines.** EBNA2.26aa.FP-RBP-J$_{8-435}$ complex was added to wells containing serially diluted competitor peptide. A control competition assay was run in parallel using an EBNA2.26aa peptide which did not have a fluoroscein tag. The flourescein tag, the WΦP RBP-Jk binding motif and the TΦFC motif are highlighted in orange, pink and green respectively in the peptide sequences below. The bars show the standard deviation for each concentration of competitor peptide, which was done in triplicate.

### 3.2.3.1 : Design of the RBP-Jκ consensus site nanolever and measuring RBP-Jκ-DNA interactions using the SwitchSense Biosensor

We wanted to study whether EBNA peptide binding caused conformational changes in RBP-Jκ similar to the effects of Notch binding (Friedmann *et al.*, 2008) or had any effect on RBP-Jκ DNA binding so we used SwitchSense to explore this. We first needed to design a DNA nanolever that contained the RBP-Jκ DNA site. RBP-Jκ consensus site nanolever was designed by Dynamic Biosensors to ensure the DNA nanolever would not fold into secondary structures which would interfere with measurements (Figure 3.35). The negative control nanolever was provided from a bank of negative controls developed by Dynamic Biosensors which are also designed not to fold into secondary structures (Figure 3.35).

C-terminally His-tagged RBP-Jκ$_{8-435}$ expressed in insect cells was incubated with Switchsense chips with RBP-Jκ DNA consensus site and control nanolever bound to different electrodes. RBP-Jκ$_{8-435}$ was added to the Switchsense chip at different concentrations (10nM, 100Nm and 1µM) to determine which concentration was optimal for producing smooth binding and disassociation curves. The dynamic response is shown to slow, producing binding curves, as RBP-Jκ$_{8-435}$ binds to both the RBP-Jκ consensus site and to the control nanolever. It was discovered that the nanolever chosen from Biosensor bank of negative controls contained a RBP-Jκ non-consensus site shown to bind RBP-Jκ (Figure 3.35 and 3.36)(Friedmann and Kovall, 2010). This unfortunately meant we had to proceed with the SwitchSense assays with no negative control. We found that 1µM of RBP-Jκ$_{8-435}$ saturated the chip too quickly and generated a noisy signal, which was difficult to measure, and 10nM of RBP-Jκ$_{8-435}$

did not result in detectable binding (Figure 3.36). 100nM of RBP-Jκ$_{8-435}$ gave suitable a signal and this concentration of RBP-Jκ was used for future experiments (Figure 3.36).

The SwitchSense software calculated $k_{on}$ from the binding curves generated from measuring the dynamic response in real time (Figure 3.36). The $k_{off}$ was measured by washing the unbound RBP-Jκ$_{8-435}$ from the chip and allowing the RBP-Jκ$_{8-435}$ to disassociate from the DNA overnight, although due to how tightly the RBP-Jκ$_{8-435}$ bound to the DNA we were not able to gather the data for a complete disassociation curve. From the $k_{on}$ and the $k_{off}$ we used the SwitchSense software to calculate the approximate $k_d$s of the interactions between RBP-Jκ$_{8-435}$ and the RBP-Jκ DNA consensus site (Figure 3.36). As expected the RBP-Jκ$_{8-435}$ bound to consensus site nanolever ($k_d$ = ~20nM) tighter than non-consensus nanolever ($k_d$ = ~70nM). The $k_d$ calculated for RBP-Jκ binding to DNA was in line with previously published data from ITC studies (70nM) (Friedmann and Kovall, 2010).

**Sequence of RBP-Jκ consensus nanolever (69 bp):**

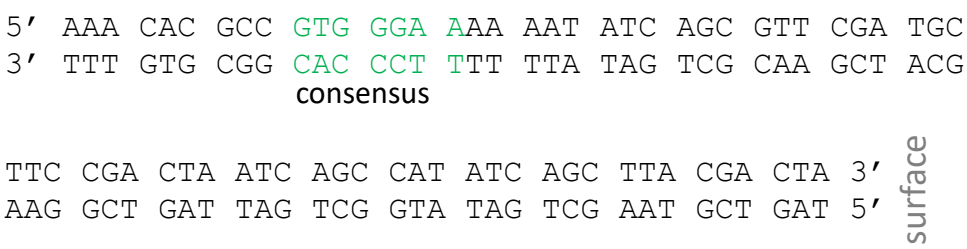


**Sequence of control nanolever (48 bp control):**

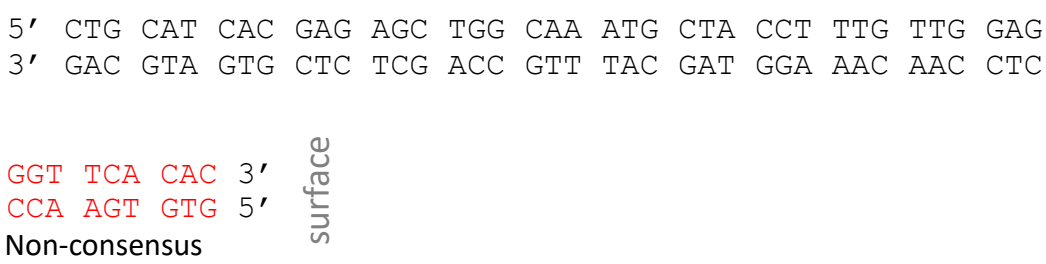


**Figure 3.35. DNA Sequences of the RBP-Jκ consensus and control Switchsense nanolevers.** Shown are the DNA sequences of the double stranded designed sequences. The RBP-Jκ consensus and non-consensus sites have been coloured in green and red respectively. The end of the DNA nanolever that is exposed to buffer are labelled surface. The single stranded sequence used to anneal the nanolever to the DNA switch which is attached to the chip is not shown.

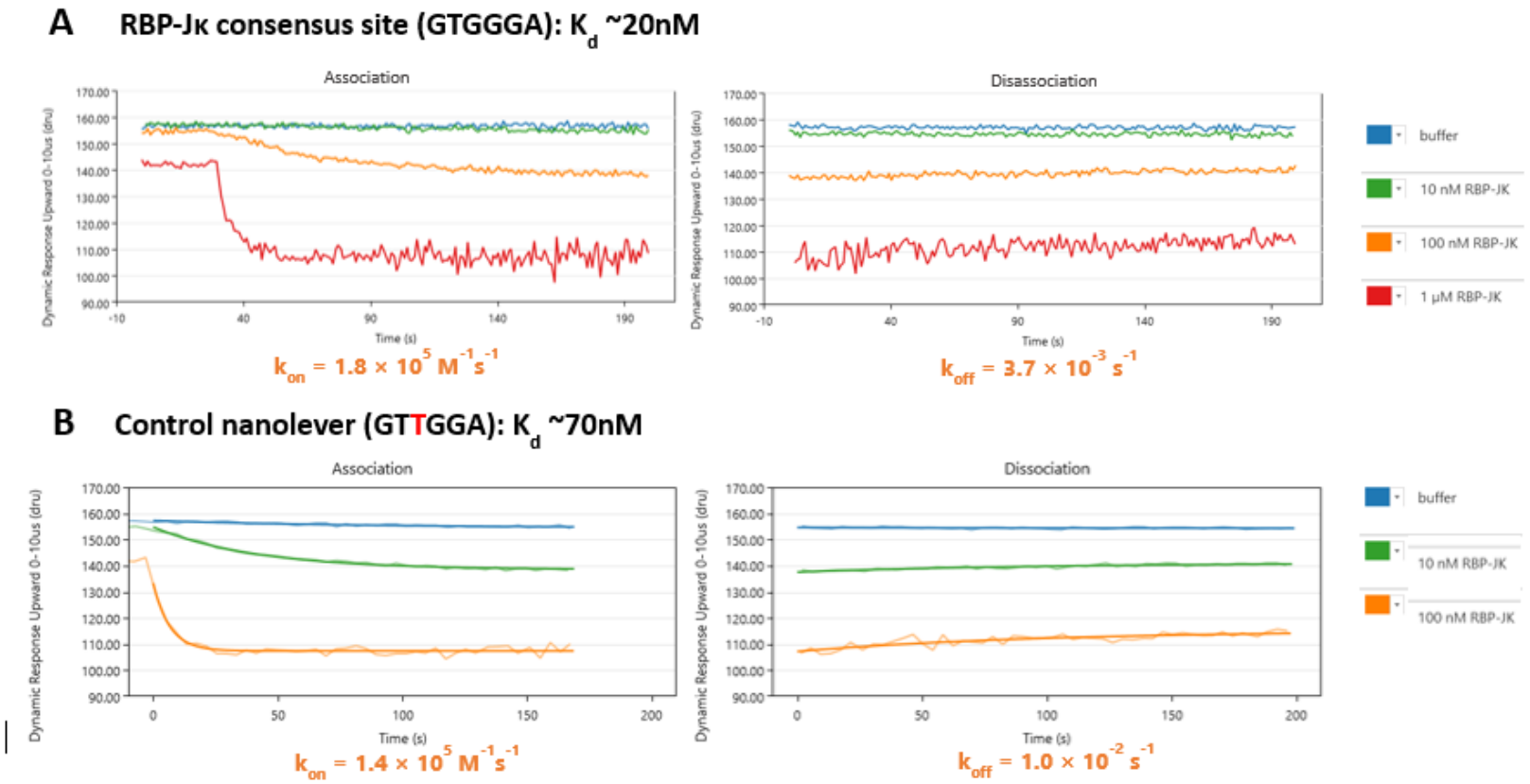


**Figure 3.36. SwitchSense assay showing C-terminally his-tagged RBP-Jκ$_{8-435}$ expressed in insect cells binding to DNA containing a RBP-Jκ consensus site or a RBP-Jκ non-consensus site. A.** Oligos containing the RBP-Jκ consensus site were annealed to the chip then RBP-Jk$_{8-435}$ at different concentrations was passed across the chip. As RBP-Jκ bound the dynamic response of the switch was measured generating binding and dissociation curves from which $K_d$s could be calculated. **B**. The chip was boiled to clean the chip, a non-consensus oligo was bound and RBP-Jk$_{8-435}$ at different concentrations was passed across to generate binding curves from which $K_d$s could be calculated.

### 3.2.3.2 : EBNA2 peptide and the Notch 2 peptide potentially induce conformational changes in RBP-Jκ$_{8-435}$

We next investigated whether EBNA peptides binding affected RBP-Jκ$_{8-435}$-DNA interactions. We preincubated C-terminally His-tagged RBP-Jκ$_{8-435}$ expressed in insect cells with each of the EBNA peptides (EBNA2.26aa, EBNA3C.33aa and EBNA3C.mTFGC.mWTP.33aa, as negative control) and the Notch2.26aa peptide and then injected the complexes over the chip with RBP-Jκ DNA consensus site nanolevers bound (Figure 3.37). The dynamic response of the RBP-Jκ consensus nanolevers slowed as each of the peptide-RBP-Jκ$_{8-435}$ complexes bound to the nanolevers generating association curves (Figure 3.37). The EBNA3C.33a peptide did not affect the ability of RBP-Jκ$_{8-435}$ to bind to DNA (Figure 3.37A). However, the RBP-Jκ$_{8-435}$ bound to Notch 2 peptide appeared to have a faster dynamic response than just RBP-Jκ$_{8-435}$ bound to the RBP-Jκ DNA consensus nanolever, which was which could indicate the induction of conformational changes reducing the hydrodynamic friction of the RBP-Jκ$_{8-435}$. This is consistent with previous reports demonstrating Notch RAM domain peptide induced conformational changes in CSL, which were essential to Notch complex assembly (Friedmann *et al.*, 2008).

Interestingly, when the EBNA2.26aa peptide bound to RBP-Jκ$_{8-435}$, it appeared to induce conformational changes in RBP-Jκ$_{8-435}$ that reduced the hydrodynamic friction and these appeared to be greater than the effects of the Notch2.26aa peptide (Figure 3.37A). This can be seen more clearly when a single recovery of the nanolever is plotted (Figure 3.37B).

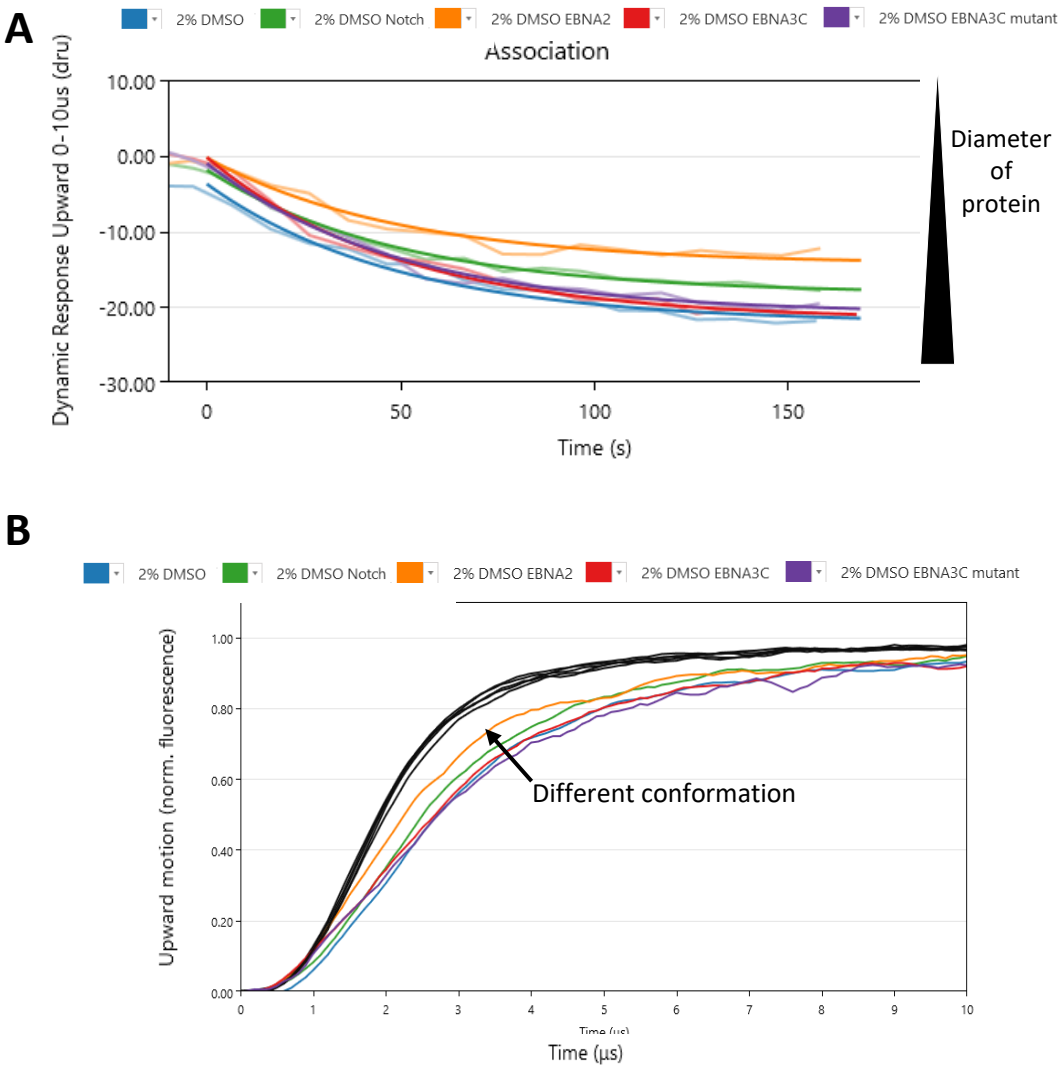


**Figure 3.37. SwitchSense assay showing C-terminally his-tagged RBP-Jκ$_{8-435}$ expressed in insect cells complexed with peptides of Notch or EBNAs binding to DNA RBP-Jk consensus. A.** RBP-Jk was incubated with different peptides and passed over the switchsense chip with nanolevers containing a RBP-Jk consensus site bound to the switches. As RBP-Jk bound this slows the dynamic response creating a binding curve. **B.** A trace of a single motion of the switch during the previously described assays. Empty switches are shown in black. Changes in RBP-Jκ were measured when Notch or EBNA2 peptide was complexed with RBP-Jκ. Hwever no changes in conformation were measured when RBP-Jκ was complexed with EBNA3C peptide.

### 3.2.3.3 : DMSO does not significantly affect RBP-Jκ$_{8-435}$ DNA binding.

Due to the SwitchSense biosensor having the sensitivity required to measure conformational changes of RBP-Jκ$_{8-435}$ we wanted to test whether the DMSO we had added to the ITC binding assay to solubilise the larger peptides had had a negative effect on RBP-Jκ$_{8-435}$. To do this, we incubated C-terminally His-tagged RBP-Jκ$_{8-435}$ expressed in insect cells in buffer with and without 2% DMSO and then injected it onto chips with RBP-Jκ consensus site nanolevers bound. In the association and disassociation curves there is no evidence to show RBP-Jκ$_{8-435}$-DNA interactions were affected by the DMSO (Figure 3.38 A and B). The RBP-Jκ$_{8-435}$ incubated in DMSO did have a marginally slower dynamic response compared to the RBP-Jκ$_{8-435}$ not incubated in DMSO suggesting that it may have a more open conformation. However we were assured by the technicians from Dynamic Biosensors that the difference shown was insignificant and that DMSO was not inducing conformational changes that would be detrimental to RBP-Jκ$_{8-435}$ functionality (Figure 3.38 A and B).

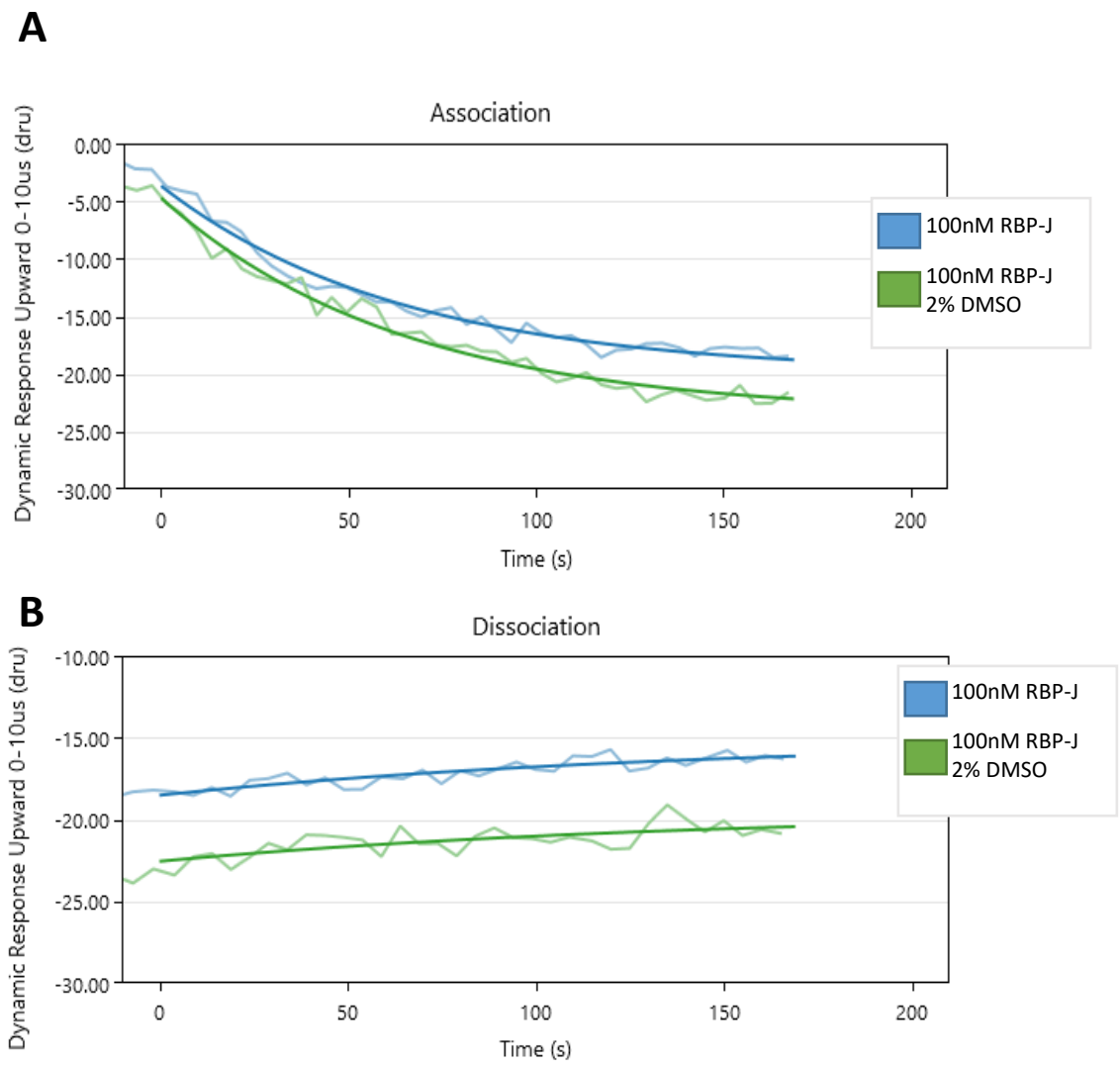


**Figure 3.38. SwitchSense assay in buffer with or without DMSO showing C-terminally his-tagged RBP-Jk$_{8-435}$ expressed in insect cells binding to DNA containing a RBP-Jk consensus site. A. B**inding curve of C-terminally his-tagged RBP-Jk$_{8-435}$ expressed in insect cells in buffer with and without 2% DMSO. **B.** A disassociation curve of C-terminally his-tagged RBP-Jk$_{8-435}$ expressed in insect cells in buffer with and without 2% DMSO.

### 3.2.4.1 : Design and optimisation of pull-down assay to study the EBNA3C RBP-Jκ binding motifs.

Previous data had indicated that mutation of the TFGC motif in EBNA3C to AAAA disrupted RBP-Jκ binding (Zhao *et al.*, 1996, Calderwood *et al.*, 2011). However, we found no binding of the TFGC motif *in vitro*. We therefore hypothesised that the TFGC-AAAA mutation may have disrupted the folding of EBNA3C. We set out to mutate residues of EBNA3C to study the effects on binding of full length EBNA3C. We introduced mutations in full length EBNA3C to generate mammalian expression vector encoding EBNA3C$_{T209A}$ (pSG53C.TA), EBNA3C$_{F210A}$ (pSG53C.FA) and EBNA3C$_{TF209AA}$ (pSG53C.TFAA) mutants of the EBNA3C TΦGC RBP-Jκ binding motif (Figure 39). We did not mutate the glycine and cysteine residues of the TΦGC RBP-Jκ binding motif as we hypothesised they may play key roles in folding. We also generated an EBNA3C$_{W227S}$ (pSG53C.STP) mutant of the WΦP RBP-Jκ binding motif and a EBNA3C$_{TFGC209AAAA.W227S}$ double mutant of both the RBP-Jκ binding motifs (EBNA3C.JK.STP) (Figure 3.39).

These vectors were then transfected into EBV negative Burkitts lymphoma cell line (DG75) alongside a previously generated EBNA3C$_{TFGC209AAAA}$ mutant and cells were harvested 48 hours post transfection (Figure 3.40 and 3.41).

C-terminally His-tagged RBP-Jκ$_{8-435}$ was expressed in *E.coli* and bound to talon beads to be used as bait for the pulldown. We ran a sample of the beads against BSA standards in order to quantify how much RBP-Jκ$_{8-435}$ bound to the talon beads (Figure 3.42).

However, when we carried out the pulldown western blot analysis showed that the EBNA3C was pulled down even when RBP-Jκ was not incubated with the $Co^{2+}$ beads (Figure 3.43). This demonstrated the EBNA3C construct was binding non-specifically to

the $Co^{2+}$ beads. Due to time constraints we were unable to optimise the pulldown conditions to remove the EBNA3C background binding to the $Co^{2+}$ beads.

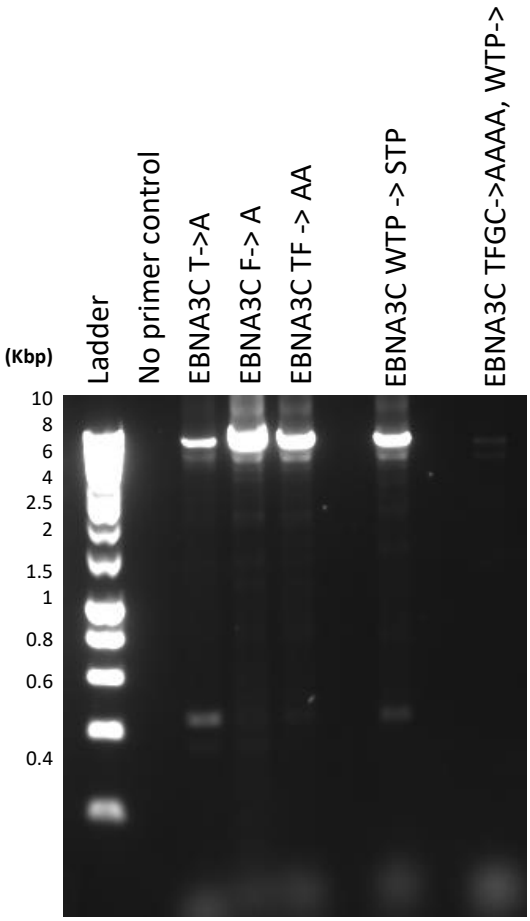


**Figure 3.39. Mutagenesis of full length EBNA3C RBP-Jk binding motifs TFGC and WTP.** Agarose gel showing PCR products after site directed mutagenesis reactions. The plasmid product predicted band size was 7055bp. All successful mutagenesis reactions were transformed in to competent *E.coli*, colonies were picked and DNA was extracted and sent for sequencing.

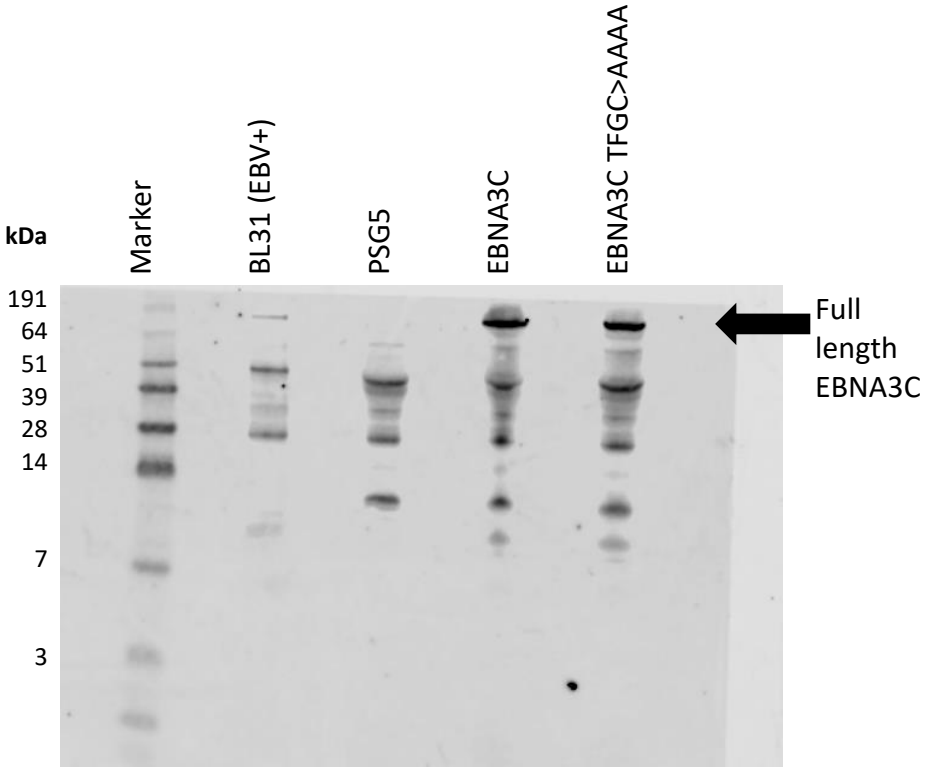


**Figure 3.40. Western blot analysis following transfection of plasmids expressing wild type EBNA3C and EBNA3C mutants.** Cells were transfected with pSG5 vector, pSG5 wild type full length EBNA3C (pSG5.3C) or pSG5 vector with EBNA3C TFGC-AAAA mutant. Whole cell and lysate samples were analysed by SDS-PAGE. The gel was probed with an anti-EBNA3C antibody and BL31 EBV positive cell line was used as a positive control. The predicted band size for EBNA3C is 90kDa.

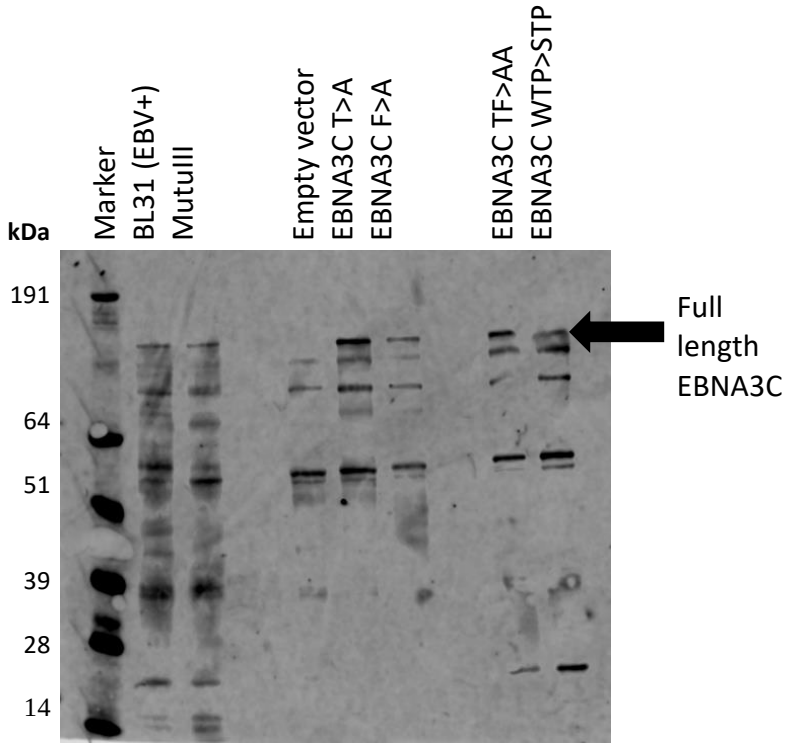


**Figure 3.41. Western blot analysis following transfection of plasmids expressing wild type EBNA3C and EBNA3C mutants.** Cells were transfected with PSG5 vector, pSG5 vector with full length EBNA3C with TFGC mutated to AFGC, TAGC or AAGC or a pSG5 vector with full length EBNA3C WTP mutated to STP. Whole cell and lysate samples were analysed by SDS-PAGE. The gel was probed with an anti-EBNA3C antibody and BL31 EBV positive cell line and MutuIII cell line was used as a positive control. The predicted band size for EBNA3C is 90kDa.

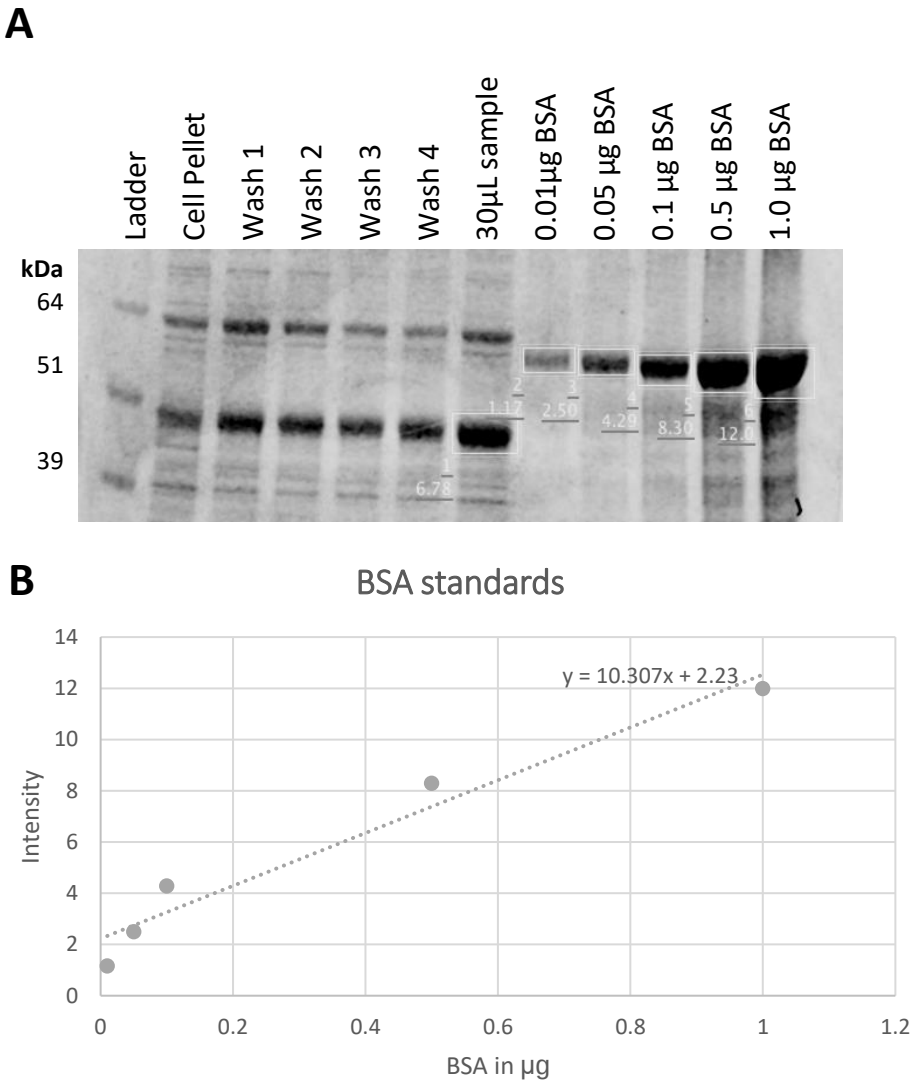


**Figure 3.42. Quantification of C-terminally His-tagged RBP-Jk$_{8-435}$ expressed in 100ml *E.coli* bound to 100µL of $Co^{2+}$ beads (Talon) . A.** Coomassie stained gel beads sampled from each step and 30µL of beads was analysed for the final quantification. Comparing to the BSA standards it was estimated there was approximately 30µM represented in the. Shown in yellow were the numbers used to calculate the concentration of RBP-Jk$_{8-435}$ on the beads. **B.** Graph of concentrations of BSA standards plotted against intensities measured for BSA controls. Formula of trend line is shown.

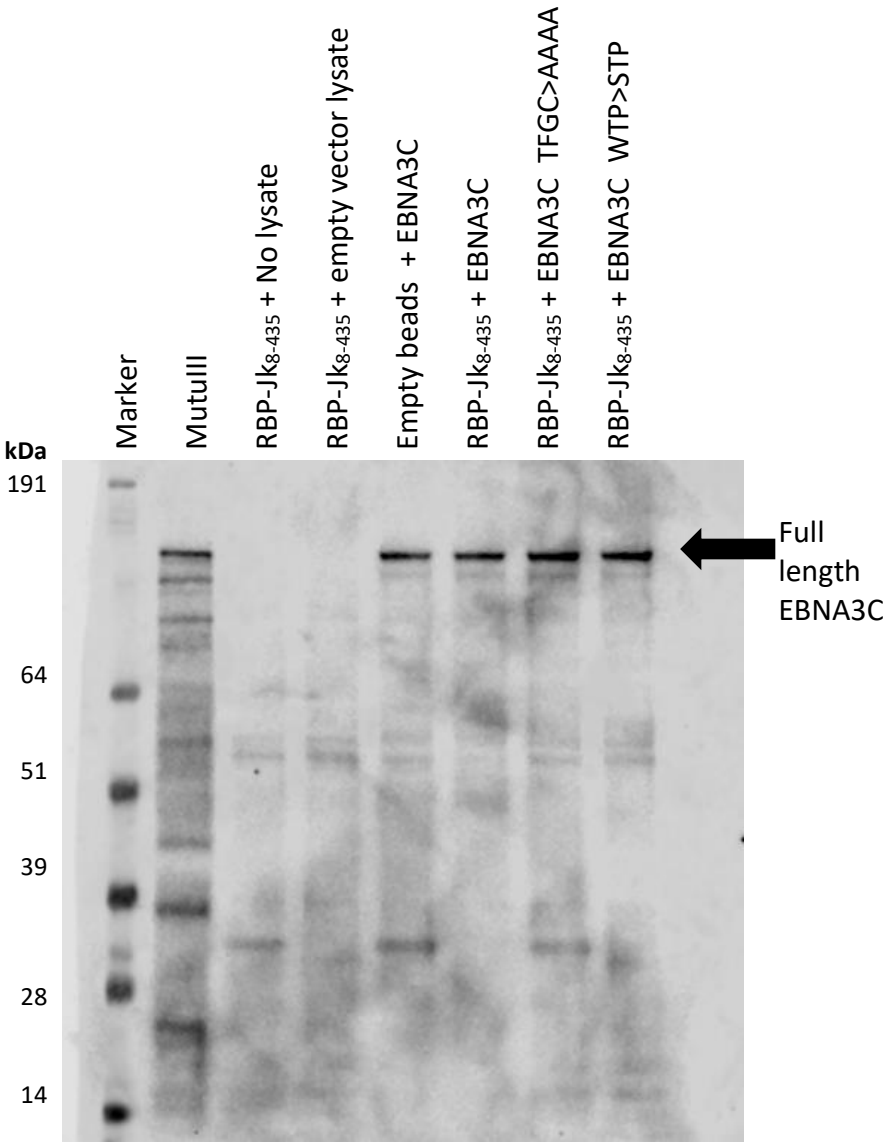


**Figure 3.43. Western blot analysis of pull down of EBNA3C wild type and EBNA3C mutants using C-terminally His-tagged RBP-Jk$_{8-435}$ expressed in *E.coli* bound to $Co^{2+}$-beads as the bait.** C-terminally His-tagged RBP-Jk$_{8-435}$ bound to $Co^{2+}$-beads was incubated with cell lysates from transfected cells overnight. After washing 30µL of the beads were boiled in GSB and analysed by SDS-PAGE and western blotting probed with anti-EBNA3C antibody. Mutu III cell lysate was used a positive control.

### 3.2.5.1 : Conclusions of the thermodynamic studies into the interactions between Epstein-Barr Virus transcription factors and RBP-Jκ

Initially we optimised an Isothermal titration calorimetry (ITC) binding assay using a 14 amino acid peptide of EBNA2, containing the WΦP RBP-Jκ binding motif, and RBP-$Jκ_{8-435}$, expressed in insect cells, to measure the affinities of the interactions between RBP-Jκ and the EBNA RBP-Jκ binding motifs (Figure 3.23).

ITC analysis showed a peptide of the Notch 2 RAM domain (Notch2.26aa) bound to RBP-Jκ an order of magnitude tighter than EBNA2 peptide (EBNA2.26aa) demonstrating that the residues surrounding the EBNA2 WΦP motif had a much weaker affinity for RBP-Jκ compared to residues surrounding the Notch 2 WΦP motif (Figure 3.24). This was confirmed by our FP competition assay in which the Notch 2 peptide to competed off all the fluorescein tagged EBNA2 peptide from RBP-Jκ (Figure 3.32).

Our ITC analysis also showed that the EBNA3s TΦGC motif in the context of a peptide did not contribute to RBP-Jκ interactions *in vitro* and that phosphorylating the threonine in the EBNA3C TFGC motif did not enable RBP-Jκ binding (Figure 3.25, 3.26 and 3.29). Additionally we showed, using FP competition assays, that the EBNA3C TΦGC motif in the context of a peptide did not compete with unlabelled EBNA2 peptide for RBP-Jκ binding (Figure 3.33 and 3.34). However, our ITC analysis did show that the EBNA3C WTP motif in the context of a peptide was essential for RBP-Jκ binding *in vitro*, which agreed with previously published data (Calderwood *et al.*, 2011)(Figure 3.26). In addition to this FP competition assays showed that the EBNA3C

WTP motif was needed to compete with EBNA2 peptide for RBP-Jκ binding (Figure 3.33 and 3.34).

In order to complete our thermodynamic studies we switched from producing RBP-Jκ in insect cells to *E.coli*. We confirmed, using ITC analysis, that this did not affect interactions between RBP-Jκ and EBNA peptides (Figure 3.27). Interestingly we measured weak binding between a 33 amino acid peptide of EBNA3A (EBNA3A.33aa) and RBP-Jκ (Figure 3.28). We had previously shown that a peptide of the EBNA3A TLGC motif did not have affinity for RBP-Jκ suggesting residues that aligned with the EBNA3C WTP motif, with similar hydrophobicity to the WΦP motif, facilitated this weak interaction (Figure 3.25 and 3.28). We were confident in the reliability of our ITC as we were able to show little difference between repeats (Figure 3.30).

We also utilised SwitchSense to measure the effects EBNA peptide binding had on RBP-Jκ-DNA interactions and on the conformation of RBP-Jκ (Figure 3.37). There were no measurable differences made to the $K_{on}$ of RBP-Jκ-DNA interactions when EBNA peptides were bound to RBP-Jκ (Figure 3.37). However, SwitchSense analysis showed that the Notch 2 peptide confers conformational changes to RBP-Jκ agreeing with previously published data (Friedmann *et al.*, 2008). Interestingly SwitchSense measured more severe conformational changes to RBP-Jκ when EBNA2 peptide was bound (Figure 3.37). However, the physiological connotations of this remain to be tested. We attempted to optimise pull downs of full length EBNA3C with mutated TFGC and WTP motifs expressed in mammalian cells to confirm the findings of our ITC and FP data. However, we encountered significant $EBNA3C_{TFGC\text{-}AAAA}$ background binding to the $Co^{2+}$ beads and, due to time constraints, were unable to optimise the assay.

## Chapter 3.3 : X-ray crystallography studies

The key aim of this chapter was to solve structure the EBNAs bound to RBP-Jκ in order study the interactions between them to regulate host transcription elucidate the mechanism of how the EBNAs hijack RBP-Jκ mediated genes. No structures of full length EBNA2 and EBNA3 proteins have been solved to date which is most likely due to their folding, which is predicted to be predominantly disordered (Yenamandra *et al.*, 2009). Additionally, few structures of truncations of EBNA2 and EBNA3 proteins exist due to them proving difficult to express in large quantities. NMR structures of dimerised EBNA2 N-terminal END domains and the EBNA2 N-terminal TAD domain bound to the Tfb1/p62 subunit of TFIIH have been solved (Chabot *et al.*, 2014, Friberg *et al.*, 2015)(Figure 1.3). These structures enabled study into how EBNA2 dimerises, which residues were involved dimerization and EBNA2-TFIIH interactions and the role of EBNA2 dimerisation and TFIIH binding in EBNA2 activation of host genes (Chabot *et al.*, 2014, Friberg *et al.*, 2015). This atomic resolution detail would not have been achievable with biomolecular techniques. In addition to this crystal structures of RBP-Jκ, CSL and Su(H) have proven essential to identifying how notch signalling is regulated in multiple species as traditional techniques, such as pulldowns of truncations RBP-Jκ, have not been reliable as RBP-Jκ relies on distal parts of its amino acid sequence to fold into its 3D structure (Arnett *et al.*, 2010, Kurth *et al.*, 2011, Choi *et al.*, 2012). Therefore, we initially attempted to co-crystallise RBP-Jκ$_{8-435}$ expressed in insect cells bound to DNA with peptides of the EBNAs which contained the TΦGC and WΦP RBP-Jκ binding motifs. We also attempt to co-express the EBNAs with RBP-Jκ as we hypothesised that RBP-Jκ binding would help stabilise the EBNAs as they were expressed.

### 3.3.1.1 : Results from the 4ºC crystal trials of RBP-Jκ$_{8-435}$-DNA-EBNA2.26aa expressed in insect cells.

RBP-Jκ$_{8-435}$ was expressed in insect cells, purified with a $Co^{2+}$ column step, an anion exchange step, incubated with DNA containing the RBP-Jκ consensus site (TTACT**GTGGGA**AAGA) and then passed through a size exclusion column. We designed the DNA to contain the RBP-Jκ consensus and have a 2bp overhang which we hoped would encourage crystal contact points to form to aid crystallisation. The RBP-Jκ$_{8-435}$-DNA complex was then concentrated to ~8mg/ml and incubated with the EBNA2.26aa peptide at a 1:1.5 ratio. The sample (~5mg/ml) was loaded onto 98 well sitting drop plates with broad crystal screening conditions (JCSG+, PacT, Proplex and Natrix). Condition screens JCSG+ and PacT were chosen for the broad screen as they offer a large range of PEGs and salts that have previously been used to produce crystal structures. Proplex was chosen as the conditions are designed for the crystallisation of protein complexes. Natrix was chosen as the conditions are designed to aid the crystallisation of protein-DNA complexes. The plates were then examined for crystals and crystalline precipitation. The plates were examined after seven days and the number of conditions that produced crystalline precipitation were counted (Figure 3.44). The optimal condition predicted from these trials was 0.1M Tris buffer pH6.5 with PEG3350 as the precipitant. Due to the long length of time it took these crystal trials took to produce only precipitant we decided not continue crystal trials at 4ºC, however we kept the plates at 4ºC to see if they would produce any crystals given more time.

After approximately 19 months we found these plates had produced prism shaped crystals (Figure 3.44), in Natrix conditions D2 (0.2M Ammonium acetate, 0.15M

Magnesium acetate tetrahydrate, 0.05M HEPES Sodium pH7.0, 5% w/v Polyethylene glycol 4000) and F7 (0.08M Sodium chloride, 0.04M Sodium cacodylate trihydrate pH6.0, 45% v/v (+/-)-2-Methyl-2,4-pentanediol, 0.012M Spermine tetrahydrochloride). The prism shaped crystal from Natrix D2 was fished and cryo-protected by increasing the PEG4000 in the buffer incrementally to 30% (Figure 3.45A). The crystals from Natrix F7 were also fished and frozen directly into liquid nitrogen due to the fact they were already in 45% (+/-)-2-Methyl-2,4-pentanediol (MPD)(Figure 3.45B). Unfortunately, the dewar leaked in transit and the crystals had dissolved by the time they had arrived at the Diamond light source synchrotron.

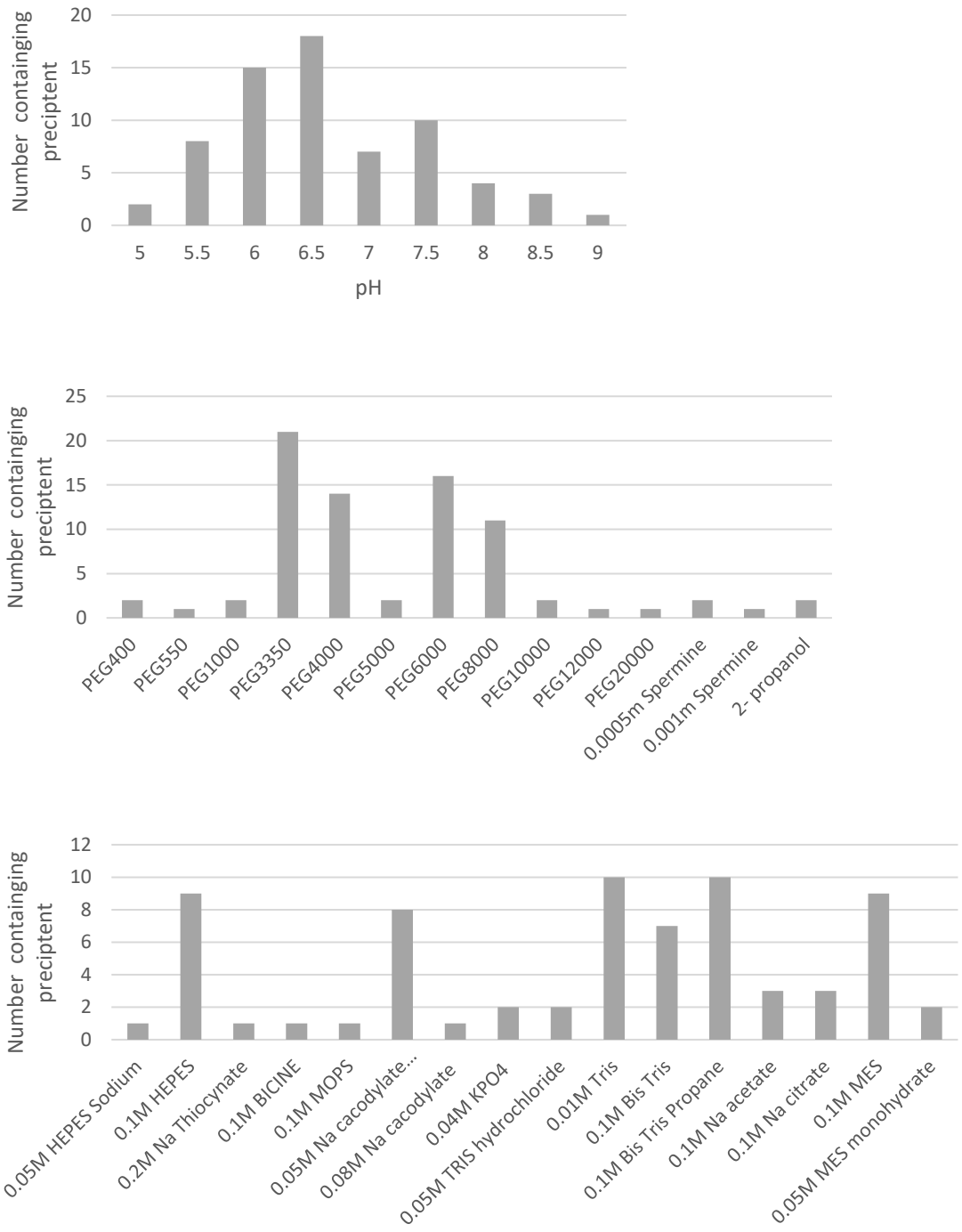


**Figure 3.44. Graphs showing the number of the number of wells containing precipitant produced during EBNA2.26aa-DNA-RBP-Jk$_{8-435}$ complex expressed in insect cells crystallisation trials at 4$^{o}$C.** EBNA2.26aa, DNA and RBP-Jk$_{8-435}$ were incubated on ice 1.5:1:1 respectively and plated into 98 well sitting drop crystallisation plates containing PacT, JCSG+, Proplex and Natrix crystallisation conditions in a 4$^{o}$C cold room. After 7 days wells containing precipitant were noted, the conditions were counted and these graphs were produced from this data.

**A**

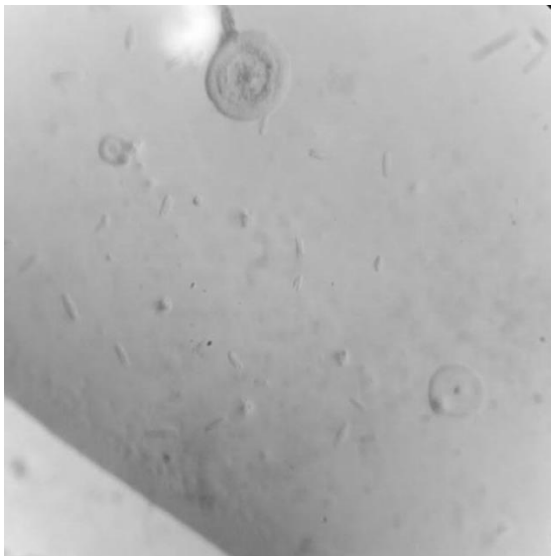

Natrix D2 0.2M Ammonium acetate 0.15M Magnesium acetate tetrahydrate 0.05M HEPES Sodium pH7.0 5% w/v Polyethylene

**B**

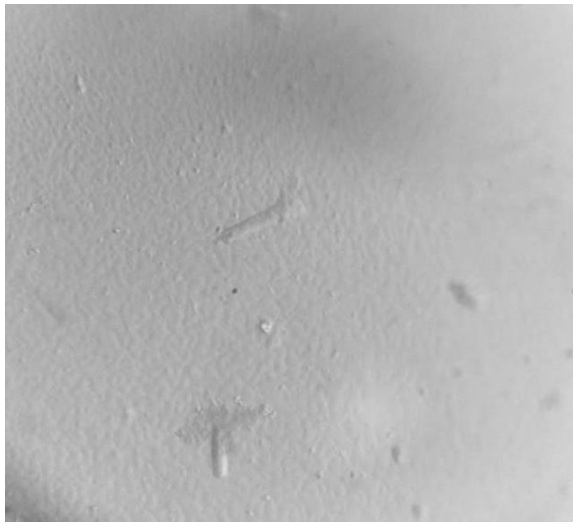

Natrix F7 0.08M Sodium chloride 0.04M Sodium cacodylate trihydrate pH6.0 45% v/v (+/-)-2-Methyl-2,4-pentanediol 0.012M Spermine tetrahydrochloride

**Figure 3.45. Crystals containing EBNA2.26aa-DNA-RBP-Jk$_{8-435}$ complex expressed in insect cells produced at 4$^{o}$C over 19 months. A.** Shows prism shaped crystals containing EBNA2.26aa-DNA-RBP-Jk$_{8-435}$ complex in a Natrix crystallisation condition described below the photo. Also seen are spherulites. **B.** Shows prism shaped crystals of EBNA2.26aa-DNA-RBP-Jk$_{8-435}$ complex emerging from phase separation and precipitant in a Natrix crystallisation condition described below the photo.

### 3.3.1.2 : Results from the room temperature crystal trials of RBP-Jκ$_{8-435}$-DNA-EBNA2.26aa complex expressed in insect cells.

The RBP-Jκ$_{8-435}$-DNA-EBNA2.26aa complex was expressed, purified and assembled as described in chapter 3.3.1.1 and the same screens were set up at room temperature (22$^{o}$C). After three days rhombus shaped crystals had grown in proplex C2 condition (0.1 M sodium citrate pH4.5, 20 % w/v PEG 4000) (Figure 3.46A). After 7 days the rhombus shaped crystals had also grown in proplex B8 conditions (0.1 M $MgCl_2$, 0.1 M sodium citrate pH5.0, 15 % w/v PEG 4000) (Figure 3.46B). These conditions were very similar to each other only varying slightly in the percentage of PEG4000 and pH.

As the crystals had grown out of phase separation we recorded the number of conditions that produced phase separation instead of precipitation with the aim of optimising conditions that would produce more rhomboid shaped crystals (Figure 3.47). As observed in the 4$^{o}$C trials 0.1M Tris buffer pH6.5 was most commonly seen to produce phase separation, however PEG6000 was the most common precipitant.

We also noticed a significant number of the wells had produced spherulites and recorded these conditions with the aim to optimise a condition that could prevent the nucleation that had caused the crystals to grow into spherulites (Figure 3.48). A Tris based buffer most commonly produced this condition, but the most common pH was pH7.5 and the most common precipitant was PEG3350 (Figure 3.48).

Due to the low levels of RBP-Jκ$_{8-435}$ being produced in insect cells and the crystals grown in conditions Proplex C2 and B8 proving difficult to replicate only a small number of trials were completed based on phase separation and spherulite information and the few that were carried out produced no crystals.

**A**

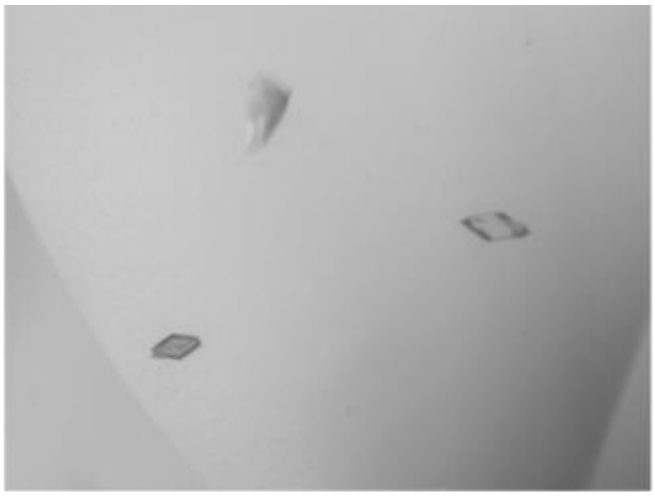

Proplex C2 0.1 M sodium citrate pH4.5 20 % w/v PEG 4000

**B**

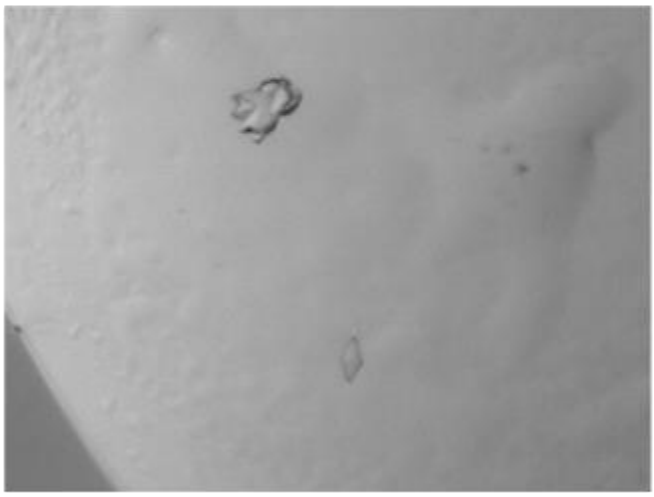

Proplex B8 0.1 M $MgCl_2$ 0.1 M sodium citrate pH5.0 15 % w/v PEG 4000

**Figure 3.46. Crystals containing EBNA2.26aa-DNA-RBP-Jk$_{8-435}$ complex expressed in insect cells produced at 22°C. A.** Shows rhomboid shaped crystals containing EBNA2.26aa-DNA-RBP-Jk$_{8-435}$ complex in a Proplex crystallisation condition described below the photo. **B.** Shows jagged cluster of crystals and small rhomboid crystal of EBNA2.26aa-DNA-RBP-Jk$_{8-435}$ complex emerging from phase separation and precipitant in a Proplex crystallisation condition described below the photo.

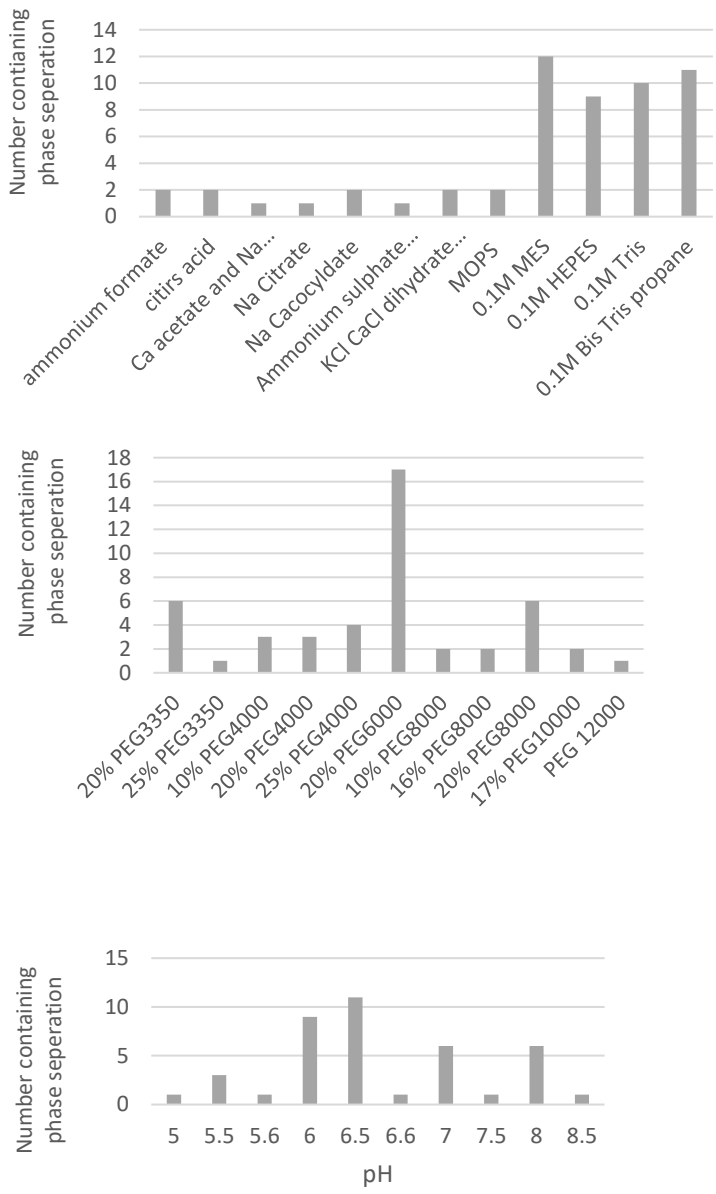


**Figure 3.47. Graphs showing the number of the number of wells containing phase separation produced during EBNA2.26aa-DNA-RBP-Jk$_{8-435}$ complex expressed in insect cells crystallisation trials at 22ºC/room temperature .** EBNA2.26aa peptide, DNA and RBP-Jk$_{8-435}$ were incubated on ice 1.5:1:1 respectively and plated into 98 well sitting drop crystallisation plates containing PacT, JCSG+, Proplex or Natrix crystallisation conditions in at room temperature. After 7 days wells containing phase separation were noted, the conditions were counted and these graphs were produced from this data.

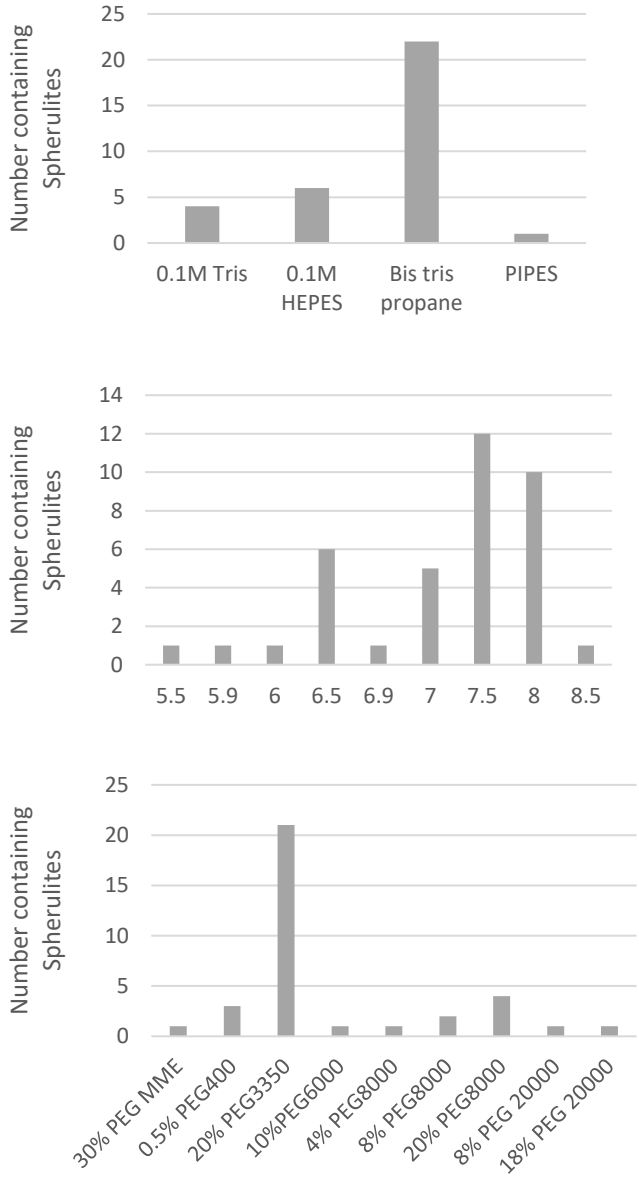


**Figure 3.48. Graphs showing the number of the number of wells containing Spherulites produced during EBNA2.26aa-DNA-RBP-Jk$_{8-435}$ complex expressed in insect cells crystallisation trials at 22°C/room temperature .** EBNA2.26aa peptide, DNA and RBP-Jk$_{8-435}$ were incubated on ice 1.5:1:1 respectively and plated into 98 well sitting drop crystallisation plates containing PacT, JCSG+, Proplex or Natrix crystallisation conditions at room temperature. After 7 days wells containing spherulites were noted, the conditions were counted and these graphs were produced from this data.

### 3.3.1.3 : RBP-Jκ$_{8-435}$ bound to RBP-Jκ consensus site crystal structure produced from Proplex C2 condition

The crystal produced in Proplex C2 condition (Figure 3.46A) was fished then cryoprotected and flash frozen in liquid nitrogen. The crystal was exposed to X-rays on the IO2 beamline at the diamond light source where a full data set with a resolution of 3.6Å was acquired.

Due to the crystal consisting of two rhomboid plates overlapping each other, the scatter data produced contained shadow spots which made the asymmetric unit and space group determination of the crystal lattice difficult to calculate. Dr Mark Roe (University of Sussex crystallography facilities manager) processed the scatter data for us. Initially Diamonds XIA2 software was used to reduce the scatter data (Winter, 2010). Next Phaser software from the CCP4 package was used for the molecular replacement. The phase data of the RBP-Jκ$_{8-435}$ and DNA from the structure of the Notch 1 transcription complex was used for molecular replacement (Choi *et al.*, 2012) (McCoy *et al.*, 2007, Winn *et al.*, 2011). The initial refinements were completed in refmac software and the phenix suite was used for completion (Vagin *et al.*, 2004, Adams *et al.*, 2010). We were confident in the quality of the model produced (Figure 49) as the $R_{free}$ and $R_{work}$ values were below the PDB cut off of 0.5 (Figure 3.50) despite the reasonably high Wilson b factor (Figure 3.50).

The crystal structure (Figure 3.49) only contained RBP-Jκ$_{8-435}$ expressed in insect cells bound to DNA (TTACT**GTGGGA**AAGA) and no EBNA2 peptide. The asymmetric unit of the crystal contained two complexes RBP-Jκ$_{8-435}$ bound to DNA that were slightly offset which were arranged into a P.21.21.2 lattice. Due to the low resolution of the crystal

structure we were unable to clearly distinguish any electron density over the beta trefoil domain that could have been produced by the EBNA2.26aa peptide being bound to RBP-J$\kappa_{8-435}$.

We modelled an EBNA2 peptide onto the structure using wincoot to mutate the residues of the NotchRAM peptide in the previous structure of the Notch 1 transcription complex to EBNA2 residues (aligned to the WΦP RBP-Jκ binding motif) then aligned the two structures (Figure 3.51) (Choi *et al.*, 2012). It Is clear from this model that the electron density from the Notch peptide sterically clashes with the opposing RBP-J$\kappa_{8-435}$-DNA complex. As expected this is also the case when the EBNA2 peptide is also modelled in place of the NotchRAM peptide (Figure 3.51). This may explain why the EBNA2 peptide was not present in the crystal and was likely forced out of the complex by crystal packing forces during crystallisation. It was unlikely that the EBNA2 peptide was not bound to RBP-Jκ before the adding it to the crystallisation conditions as the buffers that the complex was assembled in was similar to the buffer used during our ITC assays. Because of the arrangement of the RBP-Jκ molecules in the crystal we decided not to continue optimising this crystal condition.

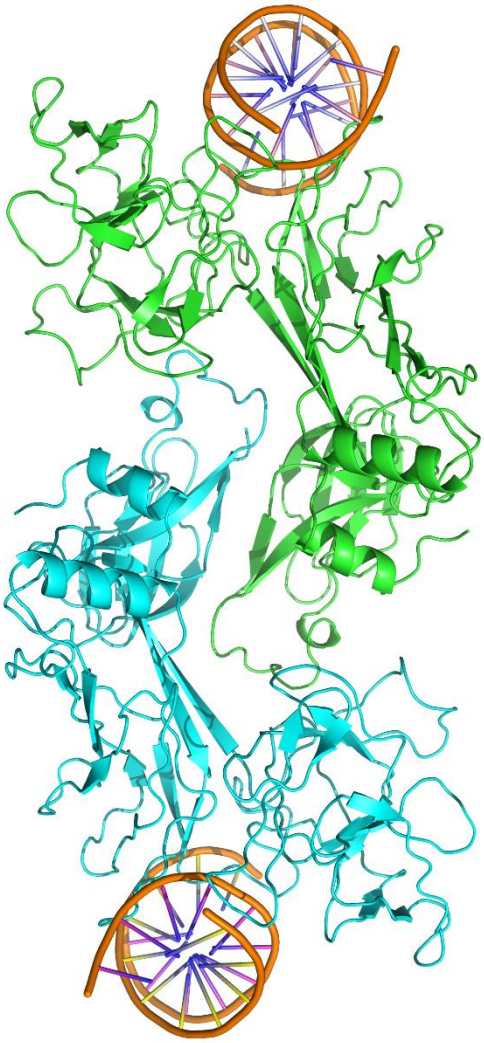

**Figure 3.49. X-ray crystal structure produced from Proplex C2 crystallisation condition. The structure contains C-terminally His tagged RBP-Jk$_{8-435}$ expressed in insect cells bound to DNA containing the RBP-Jk consensus sight.** The asymmetric unit contains two complexes of C-terminally His-tagged RBP-Jk$_{8-435}$ bound to DNA shown as cartoons one in blue and the other in green. The structure was resolved to 3.63Å, with no detectable electron density visable in the electron density map on the Beta-trefoil domain that would be present if there was a peptide bound.

| **Data Processing statistics** | |
|---|---|
| Space group | P 21 21 2 |
| Resolution Range (Å) | 3.73-3.63 |
| Molecules in asymmetric unit | 2 |
| Cell parameters a, b, c (Å) | 171.48, 68.52, 107.89 |
| Cell parameters α, β, γ (°) | 90, 90, 90 |
| X-ray source | IO2 beamline at Diamond |
| Mosaicity (°) | 0.515 |
| Number of unique reflections | 14751 |
| Multiplicity | 6.5 (4.7) |
| Completeness (%) | 98.8 (93.2) |
| $R_{merge}$ | 0.041 (1.336) |
| I/σ(I) | 0.825 |
| **Refinement statistics** | |
| $R_{work}/R_{free}$ | 0.40/0.47 |
| Number of reflections | 14459 |
| Number of atoms | 7549 |
| Complexes/ asymmetric unit | 2 |
| Wilson B score (Å$^2$) | 132.87 |
| RMSD bond length (Å) | 0.003 |
| RMSD bond angles (°) | 0.713 |
| Ramachandran plot (favoured/ outliers)(%) | 80.99/3.25 |

**Figure 3.50. Table of Data processing and Refinement Statistics for X-ray crystal structure of C-terminally His-tagged RBP-Jk$_{8-435}$ expressed in insect cells bound to RBP-Jk consensus site DNA.** The data processing and refinement statistics are poor for the model of C-terminally His-tagged RBP-Jk$_{8-435}$ expressed in insect cells bound to RBP-Jk consensus site DNA as shadow spots in the scatter data made the data challenging to process.

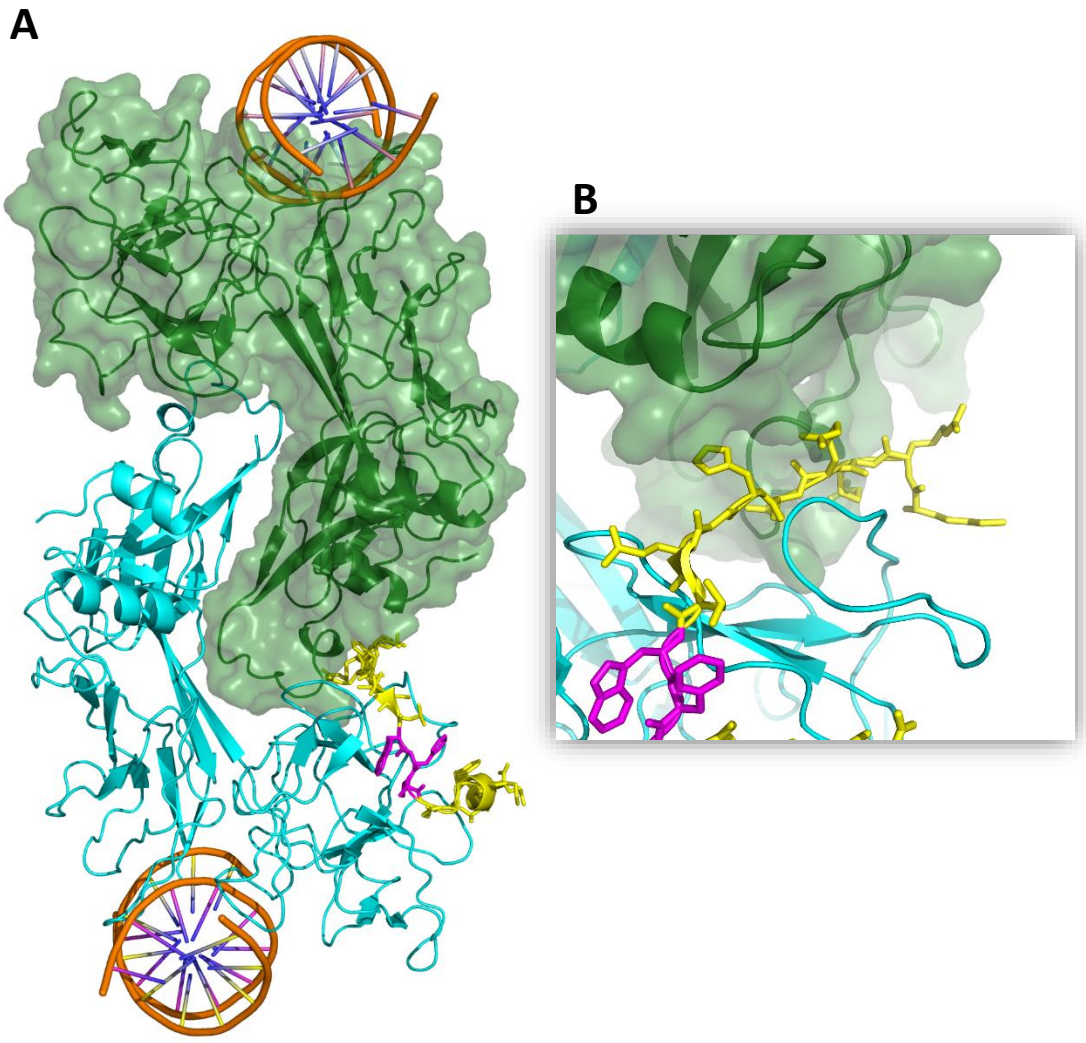


C

| | |
|---|---|
| **Notch2.26aa:** | MAKRKRKHGSLWLPEGFTLRRDASNH |
| **EBNA2.26aa:** | QQLHHLPSGPPWWPPICDPPQPSKTQ |

**Figure 3.51. X-ray crystal structure, of C-terminally His tagged RBP-Jk$_{8-435}$ expressed in insect cells bound to DNA containing the RBP-Jk consensus sight, with surface shown to reveal potential steric clashes between the EBNA2.26aa peptide and the second RBP-Jk$_{8-435}$ in the asymmetric unit of the crystal. A.** X-ray crystal structure of C-terminally His tagged RBP-Jk$_{8-435}$ expressed in insect cells bound to DNA containing the RBP-Jk consensus sight with a transparent molecular surface of the second RBP-Jk$_{8-435}$ (in green). An EBNA2 peptide (in yellow) has been modelled on to the structure by substituting the Notch-RAM residues in the 3V79 structure for EBNA2 residues using the WΦP RBP-Jk binding motif (in pink) to align the two peptides. **B.** The structure described in figure 47.A has been zoomed in to highlight the likely steric clashes between the N terminus of the EBNA.26aa peptide and the second RBP-Jk$_{8-435}$ in the asymmetric unit (shown in green). **C.** Notch26.aa and EBNA2.26aa peptide amino acid sequences have been aligned. The RBP-Jk Notch WΦP binding motif is highlighted in pink and highly conserved residues identified by S.E Johnson et al 2009 to contribute significant amount of affinity to the Notch-RBP-Jk interaction have been highlighted in blue.

### 3.3.1.3 : Results of the room temperature crystal trials of RBP-Jκ$_{8-435}$-DNA-EBNA3C.33aa expressed in insect cells.

The RBP-Jκ$_{8-435}$-DNA complex was purified as previously described and was then incubated with EBNA3C.33aa peptide in a 1:1.5 ratio. Approximately 7mg/ml of complex was loaded onto 96 well hanging drop plates with JGSC+, PacT and Proplex crystallisation screens. There was little activity in these crystallisation trials which may have been due to the RBP-Jκ$_{8-435}$ being stored at -80$^{o}$C before the crystal trials. No crystals were produced but after 7 days we recorded the conditions that phase separation had taken place (Figure 3.52). There was not a distinct pH that scored highly, however Tris buffer and the precipitants 20% PEG3350 and 20% PEG6000 gave phase separation. We chose not to continue to optimise crystallisation conditions for RBP-Jκ$_{8-435}$-DNA-EBNA3C.33aa due to poor yields of RBP-Jκ$_{8-435}$ being expressed in insect cells and no conditions producing crystals or promising crystalline precipitate. We were also concerned that the TΦGC motif in the EBNA3C.33a peptide was shown not to bind RBP-Jκ$_{8-435}$ in our ITC binding assays and that there would be a significant portion of the peptide not bound to RBP-Jκ (Figure 3.26).

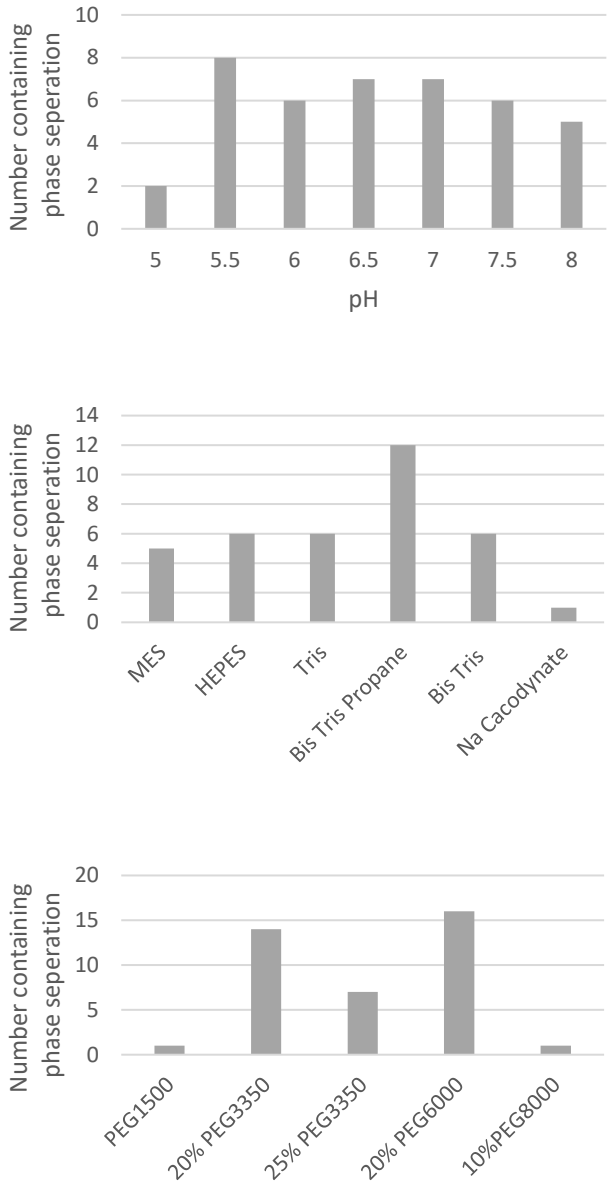


**Figure 3.52. Graphs showing the number of the number of wells containing phase separation produced during EBNA3C.33aa-DNA-RBP-Jk$_{8-435}$ complex expressed in insect cells crystallisation trials at 22$^{o}$C/room temperature.** EBNA3C.33aa peptide, DNA and RBP-Jk$_{8-435}$ were incubated on ice 1.5:1:1 respectively and plated into 98 well sitting drop crystallisation plates containing PacT, JCSG+, Proplex or Natrix crystallisation conditions at room temperature. After 7 days wells containing phase separation were noted, the conditions were counted and these graphs were produced from this data.

### 3.3.2.1 : Switching the production of RBP-Jκ$_{8-435}$ from insect cells to *E.coli* increased the number of crystallisation strategies we could attempt.

The main factor that prevented us from creating an efficient production line to attempt to crystallise C-terminally His-tagged RBP-Jκ$_{8-435}$ with EBNA peptides was due to low and inconsistent yields of RBP-Jκ$_{8-435}$ expressed in insect cells. It prevented us from increasing the concentration of protein used to 10 to 15mg/ml. Our ITC analysis had shown that interactions between the EBNA2.26aa peptide and RBP-Jκ$_{8-435}$ were not significantly impacted by which expression host was used to produce RBP-Jκ$_{8-435}$ (Figure 3.27). Therefore we decided to switch the production of RBP-Jκ$_{8-435}$ to *E.coli*. With larger and more consistent yields we could expand the number of crystallisation trials from the strategies shown in blue (Figure 3.53) to the strategies shown in yellow in (Figure 3.53). Furthermore as RBP-Jκ$_{8-435}$ took a shorter amount of time to express and purify in *E.coli*.

We had concerns that a significant number of residues of the EBNA2.26aa peptide may not be binding to RBP-Jκ$_{8-435}$ and floating freely in solution. We knew from the structure of Notch ternary complex that this could compromise the resolution of peptides bound to the BTD of RBP-Jκ$_{8-435}$ and impact crystal formation (Wilson and Kovall, 2006, Choi *et al.*, 2012). We therefore decided to use the smaller EBNA2.14aa peptide in crystal trials to address these concerns.

RBP-Jκ$_{8-435}$-DNA complex was purified as previously described in chapter 3.1.2.2, concentrated to approximately 10mg/ml, then incubated with EBNA2.14aa peptide at a 1:4 ratio to increase the amount of peptide present. We loaded the RBP-Jκ$_{8-435}$-DNA-EBNA2.14aa sample at 10mg/ml onto 96 well sitting drops plates with JCSG+, Proplex,

PacT and Natrix crystallisation condition screens. Crystals large enough to take to the synchrotron were produced in Proplex A8, E7 and B7 and Natrix G9, E2, C3 and D7 conditions. Due to issues loading the crystals into pucks some of the samples were lost. The crystals produced in Natrix conditions C3 and D7 were identified to be salt crystals when exposed to the x-ray source. The rest of the crystals were too small to produce scatter data.

We therefore designed a deep well block of crystallisation conditions to optimise the conditions producing small crystals (Figure 3.54). We also included the crystal condition Proplex C2 which produced the crystal structure (Figure 3.49). We made a gradient of the PEG in these conditions to discourage the crystals entering a nucleation phase and producing smaller crystals. Reducing the PEG did reduce the number of crystals in the Proplex A8 however these crystals were still too small to expose to an X-ray source. The Proplex A8 condition predominantly produced crystal showers however after approximately 2 weeks a larger crystal grew out of this shower (Figure 3.55) which was fished but unfortunately was lost during loading and was not exposed to an X-ray source. Surprisingly the Proplex C2 condition caused the RBP-J$\kappa_{8\text{-}435}$-DNA-EBNA2.14aa to crash out of solution which was unexpected. We also set up a plate where pH was varied, however this had little effect of the crystal growth and most of the conditions continued to produce crystal showers (Figure 3.56).

We next decided to seed the optimisation 2 plate with crystals from the Proplex A8 condition, from optimisation plate 1 well C2, to determine whether this encouraged larger crystals to grow (Figure 3.55). However seeding did not have the desired affect and simply generated more crystal showers (Figure 3.57A and B). We also added 5%

glycerol to the optimisation 2 crystallisation conditions to prevent the crystals entering a nucleation phase and slow the crystallisation process in order to grow fewer larger crystals instead of showers of small crystals. This had some success as we managed to reduce the number of nucleation points and grow fewer crystals, however the crystals were still as small as they were before the addition of glycerol (Figure 3.57D). A larger crystal did grow out of the crystal shower (Figure 3.57C), which was fished. However, this crystal was lost whilst it was being loaded onto the pucks and therefore no data was collected.

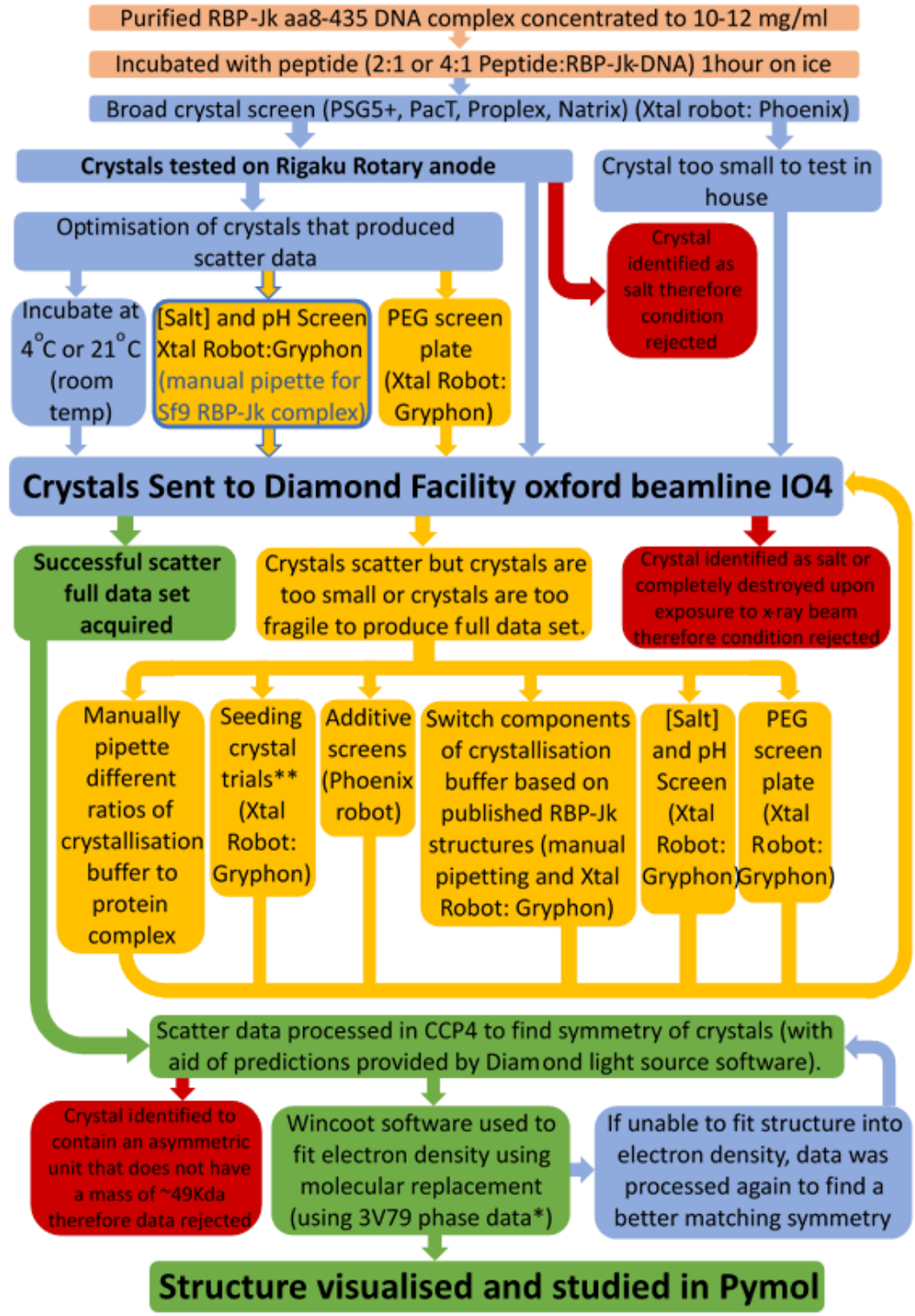


**Figure 3.53. A flow chart showing the process of optimising crystals for structure resolution.** In light pink are the preparatory steps to assemble the complex for crystallisation. Highlighted in light blue are optimisation steps that the RBP-Jk$_{8-435}$ complex produced in insect cells were restricted to due to a lack of material being produced. Highlighted in yellow are extra optimisation steps that could be achieved when expressing RBP-Jk$_{8-435}$ in *E.coli* due increased protein production. In green are the synchrotron data processing steps and dark red boxes explains why conditions would be rejected.

| Optimisation plate 1 | | 1 | 2 | 3 | 4 | 5 | 6 |
|---|---|---|---|---|---|---|---|
| A | Proplex C2 | | | | | | |
| | 0.1M Na Citrate pH4.5 | 0.1M | 0.1M | 0.1M | 0.1M | 0.1M | 0.1M |
| | PEG4000 | 7% | 9% | 12% | 15% | 17% | 20% |
| | 0.1M $MgCl_2$ | 0.1M | 0.1M | 0.1M | 0.1M | 0.1M | 0.1M |
| B | Proplex B8 | | | | | | |
| | 0.1M Na Citrate pH5 | 0.1M | 0.1M | 0.1M | 0.1M | 0.1M | 0.1M |
| | PEG4000 | 7% | 9% | 12% | 15% | 17% | 20% |
| | 0.1M $MgCl_2$ | 0.1M | 0.1M | 0.1M | 0.1M | 0.1M | 0.1M |
| C | Proplex A8 | | | | | | |
| | 0.2M Ammonium Sulphate | 0.2M | 0.2M | 0.2M | 0.2M | 0.2M | 0.2M |
| | 0.1M Na Acetate pH5.5 | 0.1M | 0.1M | 0.1M | 0.1M | 0.1M | 0.1M |
| | PEG2000 MME | 4% | 6% | 8% | 10% | 12% | 15% |
| D | PacT B6 pH9 | | | | | | |
| | 0.1M MEB buffer pH9 | 0.1M | 0.1M | 0.1M | 0.1M | 0.1M | 0.1M |
| | PEG1500 | 15% | 18% | 21% | 25% | 27% | 30% |
| E | PacT B6 pH10 | | | | | | |
| | 0.1M MEB buffer pH10 | 0.1M | 0.1M | 0.1M | 0.1M | 0.1M | 0.1M |
| | PEG1500 | 15% | 18% | 21% | 25% | 27% | 30% |
| F | PacT E4 | | | | | | |
| | 0.2M K Thiocyanate | 0.2M | 0.2M | 0.2M | 0.2M | 0.2M | 0.2M |
| | PEG3350 | 8% | 10% | 12% | 15% | 17% | 20% |
| G | PacT E4 | | | | | | |
| | 0.1M K Thiocyanate | 0.1M | 0.1M | 0.1M | 0.1M | 0.1M | 0.1M |
| | PEG3350 | 8% | 10% | 12% | 15% | 17% | 20% |

**Figure 3.54. Table showing conditions used to optimise the crystallisation of the EBNA2.14aa peptide, C-terminally His-tagged RBP-$Jk_{8-435}$ (expressed in *E.coli*) and RBP-Jk consensus site DNA complex.** Conditions were chosen from conditions that produced crystals in the broad screens (JSCG+, PacT, Proplex and Natrix 98-well crystallisation condition deep well blocks).

Opt1 plate C2 : 0.2M Ammonium Sulphate, 0.1M Na Acetate pH5.5, 6% PEG2000 MME

**Figure 3.55. Crystal of EBNA2.14aa-RBP-Jk$_{8-435}$(expressed in *E.coli*)-DNA complex grown in Optimisation plate 1 well C2.** A cuboid shaped crystal has grown out of the crystal shower surrounding it. The crystal was difficult to fish due to it being stuck to the bottom of the well.

| Optimisation plate 2 | | 1 | 2 | 3 | 4 | 5 | 6 |
|---|---|---|---|---|---|---|---|
| A | Proplex B8 | | | | | | |
| | 0.1M Na Citrate pH5 | 0.1M | 0.1M | 0.1M | 0.1M | 0.1M | 0.1M |
| | PEG4000 | 7% | 9% | 12% | 15% | 17% | 20% |
| | 0.1M $MgCl_2$ | 0.1M | 0.1M | 0.1M | 0.1M | 0.1M | 0.1M |
| B | Proplex A8 | | | | | | |
| | 0.2M Ammonium Sulphate | 0.2M | 0.2M | 0.2M | 0.2M | 0.2M | 0.2M |
| | 0.1M Na Acetate pH5.5 | 0.1M | 0.1M | 0.1M | 0.1M | 0.1M | 0.1M |
| | PEG2000 MME | 4% | 6% | 8% | 10% | 12% | 15% |
| C | PacT B6 pH9 | | | | | | |
| | 0.1M MEB buffer pH9 | 0.1M | 0.1M | 0.1M | 0.1M | 0.1M | 0.1M |
| | PEG1500 | 15% | 18% | 21% | 25% | 27% | 30% |
| D | PacT B6 pH10 | | | | | | |
| | 0.1M MEB buffer pH10 | 0.1M | 0.1M | 0.1M | 0.1M | 0.1M | 0.1M |
| | PEG1500 | 15% | 18% | 21% | 25% | 27% | 30% |
| E | PacT E4 0.1M | | | | | | |
| | 0.2M K Thiocyanate | 0.2M | 0.2M | 0.2M | 0.2M | 0.2M | 0.2M |
| | PEG3350 | 8% | 10% | 12% | 15% | 17% | 20% |
| F | PacT E4 0.2M | | | | | | |
| | 0.1M K Thiocyanate | 0.1M | 0.1M | 0.1M | 0.1M | 0.1M | 0.1M |
| | PEG3350 | 8% | 10% | 12% | 15% | 17% | 20% |
| G | PacT E7 pH6.0 | | | | | | |
| | 0.1M Na Phosphate pH6.0 | 0.1M | 0.1M | 0.1M | 0.1M | 0.1M | 0.1M |
| | PEG8000 | 8% | 10% | 12% | 15% | 17% | 20% |
| H | PacT E7 pH6.5 | | | | | | |
| | 0.1M Na Phosphate pH6.5 | 0.1M | 0.1M | 0.1M | 0.1M | 0.1M | 0.1M |
| | PEG8000 | 8% | 10% | 12% | 15% | 17% | 20% |

**Figure 3.56. Table showing conditions used to optimise the crystallisation of the EBNA2.14aa peptide, C-terminally His-tagged RBP-$Jk_{8-435}$ (expressed in *E.coli*) and RBP-Jk consensus site DNA complex.** These conditions were derived from new crystallisation conditions from the broad screen that produced crystals of the EBNA2.14aa peptide-RBP-$Jk_{8-435}$-DNA complex and those that produced crystals in optimisation plate 1.

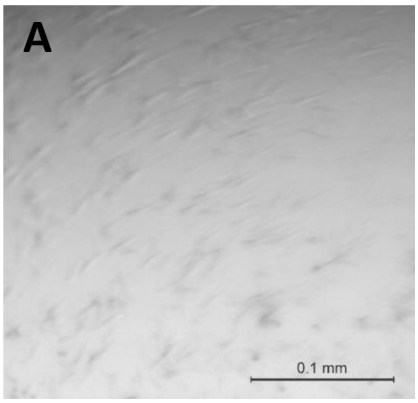


Opt 2 E1 : 0.2M K Thiocyanate, 8% PEG3350

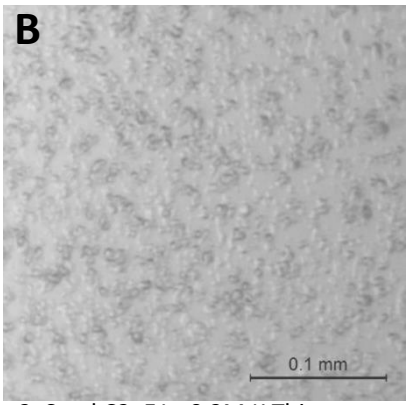


Opt 2, Seed C2, E1 : 0.2M K Thiocyanate, 8% PEG3350

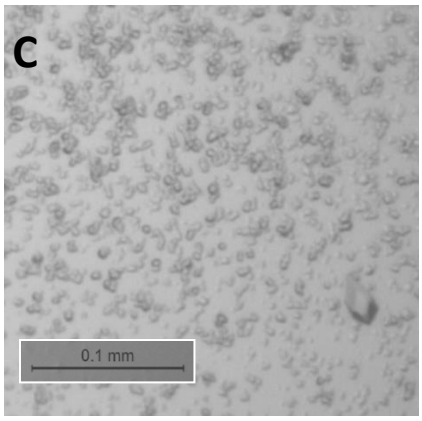


Opt 2 B5 : 0.2M Ammonium Sulphate, 0.1M Na Acetate pH5.5, 12% PEG2000 MME

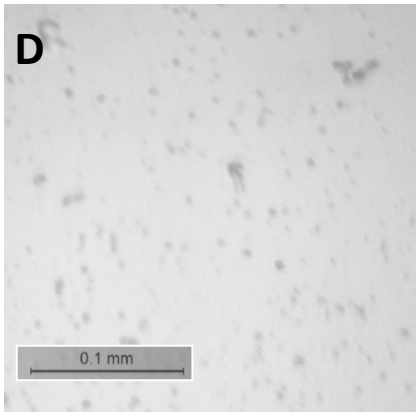


Opt 2 5% glycerol B5 : 0.2M Ammonium Sulphate, 0.1M Na Acetate pH5.5, 12% PEG2000 MME

**Figure 3.57. Pictures of crystals of EBNA2.14aa peptide, C-terminally His-tagged RBP-Jk$_{8-435}$ (expressed in *E.coli*) and RBP-Jk consensus site DNA complex summarising the effects of adding 5% glycerol or seed, from optimisation plate 1 well C2, to crystallisation conditions. A.** A shower of thin crystals needles of EBNA2.14aa peptide-RBP-Jk$_{8-435}$-DNA complex produced in optimisation plate 2 well E1. **B.** A shower of EBNA2.14aa peptide-RBP-Jk$_{8-435}$-DNA complex crystals appear to be larger but still too small to expose to an x-ray source. **C.** A rhomboid shaped crystal has grown out of the crystal shower surrounding it. **D.** The addition of seed from opt1 C2 has reduced the number of nuclearisation points but has not produced crystals large enough to expose to an x-ray source.

### 3.3.2.2 : Optimisation of crystallisation of RBP-Jκ$_{8-435}$-DNA-EBNA2.14aa complex expressed in *E.coli* in Natrix and Published conditions

Natrix conditions G9 and G10 produced small cuboid crystals and G11 produced small pyramid crystals (Figure 3.58A, B and C). Each of the Natrix conditions contained 0.04M Lithium chloride, 0.08 M Strontium chloride hexahydrate, 0.04 M Sodium cacodylate trihydrate pH 7.0, 30% (+/-)-2-Methyl-2,4-pentanediol, 0.012 M Spermine tetrahydrochloride whilst G10 and G11 also contained 0.02 M Magnesium chloride hexahydrate and 0.012 M Potassium chloride respectively. This was likely the reason why the crystals had a similar morphology.

We generated (+/-)-2-Methyl-2,4-pentanediol (MPD) screens for each of these Natrix conditions to attempt to reduce the number of nucleation points to grow fewer larger crystals (Figure 3.59). In the second half of this crystal screen we reproduced published crystal conditions that had been used to produce crystals of CSL-RAM-DNA complex (Figure 3.59)(Friedmann *et al.*, 2008).

We were unable to reproduce the cuboid crystals had previously seen (Figure 3.58). We obtained predominantly crystal showers. Unfortunately, the conditions based on the previously published structure of CSL-RAM-DNA caused the protein to come out of solution. However, a hybrid of published conditions and Proplex A8 condition did produce small rhomboid crystals (Figure 3.60 A and C).

We had also made a seed stock from the crystals grown in the Natrix G10 condition (Figure 3.58B) and seeded the Natrix and published optimisation plate with this stock. Unfortunately, the seed produced small edgeless crystals that were not suitable for collecting scatter data (Figure 3.60 B and D).

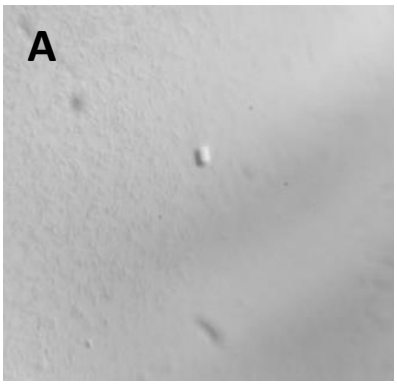


Natrix G9 : 0.04 M Lithium chloride, 0.08 M Strontium chloride hexahydrate, 0.04 M Sodium cacodylate trihydrate pH 7.0, 30% (+/-)-2-Methyl-2,4-pentanediol, 0.012 M Spermine tetrahydrochloride

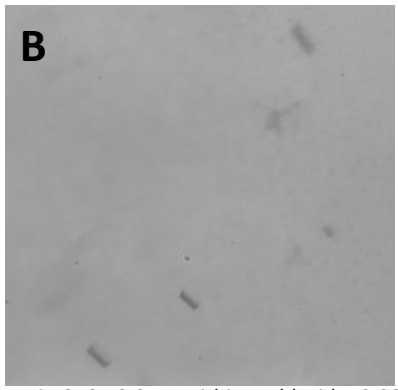


Natrix G10 : 0.04 M Lithium chloride, 0.08 M Strontium chloride hexahydrate, 0.04 M Sodium cacodylate trihydrate pH 7.0, 30% (+/-)-2-Methyl-2,4-pentanediol, 0.02 M Magnesium chloride hexahydrate, 0.012 M Spermine tetrahydrochloride

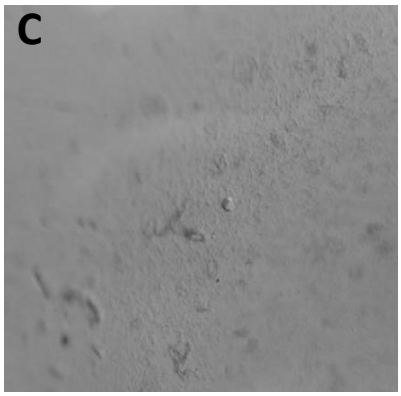


Natrix G11 : 0.04 M Lithium chloride, 0.08 M Strontium chloride hexahydrate, 0.04 M Sodium cacodylate trihydrate pH 7.0, 30% (+/-)-2-Methyl-2,4-pentanediol, 0.02 M Magnesium chloride hexahydrate, 0.012 M Spermine tetrahydrochloride, 0.012 M Potassium chloride

**Figure 3.58. Pictures of crystals of EBNA2.14aa peptide, C-terminally His-tagged RBP-Jk$_{8-435}$ (expressed in *E.coli*) and RBP-Jk consensus site DNA complex grown in Natrix HT 96 well sitting drop crystallisation conditions. A.** A small cuboid crystal of EBNA2.14aa peptide-RBP-Jk$_{8-435}$-DNA complex. Unfortunately, the crystal was too small to fish. **B.** Small cuboid crystals of EBNA2.14aa peptide-RBP-Jk$_{8-435}$-DNA complex which were fished and sent to the diamond light source. **C.** A small Hexagonal flat-topped pyramid shaped crystal of EBNA2.14aa peptide-RBP-Jk$_{8-435}$-DNA complex. Unfortunately, the crystal was also too small to fish.

| Optimisation plate: Natrix and published conditions | | 1 | 2 | 3 | 4 | 5 | 6 |
|---|---|---|---|---|---|---|---|
| A | **Natrix G9** | | | | | | |
| | 0.04 M Lithium chloride | 0.04M | 0.04M | 0.04M | 0.04M | 0.04M | 0.04M |
| | 0.08 M Strontium chloride hexahydrate | 0.08M | 0.08M | 0.08M | 0.08M | 0.08M | 0.08M |
| | 0.04 M Sodium cacodylate trihydrate pH 7.0 | 0.04M | 0.04M | 0.04M | 0.04M | 0.04M | 0.04M |
| | (+/-)-2-Methyl-2,4-pentanediol | 25% | 27% | 30% | 33% | 35% | 38% |
| | 0.012 M Spermine tetrahydrochloride | 12mM | 12mM | 12mM | 12mM | 12mM | 12mM |
| B | **Natrix G10** | | | | | | |
| | 0.04 M Lithium chloride | 0.04M | 0.04M | 0.04M | 0.04M | 0.04M | 0.04M |
| | 0.08 M Strontium chloride hexahydrate | 0.08M | 0.08M | 0.08M | 0.08M | 0.08M | 0.08M |
| | 0.04 M Sodium cacodylate trihydrate pH 7.0 | 0.04M | 0.04M | 0.04M | 0.04M | 0.04M | 0.04M |
| | (+/-)-2-Methyl-2,4-pentanediol | 25% | 27% | 30% | 33% | 35% | 38% |
| | 0.012 M Spermine tetrahydrochloride | 12mM | 12mM | 12mM | 12mM | 12mM | 12mM |
| | 0.02 M Magnesium chloride hexahydrate | 0.02M | 0.02M | 0.02M | 0.02M | 0.02M | 0.02M |
| C | **Natrix G11** | | | | | | |
| | 0.04 M Sodium chloride | 0.04M | 0.04M | 0.04M | 0.04M | 0.04M | 0.04M |
| | 0.08 M Strontium chloride hexahydrate | 0.08M | 0.08M | 0.08M | 0.08M | 0.08M | 0.08M |
| | 0.04 M Sodium cacodylate trihydrate pH 7.0 | 0.04M | 0.04M | 0.04M | 0.04M | 0.04M | 0.04M |
| | (+/-)-2-Methyl-2,4-pentanediol | 30% | 33% | 35% | 38% | 40% | 43% |
| | 0.012 M Spermine tetrahydrochloride | 12mM | 12mM | 12mM | 12mM | 12mM | 12mM |
| | 0.02 M Magnesium chloride hexahydrate | 0.02M | 0.02M | 0.02M | 0.02M | 0.02M | 0.02M |
| | 0.012 M Potassium chloride | 12mM | 12mM | 12mM | 12mM | 12mM | 12mM |
| D | **Proplex C2** | | | | | | |
| | 0.1M Na Citrate pH5 | 0.1M | 0.1M | 0.1M | 0.1M | 0.1M | 0.1M |
| | PEG3550 | 4% | 6% | 8% | 10% | 12% | 15% |
| E | **3BRD Friedmann et al 2008 Worm CSL-RAM-DNA complex** | | | | | | |
| | 0.1M bis-tris pH6 | 0.1M | 0.1M | 0.1M | 0.1M | 0.1M | 0.1M |
| | PEG3350 | 22% | 24% | 26% | 28% | 30% | 32% |
| | 0.2M MgCl2 | 0.2M | 0.2M | 0.2M | 0.2M | 0.2M | 0.2M |
| F | **3BRF Friedmann et al 2008 Worm CSL-RAM-DNA complex** | | | | | | |
| | 0.1M HEPES pH7.2 | 0.1M | 0.1M | 0.1M | 0.1M | 0.1M | 0.1M |
| | PEG3350 | 17% | 19% | 21% | 23% | 25% | 27% |
| | 0.2 M ammonium acetate | 0.2M | 0.2M | 0.2M | 0.2M | 0.2M | 0.2M |
| G | **3BRG Friedmann et al 2008 Mouse CSL-RAM-DNA complex** | | | | | | |
| | 0.1M bis-tris pH5.5 | 0.1M | 0.1M | 0.1M | 0.1M | 0.1M | 0.1M |
| | PEG3350 | 22% | 24% | 26% | 28% | 30% | 32% |
| H | **Proplex A8 PEG 3350** | | | | | | |
| | 0.2M Ammonium Sulphate | 0.2M | 0.2M | 0.2M | 0.2M | 0.2M | 0.2M |
| | 0.1M Na Acetate pH5.5 | 0.1M | 0.1M | 0.1M | 0.1M | 0.1M | 0.1M |
| | PEG3550 | 4% | 6% | 8% | 10% | 12% | 15% |

**Figure 3.59. Table showing conditions used to optimise the crystallisation of the EBNA2.14aa peptide-RBP-Jk$_{8-435}$-DNA complex.** These conditions were derived from a Natrix screen that produced crystals of the EBNA2.14aa peptide-RBP-Jk$_{8-435}$-DNA complex and conditions that produced crystals in previous publications.

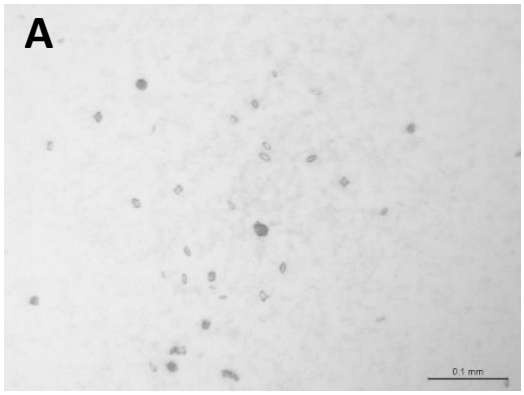


Opt 3 H2: 0.2M Ammonium Sulphate, 0.1M Na Acetate pH5.5, 6% PEG3550

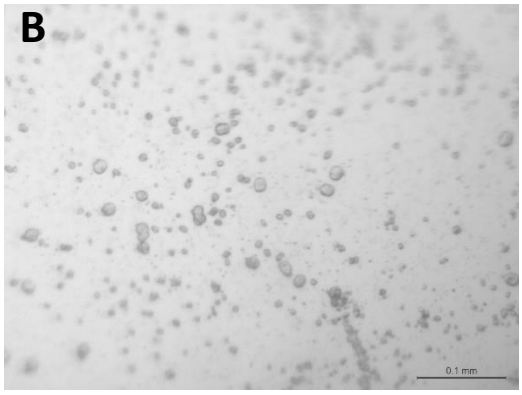


Opt3 Natrix G10 seed H2: 0.2M Ammonium Sulphate, 0.1M Na Acetate pH5.5, 6% PEG3550

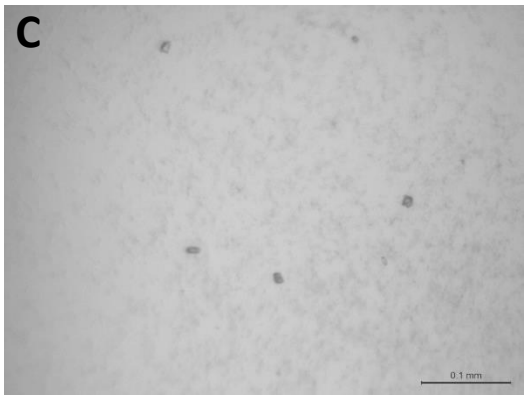


Opt 3 H3: 0.2M Ammonium Sulphate, 0.1M Na Acetate pH5.5, 8% PEG3550

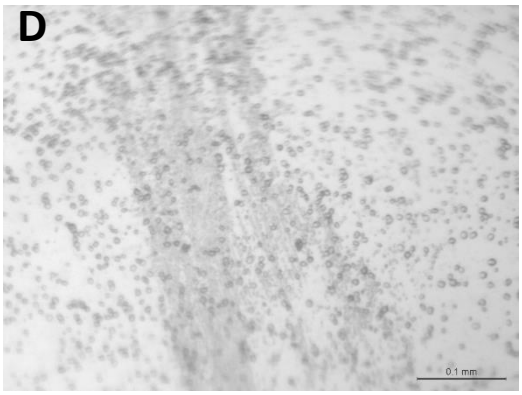


Opt3 Natrix G10 seed H3: 0.2M Ammonium Sulphate, 0.1M Na Acetate pH5.5, 8% PEG3550

**Figure 3.60. Pictures of crystals of EBNA2.14aa peptide, C-terminally His-tagged RBP-$Jk_{8-435}$ (expressed in *E.coli*) and RBP-Jk consensus site DNA complex grown in Natrix and published condition optimisation plate. A.** Small crystals of EBNA2.14aa peptide-RBP-$Jk_{8-435}$-DNA complex. Unfortunately, these crystals were too small to fish. **B.** Small crystalline precipitate of EBNA2.14aa peptide-RBP-$Jk_{8-435}$-DNA complex which were too small to be fished. **C.** Small crystals of EBNA2.14aa peptide-RBP-$Jk_{8-435}$-DNA complex. Unfortunately, these crystals were too small to fish. **D.** Small crystalline precipitate of EBNA2.14aa peptide-RBP-$Jk_{8-435}$-DNA complex which were too small to be fished.

### 3.3.2.3 : Optimisation of Proplex A8 condition

The Proplex A8 conditions had consistently produced crystal showers, even from different preparations of RBP-J$\kappa_{8-435}$-DNA-EBNA2.14aa complex. However, when we substituted PEG2000 MME for PEG3350 in the Natrix and published conditions (Figure 3.59) it produced distinctly different crystals to what we had seen in previous screens. We therefore decided to make a Proplex A8 PEG screen to see if a different PEG would grow crystals we could collect scatter data from (Figure 3.61).

The heavier PEG caused the protein to crash out of solution and the lighter PEGs still produced crystal showers. However, the PEG400 condition resulted in distinct rod shaped crystals (Figure 3.62) and lower concentrations of PEG400 produced larger rod crystals (Figure 3.62A and C). However, these crystals were unfortunately too thin to collect data from. We also reduced the concentration of protein added to the wells from 10mg/ml to 5 mg/ml to attempt to reduce the number of nucleation points which would lead to fewer but larger crystals growing. Reducing the concentration of complex to 5mg/ml did reduce the number of crystals that grew but did not increase the size of the crystals (Figure 3.62 A and D).

| Proplex A8 PEG Screen | | 1 | 2 | 3 | 4 | 5 | 6 |
|---|---|---|---|---|---|---|---|
| A | Proplex A8 PEG3550 | | | | | | |
| | 0.2M Ammonium Sulphate | 0.2M | 0.2M | 0.2M | 0.2M | 0.2M | 0.2M |
| | 0.1M Na Acetate pH5.5 | 0.1M | 0.1M | 0.1M | 0.1M | 0.1M | 0.1M |
| | PEG3550 | 4% | 6% | 8% | 10% | 12% | 15% |
| B | Proplex A8 PEG4000 | | | | | | |
| | 0.2M Ammonium Sulphate | 0.2M | 0.2M | 0.2M | 0.2M | 0.2M | 0.2M |
| | 0.1M Na Acetate pH5.5 | 0.1M | 0.1M | 0.1M | 0.1M | 0.1M | 0.1M |
| | PEG4000 | 4% | 6% | 8% | 10% | 12% | 15% |
| C | Proplex A8 PEG8000 | | | | | | |
| | 0.2M Ammonium Sulphate | 0.2M | 0.2M | 0.2M | 0.2M | 0.2M | 0.2M |
| | 0.1M Na Acetate pH5.5 | 0.1M | 0.1M | 0.1M | 0.1M | 0.1M | 0.1M |
| | PEG8000 | 4% | 6% | 8% | 10% | 12% | 15% |
| D | Proplex A8 6%PEG (salt) | | | | | | |
| | 0.2M Ammonium Sulphate | 75mM | 0.1M | 0.125M | 0.15M | 0.175M | 0.2M |
| | 0.1M Na Acetate pH5.5 | 0.1M | 0.1M | 0.1M | 0.1M | 0.1M | 0.1M |
| | PEG3550 6% | 6% | 6% | 6% | 6% | 6% | 6% |
| E | Proplex A8 8%PEG (salt) | | | | | | |
| | 0.2M Ammonium Sulphate | 75mM | 0.1M | 0.125M | 0.15M | 0.175M | 0.2M |
| | 0.1M Na Acetate pH5.5 | 0.1M | 0.1M | 0.1M | 0.1M | 0.1M | 0.1M |
| | PEG3550 8% | 8% | 8% | 8% | 8% | 8% | 8% |
| F | Proplex A8 PEG550 MME | | | | | | |
| | 0.2M Ammonium Sulphate | 0.2M | 0.2M | 0.2M | 0.2M | 0.2M | 0.2M |
| | 0.1M Na Acetate pH5.5 | 0.1M | 0.1M | 0.1M | 0.1M | 0.1M | 0.1M |
| | PEG550 MME | 6% | 10% | 15% | 20% | 25% | 30% |
| G | Proplex A8 PEG550 | | | | | | |
| | 0.2M Ammonium Sulphate | 0.2M | 0.2M | 0.2M | 0.2M | 0.2M | 0.2M |
| | 0.1M Na Acetate pH5.5 | 0.1M | 0.1M | 0.1M | 0.1M | 0.1M | 0.1M |
| | PEG550 | 6% | 10% | 15% | 20% | 25% | 30% |
| H | Proplex A8 PEG400 | | | | | | |
| | 0.2M Ammonium Sulphate | 0.2M | 0.2M | 0.2M | 0.2M | 0.2M | 0.2M |
| | 0.1M Na Acetate pH5.5 | 0.1M | 0.1M | 0.1M | 0.1M | 0.1M | 0.1M |
| | PEG400 | 6% | 10% | 15% | 20% | 25% | 30% |

**Figure 3.61. Table showing conditions used to optimise the crystallisation of the EBNA2.14aa peptide-RBP-Jk$_{8-435}$-DNA complex.** Different polymers of polyethylene glycol (PEG) were combined with proplex A8 crystallisation condition to attempt to prevent crystal showers of EBNA2.14aa peptide-RBP-Jk$_{8-435}$-DNA complex growing.

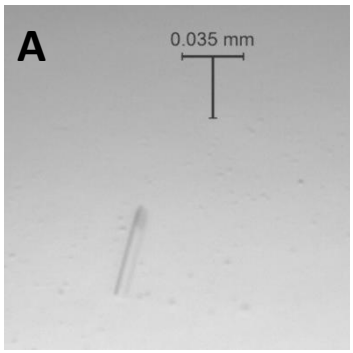


Proplex A8 opt 5mg/ml H4: 0.2M Ammonium Sulphate, 0.1M Na Acetate pH5.5, 20% PEG400

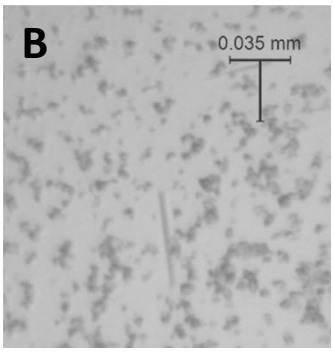


Proplex A8 opt 5mg/ml H5: 0.2M Ammonium Sulphate, 0.1M Na Acetate pH5.5, 25% PEG400

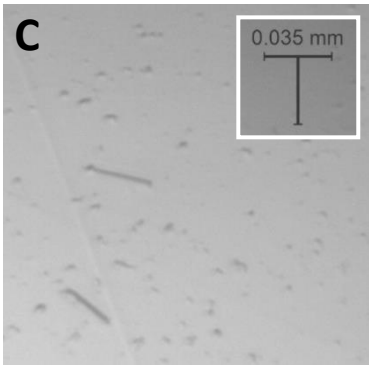


Proplex A8 opt 5mg/ml Hand pipetted: 0.2M $NH_4$

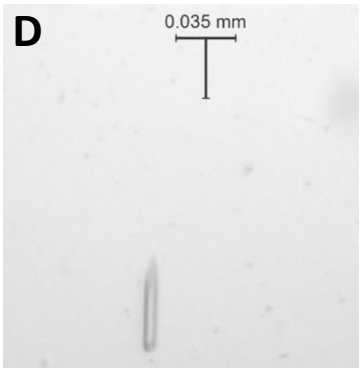


Proplex A8 opt 10mg/ml H4: 0.2M Ammonium

**Figure 3.62. Pictures of crystals of EBNA2.14aa peptide, C-terminally His-tagged RBP-$Jk_{8-435}$ (expressed in *E.coli*) and RBP-Jk consensus site DNA complex grown in Proplex A8 PEG optimisation plate at different concentrations. A.** A small rod-shaped crystal of EBNA2.14aa peptide-RBP-$Jk_{8-435}$-DNA complex. The complex did not grow crystal showers however these crystals were too thin to expose to an x-ray source. **B.** A small rod-shaped crystal of EBNA2.14aa peptide-RBP-$Jk_{8-435}$-DNA complex growing out of crystalline precipitate can be seen. These crystals were too thin to expose to an x-ray source. **C.** Small rod-shaped crystals of EBNA2.14aa peptide-RBP-$Jk_{8-435}$-DNA complex are shown growing out of crystalline precipitate. These crystals were too small to be fished. **D.** A small rod-shaped crystal of EBNA2.14aa peptide-RBP-$Jk_{8-435}$-DNA complex. Although the crystals did not grow crystal showers these crystals were too thin to expose to an x-ray source.

### 3.3.3.1 : Expression of a conserved region of EBNA2 to co-crystallise with RBP-Jκ$_{8-435}$-DNA complex

As we were unable to optimise a crystallisation condition for the RBP-Jκ$_{8-435}$-DNA-EBNA2.14aa complex we decided to express and purify larger RBP-Jκ binding region of EBNA2 (EBNA2$_{272-333}$) in insect cells to try and increase the likelihood of obtaining a structure of a RBP-Jκ-DNA-EBNA2 complex.

A Masters student from Dr Chrisostomos Prodromou group had produced a pFastBac vector that contained cDNA to express N-terminally His-tagged EBNA2$_{272-333}$ but had found the construct expressed the EBNA2 produced poorly and was not stable in solution. We therefore decided to co-express EBNA2$_{272-333}$ with RBP-Jκ$_{8-435}$ and anticipated that RBP-Jκ$_{8-435}$ would stabilise EBNA2$_{272-333}$ during expression and purification. We also decided to switch the His-tag on the EBNA2$_{272-333}$ to a StrepII tag to aid its stability during purification by inserting the EBNA2$_{272-333}$ cDNA into the polyhed MCS of the pFastBacCP17.2 vector.

The cDNA coding for EBNA2$_{272-333}$ was successfully amplified from the vector produced by Dr Chrisostomos Prodromou masters student (Figure 63A). The EBNA2$_{272-333}$ DNA fragment was ligated into a polyhed MCS of the a pFastBac co-expression vector containing either RBP-Jκ$_{8-435}$ or RBP-Jκ variant 2 cloned into the p10 MCS (pF.JK.8-435) (Figure 3.63B) . These co-expression vectors were transposed into bacmids to produce recombinant baculovirus that would co-express N-terminally His-tagged RBP-Jκ variant 2 or C-terminally His-tagged RBP-Jκ$_{8-435}$ with N-terminally StrepII-tagged EBNA2$_{272-333}$, (Figure 3.63 C and D).

We tested the expression of insect cells infected with the p1 recombinant baculovirus. N-terminally His-tagged RBP-Jκ variant 2 and C-terminally His-tagged RBP-Jκ$_{8-435}$ were shown to be expressed (Figure 3.64A). Western blot analysis also showed that the EBNA2$_{272-333}$ was being co-expressed in both the recombinant baculovirus (Figure 3.64B). Unfortunately, due to time constraints we were unable to optimise large scale purification of EBNA2$_{272-333}$ co-expressed in insect cells with RBP-Jκ$_{8-435}$.

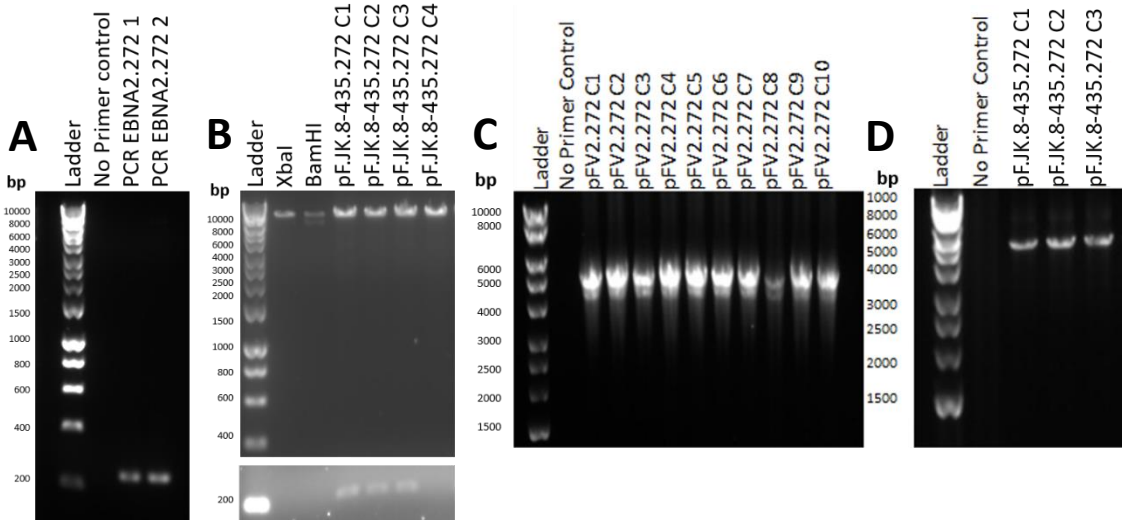


**Figure 3.63. Production of pFastBac plasmids co-expression EBNA2 aa272-333 and C-terminally His-tagged RBP-Jk$_{8-435}$ or N-terminally His-tagged RBP-Jk variant 2 and the transposition of these vectors into a bacmids. A.** PCR products of cDNA encoding a fragment of EBNA2 aa272-333. The expected band size is 187bp. **B.** Diagnostic restriction digests of different clones following ligation of cDNA of EBNA2.272-333 into a pFastBac vector containing C-terminally His-tagged RBP-Jk$_{8-435}$. Clones 1 to 3 produced products approximately the predicted size and were sent for sequencing. All clones contained the correct product. **C, D.** The pFastBac Vectors containing EBNA2.272-333 and either N-terminally His-tagged RBP-Jk variant 2 or C-terminally His-tagged RBP-Jk$_{8-435}$ were transposed into bacmids to produce recombinant baculovirus. Diagnostic PCRs amplified entire transposed region in the bacmid. Expected band sizes for transposed RBP-Jk variant 2 and RBP-Jk$_{8-435}$ were 4279bp and 3175bp respectively.

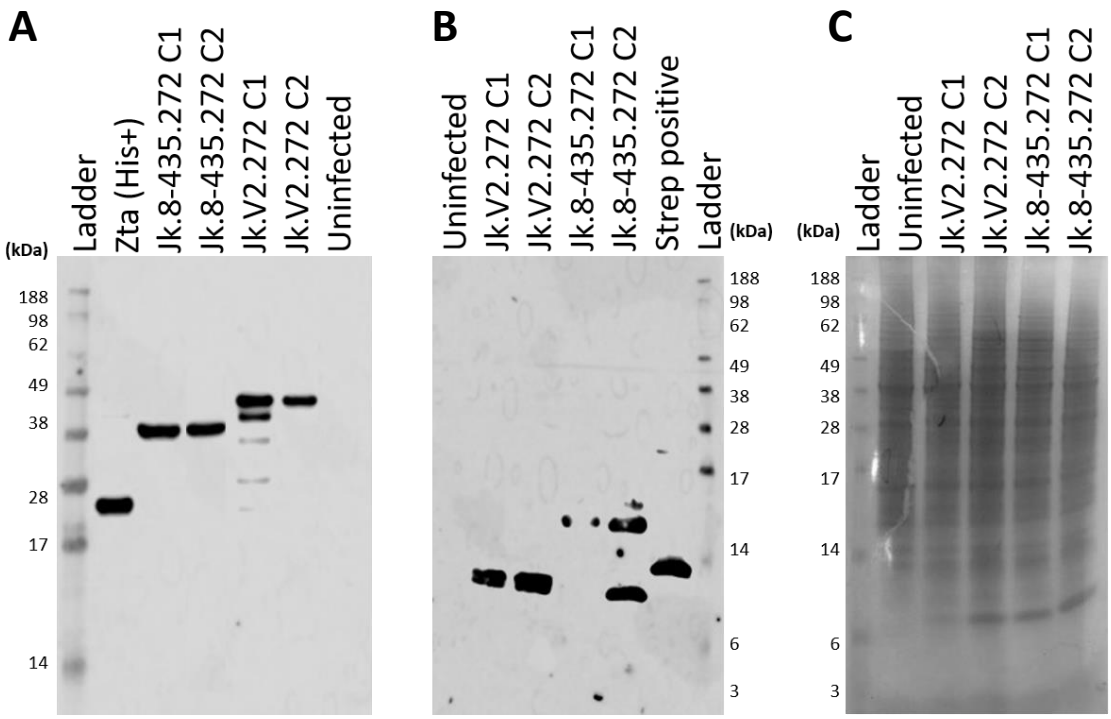


**Figure 3.64. Western blot analysis of insect cells co-expressing N-terminally Strep-tagged EBNA2$_{272-333}$ with N-terminally His-tagged RBP-Jk variant 2 or C-terminally His-tagged RBP-Jk$_{8-435}$. A.** Bacmids containing pFJK.V2.272 or pFJK.8-435.272 were transfected into Sf9 insect cells and cell lysates were prepared after 72 hours. Samples were run on a 10% Tris-SDS gel and probed with an anti-His antibody. Purified His-tagged Epstein-Barr virus ZTA protein was used as a positive control. Expected band sizes for N-terminally His-tagged RBP-Jk variant 2 and C-terminally His-tagged RBP-Jk$_{8-435}$ were 54kDa and 49kDa respectively. **B.** The same samples were run on a 10% Tris-SDS gel and probed with an anti-strep-tag antibody. Expected band size for the EBNA2$_{272-333}$ fragment was 11.2kDa. **C.** Coomassie stained gels of the transfection reactions.

### 3.3.3.2 : Expression of full length EBNA2 and the EBNA3C homology domain to co-crystallise with RBP-Jκ$_{8-435}$-DNA complex.

Due to the RBP-Jκ$_{8-435}$-DNA-EBNA2.26aa complex proving challenging to crystallise we also attempted to co-crystallise the RBP-Jκ$_{8-435}$-DNA complex with full length EBNA2 and constructs of the EBNA3C homology domain containing RBP-Jκ binding motifs.

The same Masters student from Dr Chrisostomos Prodromou group had produced a recombinant P2 baculovirus that expressed N-terminally His-tagged full length EBNA2. We tested whether it expressed EBNA2 with a small scale insect cell infection. EBNA2 was poorly expressed as we could detect EBNA2 by western blot analysis (Figure 3.65) but no clearly distinguishable bands were shown in the stained gel of the same cell pellet (Figure 3.65). EBNA2 also appears to partially degraded (Figure 3.65). We therefore decided to co-express full length EBNA2 with C-terminally His-tagged RBP-Jκ$_{8-435}$ in insect cells to attempt to improve stability.

Full length EBNA2 cDNA was successfully amplified from a vector produced by Dr Chrisostomos Prodromou Masters student (Figure 3.66A) and cloned into the pFastBac expression vectors with N-terminally His-tagged RBP-Jκ variant 1 or 2, or C-terminally His-tagged RBP-Jκ$_{8-435}$ (Figure 3.66B and C). Full length EBNA2 cDNA was successfully ligated into the polyhed MCS of the pFastBac expression vectors, which had a N-terminal StrepII-tag, with N-terminally His-tagged RBP-Jκ variant 1 or 2, or C-terminally His-tagged RBP-Jκ$_{8-435}$ cloned into the p10 MCS (Figure 3.66D).

Full length EBNA3C had previously been expressed in insect cells by Michelle West's group but was insoluble and partially degraded. The Homology domain (HD) of the EBNA3 family is predicted to contain secondary structure so we decided to focus on

expressing the EBNA3C HD (Zhao *et al.*, 1996, Yenamandra *et al.*, 2009). EBNA3C$_{100-356}$ (3CHD.1) was based on an EBNA3C construct previously used to study EBNA3C-RBP-Jκ interactions (Calderwood *et al.*, 2011). Based on alignments of the EBNA3 family we designed an additional construct, EBNA3C$_{100-431}$ (3CHD.2), to include a hydrophobic region which we predicted maybe be important for folding.

We made pFastBac vectors to express N-terminally His-tagged EBNA3C$_{100-356}$ or EBNA3C$_{100-431}$ and co-express C-terminally His-tagged RBP-Jκ$_{8-435}$ with N-terminally StrepII-tagged EBNA3C$_{100-356}$ or EBNA3C$_{100-431}$. We initially amplified cDNA to generate EBNA3C$_{100-356}$ or EBNA3C$_{100-431}$ destined for the p10 (N-terminal His-tag) or the polyhed (StrepII-tag) MCS of the pFastBac vector (Figure 3.67A). We successfully inserted cDNA to express EBNA3C$_{100-356}$ or EBNA3C$_{100-431}$ into empty pFastBac vector and pF.JK.8-435 respectively (Figure 3.67B-E).

We next transposed pF.JK.8-435.EB2, pF.EB3CHD.1, pF.EB3CHD.2, pF.JK.8-435.3CHD.1 and pF.JK.8-435.3CHD.1 into bacmids to generate recombinant baculovirus. Due to the large size of the DNA transposed into the bacmid we were unable amplify the entire transposed region to check for successful transposition as the polymerase was unable to extend such a large piece of DNA. We determined whether the vectors had been successfully transposed by amplifying the bacmid with the forward primers used to amplify each of the inserts and the M13 primer most proximal to the insert (Figure 3.68A).

Unfortunately, only the bacmid containing pF.EB3CHD.1 expressing N-terminally His-tagged EBNA3C$_{100-356}$ was successfully transfected (Figure 3.69). The insect cells should appear swollen if the cells have successfully been transfected as this is indicative of

baculovirus production. However, after this transfection it was mot clear whether the insect cells were swollen. As there was no way to quantify this swelling we were unable to show this data. Due to the cloning strategy being similar to the strategy used to produce pF.JK3.272 co-expression vector it was unlikely that there were transcriptional issues with EBNA2 and EBNA3C HD constructs. Additionally, RBP-J$\kappa_{8-435}$ and EBNA2$_{272-333}$ had been successfully expressed using the same expression system (Figure 3.64) which would suggest EBNA3C HD and EBNA2 should have been also expressed if the transfection had been successful. Therefore, it was most likely that the transfection had been unsuccessful but due to time constraints we were unable to repeat the unsuccessful transfections. However, we were able to do one large scale insect cell expression of N-terminally His-tagged EBNA3C$_{100-356}$.

A $Co^{2+}$ column (Talon 5ml) was used for the first purification step (Figure 3.70A). EBNA3C$_{100-356}$ was poorly expressed as the expected 29.5kDa bands were faint and not the dominant band on the gel (Figure 3.70A). We pooled eluates from the $Co^{2+}$ column purification for size exclusion (S200 10/300 column) to separate the EBNA3C$_{100-356}$ from the impurities. Some loss of impurities was observed but it was unclear which protein was EBNA3C$_{100-356}$ so performed a western blot of the size exclusion step fractions (Figure 3.70 B and C). The overall yield of EBNA3C$_{100-356}$ was approximately 0.4mg which was poor for a 3L prep. This was not enough EBNA3C$_{100-356}$ to set up crystal trials or ITC binding assays. The Coomassie stained gel and the western blot showed that there were still significant amounts of impurities in the sample so more purification steps would have likely been needed to improve the quality of the preparation (Figure 3.70 A and B).

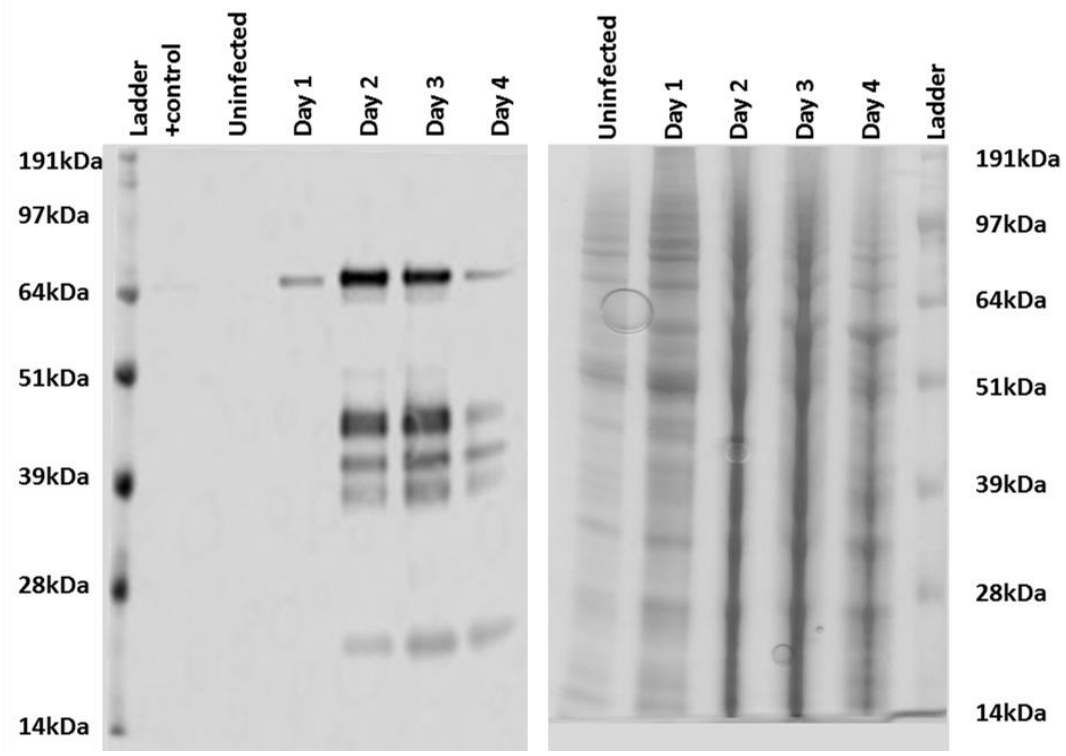


**Figure 3.65. Western blot and SDS-PAGE of analysis of baculovirus expression of N-terminally His-tagged full length EBNA2.** 100ml Sf9 insect cells were infected with baculovirus that expressed for N-terminally His-tagged full length EBNA2. Samples were taken every day, boiled in GSB and run on a 10% Bis-Tris SDS PAGE. The western was probed with an anti-EBNA2 antibody using a lysate from GM12878 cells line as a positive control. At higher exposure the positive control is visible. The Coomassie was stained in SimplyBlue gel stain. Although the expected mass of EBNA2 is 49kDa EBNA2 runs at approximately 65kDa on SDS-PAGE gels.

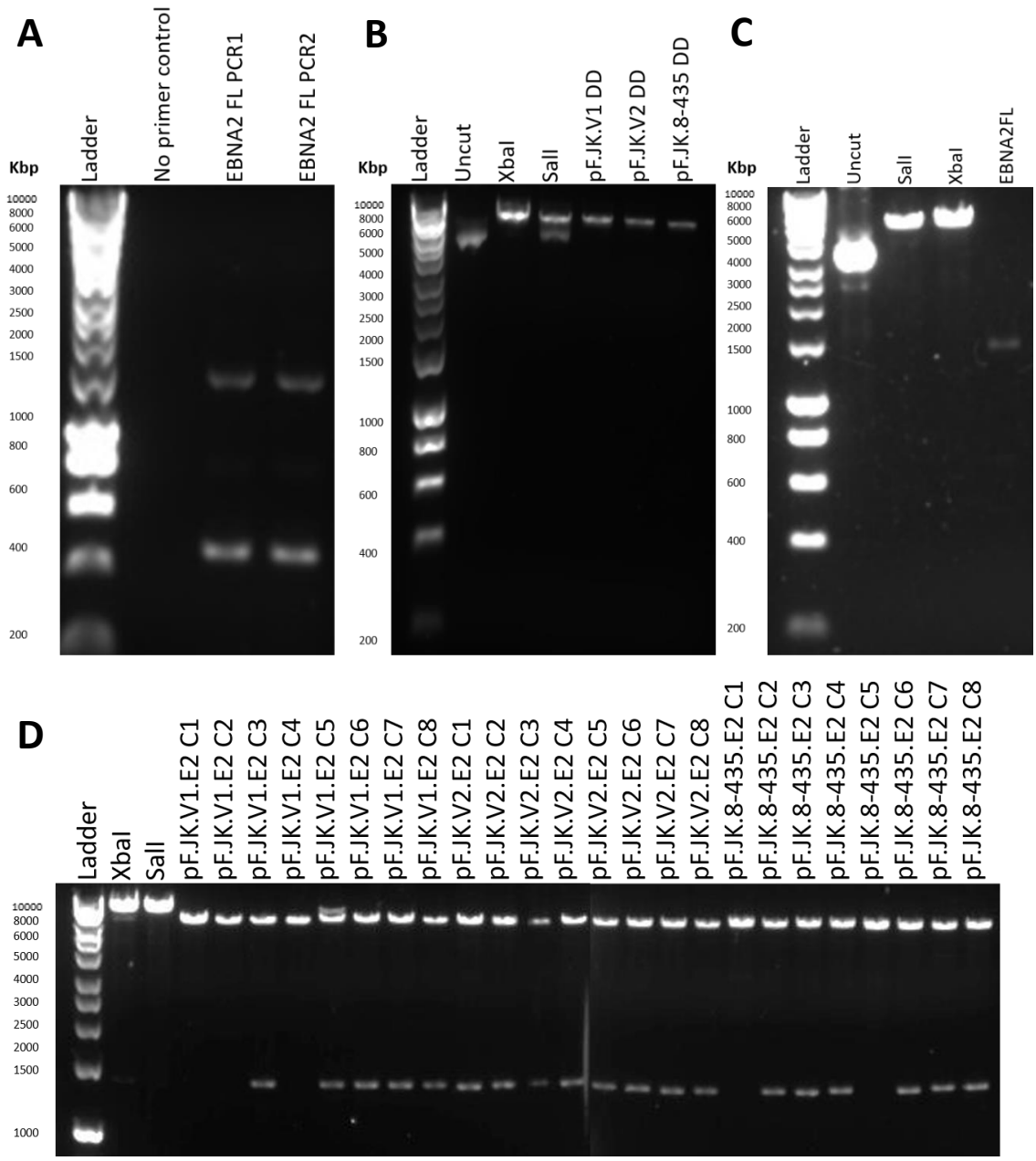


**Figure 3.66. Cloning of gene expressing Full length EBNA2 into a pFastBac co-expression vector containing C-terminally His-tagged RBP-Jk$_{8-435}$ or N-terminally His-tagged RBP-Jk variant 1 or variant 2. A.** PCR products of cDNA encoding full length EBNA2 (1464bp expected size) from pUC19.EB2. **B. R**estriction digests of pF.JK.V1, pF.JK.V2 and pF.JK.8-435. **C.** Restriction digest of full length EBNA2 cDNA. **D.** Diagnostic restriction digests of different clones following ligation of full length EBNA2 cDNA into pFastBac co-expression vectors of pF.JK.V1, pF.JK.V2 and pF.JK.8-435.

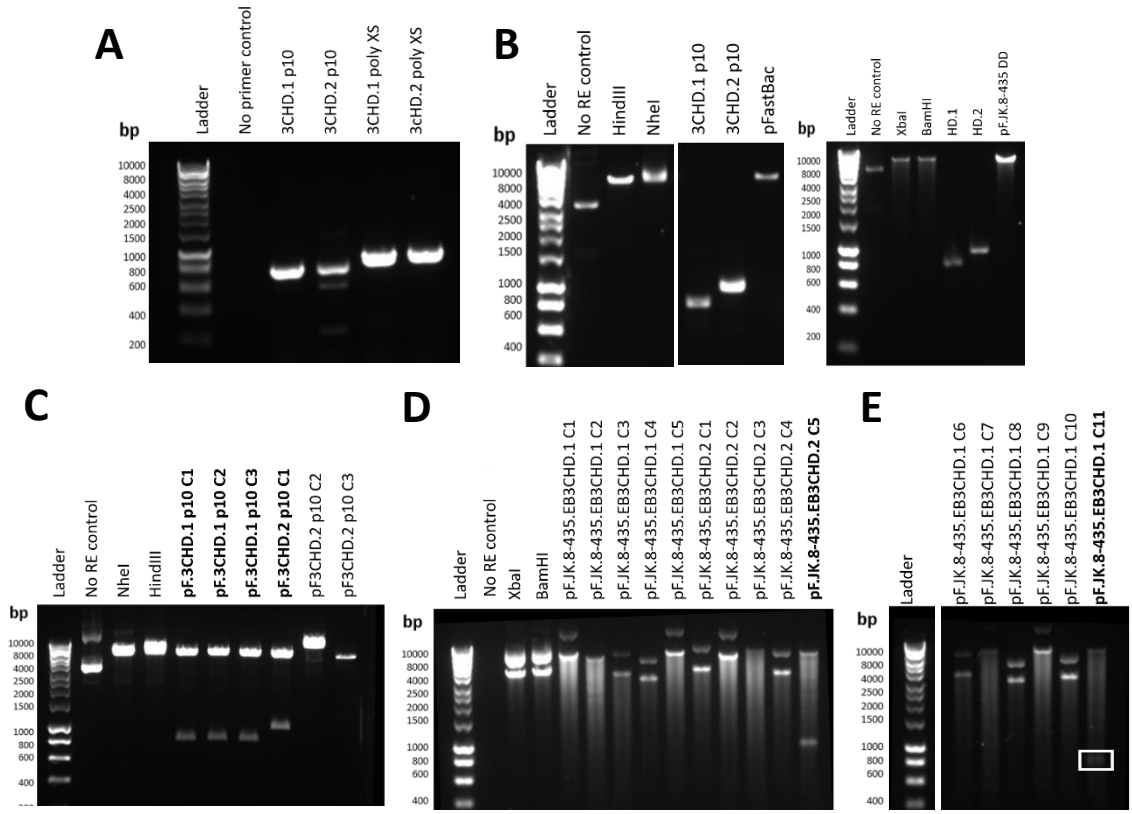


**Figure 3.67. Cloning of genes expressing EBNA3C$_{100-356}$ (3CHD.1) or EBNA3C$_{100-413}$ (3CHD.2) into a pFastBac17.2 vector or a pFastBac co-expression vector containing C-terminally His-tagged RBP-Jk$_{8-435}$. A.** PCR of cDNA encoding EBNA3C$_{100-356}$ (3CHD.1) or EBNA3C$_{100-413}$ (3CHD.2) from pUC19.EB3C. p10 (N-terminally his-tagged) and polyXS (N-terminally strep-tagged) denote the multiple cloning site (MCS) in the pFastBac vector the cDNA will be inserted to. **B. R**estriction digest of inserts and destination vectors previously described. **C.** Diagnostic restriction digests of ligation of cDNA of EBNA3C$_{100-356}$ (3CHD.1) or EBNA3C$_{100-413}$ (3CHD.2) into a pFastBac17.2 vector p10 MCS. **D.** Diagnostic restriction digests of ligation of cDNA containing EBNA3C$_{100-356}$ (3CHD.1) or EBNA3C$_{100-413}$ (3CHD.2) into a pF.JK.8-435 vector into the polyhed MCS. **E.** Diagnostic restriction digests of ligation of cDNA containing EBNA3C$_{100-356}$ (3CHD.1) into a pF.JK.8-435 vector into the polyhed MCS.

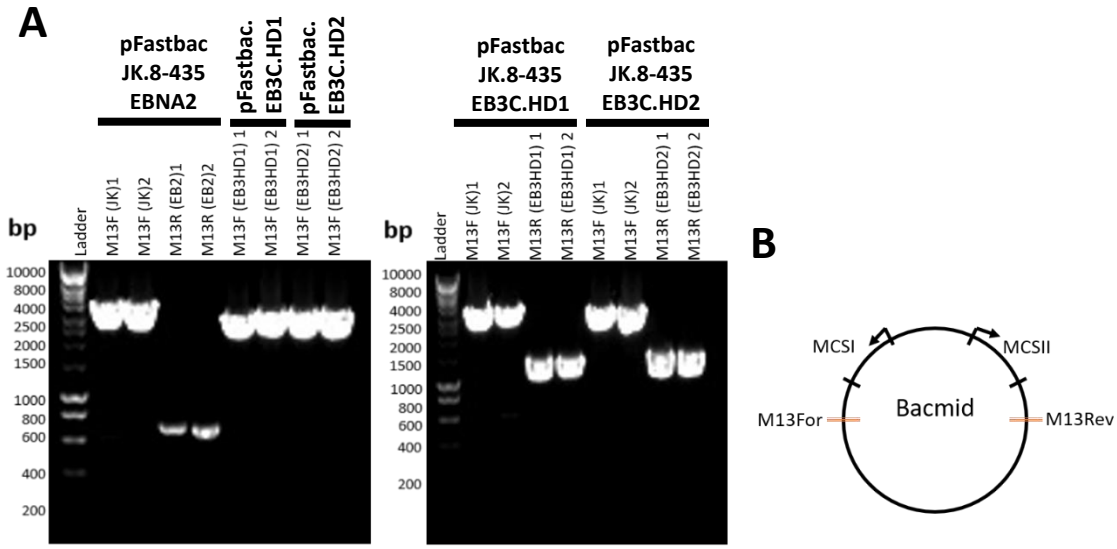


**Figure 3.68. Diagnostic PCRs of pFastBac vectors, with EBNAs cDNA or cDNA to co-express EBNAs with C-terminally His-tagged RBP-Jk$_{8\text{-}435}$, transposed into bacmids. A.** Diagnostic PCRs of vectors pF.JK.8-435.EB2, pF.EB3C.HD1, pF.EB3C.HD2, pF.JK.8-435.EB3C.HD1 and pF.JK.8-435.EB3C.HD1 transposed into bacmids. Shown are the combination of primers used in each of the diagnostic PCRs (M13 forward (M13F), M13 reverse (M13R) with the forward primer of each insert). **B.** A schematic of the bacmid showing where the M13F, M13R and insert primers would amplify from.

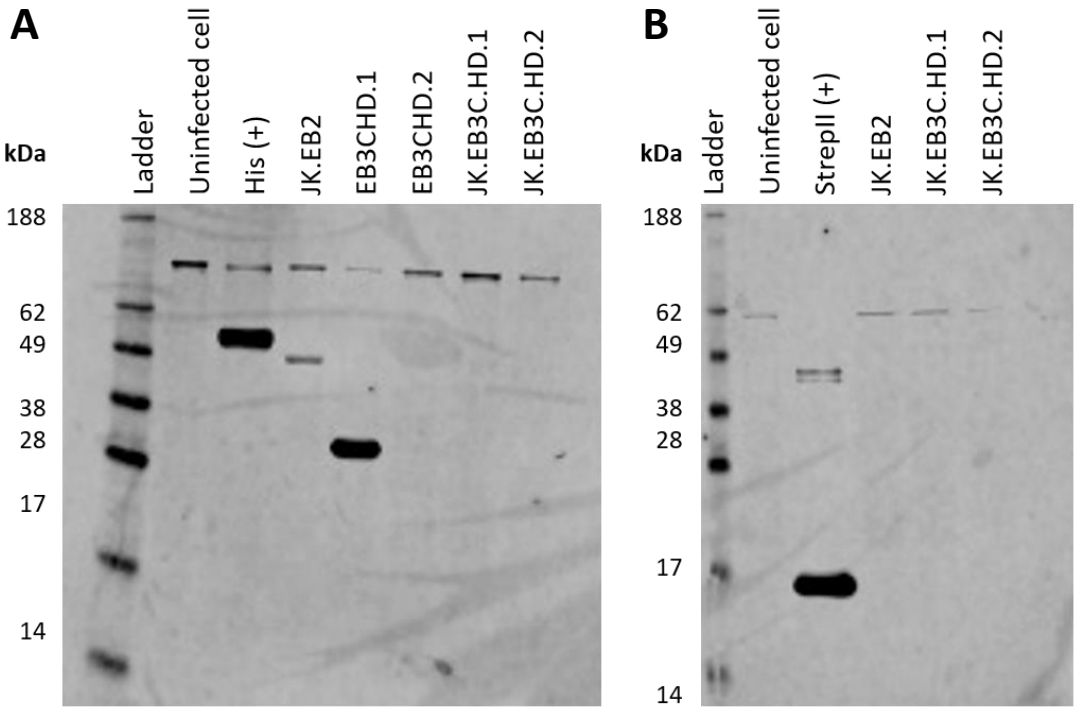


**Figure 3.69. Western blot analysis of Sf9 insect cells infected with P1 baculovirus expressing EBNAs or co-expressing EBNAs with C-terminally His-tagged RBP-Jk$_{8\text{-}435}$. A.** Bacmids containing pF.JK.8-435.EB2, pF.EB3C.HD1, pF.EB3C.HD2, pF.JK.8-435.EB3C.HD1 and pF.JK.8-435.EB3C.HD1 were transfected into Sf9 insect cells and cell lysates were prepared after 72 hours. Samples were ran on a 10% Tris-SDS gel and probed with an anti-His antibody. Purified His-tagged RBP-Jk$_{8\text{-}435}$ was used as a positive control. Expected band sizes for C-terminally His-tagged RBP-Jk$_{8\text{-}435}$, N-terminally His-tagged EBNA3C$_{100\text{-}356}$ (3CHD.1) and N-terminally His-tagged EBNA3C$_{100\text{-}413}$ (3CHD.2) were 49kDa, 32kDa and 38.2kDa respectively. **B.** The same samples previously described were run on a 10% Tris-SDS gel and probed with an anti-Strep antibody. Expected band sizes N-terminally strep-tagged EBNA3C$_{100\text{-}356}$ (3CHD.1) and N-terminally strep-tagged EBNA3C$_{100\text{-}413}$ (3CHD.2) were 33.7kDa and 39.9kDa respectively. Although the expected mass of EBNA2 is 49kDa EBNA2 runs at approximately 65kDa on SDS-PAGE gels.

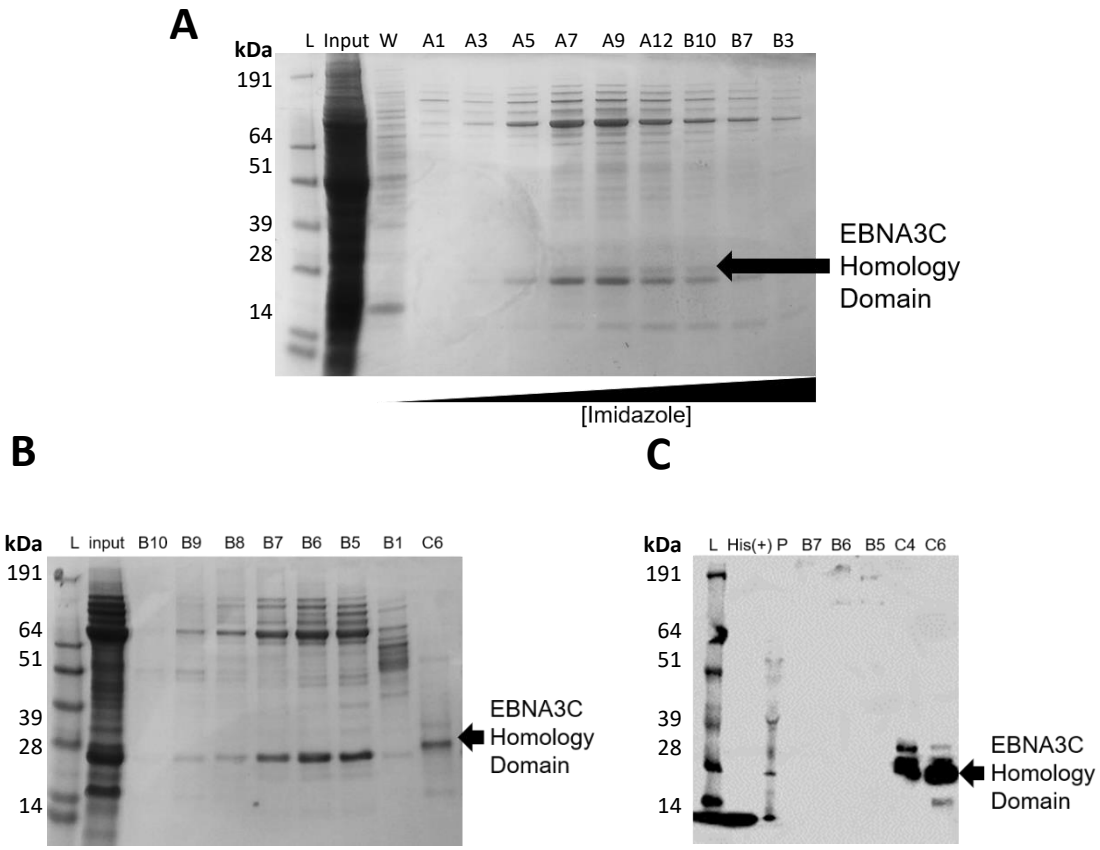


**Figure 3.70. Analysis of $Co^{2+}$ column (Talon) and size exclusion purification steps of N-terminally His tagged EBNA3C$_{100-356}$ expressed in 5 litres of insect cells. A.** Coomassie stained gel showing elution fractions from $Co^{2+}$ column (5ml Talon FF GE life sciences) as an increasing concentration of imidazole was passed through. All wells shown were pooled as it was not clear which contained EBNA3C HD. **B.** Coomassie stained gel showing elution fractions from size exclusion purification step. N-terminally His tagged EBNA3C$_{100-356}$ was loaded onto a Superdex S200 10/300 calibrated in EB3C Buffer C. **C.** Samples from the size exclusion step were boiled and run on a 4-12% Tris SDS page gel, then probed with anti-His antibody. A His-tagged PU.1 construct was used as the positive control.

### 3.3.4.1 : Conclusions of the structural studies of EBNA-RBP-Jκ complexes

We were unable to obtain crystals of EBNA2.14aa-RBP-Jκ-DNA complex that were suitable for X-ray diffraction. We showed that the EBNA2 peptide was not present in the crystal structure and had not been incorporated into the complex (Figure 3.49). This was likely caused by the contact points of the crystal that were over the BTD of RBP-Jκ forcing the peptide out of the WΦP binding pocket. In addition to this the crystal produced low resolution data. This was likely caused by the free space that was between the complexes in the lattice reducing resolution and the fact that the crystal contained two crystals stacked on top of each other. This generated shadow spots of intensity when we were exposing the crystal to the X-ray source. Shadow spots make resolving structures difficult as they create diffractions that do not represent the structure you are attempting to resolve yet are incorporated into Fourier transform calculations making the scatter data challenging to process.

One potential issue with our protocol for preparing the EBNA2.14aa-RBP-Jκ-DNA complex was that we concentrated the RBP-Jκ-DNA before adding the peptide. This potentially could have made the solution congested and sterically prevented the EBNA2.14aa peptide from binding to the RBP-Jκ. However, this was dismissed when a postdoc from Michelle West's group incubated EBNA2.14aa with RBP-Jκ-DNA before concentrating and showed that this did not improve crystallisation of the EBNA2.14aa-RBP-Jκ-DNA complex.

We then attempted to co-crystalise EBNA peptides with RBP-Jκ expressed in *E.coli*. With the higher and more consistent yields of RBP-Jκ expressed in *E.coli* we were able to broaden the range of crystallisation strategies. We also switched using EBNA2.26aa

peptide to EBNA2.14aa as amino acid chains not bound to RBP-Jκ were thought to be one of the reasons for the low quality resolution of the RAM domain of Notch in the structure of the Notch ternary complex (Wilson and Kovall, 2006). Even after testing large numbers of different crystallisation conditions to crystallise EBNA2.14aa-RBP-Jκ-DNA expressed in *E.coli* we were not able to discourage the crystals from forming crystal showers (Figure 3.57, 3.58, 3.60 and 3.62).

Finally, we attempted to express constructs of the EBNAs individually and in co-expression vectors. Again, based on previous studies of the EBNA TΦGC and WΦP RBP-Jκ binding motifs by and we chose to express the EBNAs in insect cells (Zhao *et al* 1996, Calderwood *et al* 2011)(Figure 3.69). We also tried to co-express the EBNAs with RBP-Jκ as we hypothesised that RBP-Jκ would confer stability to the EBNAs as they were being expressed (Figure 3.69). We also utilised StrepII-tag as it is eluted from StrepTactin resin using desthiobiotin which is significantly less harmful to proteins than imidazole. Time constraints and unsuccessful transfections meant we were only able to produce a baculovirus that could express his-tagged EBNA3C$_{100\text{-}356}$ (3CHD.1)(Figure 3.69 and 3.70). However, EBNA3C$_{100\text{-}356}$ expressed poorly and due to time constraints we were unable to optimise a large scale purification (Figure 3.70).

# Chapter 4 : Discussion

## 4.1 : Future strategies for the crystallisation of EBNA peptides bound to RBP-Jκ

The largest obstacles we encountered when optimising crystallisation conditions whilst expressing RBP-Jκ in insect cells was that the production of recombinant baculovirus, expression and purification processes were slow. Inconsistent yields also meant that planning crystallisation strategies was also difficult. It is possible that the quality of the RBP-Jκ expressed in insect cells was likely of a higher quality than the RBP-Jκ expressed in *E.coli*, due to processing by eukaryotic folding machinery. However, the extra time that it took to express RBP-Jκ in insect cells largely negated this benefit. Additionally, we showed using ITC that the ability of the EBNA2.14aa peptide to bind to RBP-Jκ was not affected by which expression system had been used to produce RBP-Jκ (Figure 3.27). Therefore for the purpose of crystallising the EBNA2.14aa-RBP-Jκ-DNA complex, the RBP-Jκ expressed in *E.coli* was suitable.

Even after testing large numbers of different crystallisation strategies we were not able obtain crystals of EBNA RBP-Jκ complexes. We were able to produce a 3.63Å structure of RBP-$Jκ_{8-435}$ bound to DNA where the crystal packing forces had appeared to displace EBNA2 peptide from the BTD of RBP-Jκ. This may have occurred due to the EBNA2 peptide having significantly weaker affinity for RBP-Jκ than Notch peptide (Figure 3.24).

Novel constructs of RBP-Jκ could be generated for future trials to prevent crystal packing forces from displacing EBNA2 peptide from the crystal. Adding tags to RBP-Jκ and binding RBP-Jκ to different DNA nucleotides could also encourage an EBNA2-RBP-Jκ-DNA to crystallise into different lattices and symmetries. This could potentially

prevent crystal showers from growing, encourage tighter packing to improve resolution and prevent crystal contact points being established over the hydrophobic WΦP binding pocket of the BTD.

A potential way of co-crystallising RBP-Jκ-EBNA2 peptide complex would be to reproduce the crystallisation strategy that produced structure of Hairless bound to Suppressor of hairless (Su(H)) complex (Figure 4.1)(Yuan *et al.*, 2016). Su(H) is the *D. melanogaster* homologue of RBP-Jκ and hairless, which there is no known human homologue, binds to Su(H) to silence notch signalling. Traditionally Maltose binding Protein (MBP) tags are cleaved off and are only attached to proteins to improve solubility however, in this structure the MBP tag was not cleaved off hairless as the MBP-tag formed key contact points in the crystal lattice. The lattice that was produced consisted of very tightly packed complexes, which produced a 2.14Å resolution structure, one of the highest resolution structures of a RBP-Jκ homologue (Figure 4.1). The crystallisation strategy used to produce the structure of the Notch1 transcription complex could also be attempted by substituting the RAM domain peptide for EBNA2 peptide in the Notch complex. However, our SwitchSense data indicated that the EBNA2 peptide induced conformational changes to RBP-Jκ, which may differ to the conformation induced by Notch RAM domain binding, potentially disrupting the assembly of the Notch transcription complex when attempting to co-crystallise it with the EBNA2 peptide.

Another potential solution to ensuring that the EBNA2.14aa peptide remained bound to RBP-Jκ during crystallisation would be to produce a fusion protein of RBP-Jκ and EBNA2 CR6, which contains the WΦP RBP-Jκ binding motif. A significant challenge to

designing a RBP-Jκ fusion protein is that the N and C termini of RBP-Jκ are shown in the structure of the Notch 1 transcription complex to protrude from the NTD and CTD away from the BTD (Choi *et al.*, 2012). This would mean a flexible linker chain would have to be introduced to allow the EBNA2 CR6 to interact with the BTD of RBP-Jκ. However, in the structure of the Notch transcription activation complex the amino acid linker that connects the RAM domain to the ANK repeats was suggested to contribute to the low resolution of the structure (Nam *et al.*, 2003, Choi *et al.*, 2012). Also increasing the length of the amino acid chain linker that connects the Notch ANK and RAM domains has been shown to reduce the strength of RBP-Jκ-Notch interactions (Sherry *et al.*, 2015).

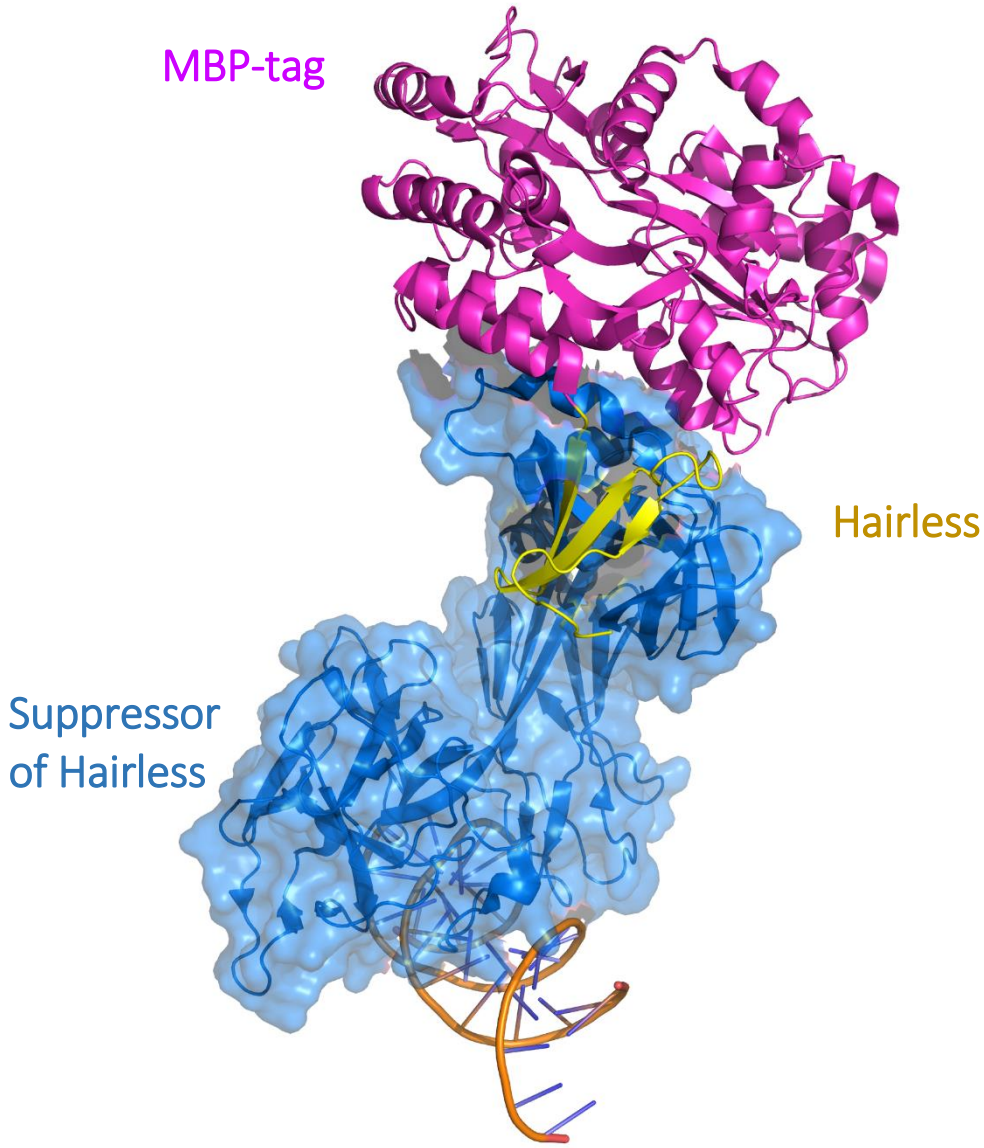


**Figure 4.1. Crystal Structure of MBP-tagged Hairless bound to the Suppressor of Hairless-Hes-1 site complex.** MBP-tag shown in pink, Hairless shown in yellow and Suppressor of Hairless shown in blue. Structure resolved by Yuan et al 2016 to 2.14Å resolution (Yuan *et al.*, 2016).

## 4.2 : Production of recombinant EBNAs

An ongoing problem that was encountered during attempts to express recombinant EBNAs was there poor solubility *in vitro*. This is likely due to the EBNAs being predicted to have predominantly disordered folding (Yenamandra *et al.*, 2009). We attempted to express the EBNA3C homology domain in insect cells due to it being predicted to fold (Yenamandra *et al.*, 2009) but despite this it expressed poorly and was unstable suggesting it relied on distal parts of the EBNA3C protein for stability. In LCLs EBNA3 levels were not affected by the addition of cyclohexamide or interferon-γ, suggesting a low turnover and were suggested to be very stable in cells (Touitou *et al.*, 2005, West, 2006). Additionally pulse chase experiments and cycloheximide treatment also showed that EBNA2 was stable in cells for over 24 hours (Grässer *et al.*, 1991). It has been suggested that the EBNAs rely on interactions with host cell folding proteins to achieve this. For example, EBNA3A induces the expression of and interacts *in vitro* with Hsp70 (Young *et al.*, 2008).

We did not attempt to express EBNA2 and EBNA3C HD in *E.coli* as previous studies showed that EBNA-RBP-Jκ interactions are influenced by whether they were expressed in eukaryotic or prokaryotic expression systems (Henning, 2006, Johnson *et al.*, 2010, Calderwood *et al.*, 2011). However, Dr Rajesh Ponnusammy, working in the group in parallel, did attempt to express EBNA2 and EBNA3C homology domain in *E.coli* and yeast expression systems. He also found that the EBNA3s and EBNA2s were insoluble and expressed at low levels.

One solution to improve solubility of the EBNAs *in vitro* would be to co-express them with binding partners such as host transcription factors they interact with. Although

we attempted to co-express the EBNAs with RBP-Jκ in insect cells we were unable to produce a recombinant virus capable of this and due to time constraints we were unable to repeat the transfections. However SKIP could be co-expressed with EBNA2 to improve stability as it has been shown to interact with EBNA2 in pull downs and mammalian two hybrid assays, and play a role in EBNA2 transactivation of RBP-Jκ mediated genes in reporter assays (Sifang Zhou, 2000). However, SKIP has not been expressed and purified in large quantities *in vitro* and not much is known about its stability.

Another solution to finding a truncation of the each of the EBNAs that expresses well and is soluble in buffer would be to process cDNA encoding EBNA2 and the EBNA3s at the Oxford Protein Production Facility UK (OPPFUK). This research facility will initially produce an array of constructs capable of expressing a multitude of iterations of your protein of interest. The cDNA produced from this PCR step are cloned into vectors capable of being transformed or transfected into a host of *E.coli* strains and eukaryotic expression systems. In addition to this they have a library of tags to add to your protein of interest, such as MBP-tags and TRX-tags, to improve solubility. The precise mechanism to how MBP tags improve solubility of fusion proteins is not well understood and MBP tags ability to improve solubility is suggested to be dependent on the protein fused to the MBP tag (Nallamsetty and Waugh, 2006). TRX tags improve solubility and prevent the formation of inclusion bodies of their fusion partners with their oxido-reductase activity (LaVallie *et al.*, 1993, Yasukawa *et al.*, 1995, LaVallie *et al.*, 2000). From here different constructs are expressed in plates in a multitude of expression hosts which can be probed for successful expression to provide a list of hits of successful constructs. Finally, the hits can be tested for solubility in a range of stock

lysis buffers the OPPFUK have designed. This broad screen could provide the key to finding a soluble and highly expressible truncation of the EBNAs suitable for thermodynamic and structural studies.

### 4.3 : EBNA interactions with RBP-Jκ.

#### 4.3.1 : The Role of TFGC and WTP RBP-Jκ motifs in EBNA-RBP-Jκ interactions

Our ITC data showed that, in the context of the peptide, Notch2 bound to RBP-Jκ an order of magnitude tighter than EBNA2. This suggests that in the context of an EBV infection it is unlikely that EBNA2 directly competes with Notch for RBP-Jκ for binding. However Notch1 is also expressed in B cells at different stages of B cell development and should also be tested to quantify how tightly it binds to RBP-Jκ to compare its affinity to EBNA2-RBP-Jκ interactions (He and Pear, 2003b). Additionally, our Switchsense data indicated that the EBNA2 peptide induced more severe conformational changes to RBP-Jκ than Notch induced. During an EBV infection this could allow EBNA2 to drive dynamic RBP-Jκ to bind specific promoters that aid the establishment of a persistent EBV infection. This unique conformation of RBP-Jκ induced by EBNA2 could also provide a unique platform to recruit transcriptional and epigenetic factors, not recruited by Notch, to manipulate host gene expression during an EBV infection.

Surprisingly we found that in the context of a peptide that the TΦGC EBNA3 RBP-Jκ binding motif did not contribute to RBP-Jκ binding and did not compete with an EBNA2 peptide for RBP-Jκ binding. We also showed that *in vitro* the WΦP motif in the EBNA3C peptide was essential for RBP-Jκ binding. In addition to this, we showed that residues in EBNA3A that mimicked the chemistry of the WΦP motif facilitated weak binding to

RBP-Jκ. This suggests that TΦGC motif may bind indirectly to RBP-Jκ via another host transcription factor or be essential to EBNA3 folding and the presentation of the WΦP or a WΦP-like motif. However, the EBNA3 peptides we tested did not include two regions, which flank the TΦGC and WΦP motif, which are predicted to fold in to β-sheets. If these regions had been included in the EBNA3 peptide designs they may have facilitated EBNA3 TΦGC motif binding to RBP-Jκ and should be tested in future studies (Yenamandra *et al.*, 2009, Calderwood *et al.*, 2011).

However, we suggest that the scanning alanine mutations that were used to identify the TΦGC motif as directly binding to RBP-Jκ in past studies may have in fact perturbed the folding of EBNA3C and the presentation of WΦP motif rather than knocking out specific RBP-Jκ binding interactions (Robertson *et al.*, 1996a). Most of the EBNA3C-RBP-Jκ interaction studies were undertaken before research had showed that alanine mutations and truncations can have serious consequences for the overall folding of the protein interest (Studer *et al.*, 2013). In addition to this mutating glycine residues is often avoided as they rotate freely allowing the protein to fold into tight turns. Glycine residues have been shown to be evolutionary conserved in kinases as they facilitate turns in protein loops essential for kinase folding but are not directly involved in protein-protein interactions (Barouch-Bentov *et al.*, 2009).

Rajesh Ponnusamy from our group produced a 3D model of the EBNA3C HD using RaptorX online modelling software (Figure 4.2). The EBNA3C model predominantly folds in to clusters of α-helices connected by disordered linkers with the TFGC and WTP motifs presented in a loop above anti-parallel β-sheets (Figure 4.2). In this model, the TFGC and the WTP RBP-Jκ binding motifs are in close proximity to each other and

presented on the surface of the protein on a loop. The two motifs appear close enough to form hydrogen bonds between the threonine residues from both motifs and could potentially have hydrophobic interactions between organic rings of the phenylanine and tryptophan residues from each of the RBP-Jκ binding motifs. We speculate from this model of the EBNA3C HD structure that the TFGC residues could play a role in the presentation of the WTP RBP-Jκ binding motif. Therefore, when the TFGC residues are mutated to alanines, EBNA3C is no longer correctly presenting the WTP motif preventing EBNA3C-RBP-Jκ binding. What this model cannot show is the effect of the TFGC-AAAA mutation on the overall structure of EBNA3C. However, it would be interesting to see if raptorX models of the EBNA3A and EBNA3B homology domains were predicted to fold in a similar conformation to the EBNA3C model and whether the RBP-Jκ binding motifs would be presented in similar positions.

We also wanted to test whether the TFGC-AAAA mutations affected EBNA3Cs ability to bind other host targets. We intended to cross-link the DG75 cells transfected with wild type and TFGC mutants of EBNA3C. This would have fixed host transcription factors known to bind EBNA3C. We then intended to pull down full length EBNA3C, with an anti EBNA3C antibody conjugated to beads, and probe the pulldowns products for RBP-Jκ and other known binding targets of EBNA3C using western blot analysis. We hypothesised that if the EBNA3C TFGC-AAAA mutation was deleterious to the folding of EBNA3C we would have seen that EBNA3C interactions with other host target proteins would have also been negatively affected by the TFGC-AAAA mutations.

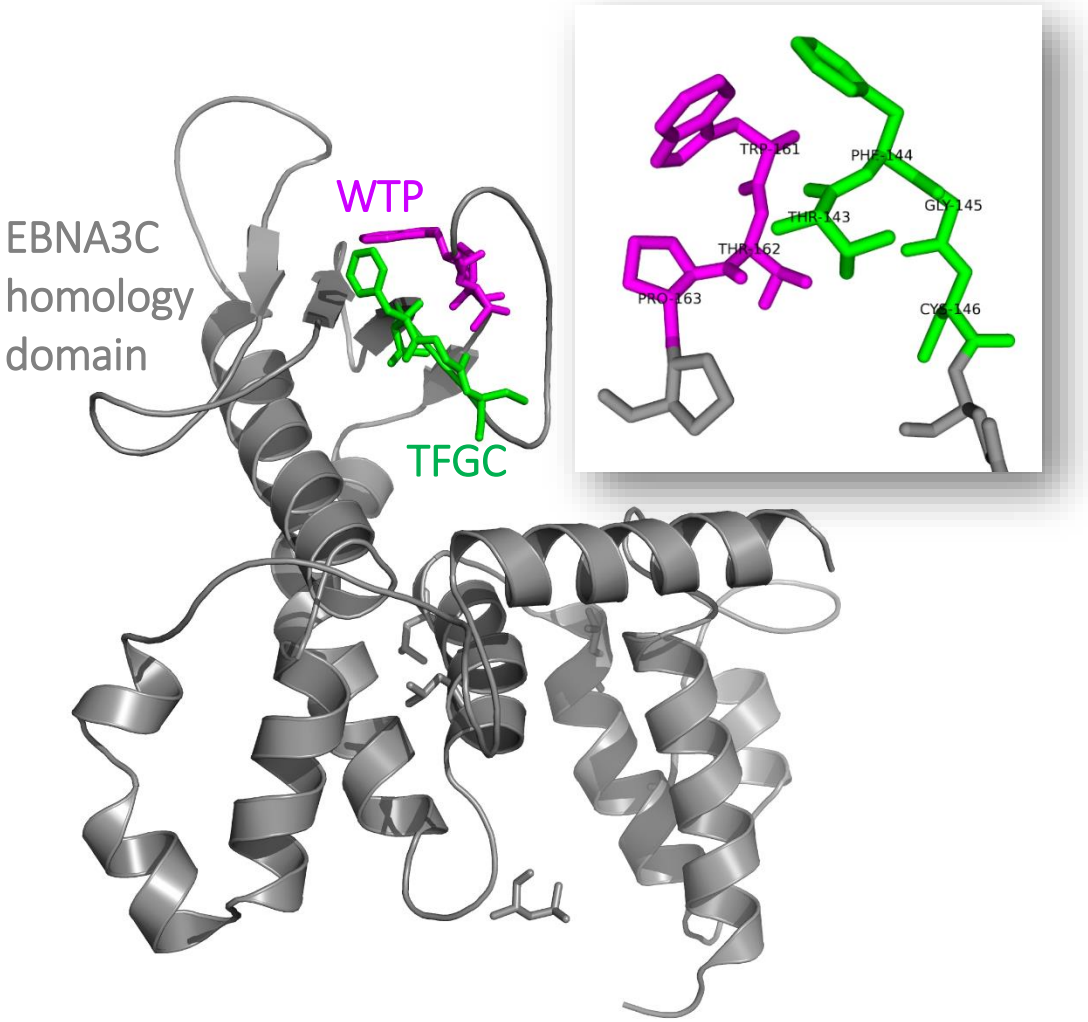


**Figure 4.2. A 3D model of the EBNA3C homology domain produced on RaptorX software.** Model was produced by Dr Rajesh Ponnusamy from Michelle West's group. Shown in grey is EBNA3C HD with the TFGC and WTP motifs shown in green pink respectively. Highlighted in the box is the TFGC and WTP EBNA3C RBP-Jκ binding motifs. In green sticks is the TFCG motif and in pink sticks if the WTP motif.

### 4.3.2 : Modelling peptides of the EBNAs binding to the Beta-trefoil domain

As we were unable to obtain structures of EBNA bound to RBP-Jκ we modelled peptides of EBNA2, EBNA3A, EBNA3B and EBNA3C on to the structure of the Lag1-Lin12 RAM-DNA complex (the worm Notch complex homologue) by mutating the residues of the lin12 RAM domain to EBNA residues using WinCoot software (Friedmann *et al.*, 2008)(Figure 4.3). We chose to use the Lag1-Lin12 RAM-DNA complex structure due to Lag-1 having a proline residue proceeding the WTP motif as the EBNAs do (Friedmann *et al.*, 2008). Whether the WTP is proceeded by a proline or not has been shown in other structures to dictate which direction the RAM domain binds to RBP-Jκ after the WΦP motif. Although the biological consequence of this has not been investigated. The tryptophan residue of the EBNA2 and EBNA3C WΦP RBP-Jκ binding motif, in the model, fits well in the a hydrophobic pocket of the BTD (Figure 4.3). This was not surprising as mutation of this tryptophan to serine ablates Notch and EBNA2 binding to RBP-Jκ (Johnson *et al.*, 2010, Calderwood *et al.*, 2011)(Figure 4.3). Even though EBNA3A lacks a WΦP RBP-Jκ binding motif we showed using ITC that FKL residues in the same position as the EBNA3C WΦP motif bound weakly to RBP-Jκ. The model of EBNA3A bound to CSL reveals that the phenylanine ring fits well into the same hydrophobic pocket the tryptophan in the WΦP motif binds (Figure 4.3). The EBNA3B Valine residue, despite being hydrophobic, does not appear to fit so tightly into the hydrophobic pocket in the BTD (Figure 4.3). This may explain why we were able to measure binding using ITC for the EBNA3A.33a-RBP-Jκ interaction but not for the EBNA3B.33a-RBP-Jκ interaction. If this interaction is shown to be biologically relevant then it may offer an explanation of the differences between each of the EBNA3s abilities to inhibit EBNA2 transactivation of RBP-Jκ mediated genes. The

evidence comparing how EBNA3s bind to RBP-Jκ is conflicting though. EBNA3A expressed in EBV infected B cells was shown to co-immunoprecipitate transfected RBP-Jκ more so than EBNA3C and EBNA3B (Robertson *et al.*, 1996a, Waltzer *et al.*, 1996). However GST-tagged EBNA3A expressed in *E.coli* pulled down RBP-Jκ less efficiently than EBNA3C (Waltzer *et al.*, 1996, Zhao *et al.*, 1996).

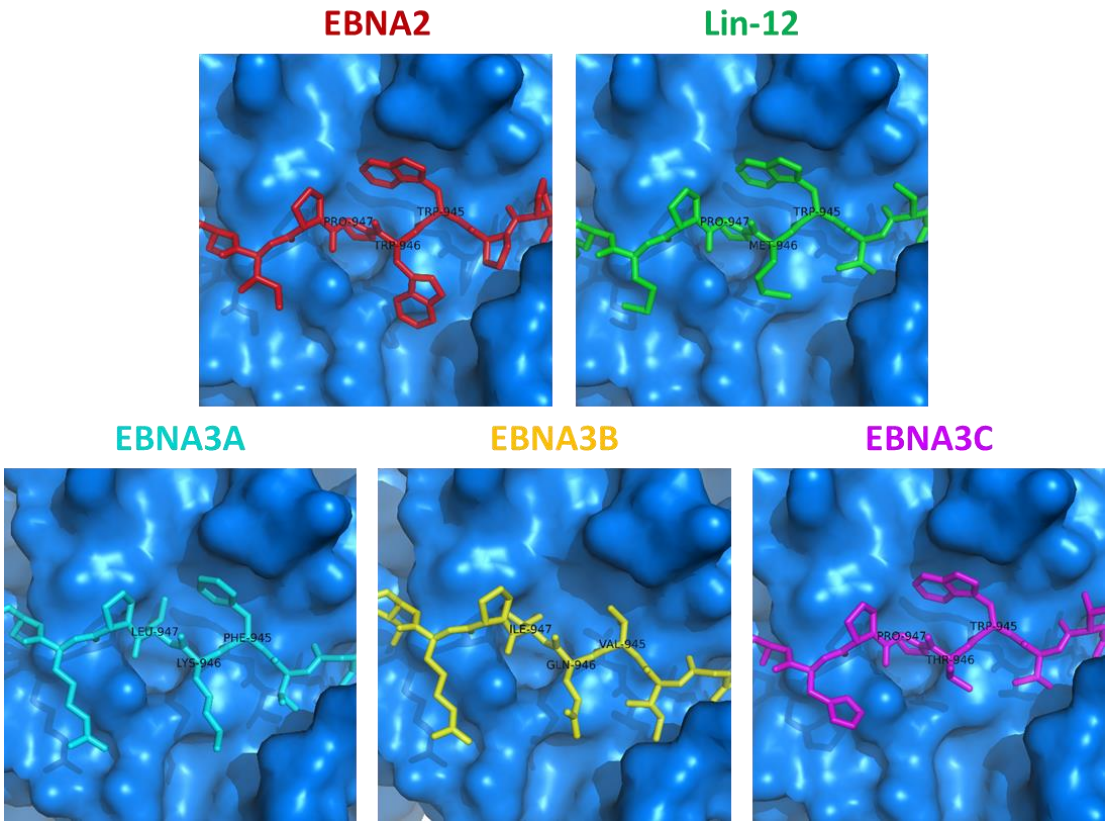


**Figure 4.3. Models of peptides of the EBNA RBP-Jκ WΦP binding motifs bound to CSL.** Models were generated by mutating the residues of the Lin-12 peptide, on Wilson et al 2007 structure of *C.Elegans* Lag-1-DNA-lin-12 structure, to residues of EBNA2, EBNA3A, EBNA3B or EBNA3C aligned to the WTP motif of Lin-12 using WinCoot software. RBP-Jκ, lin-12, EBNA2, EBNA3A, EBNA3B and EBNA3C are shown in blue, green, red, cyan, yellow and pink respectively.

### 4.3.3 : Finding potential host candidates that could facilitate indirect EBNA3C binding to RBP-Jκ.

To find potential host proteins that bridge EBNA3C and RBP-Jκ via EBNA3Cs TFGC motif ChIP-mass spectroscopy or ChroP could be used to probe latency III EBV infected cell lines such as GM1278, MutuIII or LCLs to identify chromatin interacting proteins in EBV cells. Cross-linking these cells, pulling down EBNA complexs using antibodies specific to EBNA3C and identifying the proteins bound using mass spectroscopy may identify host proteins which aid EBNA3C gene mediation and stability. In order to focus on RBP-Jκ interactions it would be useful to carry out parallel experiments using an anti-RBP-Jκ antibody to allow identification of proteins bound by both factors.

The SwitchSwense bioassay allowed us to investigate how RBP-Jκ interacts with peptides of the EBNAs containing RBP-Jκ binding motifs whilst being bound to DNA. We showed that EBNA2 peptide caused the conformation of RBP-Jκ to compact more so than Notch2 peptide. Notch Ram domain has previously been shown to be integral to Notch complex assembly as it causes conformational changes to RBP-Jκ that provide a platform for the rest of the complex to assemble upon (Friedmann *et al.*, 2008). This more compact EBNA2 induced RBP-Jκ conformation could provide a unique platform for different array host factors to bind to, to enhance EBV induced B cell immortalisation, and potentially a novel site for EBNA3C to associate with. However, this would need to be confirmed with *in vitro* assays such as the EMSA used to study the assembly of the CSL-Notch complex (Friedmann *et al.*, 2008).

### 4.3.4 : Potential mechanisms and alternative RBP-Jκ binding pockets for EBNA3C to facilitate inhibition of EBNA2 transactivation

Recent publications have shed light on how Notch signalling maybe turned off by proteins such as KyoT2 (mouse) and MINT (human) competing off Notch from RBP-Jκ via a WΦP motif (Kuroda *et al.*, 2003, VanderWielen *et al.*, 2011, Collins *et al.*, 2014). Our ITC data would suggest EBNA3A and EBNA3C may also compete with EBNA2 for RBP-Jκ binding via a WΦP/ WΦP-like motif in a similar manner to these regulators of Notch signalling. However more research needs to be carried to confirm whether EBNA3A and EBNA3C bind directly to RBP-Jκ via WΦP/ WΦP-like motifs *in vivo*.

Our ITC data also suggests that the EBNA3 TΦGC motif may require folding to interact with RBP-Jκ directly. So far no homologues of the EBNA3 TΦGC motif or the EBNA3 homology domain have been identified in humans (White *et al.*, 2010). This suggests that EBNA3s may interact with RBP-Jκ via a binding site not yet identified in mammals. Active Suppressor of hairless (Su(H)), the drosphila homologue of RBP-Jκ, is silenced by Hairless binding to a cluster of leucines which form a hydrophobic pocket in the CTD of Su(H) (Figure 4.1) (Yuan *et al.*, 2016). We had intended to investigate whether this pocket was utilised by EBNA3C to silence EBNA2 transactivation of RBP-Jκ. We designed and produced His-tagged RBP-$Jκ_{8-435}$ with alanine mutants of the CTD hairless binding pocket to use as bait to see if it was still able to pull down EBNA3C expressed in DG75 cells. However, due to time constraints we were unable to optimise this pulldown. However, this CTD hairless pocket is gaining interest as a potential therapeutic target for small molecule inhibitors to attempt to treat cancers which have deregulated Notch signalling (Yuan *et al.*, 2016).

### 4.3.5 : Connotations of TFGC-AAAA mutation not knocking out specific RBP-Jκ binding interactions to the study of EBV

The TFGC motif not contributing to direct EBNA3C-RBP-Jκ binding not only changes the model of how we think the EBNA3s interact with RBP-Jκ but potentially affects how we study EBV. The EBNA3C TFGC-AAAA mutant has often been used as a negative control for studying EBNA3-RBP-Jκ interactions *in vitro* and is increasingly being used a negative control in studies studying the global changes EBV elicits on host chromatin conformation and host gene expression. EBV research groups are using increasingly more complex techniques such as Chip-Seq, Capture Hi-C and SILAC Mass Spectroscopy to map the EBV-induced global changes to host chromatin conformation, gene expression and proteasome (McClellan *et al.*, 2013a, Ohashi *et al.*, 2015, Traylen *et al.*, 2015, Kalchschmidt *et al.*, 2016, Wood *et al.*, 2016). RBP-Jκ regulates genes, which control B cell maturation and growth making it a key target for EBV induced immortalisation of B cells and a significant area of interest to EBV researchers (Bigas *et al.*, 2010, Kalchschmidt *et al.*, 2016, Lu *et al.*, 2016). If EBNA3C$_{TFGC\text{-}AAAA}$ mutants are to be used as negative controls we need to fully understand the contributions TΦGC motif makes to EBNA3-RBP-Jκ interactions as researchers risk drawing misleading conclusions.

### 4.4 : Fluorescent Polarisation binding assay could be used to screen for inhibitors of EBNA-RBP-Jκ interactions.

Targeting the WTP binding pocket in the BTD of RBP-Jκ as a therapeutic strategy has not been pursued due to the Notch signalling pathway role in the development of many cells in the body that have a high turnover such as lymphocytes (Bigas *et al.*, 2010, Bray, 2016). However, we showed with ITC that the EBNA2 WTP motif binds to

RBP-Jκ with 10-fold weaker affinity than Notch 2 does. The FP assay, adapted to function in a drug screen machine such as a FlexStation PHERAStar FS, could be used to screen compounds that compete off the fluorescein tagged EBNA2 peptide from RBP-Jκ but do not interfere with binding between fluorescein tagged Notch peptide and RBP-Jκ. If such a compound was discovered in these screens it would at least serve as a useful tool to study how EBV infected cell lines without EBNA2 transactivated RBP-Jκ expression function, whilst avoiding the difficulties associated with inserting or deleting genes using electroporation or lentiviral techniques. In addition to this EBNA2s has a half-life of over 24 hours in immortalised B cell lines whereas Notch is turned over rapidly to tightly control notch signalling which may reduce the likelihood of an EBNA2 inhibitor interfering with Notch signalling (Grässer *et al.*, 1991, Oberg *et al.*, 2001). If compounds were considered effective at selectively inhibiting EBNA2-RBP-Jκ interactions they could be used to study EBV induced Post transplant lymphoproliferative disorder (PTLD). Patients who receive allogeneic hematopoetic stem cell transplants are at a particularly high risk of EBV associated PTLD due to their T cell count, including EBV specific T cells, being low and the high likelihood of donor cells being infected with EBV creating an environment permissive for EBV cancers to develop (Ruf *et al.*, 2011). Screening for EBV in donor stem cells and pre-emptive prescription of anti-CD23 antibodies (Rituximab) to patients with low T cell counts can greatly reduce the risk of PTLD developing (Styczynski *et al.*, 2009, Tomblyn *et al.*, 2009). In addition to this immunotherapy involving EBV specific T cells has been shown to be an effective treatment for PTLD malignancies (Heslop *et al.*, 2010). However for patients receiving cord blood transplants there is rarely more donor sample to derive EBV-specific T cells from and some patients do not respond to rituximab (Muramatsu

*et al.*, 2011, Rasche *et al.*, 2014). A small molecule inhibitor that targeted EBNA2-RBP-Jκ interactions to disrupt EBV malignancies could be used as a preventative strategy for stem cell transplant patients or potentially as a treatment for cord blood transplant patients at risk of or suffering from EBV associated PTLD.

## Bibliography


Abbot, S.D., Rowe, M., Cadwallader, K., Ricksten, A., Gordon, J., Wang, F., Rymo, L. & Rickinson, A.B. (1990) Epstein-Barr virus nuclear antigen 2 induces expression of the virus-encoded latent membrane protein. *J Virol,* Vol. 64 (5) 2126-34.

Adams, A. & Lindahl, T. (1975) Epstein-Barr virus genomes with properties of circular DNA molecules in carrier cells. *Proc Natl Acad Sci U S A,* Vol. 72 (4) 1477-81.

Adams, P.D., Afonine, P.V., Bunkoczi, G., Chen, V.B., Davis, I.W., Echols, N., Headd, J.J., Hung, L.-W., Kapral, G.J., Grosse-Kunstleve, R.W., Mccoy, A.J., Moriarty, N.W., Oeffner, R., Read, R.J., Richardson, D.C., Richardson, J.S., Terwilliger, T.C. & Zwart, P.H. (2010) PHENIX: a comprehensive Python-based system for macromolecular structure solution. *Acta Crystallographica Section D,* Vol. 66 (2) 213-221.

Akiba, S., Koriyama, C., Herrera-Goepfert, R. & Eizuru, Y. (2008) Epstein-Barr virus associated gastric carcinoma: epidemiological and clinicopathological features. *Cancer Sci,* Vol. 99 (2) 195-201.

Allday, M.J. & Crawford, D.H. (1988) Role of epithelium in EBV persistence and pathogenesis of B-cell tumours. *Lancet,* Vol. 1 (8590) 855-7.

Allday, M.J., Crawford, D.H. & Griffin, B.E. (1989) Epstein-Barr virus latent gene expression during the initiation of B cell immortalization. *J Gen Virol,* Vol. 70 ( Pt 7) 1755-64.

Allday, M.J., Crawford, D.H. & Thomas, J.A. (1993a) Epstein-Barr virus (EBV) nuclear antigen 6 induces expression of the EBV latent membrane protein and an activated phenotype in Raji cells. *J Gen Virol,* Vol. 74 ( Pt 3) 361-9.

Allday, M.J., Crawford, D.H. & Thomas, J.A. (1993b) Epstein-Barr virus (EBV) nuclear antigen 6 induces expression of the EBV latent membrane protein and an activated phenotype in Raji cells. *The Journal of general virology,* Vol. 74 ( Pt 3) 361-9.

Allday, M.J. & Farrell, P.J. (1994) Epstein-Barr virus nuclear antigen EBNA3C/6 expression maintains the level of latent membrane protein 1 in G1-arrested cells. *J Virol,* Vol. 68 (6) 3491-8.

Altmann, M. & Hammerschmidt, W. (2005) Epstein-Barr virus provides a new paradigm: a requirement for the immediate inhibition of apoptosis. *PLoS Biol,* Vol. 3 (12) e404.

Altmann, M., Pich, D., Ruiss, R., Wang, J., Sugden, B. & Hammerschmidt, W. (2006) Transcriptional activation by EBV nuclear antigen 1 is essential for the expression of EBV's transforming genes. *Proceedings of the National Academy of Sciences of the United States of America,* Vol. 103 (38) 14188-93.

Amakawa R, J.W., Ozawa K, Matsunami N, Hamaguchi Y, Matsuda F, Kawaichi M, Honjo T (1992) Human Jk recombination Signal Binding Protein Gene (IGKJRB): Comparison with its Mouse Homologue. *Genomics,* Vol. 17 301-315.

Ambinder, R.F., Shah, W.A., Rawlins, D.R., Hayward, G.S. & Hayward, S.D. (1990) Definition of the sequence requirements for binding of the EBNA-1 protein to its palindromic target sites in Epstein-Barr virus DNA. *J Virol,* Vol. 64 (5) 2369-79.

Anagnostopoulos, I., Hummel, M., Kreschel, C. & Stein, H. (1995) Morphology, immunophenotype, and distribution of latently and/or productively Epstein-Barr virus-infected cells in acute infectious mononucleosis: implications for the interindividual infection route of Epstein-Barr virus. *Blood,* Vol. 85 (3) 744-50.

Anderson, L.J. & Longnecker, R. (2008a) An auto-regulatory loop for EBV LMP2A involves activation of Notch. *Virology,* Vol. 371 (2) 257-66.

Anderson, L.J. & Longnecker, R. (2008b) EBV LMP2A provides a surrogate pre-B cell receptor signal through constitutive activation of the ERK/MAPK pathway. *J Gen Virol,* Vol. 89 (Pt 7) 1563-8.

Andersson, E.R., Sandberg, R. & Lendahl, U. (2011) Notch signaling: simplicity in design, versatility in function. *Development,* Vol. 138 (17) 3593-612.

Andersson, J. (2000) An Overview of Epstein-Barr Virus: from Discovery to Future Directions for Treatment and Prevention. *Herpes,* Vol. 7 (3) 76-82.

Ansell, S.M. (2015) Hodgkin Lymphoma: Diagnosis and Treatment. *Mayo Clin Proc,* Vol. 90 (11) 1574-83.

Ardila-Osorio, H., Clausse, B., Mishal, Z., Wiels, J., Tursz, T. & Busson, P. (1999) Evidence of LMP1-TRAF3 interactions in glycosphingolipid-rich complexes of lymphoblastoid and nasopharyngeal carcinoma cells. *Int J Cancer,* Vol. 81 (4) 645-9.

Armitage, J.O. (2010) Early-stage Hodgkin's lymphoma. *N Engl J Med,* Vol. 363 (7) 653-62.

Arnett, K.L., Hass, M., Mcarthur, D.G., Ilagan, M.X., Aster, J.C., Kopan, R. & Blacklow, S.C. (2010) Structural and mechanistic insights into cooperative assembly of dimeric Notch transcription complexes. *Nat Struct Mol Biol,* Vol. 17 (11) 1312-7.

Aster, J.C. (2014) In brief: Notch signalling in health and disease. *J Pathol,* Vol. 232 (1) 1-3.

Aw, D., Silva, A.B. & Palmer, D.B. (2007) Immunosenescence: emerging challenges for an ageing population. *Immunology,* Vol. 120 (4) 435-46.

Babcock, G.J., Decker, L.L., Freeman, R.B. & Thorley-Lawson, D.A. (1999) Epstein-barr virus-infected resting memory B cells, not proliferating lymphoblasts, accumulate in the peripheral blood of immunosuppressed patients. *J Exp Med,* Vol. 190 (4) 567-76.

Babcock, G.J., Hochberg, D. & Thorley-Lawson, A.D. (2000) The expression pattern of Epstein-Barr virus latent genes in vivo is dependent upon the differentiation stage of the infected B cell. *Immunity,* Vol. 13 (4) 497-506.

Babcock, G.J. & Thorley-Lawson, D.A. (2000) Tonsillar memory B cells, latently infected with Epstein-Barr virus, express the restricted pattern of latent genes previously found only in Epstein-Barr virus-associated tumors. *Proc Natl Acad Sci U S A,* Vol. 97 (22) 12250-5.

Baer, R., Bankier, A.T., Biggin, M.D., Deininger, P.L., Farrell, P.J., Gibson, T.J., Hatfull, G., Hudson, G.S., Satchwell, S.C. & Séguin, C. (1984) DNA sequence and expression of the B95-8 Epstein-Barr virus genome. *Nature,* Vol. 310 (5974) 207-11.

Bailey, A.M. & Posakony, J.W. (1995) Suppressor of hairless directly activates transcription of enhancer of split complex genes in response to Notch receptor activity. *Genes Dev,* Vol. 9 (21) 2609-22.

Bajaj, B.G., Murakami, M., Cai, Q., Verma, S.C., Lan, K. & Robertson, E.S. (2008) Epstein-Barr virus nuclear antigen 3C interacts with and enhances the stability of the c-Myc oncoprotein. *J Virol,* Vol. 82 (8) 4082-90.

Balfour, H.H., Dunmire, S.K. & Hogquist, K.A. (2015) Infectious mononucleosis. *Clin Transl Immunology,* Vol. 4 (2) e33.

Balfour, H.H., Odumade, O.A., Schmeling, D.O., Mullan, B.D., Ed, J.A., Knight, J.A., Vezina, H.E., Thomas, W. & Hogquist, K.A. (2013) Behavioral, virologic, and

immunologic factors associated with acquisition and severity of primary Epstein-Barr virus infection in university students. *J Infect Dis,* Vol. 207 (1) 80-8.

Baron, M. (2003) An overview of the Notch signalling pathway. *Seminars in Cell & Developmental Biology,* Vol. 14 (2) 113-119.

Barouch-Bentov, R., Che, J., Lee, C.C., Yang, Y., Herman, A., Jia, Y., Velentza, A., Watson, J., Sternberg, L., Kim, S., Ziaee, N., Miller, A., Jackson, C., Fujimoto, M., Young, M., Batalov, S., Liu, Y., Warmuth, M., Wiltshire, T., Cooke, M.P. & Sauer, K. (2009) A conserved salt bridge in the G loop of multiple protein kinases is important for catalysis and for in vivo Lyn function. *Mol Cell,* Vol. 33 (1) 43-52.

Bazot, Q., Paschos, K., Skalska, L., Kalchschmidt, J.S., Parker, G.A. & Allday, M.J. (2015) Epstein-Barr Virus Proteins EBNA3A and EBNA3C Together Induce Expression of the Oncogenic MicroRNA Cluster miR-221/miR-222 and Ablate Expression of Its Target p57KIP2. *PLoS Pathog,* Vol. 11 (7) e1005031.

Bechtel, D., Kurth, J., Unkel, C. & Küppers, R. (2005) Transformation of BCR-deficient germinal-center B cells by EBV supports a major role of the virus in the pathogenesis of Hodgkin and posttransplantation lymphomas. *Blood,* Vol. 106 (13) 4345-50.

Beltran, B.E., Castillo, J.J., Morales, D., De Mendoza, F.H., Quinones, P., Miranda, R.N., Gallo, A., Lopez-Ilasaca, M., Butera, J.N. & Sotomayor, E.M. (2011) EBV-positive diffuse large B-cell lymphoma of the elderly: a case series from Peru. *Am J Hematol,* Vol. 86 (8) 663-7.

Ben-Bassat, H., Goldblum, N., Mitrani, S., Goldblum, T., Yoffey, J.M., Cohen, M.M., Bentwich, Z., Ramot, B., Klein, E. & Klein, G. (1977) Establishment in continuous culture of a new type of lymphocyte from a "Burkitt like" malignant lymphoma (line D.G.-75). *Int J Cancer,* Vol. 19 (1) 27-33.

Benninger-Doring, G., Pepperl, S., Deml, L., Modrow, S., Wolf, H. & Jilg, W. (1999) Frequency of CD8(+) T lymphocytes specific for lytic and latent antigens of Epstein-Barr virus in healthy virus carriers. *Virology,* Vol. 264 (2) 289-97.

Bertrand, F.E., Eckfeldt, C.E., Lysholm, A.S. & Lebien, T.W. (2000) Notch-1 and Notch-2 exhibit unique patterns of expression in human B-lineage cells. *Leukemia,* Vol. 14 (12) 2095-102.

Besseyrias, V., Fiorini, E., Strobl, L.J., Zimber-Strobl, U., Dumortier, A., Koch, U., Arcangeli, M.L., Ezine, S., Macdonald, H.R. & Radtke, F. (2007) Hierarchy of Notch-Delta

interactions promoting T cell lineage commitment and maturation. *J Exp Med,* Vol. 204 (2) 331-43.

Bigas, A., Robert-Moreno, A. & Espinosa, L. (2010) The Notch pathway in the developing hematopoietic system. *Int J Dev Biol,* Vol. 54 (6-7) 1175-88.

Borggrefe, T. & Oswald, F. (2016) Setting the Stage for Notch: The Drosophila Su(H)-Hairless Repressor Complex. *PLoS Biol,* Vol. 14 (7) e1002524.

Bosch, F.X., Lorincz, A., Muñoz, N., Meijer, C.J. & Shah, K.V. (2002) The causal relation between human papillomavirus and cervical cancer. *J Clin Pathol,* Vol. 55 (4) 244-65.

Boysen, T. & Friborg, J. (2013) [Gastric carcinoma is the most frequent Epstein-Barr virus-associated malignancy]. *Ugeskr Laeger,* Vol. 175 (47A).

Brady, G., Macarthur, G.J. & Farrell, P.J. (2007) Epstein-Barr virus and Burkitt lymphoma. *J Clin Pathol,* Vol. 60 (12) 1397-402.

Bray, S.J. (2016) Notch signalling in context. *Nat Rev Mol Cell Biol,* Vol. 17 (11) 722-735.

Brooks, C.L. & Gu, W. (2011) p53 regulation by ubiquitin. *FEBS Lett,* Vol. 585 (18) 2803-9.

Brooks, L., Yao, Q.Y., Rickinson, A.B. & Young, L.S. (1992) Epstein-Barr virus latent gene transcription in nasopharyngeal carcinoma cells: coexpression of EBNA1, LMP1, and LMP2 transcripts. *J Virol,* Vol. 66 (5) 2689-97.

Buck, M., Burgess, A., Stirzaker, R., Krauer, K. & Sculley, T. (2006) Epstein-Barr virus nuclear antigen 3A contains six nuclear-localization signals. *J Gen Virol,* Vol. 87 (Pt 10) 2879-84.

Burgess, A., Buck, M., Krauer, K. & Sculley, T. (2006) Nuclear localization of the Epstein-Barr virus EBNA3B protein. *J Gen Virol,* Vol. 87 (Pt 4) 789-93.

Burkhardt, A.L., Bolen, J.B., Kieff, E. & Longnecker, R. (1992) An Epstein-Barr virus transformation-associated membrane protein interacts with src family tyrosine kinases. *J Virol,* Vol. 66 (8) 5161-7.

Burkitt, D. (1958) A sarcoma involving the jaws in African children. *Br J Surg,* Vol. 46 (197) 218-23.

Burkitt, D. (1962) A children's cancer dependent on climatic factors. *Nature,* Vol. 194 232-4.

Burns, C.E., Traver, D., Mayhall, E., Shepard, J.L. & Zon, L.I. (2005) Hematopoietic stem cell fate is established by the Notch-Runx pathway. *Genes Dev,* Vol. 19 (19) 2331-42.

Cahir-Mcfarland, E.D., Carter, K., Rosenwald, A., Giltnane, J.M., Henrickson, S.E., Staudt, L.M. & Kieff, E. (2004) Role of NF-kappa B in cell survival and transcription of latent membrane protein 1-expressing or Epstein-Barr virus latency III-infected cells. *J Virol,* Vol. 78 (8) 4108-19.

Calderwood, M.A., Lee, S., Holthaus, A.M., Blacklow, S.C., Kieff, E. & Johannsen, E. (2011) Epstein-Barr virus nuclear protein 3C binds to the N-terminal (NTD) and beta trefoil domains (BTD) of RBP/CSL; only the NTD interaction is essential for lymphoblastoid cell growth. *Virology,* Vol. 414 (1) 19-25.

Caldwell, R.G., Wilson, J.B., Anderson, S.J. & Longnecker, R. (1998) Epstein-Barr virus LMP2A drives B cell development and survival in the absence of normal B cell receptor signals. *Immunity,* Vol. 9 (3) 405-11.

Camargo, M.C., Murphy, G., Koriyama, C., Pfeiffer, R.M., Kim, W.H., Herrera-Goepfert, R., Corvalan, A.H., Carrascal, E., Abdirad, A., Anwar, M., Hao, Z., Kattoor, J., Yoshiwara-Wakabayashi, E., Eizuru, Y., Rabkin, C.S. & Akiba, S. (2011) Determinants of Epstein-Barr virus-positive gastric cancer: an international pooled analysis. *Br J Cancer,* Vol. 105 (1) 38-43.

Cancian, L., Bosshard, R., Lucchesi, W., Karstegl, C.E. & Farrell, P.J. (2011) C-terminal region of EBNA-2 determines the superior transforming ability of type 1 Epstein-Barr virus by enhanced gene regulation of LMP-1 and CXCR7. *PLoS Pathog,* Vol. 7 (7) e1002164.

Castel, D., Mourikis, P., Bartels, S.J., Brinkman, A.B., Tajbakhsh, S. & Stunnenberg, H.G. (2013) Dynamic binding of RBPJ is determined by Notch signaling status. *Genes Dev,* Vol. 27 (9) 1059-71.

Castillo, J.J., Beltran, B.E., Miranda, R.N., Paydas, S., Winer, E.S. & Butera, J.N. (2011) Epstein-barr virus-positive diffuse large B-cell lymphoma of the elderly: what we know so far. *Oncologist,* Vol. 16 (1) 87-96.

Chabot, P.R., Raiola, L., Lussier-Price, M., Morse, T., Arseneault, G., Archambault, J. & Omichinski, J.G. (2014) Structural and functional characterization of a complex

between the acidic transactivation domain of EBNA2 and the Tfb1/p62 subunit of TFIIH. *PLoS Pathog,* Vol. 10 (3) e1004042.

Chan, A.S., To, K.F., Lo, K.W., Ding, M., Li, X., Johnson, P. & Huang, D.P. (2002) Frequent chromosome 9p losses in histologically normal nasopharyngeal epithelia from southern Chinese. *Int J Cancer,* Vol. 102 (3) 300-3.

Chen, A., Divisconte, M., Jiang, X., Quink, C. & Wang, F. (2005) Epstein-Barr virus with the latent infection nuclear antigen 3B completely deleted is still competent for B-cell growth transformation in vitro. *J Virol,* Vol. 79 (7) 4506-9.

Chesnokova, L.S., Nishimura, S.L. & Hutt-Fletcher, L.M. (2009) Fusion of epithelial cells by Epstein-Barr virus proteins is triggered by binding of viral glycoproteins gHgL to integrins alphavbeta6 or alphavbeta8. *Proc Natl Acad Sci U S A,* Vol. 106 (48) 20464-9.

Choi, S.H., Wales, T.E., Nam, Y., O'donovan, D.J., Sliz, P., Engen, J.R. & Blacklow, S.C. (2012) Conformational locking upon cooperative assembly of notch transcription complexes. *Structure,* Vol. 20 (2) 340-9.

Ciofani, M. & Zúñiga-Pflücker, J.C. (2005) Notch promotes survival of pre-T cells at the beta-selection checkpoint by regulating cellular metabolism. *Nat Immunol,* Vol. 6 (9) 881-8.

Cohen, J.I. (1992) A region of herpes simplex virus VP16 can substitute for a transforming domain of Epstein-Barr virus nuclear protein 2. *Proc Natl Acad Sci U S A,* Vol. 89 (17) 8030-4.

Cohen, J.I. & Kieff, E. (1991a) An Epstein-Barr virus nuclear protein 2 domain essential for transformation is a direct transcriptional activator. *Journal of virology,* Vol. 65 (11) 5880-5.

Cohen, J.I. & Kieff, E. (1991b) An Epstein-Barr virus nuclear protein 2 domain essential for transformation is a direct transcriptional activator. *J Virol,* Vol. 65 (11) 5880-5.

Cohen, J.I., Wang, F. & Kieff, E. (1991) Epstein-Barr virus nuclear protein 2 mutations define essential domains for transformation and transactivation. *Journal of virology,* Vol. 65 (5) 2545-54.

Cohen, M., Narbaitz, M., Metrebian, F., De Matteo, E., Preciado, M.V. & Chabay, P.A. (2014) Epstein-Barr virus-positive diffuse large B-cell lymphoma association is not only restricted to elderly patients. *Int J Cancer,* Vol. 135 (12) 2816-24.

Collins, K.J., Yuan, Z. & Kovall, R.A. (2014) Structure and function of the CSL-KyoT2 corepressor complex: a negative regulator of notch signaling. *Structure,* Vol. 22 (1) 70-81.

Dai, Q., Andreu-Agullo, C., Insolera, R., Wong, L.C., Shi, S.H. & Lai, E.C. (2013) BEND6 is a nuclear antagonist of Notch signaling during self-renewal of neural stem cells. *Development,* Vol. 140 (9) 1892-902.

Delano, W.L. Pymol: An open-source molecular graphics tool. *CCP4 Newsletter On Protein Crystallography,* Vol. 40 82-92.

Devergne, O., Cahir Mcfarland, E.D., Mosialos, G., Izumi, K.M., Ware, C.F. & Kieff, E. (1998) Role of the TRAF binding site and NF-kappaB activation in Epstein-Barr virus latent membrane protein 1-induced cell gene expression. *J Virol,* Vol. 72 (10) 7900-8.

Devergne, O., Hatzivassiliou, E., Izumi, K.M., Kaye, K.M., Kleijnen, M.F., Kieff, E. & Mosialos, G. (1996) Association of TRAF1, TRAF2, and TRAF3 with an Epstein-Barr virus LMP1 domain important for B-lymphocyte transformation: role in NF-kappaB activation. *Mol Cell Biol,* Vol. 16 (12) 7098-108.

Dhar, S.K., Yoshida, K., Machida, Y., Khaira, P., Chaudhuri, B., Wohlschlegel, J.A., Leffak, M., Yates, J. & Dutta, A. (2001) Replication from oriP of Epstein-Barr virus requires human ORC and is inhibited by geminin. *Cell,* Vol. 106 (3) 287-96.

Ding, L., Li, L., Yang, J., Zhou, S., Li, W., Tang, M., Shi, Y., Yi, W. & Cao, Y. (2007) Latent membrane protein 1 encoded by Epstein-Barr virus induces telomerase activity via p16INK4A/Rb/E2F1 and JNK signaling pathways. *J Med Virol,* Vol. 79 (8) 1153-63.

E Johannsen, E.K., G Mosialos, X Tong, E Kieff and S R Grossman (1995) Epstein-Barr virus nuclear protein 2 transactivation of the latent membrane protein 1 promoter is mediated by J kappa and PU.1. *Journal of Virology,* Vol. 69 (1) 253.

Emsley, P., Lohkamp, B., Scott, W.G. & Cowtan, K. (2010) Features and development of Coot. *Acta Crystallographica Section D,* Vol. 66 (4) 486-501.

Epstein, A. (2012) Burkitt lymphoma and the discovery of Epstein-Barr virus. *Br J Haematol,* Vol. 156 (6) 777-9.

Epstein, M.A., Achong, B.G. & Barr, Y.M. (1964a) Virus Particles in Cultured Lymphoblasts from Burkitt's Lymphoma. *Lancet,* Vol. 15 702-3.

Epstein, M.A., Achong, B.G. & Barr, Y.M. (1964b) Virus Particles in Cultured Lymphoblasts from Burkitt's Lymphoma. *Lancet,* Vol. 1 (7335) 702-3.

Epstein, M.A. & Barr, Y.M. (1964) Cultivation in Vitro of Human Lymphoblasts from Burkitt's Malignant Lymphoma. *Lancet,* Vol. 41 252-3.

Epstein, M.A., Henle, G., Achong, B.G. & Barr, Y.M. (1965) Morphological and Biological Studies on a Virus in Cultured Lymphoblasts from Burkitt's Lymphoma. *J Exp Med,* Vol. 121 761-70.

Espinosa, A.B.A.L. (2012) To Be or Notch to Be. *Blood,* Vol. 119 (14) 3226-3235.

Farrell, P.J. (2001) Epstein-Barr virus. The B95-8 strain map. *Methods Mol Biol,* Vol. 174 3-12.

Fennewald, S., Van Santen, V. & Kieff, E. (1984) Nucleotide sequence of an mRNA transcribed in latent growth-transforming virus infection indicates that it may encode a membrane protein. *J Virol,* Vol. 51 (2) 411-9.

Fingeroth, J.D., Weis, J.J., Tedder, T.F., Strominger, J.L., Biro, P.A. & Fearon, D.T. (1984) Epstein-Barr virus receptor of human B lymphocytes is the C3d receptor CR2. *Proc Natl Acad Sci U S A,* Vol. 81 (14) 4510-4.

Fish, K., Chen, J. & Longnecker, R. (2014) Epstein-Barr virus latent membrane protein 2A enhances MYC-driven cell cycle progression in a mouse model of B lymphoma. *Blood,* Vol. 123 (4) 530-40.

Fortini, M.E. (2009) Notch signaling: the core pathway and its posttranslational regulation. *Dev Cell,* Vol. 16 (5) 633-47.

Frappier, L. & O'donnell, M. (1991) Overproduction, purification, and characterization of EBNA1, the origin binding protein of Epstein-Barr virus. *J Biol Chem,* Vol. 266 (12) 7819-26.

Freyer, M.W. & Lewis, E.A. (2008) Isothermal titration calorimetry: experimental design, data analysis, and probing macromolecule/ligand binding and kinetic interactions. *Methods Cell Biol,* Vol. 84 79-113.

Friberg, A., Thumann, S., Hennig, J., Zou, P., Nössner, E., Ling, P.D., Sattler, M. & Kempkes, B. (2015) The EBNA-2 N-Terminal Transactivation Domain Folds into a

Dimeric Structure Required for Target Gene Activation. *PLoS Pathog,* Vol. 11 (5) e1004910.

Friedmann, D.R. & Kovall, R.A. (2010) Thermodynamic and structural insights into CSL-DNA complexes. *Protein Sci,* Vol. 19 (1) 34-46.

Friedmann, D.R., Wilson, J.J. & Kovall, R.A. (2008) RAM-induced allostery facilitates assembly of a notch pathway active transcription complex. *J Biol Chem,* Vol. 283 (21) 14781-91.

Fruehling, S., Swart, R., Dolwick, K.M., Kremmer, E. & Longnecker, R. (1998) Tyrosine 112 of latent membrane protein 2A is essential for protein tyrosine kinase loading and regulation of Epstein-Barr virus latency. *J Virol,* Vol. 72 (10) 7796-806.

Gahn, T.A. & Sugden, B. (1995) An EBNA-1-dependent enhancer acts from a distance of 10 kilobase pairs to increase expression of the Epstein-Barr virus LMP gene. *Journal of virology,* Vol. 69 (4) 2633-6.

Gale, N.W., Dominguez, M.G., Noguera, I., Pan, L., Hughes, V., Valenzuela, D.M., Murphy, A.J., Adams, N.C., Lin, H.C., Holash, J., Thurston, G. & Yancopoulos, G.D. (2004) Haploinsufficiency of delta-like 4 ligand results in embryonic lethality due to major defects in arterial and vascular development. *Proc Natl Acad Sci U S A,* Vol. 101 (45) 15949-54.

Geimer Le Lay, A.S., Oravecz, A., Mastio, J., Jung, C., Marchal, P., Ebel, C., Dembélé, D., Jost, B., Le Gras, S., Thibault, C., Borggrefe, T., Kastner, P. & Chan, S. (2014) The tumor suppressor Ikaros shapes the repertoire of notch target genes in T cells. *Sci Signal,* Vol. 7 (317) ra28.

Gires, O., Zimber-Strobl, U., Gonnella, R., Ueffing, M., Marschall, G., Zeidler, R., Pich, D. & Hammerschmidt, W. (1997) Latent membrane protein 1 of Epstein-Barr virus mimics a constitutively active receptor molecule. *Embo J,* Vol. 16 (20) 6131-40.

Glaser, L.V., Rieger, S., Thumann, S., Beer, S., Kuklik-Roos, C., Martin, D.E., Maier, K.C., Harth-Hertle, M.L., Grüning, B., Backofen, R., Krebs, S., Blum, H., Zimmer, R., Erhard, F. & Kempkes, B. (2017) EBF1 binds to EBNA2 and promotes the assembly of EBNA2 chromatin complexes in B cells. *PLoS Pathog,* Vol. 13 (10) e1006664.

Gonçalves, P.H., Uldrick, T.S. & Yarchoan, R. (2017) HIV-associated Kaposi sarcoma and related diseases. *AIDS,* Vol. 31 (14) 1903-1916.

Gordadze, A.V., Onunwor, C.W., Peng, R., Poston, D., Kremmer, E. & Ling, P.D. (2004) EBNA2 Amino Acids 3 to 30 Are Required for Induction of LMP-1 and Immortalization Maintenance. *Journal of Virology,* Vol. 78 (8) 3919-3929.

Greenspan, J.S., Greenspan, D., Lennette, E.T., Abrams, D.I., Conant, M.A., Petersen, V. & Freese, U.K. (1985) Replication of Epstein-Barr virus within the epithelial cells of oral "hairy" leukoplakia, an AIDS-associated lesion. *N Engl J Med,* Vol. 313 (25) 1564-71.

Gregory, C.D., Rowe, M. & Rickinson, A.B. (1990) Different Epstein-Barr virus-B cell interactions in phenotypically distinct clones of a Burkitt's lymphoma cell line. *J Gen Virol,* Vol. 71 ( Pt 7) 1481-95.

Grossman, S.R., Johannsen, E., Tong, X., Yalamanchili, R. & Kieff, E. (1994a) The Epstein-Barr virus nuclear antigen 2 transactivator is directed to response elements by the J kappa recombination signal binding protein. *Proceedings of the National Academy of Sciences of the United States of America,* Vol. 91 (16) 7568-72.

Grossman, S.R., Johannsen, E., Tong, X., Yalamanchili, R. & Kieff, E. (1994b) The Epstein-Barr virus nuclear antigen 2 transactivator is directed to response elements by the J kappa recombination signal binding protein. *Proc Natl Acad Sci U S A,* Vol. 91 (16) 7568-72.

Grässer, F.A., Haiss, P., Göttel, S. & Mueller-Lantzsch, N. (1991) Biochemical characterization of Epstein-Barr virus nuclear antigen 2A. *J Virol,* Vol. 65 (7) 3779-88.

Gudgeon, N.H., Taylor, G.S., Long, H.M., Haigh, T.A. & Rickinson, A.B. (2005) Regression of Epstein-Barr virus-induced B-cell transformation in vitro involves virus-specific CD8+ T cells as the principal effectors and a novel CD4+ T-cell reactivity. *J Virol,* Vol. 79 (9) 5477-88.

Guech-Ongey, M., Simard, E.P., Anderson, W.F., Engels, E.A., Bhatia, K., Devesa, S.S. & Mbulaiteye, S.M. (2010) AIDS-related Burkitt lymphoma in the United States: what do age and CD4 lymphocyte patterns tell us about etiology and/or biology? *Blood,* Vol. 116 (25) 5600-4.

Gunnell, A., Webb, H.M., Wood, C.D., Mcclellan, M.J., Wichaidit, B., Kempkes, B., Jenner, R.G., Osborne, C., Farrell, P.J. & West, M.J. (2016) RUNX super-enhancer control through the Notch pathway by Epstein-Barr virus transcription factors regulates B cell growth. *Nucleic Acids Res,* Vol. 44 (10) 4636-50.

Gyory, I. & Minarovits, J. (2005) Epigenetic regulation of lymphoid specific gene sets. *Biochem Cell Biol,* Vol. 83 (3) 286-95.

H, H. (2005) *The early days of Epstein-Barr virus research: the Henle years In.* Vol. 200515–22 Caister Academic Press: Norfolk, England.

Hamilton-Dutoit, S.J., Raphael, M., Audouin, J., Diebold, J., Lisse, I., Pedersen, C., Oksenhendler, E., Marelle, L. & Pallesen, G. (1993) In situ demonstration of Epstein-Barr virus small RNAs (EBER 1) in acquired immunodeficiency syndrome-related lymphomas: correlation with tumor morphology and primary site. *Blood,* Vol. 82 (2) 619-24.

Harada, S. & Kieff, E. (1997a) Epstein-Barr virus nuclear protein LP stimulates EBNA-2 acidic domain-mediated transcriptional activation. *J Virol,* Vol. 71 (9) 6611-8.

Harada, S. & Kieff, E. (1997b) Epstein-Barr virus nuclear protein LP stimulates EBNA-2 acidic domain-mediated transcriptional activation. *Journal of virology,* Vol. 71 (9) 6611-8.

He, Y. & Pear, W. (2003a) Notch signalling in B cells. *Seminars in Cell & Developmental Biology,* Vol. 14 (2) 135-142.

He, Y. & Pear, W.S. (2003b) Notch signalling in B cells. *Semin Cell Dev Biol,* Vol. 14 (2) 135-42.

Henderson, S., Rowe, M., Gregory, C., Croom-Carter, D., Wang, F., Longnecker, R., Kieff, E. & Rickinson, A. (1991) Induction of bcl-2 expression by Epstein-Barr virus latent membrane protein 1 protects infected B cells from programmed cell death. *Cell,* Vol. 65 (7) 1107-15.

Henkel, T., Ling, P.D., Hayward, S.D. & Peterson, M.G. (1994) Mediation of Epstein-Barr virus EBNA2 transactivation by recombination signal-binding protein J kappa. *Science,* Vol. 265 (5168) 92-5.

Henle, G., Henle, W., Clifford, P., Diehl, V., Kafuko, G.W., Kirya, B.G., Klein, G., Morrow, R.H., Munube, G.M., Pike, P., Tukei, P.M. & Ziegler, J.L. (1969) Antibodies to Epstein-Barr virus in Burkitt's lymphoma and control groups. *J Natl Cancer Inst,* Vol. 43 (5) 1147-57.

Henle, G., Henle, W. & Diehl, V. (1968) Relation of Burkitt's tumor-associated herpes-ytpe virus to infectious mononucleosis. *Proc Natl Acad Sci U S A,* Vol. 59 (1) 94-101.

Henle, W., Henle, G., Ho, H.C., Burtin, P., Cachin, Y., Clifford, P., De Schryver, A., De-Thé, G., Diehl, V. & Klein, G. (1970) Antibodies to Epstein-Barr virus in nasopharyngeal

carcinoma, other head and neck neoplasms, and control groups. *J Natl Cancer Inst,* Vol. 44 (1) 225-31.

Hennessy, K., Fennewald, S. & Kieff, E. (1985) A third viral nuclear protein in lymphoblasts immortalized by Epstein-Barr virus. *Proc Natl Acad Sci U S A,* Vol. 82 (17) 5944-8.

Hennessy, K., Wang, F., Bushman, E.W. & Kieff, E. (1986) Definitive identification of a member of the Epstein-Barr virus nuclear protein 3 family. *Proc Natl Acad Sci U S A,* Vol. 83 (15) 5693-7.

Henning, K., (2006) Structural, biochemical and biophysical characterisation of human transcription factor RBP-Jκ Ludwig-Maximilians-Universität München

Hertle, M.L., Popp, C., Petermann, S., Maier, S., Kremmer, E., Lang, R., Mages, J. & Kempkes, B. (2009) Differential gene expression patterns of EBV infected EBNA-3A positive and negative human B lymphocytes. *PLoS Pathog,* Vol. 5 (7) e1000506.

Heslop, H.E., Slobod, K.S., Pule, M.A., Hale, G.A., Rousseau, A., Smith, C.A., Bollard, C.M., Liu, H., Wu, M.F., Rochester, R.J., Amrolia, P.J., Hurwitz, J.L., Brenner, M.K. & Rooney, C.M. (2010) Long-term outcome of EBV-specific T-cell infusions to prevent or treat EBV-related lymphoproliferative disease in transplant recipients. *Blood,* Vol. 115 (5) 925-35.

Heussinger, N., Büttner, M., Ott, G., Brachtel, E., Pilch, B.Z., Kremmer, E. & Niedobitek, G. (2004) Expression of the Epstein-Barr virus (EBV)-encoded latent membrane protein 2A (LMP2A) in EBV-associated nasopharyngeal carcinoma. *J Pathol,* Vol. 203 (2) 696-9.

Hickabottom, M., Parker, G.A., Freemont, P., Crook, T. & Allday, M.J. (2002) Two nonconsensus sites in the Epstein-Barr virus oncoprotein EBNA3A cooperate to bind the co-repressor carboxyl-terminal-binding protein (CtBP). *J Biol Chem,* Vol. 277 (49) 47197-204.

Higuchi, M., Izumi, K.M. & Kieff, E. (2001) Epstein-Barr virus latent-infection membrane proteins are palmitoylated and raft-associated: protein 1 binds to the cytoskeleton through TNF receptor cytoplasmic factors. *Proc Natl Acad Sci U S A,* Vol. 98 (8) 4675-80.

Hislop, A.D., Kuo, M., Drake-Lee, A.B., Akbar, A.N., Bergler, W., Hammerschmitt, N., Khan, N., Palendira, U., Leese, A.M., Timms, J.M., Bell, A.I., Buckley, C.D. & Rickinson, A.B. (2005) Tonsillar homing of Epstein-Barr virus-specific CD8+ T cells and the virus-host balance. *J Clin Invest,* Vol. 115 (9) 2546-55.

Hodin, T.L., Najrana, T. & Yates, J.L. (2013) Efficient replication of Epstein-Barr virus-derived plasmids requires tethering by EBNA1 to host chromosomes. *J Virol,* Vol. 87 (23) 13020-8.

Holowaty, M.N., Sheng, Y., Nguyen, T., Arrowsmith, C. & Frappier, L. (2003) Protein interaction domains of the ubiquitin-specific protease, USP7/HAUSP. *J Biol Chem,* Vol. 278 (48) 47753-61.

Hong, J.Y., Yoon, D.H., Suh, C., Huh, J., Do, I.G., Sohn, I., Jo, J., Jung, S.H., Hong, M.E., Yoon, H., Ko, Y.H., Kim, S.J. & Kim, W.S. (2015) EBV-positive diffuse large B-cell lymphoma in young adults: is this a distinct disease entity? *Ann Oncol,* Vol. 26 (3) 548-55.

Hsieh, J.J. & Hayward, S.D. (1995) Masking of the CBF1/RBPJ kappa transcriptional repression domain by Epstein-Barr virus EBNA2. *Science,* Vol. 268 (5210) 560-3.

Hsieh, J.J., Nofziger, D.E., Weinmaster, G. & Hayward, S.D. (1997) Epstein-Barr virus immortalization: Notch2 interacts with CBF1 and blocks differentiation. *J Virol,* Vol. 71 (3) 1938-45.

Huang, D.P., Ho, J.H., Chan, W.K., Lau, W.H. & Lui, M. (1989) Cytogenetics of undifferentiated nasopharyngeal carcinoma xenografts from southern Chinese. *Int J Cancer,* Vol. 43 (5) 936-9.

Huang, D.P., Ho, J.H., Saw, D. & Teoh, T.B. (1978) Carcinoma of the nasal and paranasal regions in rats fed Cantonese salted marine fish. *IARC Sci Publ,* (20) 315-28.

Hubmann, R., Schwarzmeier, J.D., Shehata, M., Hilgarth, M., Duechler, M., Dettke, M. & Berger, R. (2002) Notch2 is involved in the overexpression of CD23 in B-cell chronic lymphocytic leukemia. *Blood,* Vol. 99 (10) 3742-7.

Hudnall, S.D., Ge, Y., Wei, L., Yang, N.P., Wang, H.Q. & Chen, T. (2005) Distribution and phenotype of Epstein-Barr virus-infected cells in human pharyngeal tonsils. *Mod Pathol,* Vol. 18 (4) 519-27.

Humme, S., Reisbach, G., Feederle, R., Delecluse, H.J., Bousset, K., Hammerschmidt, W. & Schepers, A. (2003) The EBV nuclear antigen 1 (EBNA1) enhances B cell immortalization several thousandfold. *Proc Natl Acad Sci U S A,* Vol. 100 (19) 10989-94.

Huye, L.E., Ning, S., Kelliher, M. & Pagano, J.S. (2007) Interferon regulatory factor 7 is activated by a viral oncoprotein through RIP-dependent ubiquitination. *Mol Cell Biol,* Vol. 27 (8) 2910-8.

Höfelmayr, H., Strobl, L.J., Marschall, G., Bornkamm, G.W. & Zimber-Strobl, U. (2001) Activated Notch1 can transiently substitute for EBNA2 in the maintenance of proliferation of LMP1-expressing immortalized B cells. *J Virol,* Vol. 75 (5) 2033-40.

Ikeda, A., Caldwell, R.G., Longnecker, R. & Ikeda, M. (2003) Itchy, a Nedd4 ubiquitin ligase, downregulates latent membrane protein 2A activity in B-cell signaling. *J Virol,* Vol. 77 (9) 5529-34.

Imai, S., Sugiura, M., Oikawa, O., Koizumi, S., Hirao, M., Kimura, H., Hayashibara, H., Terai, N., Tsutsumi, H., Oda, T., Chiba, S. & Osato, T. (1996) Epstein-Barr virus (EBV)-carrying and -expressing T-cell lines established from severe chronic active EBV infection. *Blood,* Vol. 87 (4) 1446-57.

Inman, G.J. & Farrell, P.J. (1995) Epstein-Barr virus EBNA-LP and transcription regulation properties of pRB, p107 and p53 in transfection assays. *J Gen Virol,* Vol. 76 ( Pt 9) 2141-9.

Ito, Y., Bae, S.C. & Chuang, L.S. (2015) The RUNX family: developmental regulators in cancer. *Nat Rev Cancer,* Vol. 15 (2) 81-95.

Izumi, K.M. & Kieff, E.D. (1997) The Epstein-Barr virus oncogene product latent membrane protein 1 engages the tumor necrosis factor receptor-associated death domain protein to mediate B lymphocyte growth transformation and activate NF-kappaB. *Proc Natl Acad Sci U S A,* Vol. 94 (23) 12592-7.

Jang, M.K., Mochizuki, K., Zhou, M., Jeong, H.S., Brady, J.N. & Ozato, K. (2005) The bromodomain protein Brd4 is a positive regulatory component of P-TEFb and stimulates RNA polymerase II-dependent transcription. *Mol Cell,* Vol. 19 (4) 523-34.

Jarriault, S., Brou, C., Logeat, F., Schroeter, E.H., Kopan, R. & Israel, A. (1995) Signalling downstream of activated mammalian Notch. *Nature,* Vol. 377 (6547) 355-8.

Jha, H.C., Lu, J., Saha, A., Cai, Q., Banerjee, S., Prasad, M.A. & Robertson, E.S. (2013) EBNA3C-Mediated Regulation of Aurora Kinase B Contributes to Epstein-Barr Virus-Induced B-Cell Proliferation through Modulation of the Activities of the Retinoblastoma Protein and Apoptotic Caspases. *J Virol,* Vol. 87 (22) 12121-38.

Johannsen, E., Koh, E., Mosialos, G., Tong, X., Kieff, E. & Grossman, S.R. (1995) Epstein-Barr virus nuclear protein 2 transactivation of the latent membrane protein 1 promoter is mediated by J kappa and PU.1. *Journal of virology,* Vol. 69 (1) 253-62.

Johannsen, E., Miller, C.L., Grossman, S.R. & Kieff, E. (1996) EBNA-2 and EBNA-3C extensively and mutually exclusively associate with RBPJkappa in Epstein-Barr virus-transformed B lymphocytes. *J Virol,* Vol. 70 (6) 4179-83.

Johnson, S.E., Ilagan, M.X., Kopan, R. & Barrick, D. (2010) Thermodynamic analysis of the CSL x Notch interaction: distribution of binding energy of the Notch RAM region to the CSL beta-trefoil domain and the mode of competition with the viral transactivator EBNA2. *J Biol Chem,* Vol. 285 (9) 6681-92.

Jones, C.H., Hayward, S.D. & Rawlins, D.R. (1989) Interaction of the lymphocyte-derived Epstein-Barr virus nuclear antigen EBNA-1 with its DNA-binding sites. *J Virol,* Vol. 63 (1) 101-10.

Jones, J.F., Shurin, S., Abramowsky, C., Tubbs, R.R., Sciotto, C.G., Wahl, R., Sands, J., Gottman, D., Katz, B.Z. & Sklar, J. (1988) T-cell lymphomas containing Epstein-Barr viral DNA in patients with chronic Epstein-Barr virus infections. *N Engl J Med,* Vol. 318 (12) 733-41.

Jox, A., Zander, T., Küppers, R., Irsch, J., Kanzler, H., Kornacker, M., Bohlen, H., Diehl, V. & Wolf, J. (1999) Somatic mutations within the untranslated regions of rearranged Ig genes in a case of classical Hodgkin's disease as a potential cause for the absence of Ig in the lymphoma cells. *Blood,* Vol. 93 (11) 3964-72.

Jundt, F., Anagnostopoulos, I., Förster, R., Mathas, S., Stein, H. & Dörken, B. (2002) Activated Notch1 signaling promotes tumor cell proliferation and survival in Hodgkin and anaplastic large cell lymphoma. *Blood,* Vol. 99 (9) 3398-403.

Jung, J., Mo, J.S., Kim, M.Y., Ann, E.J., Yoon, J.H. & Park, H.S. (2011) Regulation of Notch1 signaling by Delta-like ligand 1 intracellular domain through physical interaction. *Mol Cells,* Vol. 32 (2) 161-5.

Kalchschmidt, J.S., Gillman, A.C., Paschos, K., Bazot, Q., Kempkes, B. & Allday, M.J. (2016) EBNA3C Directs Recruitment of RBPJ (CBF1) to Chromatin during the Process of Gene Repression in EBV Infected B Cells. *PLoS Pathog,* Vol. 12 (1) e1005383.

Kanemitsu, N., Isobe, Y., Masuda, A., Momose, S., Higashi, M., Tamaru, J., Sugimoto, K. & Komatsu, N. (2012) Expression of Epstein-Barr virus-encoded proteins in extranodal

NK/T-cell Lymphoma, nasal type (ENKL): differences in biologic and clinical behaviors of LMP1-positive and -negative ENKL. *Clin Cancer Res,* Vol. 18 (8) 2164-72.

Kanzler, H., Küppers, R., Hansmann, M.L. & Rajewsky, K. (1996) Hodgkin and Reed-Sternberg cells in Hodgkin's disease represent the outgrowth of a dominant tumor clone derived from (crippled) germinal center B cells. *J Exp Med,* Vol. 184 (4) 1495-505.

Kato, S., Takahashi, E., Asano, N., Tanaka, T., Megahed, N., Kinoshita, T. & Nakamura, S. (2012) Nodal cytotoxic molecule (CM)-positive Epstein-Barr virus (EBV)-associated peripheral T cell lymphoma (PTCL): a clinicopathological study of 26 cases. *Histopathology,* Vol. 61 (2) 186-99.

Katzman, R.B. & Longnecker, R. (2004) LMP2A does not require palmitoylation to localize to buoyant complexes or for function. *J Virol,* Vol. 78 (20) 10878-87.

Kenia G. Krauer, M.B.A.T.S. (1999) Characterization of the transcriptional repressor RBP in Epstein-Barr virus-transformed B cells. *Journal of Geberal Virology,* Vol. 80 3217-3226.

Kitagawa, M. (2016) Notch signalling in the nucleus: roles of Mastermind-like (MAML) transcriptional coactivators. *J Biochem,* Vol. 159 (3) 287-94.

Klaus Peter Fuchs1, G.B., Elisabeth Dumont1, Barbara Christoph1, Marc Vidal, Elisabeth Kremmer and Bettina Kempkes (2001) Mutational analysis of the J recombination signal sequence binding protein (RBP-J)/Epstein±Barr virus nuclear antigen 2 (EBNA2) and RBP-J/Notch interaction. *Journal of Biological Chemistry,* Vol. 268 4639-4646.

Knight, J.S., Lan, K., Subramanian, C. & Robertson, E.S. (2003) Epstein-Barr virus nuclear antigen 3C recruits histone deacetylase activity and associates with the corepressors mSin3A and NCoR in human B-cell lines. *Journal of virology,* Vol. 77 (7) 4261-72.

Knight, J.S. & Robertson, E.S. (2004) Epstein-Barr virus nuclear antigen 3C regulates cyclin A/p27 complexes and enhances cyclin A-dependent kinase activity. *J Virol,* Vol. 78 (4) 1981-91.

Knight, J.S., Sharma, N., Kalman, D.E. & Robertson, E.S. (2004) A cyclin-binding motif within the amino-terminal homology domain of EBNA3C binds cyclin A and modulates cyclin A-dependent kinase activity in Epstein-Barr virus-infected cells. *J Virol,* Vol. 78 (23) 12857-67.

Knight, J.S., Sharma, N. & Robertson, E.S. (2005) Epstein-Barr virus latent antigen 3C can mediate the degradation of the retinoblastoma protein through an SCF cellular ubiquitin ligase. *Proc Natl Acad Sci U S A,* Vol. 102 (51) 18562-6.

Kuppuswamy, M., Vijayalingam, S., Zhao, L.J., Zhou, Y., Subramanian, T., Ryerse, J. & Chinnadurai, G. (2008) Role of the PLDLS-binding cleft region of CtBP1 in recruitment of core and auxiliary components of the corepressor complex. *Molecular and cellular biology,* Vol. 28 (1) 269-81.

Kuroda, K., Han, H., Tani, S., Tanigaki, K., Tun, T., Furukawa, T., Taniguchi, Y., Kurooka, H., Hamada, Y., Toyokuni, S. & Honjo, T. (2003) Regulation of marginal zone B cell development by MINT, a suppressor of Notch/RBP-J signaling pathway. *Immunity,* Vol. 18 (2) 301-12.

Kurth, J., Hansmann, M.L., Rajewsky, K. & Küppers, R. (2003) Epstein-Barr virus-infected B cells expanding in germinal centers of infectious mononucleosis patients do not participate in the germinal center reaction. *Proc Natl Acad Sci U S A,* Vol. 100 (8) 4730-5.

Kurth, P., Preiss, A., Kovall, R.A. & Maier, D. (2011) Molecular analysis of the notch repressor-complex in Drosophila: characterization of potential hairless binding sites on suppressor of hairless. *PLoS One,* Vol. 6 (11) e27986.

Landais, E., Saulquin, X. & Houssaint, E. (2005) The human T cell immune response to Epstein-Barr virus. *The International journal of developmental biology,* Vol. 49 (2-3) 285-92.

Laux, G., Dugrillon, F., Eckert, C., Adam, B., Zimber-Strobl, U. & Bornkamm, G.W. (1994a) Identification and characterization of an Epstein-Barr virus nuclear antigen 2-responsive cis element in the bidirectional promoter region of latent membrane protein and terminal protein 2 genes. *Journal of virology,* Vol. 68 (11) 6947-58.

Laux, G., Dugrillon, F., Eckert, C., Adam, B., Zimber-Strobl, U. & Bornkamm, G.W. (1994b) Identification and characterization of an Epstein-Barr virus nuclear antigen 2-responsive cis element in the bidirectional promoter region of latent membrane protein and terminal protein 2 genes. *J Virol,* Vol. 68 (11) 6947-58.

Laux, G., Economou, A. & Farrell, P.J. (1989) The terminal protein gene 2 of Epstein-Barr virus is transcribed from a bidirectional latent promoter region. *J Gen Virol,* Vol. 70 ( Pt 11) 3079-84.

Laux, G., Perricaudet, M. & Farrell, P.J. (1988) A spliced Epstein-Barr virus gene expressed in immortalized lymphocytes is created by circularization of the linear viral genome. *EMBO J,* Vol. 7 (3) 769-74.

Lavallie, E.R., Diblasio, E.A., Kovacic, S., Grant, K.L., Schendel, P.F. & Mccoy, J.M. (1993) A thioredoxin gene fusion expression system that circumvents inclusion body formation in the E. coli cytoplasm. *Biotechnology (N Y),* Vol. 11 (2) 187-93.

Lavallie, E.R., Lu, Z., Diblasio-Smith, E.A., Collins-Racie, L.A. & Mccoy, J.M. (2000) Thioredoxin as a fusion partner for production of soluble recombinant proteins in Escherichia coli. *Methods Enzymol,* Vol. 326 322-40.

Le Roux, A., Berebbi, M., Moukaddem, M., Perricaudet, M. & Joab, I. (1993) Identification of a short amino acid sequence essential for efficient nuclear targeting of the Epstein-Barr virus nuclear antigen 3A. *J Virol,* Vol. 67 (3) 1716-20.

Le Roux, A., Kerdiles, B., Walls, D., Dedieu, J.F. & Perricaudet, M. (1994) The Epstein-Barr virus determined nuclear antigens EBNA-3A, -3B, and -3C repress EBNA-2-mediated transactivation of the viral terminal protein 1 gene promoter. *Virology,* Vol. 205 (2) 596-602.

Lee, M.A., Diamond, M.E. & Yates, J.L. (1999) Genetic evidence that EBNA-1 is needed for efficient, stable latent infection by Epstein-Barr virus. *J Virol,* Vol. 73 (4) 2974-82.

Lee, S., Sakakibara, S., Maruo, S., Zhao, B., Calderwood, M.A., Holthaus, A.M., Lai, C.Y., Takada, K., Kieff, E. & Johannsen, E. (2009) Epstein-Barr virus nuclear protein 3C domains necessary for lymphoblastoid cell growth: interaction with RBP-Jkappa regulates TCL1. *J Virol,* Vol. 83 (23) 12368-77.

Lee, S.P., Brooks, J.M., Al-Jarrah, H., Thomas, W.A., Haigh, T.A., Taylor, G.S., Humme, S., Schepers, A., Hammerschmidt, W., Yates, J.L., Rickinson, A.B. & Blake, N.W. (2004) CD8 T cell recognition of endogenously expressed epstein-barr virus nuclear antigen 1. *The Journal of experimental medicine,* Vol. 199 (10) 1409-20.

Lefebvre, J.S., Maue, A.C., Eaton, S.M., Lanthier, P.A., Tighe, M. & Haynes, L. (2012) The aged microenvironment contributes to the age-related functional defects of CD4 T cells in mice. *Aging Cell,* Vol. 11 (5) 732-40.

**Levine** , P.H., **Ablashi** , D.V., **Pearson** , G.R., **Kottaridis** , S.D. (1985) *Epstein-Barr Virus and Associated Diseases. Proceedings of the First International Symposium on Epstein-Barr Virus-Associated Malignant Diseases (Loutraki, Greece—September 24–28, 1984).*

Li, Q., Spriggs, M.K., Kovats, S., Turk, S.M., Comeau, M.R., Nepom, B. & Hutt-Fletcher, L.M. (1997) Epstein-Barr virus uses HLA class II as a cofactor for infection of B lymphocytes. *J Virol,* Vol. 71 (6) 4657-62.

Ling, P.D. & Hayward, S.D. (1995) Contribution of conserved amino acids in mediating the interaction between EBNA2 and CBF1/RBPJk. *J Virol,* Vol. 69 (3) 1944-50.

Ling, P.D., Hsieh, J.J., Ruf, I.K., Rawlins, D.R. & Hayward, S.D. (1994) EBNA-2 upregulation of Epstein-Barr virus latency promoters and the cellular CD23 promoter utilizes a common targeting intermediate, CBF1. *J Virol,* Vol. 68 (9) 5375-83.

Ling, P.D., Rawlins, D.R. & Hayward, S.D. (1993a) The Epstein-Barr virus immortalizing protein EBNA-2 is targeted to DNA by a cellular enhancer-binding protein. *Proc Natl Acad Sci U S A,* Vol. 90 (20) 9237-41.

Ling, P.D., Ryon, J.J. & Hayward, S.D. (1993b) EBNA-2 of herpesvirus papio diverges significantly from the type A and type B EBNA-2 proteins of Epstein-Barr virus but retains an efficient transactivation domain with a conserved hydrophobic motif. *J Virol,* Vol. 67 (6) 2990-3003.

Lo, K.W., Cheung, S.T., Leung, S.F., Van Hasselt, A., Tsang, Y.S., Mak, K.F., Chung, Y.F., Woo, J.K., Lee, J.C. & Huang, D.P. (1996) Hypermethylation of the p16 gene in nasopharyngeal carcinoma. *Cancer Res,* Vol. 56 (12) 2721-5.

Lo, K.W., Kwong, J., Hui, A.B., Chan, S.Y., To, K.F., Chan, A.S., Chow, L.S., Teo, P.M., Johnson, P.J. & Huang, D.P. (2001) High frequency of promoter hypermethylation of RASSF1A in nasopharyngeal carcinoma. *Cancer Res,* Vol. 61 (10) 3877-81.

Longnecker, R., Druker, B., Roberts, T.M. & Kieff, E. (1991) An Epstein-Barr virus protein associated with cell growth transformation interacts with a tyrosine kinase. *J Virol,* Vol. 65 (7) 3681-92.

Lu, F., Chen, H.S., Kossenkov, A.V., Dewispeleare, K., Won, K.J. & Lieberman, P.M. (2016) EBNA2 Drives Formation of New Chromosome Binding Sites and Target Genes for B-Cell Master Regulatory Transcription Factors RBP-jκ and EBF1. *PLoS Pathog,* Vol. 12 (1) e1005339.

Lu, F., Wikramasinghe, P., Norseen, J., Tsai, K., Wang, P., Showe, L., Davuluri, R.V. & Lieberman, P.M. (2010) Genome-wide analysis of host-chromosome binding sites for Epstein-Barr Virus Nuclear Antigen 1 (EBNA1). *Virol J,* Vol. 7 262.

Luftig, M., Prinarakis, E., Yasui, T., Tsichritzis, T., Cahir-Mcfarland, E., Inoue, J., Nakano, H., Mak, T.W., Yeh, W.C., Li, X., Akira, S., Suzuki, N., Suzuki, S., Mosialos, G. & Kieff, E. (2003) Epstein-Barr virus latent membrane protein 1 activation of NF-kappaB through IRAK1 and TRAF6. *Proc Natl Acad Sci U S A,* Vol. 100 (26) 15595-600.

Macarthur, G.J., Wilson, A.D., Birchall, M.A. & Morgan, A.J. (2007) Primary CD4+ T-cell responses provide both helper and cytotoxic functions during Epstein-Barr virus infection and transformation of fetal cord blood B cells. *J Virol,* Vol. 81 (9) 4766-75.

Magrath, I. (1990) The pathogenesis of Burkitt's lymphoma. *Adv Cancer Res,* Vol. 55 133-270.

Maier, D., Kurth, P., Schulz, A., Russell, A., Yuan, Z., Gruber, K., Kovall, R.A. & Preiss, A. (2011) Structural and functional analysis of the repressor complex in the Notch signaling pathway of Drosophila melanogaster. *Mol Biol Cell,* Vol. 22 (17) 3242-52.

Maier, S., Staffler, G., Hartmann, A., Hock, J., Henning, K., Grabusic, K., Mailhammer, R., Hoffmann, R., Wilmanns, M., Lang, R., Mages, J. & Kempkes, B. (2006) Cellular target genes of Epstein-Barr virus nuclear antigen 2. *J Virol,* Vol. 80 (19) 9761-71.

Maini, M.K., Gudgeon, N., Wedderburn, L.R., Rickinson, A.B. & Beverley, P.C. (2000) Clonal expansions in acute EBV infection are detectable in the CD8 and not the CD4 subset and persist with a variable CD45 phenotype. *Journal of immunology,* Vol. 165 (10) 5729-37.

Mancao, C., Altmann, M., Jungnickel, B. & Hammerschmidt, W. (2005) Rescue of "crippled" germinal center B cells from apoptosis by Epstein-Barr virus. *Blood,* Vol. 106 (13) 4339-44.

Mancao, C. & Hammerschmidt, W. (2007) Epstein-Barr virus latent membrane protein 2A is a B-cell receptor mimic and essential for B-cell survival. *Blood,* Vol. 110 (10) 3715-21.

Mann, K.P., Staunton, D. & Thorley-Lawson, D.A. (1985) Epstein-Barr virus-encoded protein found in plasma membranes of transformed cells. *J Virol,* Vol. 55 (3) 710-20.

Marafioti, T., Hummel, M., Foss, H.D., Laumen, H., Korbjuhn, P., Anagnostopoulos, I., Lammert, H., Demel, G., Theil, J., Wirth, T. & Stein, H. (2000) Hodgkin and reed-sternberg cells represent an expansion of a single clone originating from a germinal center B-cell with functional immunoglobulin gene rearrangements but defective immunoglobulin transcription. *Blood,* Vol. 95 (4) 1443-50.

Marshall, D. & Sample, C. (1995) Epstein-Barr virus nuclear antigen 3C is a transcriptional regulator. *J Virol,* Vol. 69 (6) 3624-30.

Maruo, S., Johannsen, E., Illanes, D., Cooper, A. & Kieff, E. (2003) Epstein-Barr Virus nuclear protein EBNA3A is critical for maintaining lymphoblastoid cell line growth. *J Virol,* Vol. 77 (19) 10437-47.

Maruo, S., Johannsen, E., Illanes, D., Cooper, A., Zhao, B. & Kieff, E. (2005) Epstein-Barr virus nuclear protein 3A domains essential for growth of lymphoblasts: transcriptional regulation through RBP-Jkappa/CBF1 is critical. *J Virol,* Vol. 79 (16) 10171-9.

Maruo, S., Wu, Y., Ishikawa, S., Kanda, T., Iwakiri, D. & Takada, K. (2006) Epstein-Barr virus nuclear protein EBNA3C is required for cell cycle progression and growth maintenance of lymphoblastoid cells. *Proc Natl Acad Sci U S A,* Vol. 103 (51) 19500-5.

Maruo, S., Wu, Y., Ito, T., Kanda, T., Kieff, E.D. & Takada, K. (2009) Epstein-Barr virus nuclear protein EBNA3C residues critical for maintaining lymphoblastoid cell growth. *Proc Natl Acad Sci U S A,* Vol. 106 (11) 4419-24.

Maruo, S., Zhao, B., Johannsen, E., Kieff, E., Zou, J. & Takada, K. Epstein-Barr virus nuclear antigens 3C and 3A maintain lymphoblastoid cell growth by repressing p16INK4A and p14ARF expression. *Proc Natl Acad Sci U S A,* Vol. 108 (5) 1919-24.

Maruo, S., Zhao, B., Johannsen, E., Kieff, E., Zou, J. & Takada, K. (2011) Epstein-Barr virus nuclear antigens 3C and 3A maintain lymphoblastoid cell growth by repressing p16INK4A and p14ARF expression. *Proc Natl Acad Sci U S A,* Vol. 108 (5) 1919-24.

Masashi Kawaichi, C.O., Shiro Shibayama, Antonis E. Koromilas, Norisada Matsunami, Yasushi Hamaguchi, and Tasuku Honjo (1991) Genomic organisation of Mouse RBP-Jk Recombination Signal Binding Protien (RBP-Jk) Gene. *The Journal of Biochemistry,* Vol. 267 (6) 4016-4022.

Matskova, L., Ernberg, I., Pawson, T. & Winberg, G. (2001) C-terminal domain of the Epstein-Barr virus LMP2A membrane protein contains a clustering signal. *J Virol,* Vol. 75 (22) 10941-9.

Mccann, E.M., Kelly, G.L., Rickinson, A.B. & Bell, A.I. (2001) Genetic analysis of the Epstein-Barr virus-coded leader protein EBNA-LP as a co-activator of EBNA2 function. *J Gen Virol,* Vol. 82 (Pt 12) 3067-79.

Mcclellan, M.J., Khasnis, S., Wood, C.D., Palermo, R.D., Schlick, S.N., Kanhere, A.S., Jenner, R.G. & West, M.J. (2012) Downregulation of integrin receptor-signaling genes

by Epstein-Barr virus EBNA 3C via promoter-proximal and -distal binding elements. *J Virol,* Vol. 86 (9) 5165-78.

Mcclellan, M.J., Wood, C.D., Ojeniyi, O., Cooper, T.J., Kanhere, A., Arvey, A., Webb, H.M., Palermo, R.D., Harth-Hertle, M.L., Kempkes, B., Jenner, R.G. & West, M.J. (2013a) Modulation of enhancer looping and differential gene targeting by Epstein-Barr virus transcription factors directs cellular reprogramming. *PLoS Pathog,* Vol. 9 (9) e1003636.

Mcclellan, M.J., Wood, C.D., Ojeniyi, O., Cooper, T.J., Kanhere, A., Arvey, A., Webb, H.M., Palermo, R.D., Harth-Hertle, M.L., Kempkes, B., Jenner, R.G. & West, M.J. (2013b) Modulation of enhancer looping and differential gene targeting by Epstein-Barr virus transcription factors directs cellular reprogramming. *PLoS pathogens,* Vol. 9 (9) e1003636.

Mccoy, A.J., Grosse-Kunstleve, R.W., Adams, P.D., Winn, M.D., Storoni, L.C. & Read, R.J. (2007) Phaser crystallographic software. *Journal of Applied Crystallography,* Vol. 40 (4) 658-674.

Mciver, Z., Stephens, N., Grim, A. & Barrett, A.J. (2010) Rituximab administration within 6 months of T cell-depleted allogeneic SCT is associated with prolonged life-threatening cytopenias. *Biol Blood Marrow Transplant,* Vol. 16 (11) 1549-56.

Meier-Stiegen, F., Schwanbeck, R., Bernoth, K., Martini, S., Hieronymus, T., Ruau, D., Zenke, M. & Just, U. (2010) Activated Notch1 target genes during embryonic cell differentiation depend on the cellular context and include lineage determinants and inhibitors. *PLoS One,* Vol. 5 (7) e11481.

Menezes, J., Leibold, W., Klein, G. & Clements, G. (1975) Establishment and characterization of an Epstein-Barr virus (EBC)-negative lymphoblastoid B cell line (BJA-B) from an exceptional, EBV-genome-negative African Burkitt's lymphoma. *Biomedicine,* Vol. 22 (4) 276-84.

Miyashita, E.M., Yang, B., Babcock, G.J. & Thorley-Lawson, D.A. (1997) Identification of the site of Epstein-Barr virus persistence in vivo as a resting B cell. *J Virol,* Vol. 71 (7) 4882-91.

Moghaddam, A., Rosenzweig, M., Lee-Parritz, D., Annis, B., Johnson, R.P. & Wang, F. (1997) An animal model for acute and persistent Epstein-Barr virus infection. *Science,* Vol. 276 (5321) 2030-3.

Montes-Moreno, S., Odqvist, L., Diaz-Perez, J.A., Lopez, A.B., De Villambrosía, S.G., Mazorra, F., Castillo, M.E., Lopez, M., Pajares, R., García, J.F., Mollejo, M., Camacho,

F.I., Ruiz-Marcellán, C., Adrados, M., Ortiz, N., Franco, R., Ortiz-Hidalgo, C., Suarez-Gauthier, A., Young, K.H. & Piris, M.A. (2012) EBV-positive diffuse large B-cell lymphoma of the elderly is an aggressive post-germinal center B-cell neoplasm characterized by prominent nuclear factor-kB activation. *Mod Pathol,* Vol. 25 (7) 968-82.

Morton, L.M., Wang, S.S., Devesa, S.S., Hartge, P., Weisenburger, D.D. & Linet, M.S. (2006) Lymphoma incidence patterns by WHO subtype in the United States, 1992-2001. *Blood,* Vol. 107 (1) 265-76.

Mosialos, G., Birkenbach, M., Yalamanchili, R., Vanarsdale, T., Ware, C. & Kieff, E. (1995) The Epstein-Barr virus transforming protein LMP1 engages signaling proteins for the tumor necrosis factor receptor family. *Cell,* Vol. 80 (3) 389-99.

Muramatsu, H., Takahashi, Y., Shimoyama, Y., Doisaki, S., Nishio, N., Ito, Y., Hama, A., Shimada, A., Yagasaki, H., Ito, M. & Kojima, S. (2011) CD20-negative Epstein-Barr virus-associated post-transplant lymphoproliferative disease refractory to rituximab in a patient with severe aplastic anemia. *Int J Hematol,* Vol. 93 (6) 779-81.

Murray, R.J., Kurilla, M.G., Brooks, J.M., Thomas, W.A., Rowe, M., Kieff, E. & Rickinson, A.B. (1992) Identification of target antigens for the human cytotoxic T cell response to Epstein-Barr virus (EBV): implications for the immune control of EBV-positive malignancies. *J Exp Med,* Vol. 176 (1) 157-68.

Nakagawa, M., Ichikawa, M., Kumano, K., Goyama, S., Kawazu, M., Asai, T., Ogawa, S., Kurokawa, M. & Chiba, S. (2006) AML1/Runx1 rescues Notch1-null mutation-induced deficiency of para-aortic splanchnopleural hematopoiesis. *Blood,* Vol. 108 (10) 3329-34.

Nakayama, T., Fujisawa, R., Izawa, D., Hieshima, K., Takada, K. & Yoshie, O. (2002) Human B cells immortalized with Epstein-Barr virus upregulate CCR6 and CCR10 and downregulate CXCR4 and CXCR5. *J Virol,* Vol. 76 (6) 3072-7.

Nallamsetty, S. & Waugh, D.S. (2006) Solubility-enhancing proteins MBP and NusA play a passive role in the folding of their fusion partners. *Protein Expr Purif,* Vol. 45 (1) 175-82.

Nam, Y., Aster, J.C. & Blacklow, S.C. (2002) Notch signaling as a therapeutic target. *Curr Opin Chem Biol,* Vol. 6 (4) 501-9.

Nam, Y., Sliz, P., Song, L., Aster, J.C. & Blacklow, S.C. (2006) Structural basis for cooperativity in recruitment of MAML coactivators to Notch transcription complexes. *Cell,* Vol. 124 (5) 973-83.

Nam, Y., Weng, A.P., Aster, J.C. & Blacklow, S.C. (2003) Structural requirements for assembly of the CSL.intracellular Notch1.Mastermind-like 1 transcriptional activation complex. *J Biol Chem,* Vol. 278 (23) 21232-9.

Nanbo, A. & Takada, K. (2002) The role of Epstein-Barr virus-encoded small RNAs (EBERs) in oncogenesis. *Rev Med Virol,* Vol. 12 (5) 321-6.

Nanbo, A., Yoshiyama, H. & Takada, K. (2005) Epstein-Barr virus-encoded poly(A)- RNA confers resistance to apoptosis mediated through Fas by blocking the PKR pathway in human epithelial intestine 407 cells. *J Virol,* Vol. 79 (19) 12280-5.

Nemerow, G.R., Mold, C., Schwend, V.K., Tollefson, V. & Cooper, N.R. (1987) Identification of gp350 as the viral glycoprotein mediating attachment of Epstein-Barr virus (EBV) to the EBV/C3d receptor of B cells: sequence homology of gp350 and C3 complement fragment C3d. *J Virol,* Vol. 61 (5) 1416-20.

Nguyen-Van, D., Keane, C., Han, E., Jones, K., Nourse, J.P., Vari, F., Ross, N., Crooks, P., Ramuz, O., Green, M., Griffith, L., Trappe, R., Grigg, A., Mollee, P. & Gandhi, M.K. (2011) Epstein-Barr virus-positive diffuse large B-cell lymphoma of the elderly expresses EBNA3A with conserved CD8 T-cell epitopes. *Am J Blood Res,* Vol. 1 (2) 146-59.

Niederman, J.C., Miller, G., Pearson, H.A., Pagano, J.S. & Dowaliby, J.M. (1976) Infectious mononucleosis. Epstein-Barr-virus shedding in saliva and the oropharynx. *N Engl J Med,* Vol. 294 (25) 1355-9.

Niedobitek, G., Agathanggelou, A., Herbst, H., Whitehead, L., Wright, D.H. & Young, L.S. (1997) Epstein-Barr virus (EBV) infection in infectious mononucleosis: virus latency, replication and phenotype of EBV-infected cells. *J Pathol,* Vol. 182 (2) 151-9.

Nikiforow, S., Bottomly, K. & Miller, G. (2001) CD4+ T-cell effectors inhibit Epstein-Barr virus-induced B-cell proliferation. *J Virol,* Vol. 75 (8) 3740-52.

Nitsche, F., Bell, A. & Rickinson, A. (1997) Epstein-Barr virus leader protein enhances EBNA-2-mediated transactivation of latent membrane protein 1 expression: a role for the W1W2 repeat domain. *J Virol,* Vol. 71 (9) 6619-28.

Nonkwelo, C., Skinner, J., Bell, A., Rickinson, A. & Sample, J. (1996) Transcription start sites downstream of the Epstein-Barr virus (EBV) Fp promoter in early-passage Burkitt lymphoma cells define a fourth promoter for expression of the EBV EBNA-1 protein. *J Virol,* Vol. 70 (1) 623-7.

Oberg, C., Li, J., Pauley, A., Wolf, E., Gurney, M. & Lendahl, U. (2001) The Notch intracellular domain is ubiquitinated and negatively regulated by the mammalian Sel-10 homolog. *J Biol Chem,* Vol. 276 (38) 35847-53.

Oh, S.T., Seo, J.S., Moon, U.Y., Kang, K.H., Shin, D.J., Yoon, S.K., Kim, W.H., Park, J.G. & Lee, S.K. (2004) A naturally derived gastric cancer cell line shows latency I Epstein-Barr virus infection closely resembling EBV-associated gastric cancer. *Virology,* Vol. 320 (2) 330-6.

Ohashi, M., Holthaus, A.M., Calderwood, M.A., Lai, C.Y., Krastins, B., Sarracino, D. & Johannsen, E. (2015) The EBNA3 family of Epstein-Barr virus nuclear proteins associates with the USP46/USP12 deubiquitination complexes to regulate lymphoblastoid cell line growth. *PLoS Pathog,* Vol. 11 (4) e1004822.

Ok, C.Y., Li, L., Xu-Monette, Z.Y., Visco, C., Tzankov, A., Manyam, G.C., Montes-Moreno, S., Dybkaer, K., Dybaer, K., Chiu, A., Orazi, A., Zu, Y., Bhagat, G., Chen, J., Richards, K.L., Hsi, E.D., Choi, W.W., Van Krieken, J.H., Huh, J., Ai, W., Ponzoni, M., Ferreri, A.J., Farnen, J.P., Møller, M.B., Bueso-Ramos, C.E., Miranda, R.N., Winter, J.N., Piris, M.A., Medeiros, L.J. & Young, K.H. (2014) Prevalence and clinical implications of epstein-barr virus infection in de novo diffuse large B-cell lymphoma in Western countries. *Clin Cancer Res,* Vol. 20 (9) 2338-49.

Ok, C.Y., Papathomas, T.G., Medeiros, L.J. & Young, K.H. (2013) EBV-positive diffuse large B-cell lymphoma of the elderly. *Blood,* Vol. 122 (3) 328-40.

Ong, C.T., Cheng, H.T., Chang, L.W., Ohtsuka, T., Kageyama, R., Stormo, G.D. & Kopan, R. (2006) Target selectivity of vertebrate notch proteins. Collaboration between discrete domains and CSL-binding site architecture determines activation probability. *J Biol Chem,* Vol. 281 (8) 5106-19.

Oswald, F., Kostezka, U., Astrahantseff, K., Bourteele, S., Dillinger, K., Zechner, U., Ludwig, L., Wilda, M., Hameister, H., Knöchel, W., Liptay, S. & Schmid, R.M. (2002) SHARP is a novel component of the Notch/RBP-Jkappa signalling pathway. *EMBO J,* Vol. 21 (20) 5417-26.

Oswald, F., Täuber, B., Dobner, T., Bourteele, S., Kostezka, U., Adler, G., Liptay, S. & Schmid, R.M. (2001) p300 acts as a transcriptional coactivator for mammalian Notch-1. *Mol Cell Biol,* Vol. 21 (22) 7761-74.

Oswald, F., Winkler, M., Cao, Y., Astrahantseff, K., Bourteele, S., Knöchel, W. & Borggrefe, T. (2005) RBP-Jkappa/SHARP recruits CtIP/CtBP corepressors to silence Notch target genes. *Mol Cell Biol,* Vol. 25 (23) 10379-90.

Oyama, T., Yamamoto, K., Asano, N., Oshiro, A., Suzuki, R., Kagami, Y., Morishima, Y., Takeuchi, K., Izumo, T., Mori, S., Ohshima, K., Suzumiya, J., Nakamura, N., Abe, M., Ichimura, K., Sato, Y., Yoshino, T., Naoe, T., Shimoyama, Y., Kamiya, Y., Kinoshita, T. & Nakamura, S. (2007) Age-related EBV-associated B-cell lymphoproliferative disorders constitute a distinct clinicopathologic group: a study of 96 patients. *Clin Cancer Res,* Vol. 13 (17) 5124-32.

Pajic, A., Staege, M.S., Dudziak, D., Schuhmacher, M., Spitkovsky, D., Eissner, G., Brielmeier, M., Polack, A. & Bornkamm, G.W. (2001) Antagonistic effects of c-myc and Epstein-Barr virus latent genes on the phenotype of human B cells. *Int J Cancer,* Vol. 93 (6) 810-6.

Palermo, R.D., Webb, H.M. & West, M.J. (2011) RNA polymerase II stalling promotes nucleosome occlusion and pTEFb recruitment to drive immortalization by Epstein-Barr virus. *PLoS Pathog,* Vol. 7 (10) e1002334.

Park, S., Lee, J., Ko, Y.H., Han, A., Jun, H.J., Lee, S.C., Hwang, I.G., Park, Y.H., Ahn, J.S., Jung, C.W., Kim, K., Ahn, Y.C., Kang, W.K., Park, K. & Kim, W.S. (2007) The impact of Epstein-Barr virus status on clinical outcome in diffuse large B-cell lymphoma. *Blood,* Vol. 110 (3) 972-8.

Parkin, D.M., Stiller, C.A., Draper, G.J. & Bieber, C.A. (1988) The international incidence of childhood cancer. *Int J Cancer,* Vol. 42 (4) 511-20.

Paschos, K., Parker, G.A., Watanatanasup, E., White, R.E. & Allday, M.J. (2012) BIM promoter directly targeted by EBNA3C in polycomb-mediated repression by EBV. *Nucleic Acids Res,* Vol. 40 (15) 7233-46.

Paschos, K., Smith, P., Anderton, E., Middeldorp, J.M., White, R.E. & Allday, M.J. (2009) Epstein-barr virus latency in B cells leads to epigenetic repression and CpG methylation of the tumour suppressor gene Bim. *PLoS Pathog,* Vol. 5 (6) e1000492.

Paulin, F.E., West, M.J., Sullivan, N.F., Whitney, R.L., Lyne, L. & Willis, A.E. (1996) Aberrant translational control of the c-myc gene in multiple myeloma. *Oncogene,* Vol. 13 (3) 505-13.

Pegtel, D.M., Subramanian, A., Sheen, T.S., Tsai, C.H., Golub, T.R. & Thorley-Lawson, D.A. (2005) Epstein-Barr-Virus-Encoded LMP2A Induces Primary Epithelial Cell Migration and Invasion: Possible Role in Nasopharyngeal Carcinoma Metastasis. *J Virol,* Vol. 79 (24) 15430-42.

Peng, R., Tan, J. & Ling, P.D. (2000) Conserved regions in the Epstein-Barr virus leader protein define distinct domains required for nuclear localization and transcriptional cooperation with EBNA2. *J Virol,* Vol. 74 (21) 9953-63.

Petti, L. & Kieff, E. (1988) A sixth Epstein-Barr virus nuclear protein (EBNA3B) is expressed in latently infected growth-transformed lymphocytes. *J Virol,* Vol. 62 (6) 2173-8.

Petti, L., Sample, J., Wang, F. & Kieff, E. (1988) A fifth Epstein-Barr virus nuclear protein (EBNA3C) is expressed in latently infected growth-transformed lymphocytes. *J Virol,* Vol. 62 (4) 1330-8.

Pope, J.H., Horne, M.K. & Scott, W. (1968) Transformation of foetal human keukocytes in vitro by filtrates of a human leukaemic cell line containing herpes-like virus. *Int J Cancer,* Vol. 3 (6) 857-66.

Portal, D., Rosendorff, A. & Kieff, E. (2006) Epstein-Barr nuclear antigen leader protein coactivates transcription through interaction with histone deacetylase 4. *Proc Natl Acad Sci U S A,* Vol. 103 (51) 19278-83.

Portal, D., Zhou, H., Zhao, B., Kharchenko, P.V., Lowry, E., Wong, L., Quackenbush, J., Holloway, D., Jiang, S., Lu, Y. & Kieff, E. (2013) Epstein-Barr virus nuclear antigen leader protein localizes to promoters and enhancers with cell transcription factors and EBNA2. *Proc Natl Acad Sci U S A,* Vol. 110 (46) 18537-42.

Portis, T. & Longnecker, R. (2004) Epstein-Barr virus (EBV) LMP2A mediates B-lymphocyte survival through constitutive activation of the Ras/PI3K/Akt pathway. *Oncogene,* Vol. 23 (53) 8619-28.

Precopio, M.L., Sullivan, J.L., Willard, C., Somasundaran, M. & Luzuriaga, K. (2003) Differential kinetics and specificity of EBV-specific CD4+ and CD8+ T cells during primary infection. *Journal of immunology,* Vol. 170 (5) 2590-8.

Radkov, S.A., Touitou, R., Brehm, A., Rowe, M., West, M., Kouzarides, T. & Allday, M.J. (1999) Epstein-Barr virus nuclear antigen 3C interacts with histone deacetylase to repress transcription. *J Virol,* Vol. 73 (7) 5688-97.

Randahl, H., Fåhraeus, R. & Klein, G. (1992) Biochemical characterization of Epstein-Barr virus nuclear antigen 2A and an associated ATPase activity. *Eur J Biochem,* Vol. 207 (1) 55-9.

Rasche, L., Kapp, M., Einsele, H. & Mielke, S. (2014) EBV-induced post transplant lymphoproliferative disorders: a persisting challenge in allogeneic hematopoetic SCT. *Bone Marrow Transplant,* Vol. 49 (2) 163-7.

Rawlins, D.R., Milman, G., Hayward, S.D. & Hayward, G.S. (1985) Sequence-specific DNA binding of the Epstein-Barr virus nuclear antigen (EBNA-1) to clustered sites in the plasmid maintenance region. *Cell,* Vol. 42 (3) 859-68.

Reedman, B.M. & Klein, G. (1973) Cellular localization of an Epstein-Barr virus (EBV)-associated complement-fixing antigen in producer and non-producer lymphoblastoid cell lines. *Int J Cancer,* Vol. 11 (3) 499-520.

Robertson, E.S., Lin, J. & Kieff, E. (1996a) The amino-terminal domains of Epstein-Barr virus nuclear proteins 3A, 3B, and 3C interact with RBPJ(kappa). *J Virol,* Vol. 70 (5) 3068-74.

Robertson, E.S., Lin, J. & Kieff, E. (1996b) The amino-terminal domains of Epstein-Barr virus nuclear proteins 3A, 3B, and 3C interact with RBPJ(kappa). *Journal of virology,* Vol. 70 (5) 3068-74.

Rowe, D.T., Hall, L., Joab, I. & Laux, G. (1990) Identification of the Epstein-Barr virus terminal protein gene products in latently infected lymphocytes. *J Virol,* Vol. 64 (6) 2866-75.

Rowe, M., Finke, J., Szigeti, R. & Klein, G. (1988) Characterization of the serological response in man to the latent membrane protein and the six nuclear antigens encoded by Epstein-Barr virus. *J Gen Virol,* Vol. 69 ( Pt 6) 1217-28.

Rowe, M., Raithatha, S. & Shannon-Lowe, C. (2014) Counteracting effects of cellular Notch and Epstein-Barr virus EBNA2: implications for stromal effects on virus-host interactions. *J Virol,* Vol. 88 (20) 12065-76.

Ruf, S., Moser, O., Wössmann, W., Kreyenberg, H. & Wagner, H.J. (2011) Examining the origin of posttransplant lymphoproliferative disorder in a patient after a second allogeneic hematopoeitic stem cell transplantation for relapsed BCR-ABL positive acute lymphoblastic leukemia. *J Pediatr Hematol Oncol,* Vol. 33 (1) 50-4.

Rymo, L. (1995) Domains of the Epstein-Barr virus nuclear antigen 2 (EBNA2) involved in the transactivation of the latent membrane protein 1 and the EBNA Cp promoters. *Journal of General Virology,* Vol. 76 2669-2678.

Saha, A., Halder, S., Upadhyay, S.K., Lu, J., Kumar, P., Murakami, M., Cai, Q. & Robertson, E.S. (2011) Epstein-Barr virus nuclear antigen 3C facilitates G1-S transition by stabilizing and enhancing the function of cyclin D1. *PLoS Pathog,* Vol. 7 (2) e1001275.

Saito, T., Chiba, S., Ichikawa, M., Kunisato, A., Asai, T., Shimizu, K., Yamaguchi, T., Yamamoto, G., Seo, S., Kumano, K., Nakagami-Yamaguchi, E., Hamada, Y., Aizawa, S. & Hirai, H. (2003) Notch2 is preferentially expressed in mature B cells and indispensable for marginal zone B lineage development. *Immunity,* Vol. 18 (5) 675-85.

Sample, C. & Parker, B. (1994) Biochemical characterization of Epstein-Barr virus nuclear antigen 3A and 3C proteins. *Virology,* Vol. 205 (2) 534-9.

Sample, J., Liebowitz, D. & Kieff, E. (1989) Two related Epstein-Barr virus membrane proteins are encoded by separate genes. *J Virol,* Vol. 63 (2) 933-7.

Santos, M.A., Sarmento, L.M., Rebelo, M., Doce, A.A., Maillard, I., Dumortier, A., Neves, H., Radtke, F., Pear, W.S., Parreira, L. & Demengeot, J. (2007) Notch1 engagement by Delta-like-1 promotes differentiation of B lymphocytes to antibody-secreting cells. *Proc Natl Acad Sci U S A,* Vol. 104 (39) 15454-9.

Saridakis, V., Sheng, Y., Sarkari, F., Holowaty, M.N., Shire, K., Nguyen, T., Zhang, R.G., Liao, J., Lee, W., Edwards, A.M., Arrowsmith, C.H. & Frappier, L. (2005) Structure of the p53 binding domain of HAUSP/USP7 bound to Epstein-Barr nuclear antigen 1 implications for EBV-mediated immortalization. *Mol Cell,* Vol. 18 (1) 25-36.

Schepers, A., Ritzi, M., Bousset, K., Kremmer, E., Yates, J.L., Harwood, J., Diffley, J.F. & Hammerschmidt, W. (2001) Human origin recognition complex binds to the region of the latent origin of DNA replication of Epstein-Barr virus. *EMBO J,* Vol. 20 (16) 4588-602.

Schmitz, R., Stanelle, J., Hansmann, M.L. & Küppers, R. (2009) Pathogenesis of classical and lymphocyte-predominant Hodgkin lymphoma. *Annu Rev Pathol,* Vol. 4 151-74.

Schroeter, E.H., Kisslinger, J.A. & Kopan, R. (1998) Notch-1 signalling requires ligand-induced proteolytic release of intracellular domain. *Nature,* Vol. 393 (6683) 382-6.

Schultheiss, U., Püschner, S., Kremmer, E., Mak, T.W., Engelmann, H., Hammerschmidt, W. & Kieser, A. (2001) TRAF6 is a critical mediator of signal transduction by the viral oncogene latent membrane protein 1. *EMBO J,* Vol. 20 (20) 5678-91.

Shah, W.A., Ambinder, R.F., Hayward, G.S. & Hayward, S.D. (1992) Binding of EBNA-1 to DNA creates a protease-resistant domain that encompasses the DNA recognition and dimerization functions. *J Virol,* Vol. 66 (6) 3355-62.

Shair, K.H., Bendt, K.M., Edwards, R.H., Bedford, E.C., Nielsen, J.N. & Raab-Traub, N. (2007) EBV latent membrane protein 1 activates Akt, NFkappaB, and Stat3 in B cell lymphomas. *PLoS Pathog,* Vol. 3 (11) e166.

Shair, K.H., Bendt, K.M., Edwards, R.H., Nielsen, J.N., Moore, D.T. & Raab-Traub, N. (2012) Epstein-Barr virus-encoded latent membrane protein 1 (LMP1) and LMP2A function cooperatively to promote carcinoma development in a mouse carcinogenesis model. *J Virol,* Vol. 86 (9) 5352-65.

Sherry, K.P., Johnson, S.E., Hatem, C.L., Majumdar, A. & Barrick, D. (2015) Effects of Linker Length and Transient Secondary Structure Elements in the Intrinsically Disordered Notch RAM Region on Notch Signaling. *J Mol Biol,* Vol. 427 (22) 3587-3597.

Shi, W., Bastianutto, C., Li, A., Perez-Ordonez, B., Ng, R., Chow, K.Y., Zhang, W., Jurisica, I., Lo, K.W., Bayley, A., Kim, J., O'sullivan, B., Siu, L., Chen, E. & Liu, F.F. (2006) Multiple dysregulated pathways in nasopharyngeal carcinoma revealed by gene expression profiling. *Int J Cancer,* Vol. 119 (10) 2467-75.

Shibata, D. & Weiss, L.M. (1992) Epstein-Barr virus-associated gastric adenocarcinoma. *Am J Pathol,* Vol. 140 (4) 769-74.

Sifang Zhou, M.F., James J.-D. Hsieh, Lin Chen and S. Diane Hayward (2000) A Role for SKIP in EBNA2 Activation of CBF1-Repressed Promoters. *Journal of Virology,* Vol. 74 (4) 1939-1947.

Sinclair, A.J., Palmero, I., Peters, G. & Farrell, P.J. (1994) EBNA-2 and EBNA-LP cooperate to cause G0 to G1 transition during immortalization of resting human B lymphocytes by Epstein-Barr virus. *EMBO J,* Vol. 13 (14) 3321-8.

Sixbey, J.W., Nedrud, J.G., Raab-Traub, N., Hanes, R.A. & Pagano, J.S. (1984) Epstein-Barr virus replication in oropharyngeal epithelial cells. *N Engl J Med,* Vol. 310 (19) 1225-30.

Sixbey, J.W. & Pagano, J.S. (1985) Epstein-Barr virus transformation of human B lymphocytes despite inhibition of viral polymerase. *J Virol,* Vol. 53 (1) 299-301.

Sjoblom, A., Jansson, A., Yang, W., Lain, S., Nilsson, T. & Rymo, L. (1995) PU box-binding transcription factors and a POU domain protein cooperate in the Epstein-Barr virus (EBV) nuclear antigen 2-induced transactivation of the EBV latent membrane protein 1 promoter. *The Journal of general virology,* Vol. 76 ( Pt 11) 2679-92.

Sjoblom, A., Yang, W., Palmqvist, L., Jansson, A. & Rymo, L. (1998a) An ATF/CRE element mediates both EBNA2-dependent and EBNA2-independent activation of the Epstein-Barr virus LMP1 gene promoter. *Journal of virology,* Vol. 72 (2) 1365-76.

Sjoblom, A., Yang, W., Palmqvist, L., Jansson, A. & Rymo, L. (1998b) An ATF/CRE element mediates both EBNA2-dependent and EBNA2-independent activation of the Epstein-Barr virus LMP1 gene promoter. *J Virol,* Vol. 72 (2) 1365-76.

Skalska, L., White, R.E., Franz, M., Ruhmann, M. & Allday, M.J. (2010a) Epigenetic repression of p16(INK4A) by latent Epstein-Barr virus requires the interaction of EBNA3A and EBNA3C with CtBP. *PLoS Pathog,* Vol. 6 (6) e1000951.

Skalska, L., White, R.E., Franz, M., Ruhmann, M. & Allday, M.J. (2010b) Epigenetic repression of p16(INK4A) by latent Epstein-Barr virus requires the interaction of EBNA3A and EBNA3C with CtBP. *PLoS pathogens,* Vol. 6 (6) e1000951.

Spender, L.C., Lucchesi, W., Bodelon, G., Bilancio, A., Karstegl, C.E., Asano, T., Dittrich-Breiholz, O., Kracht, M., Vanhaesebroeck, B. & Farrell, P.J. (2006) Cell target genes of Epstein-Barr virus transcription factor EBNA-2: induction of the p55alpha regulatory subunit of PI3-kinase and its role in survival of EREB2.5 cells. *J Gen Virol,* Vol. 87 (Pt 10) 2859-67.

Spender, L.C., Whiteman, H.J., Karstegl, C.E. & Farrell, P.J. (2005) Transcriptional cross-regulation of RUNX1 by RUNX3 in human B cells. *Oncogene,* Vol. 24 (11) 1873-81.

Stewart, S., Dawson, C.W., Takada, K., Curnow, J., Moody, C.A., Sixbey, J.W. & Young, L.S. (2004) Epstein-Barr virus-encoded LMP2A regulates viral and cellular gene expression by modulation of the NF-kappaB transcription factor pathway. *Proc Natl Acad Sci U S A,* Vol. 101 (44) 15730-5.

Strobl, L.J., Höfelmayr, H., Marschall, G., Brielmeier, M., Bornkamm, G.W. & Zimber-Strobl, U. (2000) Activated Notch1 modulates gene expression in B cells similarly to Epstein-Barr viral nuclear antigen 2. *J Virol,* Vol. 74 (4) 1727-35.

Studer, R.A., Dessailly, B.H. & Orengo, C.A. (2013) Residue mutations and their impact on protein structure and function: detecting beneficial and pathogenic changes. *Biochem J,* Vol. 449 (3) 581-94.

Stuhler, G., Knop, S., Topp, M.S., Kröber, S.M., Ernemann, U., Herrlinger, U., Einsele, H., Kanz, L. & Hebart, H. (2006) Intravenously administered rituximab induces remission of EBV associated non Hodgkin lymphoma confined to the brain in a patient after allogeneic stem cell transplantation. *Haematologica,* Vol. 91 (3) ECR01.

Styczynski, J., Einsele, H., Gil, L. & Ljungman, P. (2009) Outcome of treatment of Epstein-Barr virus-related post-transplant lymphoproliferative disorder in hematopoietic stem cell recipients: a comprehensive review of reported cases. *Transpl Infect Dis,* Vol. 11 (5) 383-92.

Sugden, B. & Warren, N. (1989) A promoter of Epstein-Barr virus that can function during latent infection can be transactivated by EBNA-1, a viral protein required for viral DNA replication during latent infection. *J Virol,* Vol. 63 (6) 2644-9.

Sung, N.S., Kenney, S., Gutsch, D. & Pagano, J.S. (1991) EBNA-2 transactivates a lymphoid-specific enhancer in the BamHI C promoter of Epstein-Barr virus. *J Virol,* Vol. 65 (5) 2164-9.

Tabiasco, J., Vercellone, A., Meggetto, F., Hudrisier, D., Brousset, P. & Fournié, J.J. (2003) Acquisition of viral receptor by NK cells through immunological synapse. *J Immunol,* Vol. 170 (12) 5993-8.

*The PyMOL Molecular Graphics System, Version 1.2r3pre, Schrödinger, LLC*.

Thomas, J.A., Hotchin, N.A., Allday, M.J., Amlot, P., Rose, M., Yacoub, M. & Crawford, D.H. (1990) Immunohistology of Epstein-Barr virus-associated antigens in B cell disorders from immunocompromised individuals. *Transplantation,* Vol. 49 (5) 944-53.

Thorley-Lawson, D.A. & Babcock, G.J. (1999) A model for persistent infection with Epstein-Barr virus: the stealth virus of human B cells. *Life Sci,* Vol. 65 (14) 1433-53.

Tobollik, S., Meyer, L., Buettner, M., Klemmer, S., Kempkes, B., Kremmer, E., Niedobitek, G. & Jungnickel, B. (2006) Epstein-Barr virus nuclear antigen 2 inhibits AID expression during EBV-driven B-cell growth. *Blood,* Vol. 108 (12) 3859-64.

Tokunaga, M., Land, C.E., Uemura, Y., Tokudome, T., Tanaka, S. & Sato, E. (1993) Epstein-Barr virus in gastric carcinoma. *Am J Pathol,* Vol. 143 (5) 1250-4.

Tomblyn, M., Chiller, T., Einsele, H., Gress, R., Sepkowitz, K., Storek, J., Wingard, J.R., Young, J.A. & Boeckh, M.J. (2009) Guidelines for preventing infectious complications among hematopoietic cell transplant recipients: a global perspective. Preface. *Bone Marrow Transplant,* Vol. 44 (8) 453-5.

Tomkinson, B. & Kieff, E. (1992) Use of second-site homologous recombination to demonstrate that Epstein-Barr virus nuclear protein 3B is not important for lymphocyte infection or growth transformation in vitro. *J Virol,* Vol. 66 (5) 2893-903.

Tomkinson, B., Robertson, E. & Kieff, E. (1993) Epstein-Barr virus nuclear proteins EBNA-3A and EBNA-3C are essential for B-lymphocyte growth transformation. *J Virol,* Vol. 67 (4) 2014-25.

Tong, X., Drapkin, R., Reinberg, D. & Kieff, E. (1995a) The 62- and 80-kDa subunits of transcription factor IIH mediate the interaction with Epstein-Barr virus nuclear protein 2. *Proc Natl Acad Sci U S A,* Vol. 92 (8) 3259-63.

Tong, X., Drapkin, R., Yalamanchili, R., Mosialos, G. & Kieff, E. (1995b) The Epstein-Barr virus nuclear protein 2 acidic domain forms a complex with a novel cellular coactivator that can interact with TFIIE. *Mol Cell Biol,* Vol. 15 (9) 4735-44.

Tong, X., Wang, F., Thut, C.J. & Kieff, E. (1995c) The Epstein-Barr virus nuclear protein 2 acidic domain can interact with TFIIB, TAF40, and RPA70 but not with TATA-binding protein. *J Virol,* Vol. 69 (1) 585-8.

Touitou, R., Hickabottom, M., Parker, G., Crook, T. & Allday, M.J. (2001) Physical and functional interactions between the corepressor CtBP and the Epstein-Barr virus nuclear antigen EBNA3C. *J Virol,* Vol. 75 (16) 7749-55.

Touitou, R., O'nions, J., Heaney, J. & Allday, M.J. (2005) Epstein-Barr virus EBNA3 proteins bind to the C8/alpha7 subunit of the 20S proteasome and are degraded by 20S proteasomes in vitro, but are very stable in latently infected B cells. *J Gen Virol,* Vol. 86 (Pt 5) 1269-77.

Traylen, C., Ramasubramanyan, S., Zuo, J., Rowe, M., Almohammad, R., Heesom, K., Sweet, S.M., Matthews, D.A. & Sinclair, A.J. (2015) Identification of Epstein-Barr Virus Replication Proteins in Burkitt's Lymphoma Cells. *Pathogens,* Vol. 4 (4) 739-51.

Trempat, P., Tabiasco, J., Andre, P., Faumont, N., Meggetto, F., Delsol, G., Gascoyne, R.D., Fournie, J.J., Vivier, E. & Brousset, P. (2002) Evidence for early infection of nonneoplastic natural killer cells by Epstein-Barr virus. *J Virol,* Vol. 76 (21) 11139-42.

Tsuchiyama, J., Yoshino, T., Mori, M., Kondoh, E., Oka, T., Akagi, T., Hiraki, A., Nakayama, H., Shibuya, A., Ma, Y., Kawabata, T., Okada, S. & Harada, M. (1998) Characterization of a novel human natural killer-cell line (NK-YS) established from natural killer cell lymphoma/leukemia associated with Epstein-Barr virus infection. *Blood,* Vol. 92 (4) 1374-83.

Tsui, S. & Schubach, W.H. (1994) Epstein-Barr virus nuclear protein 2A forms oligomers in vitro and in vivo through a region required for B-cell transformation. *J Virol,* Vol. 68 (7) 4287-94.

Tsurumi, T., Fujita, M. & Kudoh, A. (2005) Latent and lytic Epstein-Barr virus replication strategies. *Rev Med Virol,* Vol. 15 (1) 3-15.

Uchida, J., Yasui, T., Takaoka-Shichijo, Y., Muraoka, M., Kulwichit, W., Raab-Traub, N. & Kikutani, H. (1999) Mimicry of CD40 signals by Epstein-Barr virus LMP1 in B lymphocyte responses. *Science,* Vol. 286 (5438) 300-3.

Uhlin, M., Okas, M., Gertow, J., Uzunel, M., Brismar, T.B. & Mattsson, J. (2010) A novel haplo-identical adoptive CTL therapy as a treatment for EBV-associated lymphoma after stem cell transplantation. *Cancer Immunol Immunother,* Vol. 59 (3) 473-7.

Ushmorov, A., Ritz, O., Hummel, M., Leithäuser, F., Möller, P., Stein, H. & Wirth, T. (2004) Epigenetic silencing of the immunoglobulin heavy-chain gene in classical Hodgkin lymphoma-derived cell lines contributes to the loss of immunoglobulin expression. *Blood,* Vol. 104 (10) 3326-34.

Vagin, A.A., Steiner, R.A., Lebedev, A.A., Potterton, L., Mcnicholas, S., Long, F. & Murshudov, G.N. (2004) REFMAC5 dictionary: organization of prior chemical knowledge and guidelines for its use. *Acta Crystallogr D Biol Crystallogr,* Vol. 60 (Pt 12 Pt 1) 2184-95.

Valentine, R., Dawson, C.W., Hu, C., Shah, K.M., Owen, T.J., Date, K.L., Maia, S.P., Shao, J., Arrand, J.R., Young, L.S. & O'neil, J.D. (2010) Epstein-Barr virus-encoded EBNA1 inhibits the canonical NF-kappaB pathway in carcinoma cells by inhibiting IKK phosphorylation. *Mol Cancer,* Vol. 9 1.

Vanderwielen, B.D., Yuan, Z., Friedmann, D.R. & Kovall, R.A. (2011) Transcriptional repression in the Notch pathway: thermodynamic characterization of CSL-MINT (Msx2-interacting nuclear target protein) complexes. *J Biol Chem,* Vol. 286 (17) 14892-902.

Vasquez-Del Carpio, R., Kaplan, F.M., Weaver, K.L., Vanwye, J.D., Alves-Guerra, M.C., Robbins, D.J. & Capobianco, A.J. (2011) Assembly of a Notch transcriptional activation complex requires multimerization. *Mol Cell Biol,* Vol. 31 (7) 1396-408.

Visel, A., Blow, M.J., Li, Z., Zhang, T., Akiyama, J.A., Holt, A., Plajzer-Frick, I., Shoukry, M., Wright, C., Chen, F., Afzal, V., Ren, B., Rubin, E.M. & Pennacchio, L.A. (2009) ChIP-seq accurately predicts tissue-specific activity of enhancers. *Nature,* Vol. 457 (7231) 854-8.

Visone, R., Russo, L., Pallante, P., De Martino, I., Ferraro, A., Leone, V., Borbone, E., Petrocca, F., Alder, H., Croce, C.M. & Fusco, A. (2007) MicroRNAs (miR)-221 and miR-222, both overexpressed in human thyroid papillary carcinomas, regulate p27Kip1 protein levels and cell cycle. *Endocr Relat Cancer,* Vol. 14 (3) 791-8.

Voss, M.D., Hille, A., Barth, S., Spurk, A., Hennrich, F., Holzer, D., Mueller-Lantzsch, N., Kremmer, E. & Grasser, F.A. (2001) Functional cooperation of Epstein-Barr virus nuclear antigen 2 and the survival motor neuron protein in transactivation of the viral LMP1 promoter. *J Virol,* Vol. 75 (23) 11781-90.

Waghray, M., Parhar, R.S., Taibah, K. & Al-Sedairy, S. (1992) Rearrangements of chromosome arm 3q in poorly differentiated nasopharyngeal carcinoma. *Genes Chromosomes Cancer,* Vol. 4 (4) 326-30.

Waltzer, L., Logeat, F., Brou, C., Israel, A., Sergeant, A. & Manet, E. (1994) The human J kappa recombination signal sequence binding protein (RBP-J kappa) targets the Epstein-Barr virus EBNA2 protein to its DNA responsive elements. *Embo J,* Vol. 13 (23) 5633-8.

Waltzer, L., Perricaudet, M., Sergeant, A. & Manet, E. (1996) Epstein-Barr virus EBNA3A and EBNA3C proteins both repress RBP-J kappa-EBNA2-activated transcription by inhibiting the binding of RBP-J kappa to DNA. *J Virol,* Vol. 70 (9) 5909-15.

Wang, A., Welch, R., Zhao, B., Ta, T., Keleş, S. & Johannsen, E. (2015) Epstein-Barr Virus Nuclear Antigen 3 (EBNA3) Proteins Regulate EBNA2 Binding to Distinct RBPJ Genomic Sites. *J Virol,* Vol. 90 (6) 2906-19.

Wang, C.Q. & He, J. (2016) Ubiquitous Distribution of Epstein-Barr Virus and the Highly Uneven Distribution of Nasopharyngeal Carcinoma. *Chin Med J (Engl),* Vol. 129 (20) 2506-2507.

Wang, D., Liebowitz, D. & Kieff, E. (1985) An EBV membrane protein expressed in immortalized lymphocytes transforms established rodent cells. *Cell,* Vol. 43 (3 Pt 2) 831-40.

Wang, F., Gregory, C.D., Rowe, M., Rickinson, A.B., Wang, D., Birkenbach, M., Kikutani, H., Kishimoto, T. & Kieff, E. (1987a) Epstein-Barr virus nuclear antigen 2 specifically induces expression of the B-cell activation antigen CD23. *Proc Natl Acad Sci U S A,* Vol. 84 (10) 3452-6.

Wang, F., Kikutani, H., Tsang, S.F., Kishimoto, T. & Kieff, E. (1991) Epstein-Barr virus nuclear protein 2 transactivates a cis-acting CD23 DNA element. *J Virol,* Vol. 65 (8) 4101-6.

Wang, F., Petti, L., Braun, D., Seung, S. & Kieff, E. (1987b) A bicistronic Epstein-Barr virus mRNA encodes two nuclear proteins in latently infected, growth-transformed lymphocytes. *J Virol,* Vol. 61 (4) 945-54.

Wang, F., Tsang, S.F., Kurilla, M.G., Cohen, J.I. & Kieff, E. (1990) Epstein-Barr virus nuclear antigen 2 transactivates latent membrane protein LMP1. *J Virol,* Vol. 64 (7) 3407-16.

Wang, L., Grossman, S.R. & Kieff, E. (2000) Epstein-Barr virus nuclear protein 2 interacts with p300, CBP, and PCAF histone acetyltransferases in activation of the LMP1 promoter. *Proc Natl Acad Sci U S A,* Vol. 97 (1) 430-5.

West, M.J. (2006) Structure and function of the Epstein-Barr virus transcription factor, EBNA 3C. *Curr Protein Pept Sci,* Vol. 7 (2) 123-36.

West, M.J., Webb, H.M., Sinclair, A.J. & Woolfson, D.N. (2004) Biophysical and mutational analysis of the putative bZIP domain of Epstein-Barr virus EBNA 3C. *J Virol,* Vol. 78 (17) 9431-45.

White, R.E., Groves, I.J., Turro, E., Yee, J., Kremmer, E. & Allday, M.J. (2010) Extensive co-operation between the Epstein-Barr virus EBNA3 proteins in the manipulation of host gene expression and epigenetic chromatin modification. *PLoS One,* Vol. 5 (11) e13979.

White, R.E., Ramer, P.C., Naresh, K.N., Meixlsperger, S., Pinaud, L., Rooney, C., Savoldo, B., Coutinho, R., Bodor, C., Gribben, J., Ibrahim, H.A., Bower, M., Nourse, J.P., Gandhi, M.K., Middeldorp, J., Cader, F.Z., Murray, P., Munz, C. & Allday, M.J. (2012) EBNA3B-deficient EBV promotes B cell lymphomagenesis in humanized mice and is found in human tumors. *J Clin Invest,* Vol. 122 (4) 1487-502.

Wilson, J.J. & Kovall, R.A. (2006) Crystal structure of the CSL-Notch-Mastermind ternary complex bound to DNA. *Cell,* Vol. 124 (5) 985-96.

Winn, M.D., Ballard, C.C., Cowtan, K.D., Dodson, E.J., Emsley, P., Evans, P.R., Keegan, R.M., Krissinel, E.B., Leslie, A.G., Mccoy, A., Mcnicholas, S.J., Murshudov, G.N., Pannu, N.S., Potterton, E.A., Powell, H.R., Read, R.J., Vagin, A. & Wilson, K.S. (2011) Overview of the CCP4 suite and current developments. *Acta Crystallogr D Biol Crystallogr,* Vol. 67 (Pt 4) 235-42.

Winter, G. (2010) *XIA2: an expert system for macromolecular crystallography data reduction.* Vol. 43.

Woisetschlaeger, M., Jin, X.W., Yandava, C.N., Furmanski, L.A., Strominger, J.L. & Speck, S.H. (1991) Role for the Epstein-Barr virus nuclear antigen 2 in viral promoter switching during initial stages of infection. *Proceedings of the National Academy of Sciences of the United States of America,* Vol. 88 (9) 3942-6.

Woisetschlaeger, M., Yandava, C.N., Furmanski, L.A., Strominger, J.L. & Speck, S.H. (1990) Promoter switching in Epstein-Barr virus during the initial stages of infection of B lymphocytes. *Proc Natl Acad Sci U S A,* Vol. 87 (5) 1725-9.

Wood, C.D., Veenstra, H., Khasnis, S., Gunnell, A., Webb, H.M., Shannon-Lowe, C., Andrews, S., Osborne, C.S. & West, M.J. (2016) MYC activation and BCL2L11 silencing by a tumour virus through the large-scale reconfiguration of enhancer-promoter hubs. *Elife,* Vol. 5.

Wood, V.H., O'neil, J.D., Wei, W., Stewart, S.E., Dawson, C.W. & Young, L.S. (2007) Epstein-Barr virus-encoded EBNA1 regulates cellular gene transcription and modulates the STAT1 and TGFbeta signaling pathways. *Oncogene,* Vol. 26 (28) 4135-47.

World.Health.Organisation (2014) *World Cancer Report 2014*

Wu, D.Y., Kalpana, G.V., Goff, S.P. & Schubach, W.H. (1996) Epstein-Barr virus nuclear protein 2 (EBNA2) binds to a component of the human SNF-SWI complex, hSNF5/Ini1. *J Virol,* Vol. 70 (9) 6020-8.

Wu, D.Y., Krumm, A. & Schubach, W.H. (2000a) Promoter-specific targeting of human SWI-SNF complex by Epstein-Barr virus nuclear protein 2. *J Virol,* Vol. 74 (19) 8893-903.

Wu, D.Y., Krumm, A. & Schubach, W.H. (2000b) Promoter-specific targeting of human SWI-SNF complex by Epstein-Barr virus nuclear protein 2. *Journal of virology,* Vol. 74 (19) 8893-903.

Xiao, J., Palefsky, J.M., Herrera, R., Berline, J. & Tugizov, S.M. (2009) EBV BMRF-2 facilitates cell-to-cell spread of virus within polarized oral epithelial cells. *Virology,* Vol. 388 (2) 335-43.

Xue, Y., Ren, J., Gao, X., Jin, C., Wen, L. & Yao, X. (2008) GPS 2.0, a tool to predict kinase-specific phosphorylation sites in hierarchy. *Mol Cell Proteomics,* Vol. 7 (9) 1598-608.

Yang, L., Xu, Z., Liu, L., Luo, X., Lu, J., Sun, L. & Cao, Y. (2014) Targeting EBV-LMP1 DNAzyme enhances radiosensitivity of nasopharyngeal carcinoma cells by inhibiting telomerase activity. *Cancer Biol Ther,* Vol. 15 (1) 61-8.

Yao, Q.Y., Rickinson, A.B. & Epstein, M.A. (1985) A re-examination of the Epstein-Barr virus carrier state in healthy seropositive individuals. *Int J Cancer,* Vol. 35 (1) 35-42.

Yasukawa, T., Kanei-Ishii, C., Maekawa, T., Fujimoto, J., Yamamoto, T. & Ishii, S. (1995) Increase of solubility of foreign proteins in Escherichia coli by coproduction of the bacterial thioredoxin. *J Biol Chem,* Vol. 270 (43) 25328-31.

Yates, J., Warren, N., Reisman, D. & Sugden, B. (1984) A cis-acting element from the Epstein-Barr viral genome that permits stable replication of recombinant plasmids in latently infected cells. *Proc Natl Acad Sci U S A,* Vol. 81 (12) 3806-10.

Yates, J.L. & Guan, N. (1991) Epstein-Barr virus-derived plasmids replicate only once per cell cycle and are not amplified after entry into cells. *J Virol,* Vol. 65 (1) 483-8.

Yates, J.L., Warren, N. & Sugden, B. (1985) Stable replication of plasmids derived from Epstein-Barr virus in various mammalian cells. *Nature,* Vol. 313 (6005) 812-5.

Yenamandra, S.P., Sompallae, R., Klein, G. & Kashuba, E. (2009) Comparative analysis of the Epstein-Barr virus encoded nuclear proteins of EBNA-3 family. *Comput Biol Med,* Vol. 39 (11) 1036-42.

Yi, F., Saha, A., Murakami, M., Kumar, P., Knight, J.S., Cai, Q., Choudhuri, T. & Robertson, E.S. (2009) Epstein-Barr virus nuclear antigen 3C targets p53 and modulates its transcriptional and apoptotic activities. *Virology,* Vol. 388 (2) 236-47.

Yoo, L.I., Mooney, M., Puglielli, M.T. & Speck, S.H. (1997) B-cell lines immortalized with an Epstein-Barr virus mutant lacking the Cp EBNA2 enhancer are biased toward utilization of the oriP-proximal EBNA gene promoter Wp1. *J Virol,* Vol. 71 (12) 9134-42.

Yoo, L.I., Woloszynek, J., Templeton, S. & Speck, S.H. (2002) Deletion of Epstein-Barr virus regulatory sequences upstream of the EBNA gene promoter Wp1 is unfavorable for B-Cell immortalization. *J Virol,* Vol. 76 (22) 11763-9.

Young, L.S., Dawson, C.W., Clark, D., Rupani, H., Busson, P., Tursz, T., Johnson, A. & Rickinson, A.B. (1988) Epstein-Barr virus gene expression in nasopharyngeal carcinoma. *J Gen Virol,* Vol. 69 ( Pt 5) 1051-65.

Young, P., Anderton, E., Paschos, K., White, R. & Allday, M.J. (2008) Epstein-Barr virus nuclear antigen (EBNA) 3A induces the expression of and interacts with a subset of chaperones and co-chaperones. *J Gen Virol,* Vol. 89 (Pt 4) 866-77.

Yu, M.C. & Yuan, J.M. (2002) Epidemiology of nasopharyngeal carcinoma. *Semin Cancer Biol,* Vol. 12 (6) 421-9.

Yuan, Z., Friedmann, D.R., Vanderwielen, B.D., Collins, K.J. & Kovall, R.A. (2012) Characterization of CSL (CBF-1, Su(H), Lag-1) mutants reveals differences in signaling mediated by Notch1 and Notch2. *J Biol Chem,* Vol. 287 (42) 34904-16.

Yuan, Z., Praxenthaler, H., Tabaja, N., Torella, R., Preiss, A., Maier, D. & Kovall, R.A. (2016) Structure and Function of the Su(H)-Hairless Repressor Complex, the Major Antagonist of Notch Signaling in Drosophila melanogaster. *PLoS Biol,* Vol. 14 (7) e1002509.

Yue, W., Gershburg, E. & Pagano, J.S. (2005) Hyperphosphorylation of EBNA2 by Epstein-Barr virus protein kinase suppresses transactivation of the LMP1 promoter. *J Virol,* Vol. 79 (9) 5880-5.

Yue, W., Shackelford, J. & Pagano, J.S. (2006) cdc2/cyclin B1-dependent phosphorylation of EBNA2 at Ser243 regulates its function in mitosis. *J Virol,* Vol. 80 (4) 2045-50.

Zhao, B., Marshall, D.R. & Sample, C.E. (1996) A conserved domain of the Epstein-Barr virus nuclear antigens 3A and 3C binds to a discrete domain of Jkappa. *J Virol,* Vol. 70 (7) 4228-36.

Zhao, B., Maruo, S., Cooper, A., M, R.C., Johannsen, E., Kieff, E. & Cahir-Mcfarland, E. (2006) RNAs induced by Epstein-Barr virus nuclear antigen 2 in lymphoblastoid cell lines. *Proc Natl Acad Sci U S A,* Vol. 103 (6) 1900-5.

Zhao, B. & Sample, C.E. (2000) Epstein-barr virus nuclear antigen 3C activates the latent membrane protein 1 promoter in the presence of Epstein-Barr virus nuclear antigen 2 through sequences encompassing an spi-1/Spi-B binding site. *J Virol,* Vol. 74 (11) 5151-60.

Zhao, B., Zou, J., Wang, H., Johannsen, E., Peng, C.W., Quackenbush, J., Mar, J.C., Morton, C.C., Freedman, M.L., Blacklow, S.C., Aster, J.C., Bernstein, B.E. & Kieff, E. (2011) Epstein-Barr virus exploits intrinsic B-lymphocyte transcription programs to achieve immortal cell growth. *Proc Natl Acad Sci U S A,* Vol. 108 (36) 14902-7.

Zhu, K., Zhao, J., Lubman, D.M., Miller, F.R. & Barder, T.J. (2005) Protein pI shifts due to posttranslational modifications in the separation and characterization of proteins. *Anal Chem,* Vol. 77 (9) 2745-55.

Zimber-Strobl, U., Kremmer, E., Grasser, F., Marschall, G., Laux, G. & Bornkamm, G.W. (1993) The Epstein-Barr virus nuclear antigen 2 interacts with an EBNA2 responsive cis-element of the terminal protein 1 gene promoter. *Embo J,* Vol. 12 (1) 167-75.

Zimber-Strobl, U. & Strobl, L.J. (2001) EBNA2 and Notch signalling in Epstein-Barr virus mediated immortalization of B lymphocytes. *Semin Cancer Biol,* Vol. 11 (6) 423-34.

Zimber-Strobl, U., Strobl, L.J., Meitinger, C., Hinrichs, R., Sakai, T., Furukawa, T., Honjo, T. & Bornkamm, G.W. (1994) Epstein-Barr virus nuclear antigen 2 exerts its transactivating function through interaction with recombination signal binding protein RBP-J kappa, the homologue of Drosophila Suppressor of Hairless. *Embo J,* Vol. 13 (20) 4973-82.

Zimber-Strobl, U., Suentzenich, K.O., Laux, G., Eick, D., Cordier, M., Calender, A., Billaud, M., Lenoir, G.M. & Bornkamm, G.W. (1991) Epstein-Barr virus nuclear antigen 2 activates transcription of the terminal protein gene. *J Virol,* Vol. 65 (1) 415-23.

Zolkiewska, A. (2008) ADAM proteases: ligand processing and modulation of the Notch pathway. *Cell Mol Life Sci,* Vol. 65 (13) 2056-68.

Zur Hausen, H., Schulte-Holthausen, H., Klein, G., Henle, W., Henle, G., Clifford, P. & Santesson, L. (1970) EBV DNA in biopsies of Burkitt tumours and anaplastic carcinomas of the nasopharynx. *Nature,* Vol. 228 (5276) 1056-8.

Zweidler-Mckay, P.A., He, Y., Xu, L., Rodriguez, C.G., Karnell, F.G., Carpenter, A.C., Aster, J.C., Allman, D. & Pear, W.S. (2005) Notch signaling is a potent inducer of growth arrest and apoptosis in a wide range of B-cell malignancies. *Blood,* Vol. 106 (12) 3898-906.

# Appendix 1 : Table of primers

| Primer | Primer Target | Sequence 5' to 3' |
|---|---|---|
| RBP-Jκ 8-435 Forward SmaI | RBP-Jκ (aa8-435) with the C-terminal His-tag cDNA | TAACCCGGGATGGGTGAGCGGCCTCCA |
| RBP-Jκ 8-435 Reverse XbaI | | GCGAAGCTTTCAGTGGTGGTGGTGGTG |
| pUC/M13 Forward * | Diagnostic PCR of Transposition site of Bacmid | CCCAGTCACGACGTTGTAAAACG |
| pUC/M13 Reverse * | | AGCGGATAACAATTTCACACAGG |
| EBNA3C T>A Forward | Mutagenesis of TFGC RBP-Jκ binding motif of EBNA3C | TTAACTGCC**GCA**TTTGGATGCCAAAAT |
| EBNA3C F>A Forward | | TTAACTGCCACA**GCT**GGATGCCAAAAT |
| EBNA3C TF>AA Forward | | TTAACTGCC**GCAGCT**GGATGCCAAAAT |
| EBNA3C TFGC mutant Reverse | | CATGATGCTGTCAGCCCCAACC |
| EBNA3C STP Forward | Mutagenesis of WTP RBP-Jκ binding motif of EBNA3C | ACCGTGTCGACACCACCC |
| EBNA3C STP Reverse | | GGCAGAGAAGGTGTTTAGAGTTCGTGC |
| T7 sequencing primer ** | Sequence pSG5 vector from T7 promoter | TAATACGACTCACTATAGGG |
| EBNA2 fragment Forward NheI, XbaI *** | EBNA2 fragment (aa272-333) cDNA | CGGACGGAGCTCTCTAGAGCTAGCGATA GTCCAGAACCACGGT |
| EBNA2 fragment Reverse HindIII, XheI *** | | CGGACGCTGCAGCTCGAGAAGCTTAGG GTTGCGGGGGGTCG |
| EBNA2 fragment Reverse BamHI | | TATGGATCCTTAGGGTTGCGGGGGGTCG |
| EBNA2FL Reverse SalI | Full length EBNA2 cDNA | TATGTCGACTTACTGGATGGAGGGGCGA |
| EBNA2FL Forward NheI, XbaI *** | | CGGACGGAGCTCTCTAGAGCTAGCATG CCTACATTCTATCTTGCG |
| 3CHD p10 Forward HindIII | $EBNA3C_{100-356}$ and $EBNA3C_{100-413}$ cDNA destined for p10 MCS | ATAGCTAGCCACGACATCACACCATAT |
| 3CHD.1 p10 Reverse NheI | | AATAAGCTTTCACGTTGCTAACATTGATAA |
| 3CHD.2 p10 Reverse NheI | | AATAAGCTTTCATGCAGGCACACGGCTCAC |
| 3CHD polyhed Forward XbaI | $EBNA3C_{100-356}$ and $EBNA3C_{100-413}$ cDNA destined for polyhed MCS | TAATCTAGACACGACATCACACCATAT |
| 3CHD.1 polyhed Reverse BamHI | | ATTGGATCCTCACGTTGCTAACATTGATAA |
| 3CHD.2 polyhed Reverse BamHI | | AATGGATCCTCATGCAGGCACACGGCTCAC |
| pFastBac F sequencing primer ** | Sequence DNA inserted into pFastBac p10 MCS | TCCGGATTATTCATACCGTCCC |
| pFastBac R sequencing primer ** | | CCTCTACAAATGTGGTATGGCTG |
| Polyhed_fwd | Sequence DNA inserted into pFastBac polyhed MCS | AAAATGATAACCATCTCG |
| Polyhed reverse *** | | GTCGAGAAGTACTAGAGGAT |

**primers designed by Invitogen Bac-to-Bac expression kit*

*** designed by Eurofins sequencing service*

****primers were produced by Dr Christomous Prodromou group.*

# Appendix 2 : Table of vectors

| Vector | Inserts | |
|---|---|---|
| pET28B.JK.8-435* | RBP-Jκ$_{8-435}$ with a C terminal His tag | |
| pFastBac.CP17.2 | pFastBac co-expression vector produced by Dr Christomous Prodromou with a p10 MCS with a N-terminal His-tag, a polyhed MCS with a N-terminal StrepII-tag and a LoxP site for combining two pFastBac.CP17.2 vectors. | |
| pF.JK.V1 | p10 MCS: Full length RBP-Jκ Variant 1 with an N-terminal His-tag | polyhed MCS: Empty |
| pF.JK.V2 | p10 MCS: Full length RBP-Jκ Variant 2 with an N-terminal His-tag | polyhed MCS: Empty |
| pF.JK.8-435 | p10 MCS: RBP-Jκ (aa8-435) with a C-terminal His-tag | polyhed MCS: Empty |
| pSG5 | Vector that can be transfected into DG75 cell line to overexpress insert | |
| pSG53C** | Full length EBNA3C Cdna | |
| pSG53C.Jκ** | Full length EBNA3C cDNA with TFGC mutated to AAAA | |
| pSG53C.STP | Full length EBNA3C cDNA with WTP mutated to STP | |
| pSG53C.Jκ.STP | Full length EBNA3C cDNA with TFGC mutated to AAAA and WTP mutated to STP | |
| pSG53C.TA | Full length EBNA3C cDNA with TFGC mutated to AFGC | |
| pSG53C.FA | Full length EBNA3C cDNA with TFGC mutated to TAGC | |
| pSG53C.TFAA | Full length EBNA3C cDNA with TFGC mutated to AAGC | |
| pF.CP17.272*** | p10 MCS: EBNA2$_{272-333}$ with an N-terminal His-tag | polyhed MCS: Empty |
| pF.JK.V1.272*** | p10 MCS: Full length RBP-Jκ Variant 1 with an N-terminal His-tag | polyhed MCS: EBNA2$_{272-333}$ with an N-terminal StrepII-tag |
| pF.JK.V2.272*** | p10 MCS: Full length RBP-Jκ Variant 2 with a N-terminal His-tag | polyhed MCS: EBNA2$_{272-333}$ with an N-terminal StrepII-tag |
| pF.JK.8-435.272 | p10 MCS: RBP-Jκ$_{8-435}$ with a C-terminal His-tag | polyhed MCS: EBNA2$_{272-333}$ with an N-terminal StrepII-tag |
| pF.CP17.EB2*** | p10 MCS: Full length EBNA2 with an N-terminal His-tag | polyhed MCS: Empty |
| pF.JK.V1.EB2 | p10 MCS: Full length RBP-Jκ Variant 1 with an N-terminal His-tag | polyhed MCS: Full length EBNA2 with an N-terminal StrepII-tag |
| pF.JK.V2.EB2 | p10 MCS: Full length RBP-Jκ Variant 2 with a N-terminal His-tag | polyhed MCS: Full length EBNA2 with an N-terminal StrepII-tag |
| pF.JK.8-435.EB2 | p10 MCS: RBP-Jκ (aa8-435) with a C-terminal His-tag | polyhed MCS: Full length EBNA2 with an N-terminal StrepII-tag |
| pcDNA3.EBNA3C**** | pcDNA3 vector containing full length EBNA3C cDNA | |
| pF.EB3C.HD1 | p10 MCS: EBNA3C$_{100-356}$ with an N-terminal his-tag | polyhed MCS: Empty |
| pF.EB3C.HD2 | p10 MCS: EBNA3C$_{100-413}$ with an N-terminal his-tag | polyhed MCS: Empty |
| pF.JK.8-435. EB3C.HD1 | p10 MCS: RBP-Jκ (aa8-435) with a C-terminal His-tag | polyhed MCS: EBNA3C$_{100-356}$ with a N-terminal StrepII-tag |
| pF.JK.8-435. EB3C.HD2 | p10 MCS: RBP-Jκ (aa8-435) with a C-terminal His-tag | polyhed MCS: EBNA3C$_{100-413}$ with a N-terminal StrepII-tag |

** pET28B.JK.8-435 was produced by a summer student in Michelle West's Group.*

***pSG53C and pSG53C.Jκ were produced by Dr Helen Webb from Michelle West's Group.*

****pF.CP17.272 and pF.CP17.EB2 vectors were produced by a masters student from Dr Christomous Prodromou group.*

***** pcDNA3.EBNA3C vector was given to our lab from Dr A. Bell, University of Birmingham.*

# Appendix 3 : Table of Buffers and Reagents

| | |
|---|---|
| **Agarose Gel** | |
| TBE | Tris base, Boric acid and EDTA |
| Agarose tablets | Bioline 0.5g DNase and RNAse free agarose tablets |
| DNA loading dye | Bromothenol blue and cyanol F |
| Gel red | Biotium Gel Red$^{Tm}$ Nucleic acid gel stain |
| **SDS-PAGE, Coomassie and Western blotting** | |
| Gel sample buffer (GSB) | 50mM Tris pH6.8, 4% SDS, 10% β-Mercaptoethanol, 0.01% Bromophenol blue, 10% Glycerol, 1mM EDTA |
| SDS-PAGE gel (10% and 4-12% Bis-tris gel) | Supplied by Novex (LifeTechnologies) |
| SDS running buffer (MOPS) | |
| Simply blue stain | Supplied by Invitrogen |
| Ponceau | Supplied by Sigma Bioreagents |
| ECL | Solution 1: Luminol Stock, Coomaric acid, 1M tris pH8.5<br>Solution 2: $H_2O_2$, 1M tris pH8.5<br>Mixed immediately prior to use |
| Milk powder | The Co-operative powdered milk |
| Transfer buffer | 4 litre dH2O, 1 litre methanol (Fisher), 75g Glycine (Fisher), 15g Tris(hydroxymethyl)-methylamine (Fisher) |
| PBS Tween | 100 tablets PBS (Fisher) in 10 litre of water, Tween 20 (Fisher) |
| **Antibodies** | |
| Anti-His tag | Target: 6xHis-tag, Species: mouse, Supplied by Sigma Aldrich |
| Anti-StrepII tag | Target: strepII-tag, Species mouse, Supplied by Life Technologies |
| Anti EBNA2 | Target: EBNA2, Species: mouse, Produced in Lab |
| Anti EBNA3C | Target: EBNA3C, Species: mouse, Supplied by Sigma Aldrich |
| **Insect cell culture** | |
| SF900II medium | Supplied by LifeTechnologies |
| Sf9 cells | |
| Trypan Blue | Supplied by Invitrogen |
| **Bacmid preparation** | |
| MAX Efficiency DH10Bac™ Competent *E.coli* | Supplied by LifeTechnologies |
| SOC medium | |
| Gentamicin | |
| Tetracyclin | Supplied by Thermo-Scientific |
| Kanamycin | Supplied by Fisher Bioreagents |
| IPTG | |
| X-Gal | |
| 70% ethanol | Supplied by Fisher Scientific |
| 3M potassium acetate pH 5.5 | |
| **Transfection and baculvirus plaque assay** | |
| CellfectinII | Supplied by LifeTechnologies |
| Neutral red | |
| High purity agar | |
| **EMSA** | |
| EMSA stock buffer | 5 x Buffer: 50mM Tris pH7.5, 5mM MgCl, 2.5mM EDTA, 2.5mM DTT, 250mM NaCl, 0.25µg/µl PolydIdC, 20% glycerol |
| 6% DNA retardation gel | Supplied by Novex (LifeTechnologies) |
| ***E.coli* Cells** | |
| DH5α compotent cells | Supplied by Invitrogen |
| LB | Supplied by Fisher Scientific |
| LB Agar | |
| Competent Rosetta ply5 De3 | Supplied by Invitrogen |
| NEB DH5α competent *E.coli* | Supplied by NEB |
| **Enzymes and Buffers** | |
| Phosphatase Alkaline | Supplied by Roche |
| DNA T4 Ligase | Supplied by New England Biolabs |
| Ligase Buffer (10x buffer) | Supplied by New England Biolabs : 50mM Tris-HCl, 10mM $MgCl_2$, 1mM ATP, 10mM DTT, pH 7.5 |
| High fidelity Phusion DNA Polymerase | Supplied by New England Biolabs |
| Phusion HF buffer (5x) | |
| Phusion GC buffer (5x) | |
| Taq DNApolymerase | |
| Standard Taqpol (10x buffer) | |

| | |
|---|---|
| dNTPs | |
| Hot start Q5 high fidelity mix | |
| KLD mix | |
| λ-phosphatase | Supplied by Sigma Aldrich |
| **Competent cells** | |
| Buffer I | 100mM RbCl, 50mM $MnCl_2$.4H2O, 30mM KOAc, 10mM $CaCl_2$, 15% v/v Glycerol, pH to 5.8 with 0.2M Acetic Acid |
| Buffer II | 10mM RbCl, 10mM MOPS, 75mM $CaCl_2$,15% v/v Glycerol<br>pH to 6.8 with 1M NaOH |
| **In-gel digestion and Mass spectroscopy** | |
| Coomassie destain | 50% MeCN, 25 mM $NH_4HCO_3$ |
| Reduction buffer | 10 mM DTT, 25 mM $NH_4HCO_3$ |
| Alkylation buffer | 50 mM iodoacetamide, 25 mM $NH_4HCO_3$ |
| Trypsin solution | 12.5 ng/ul trypsin, 25 mM $NH_4HCO_3$ |
| Formic acid | Supplied by Fisher Bioreagents |
| MeCN | Supplied by Fisher Bioreagents |
| Mass Spectrometer loading buffer | 0.1% Trifluoroacetic acid (TFA) |
| NanoLC buffer A | 0.1% Formic acid |
| NanoLC buffer B | MeCN, 0.1% Formic acid |
| **Crystallisation trials** | |
| PacT 96 deep well block | Supplied by Molecular Dimensions |
| JCSG plus 96 deep well block | |
| Proplex 96 deep well block | |
| Natrix 96 deep well block | Supplied by Hampton Research |
| Additive screen 96 deep well block | Supplied by Molecular Dimensions |
| **CsCl prep and pull downs** | |
| SolI | 50 mM Glucose, 25 mM Tris HCl pH8,10 mM EDTA |
| SolII | 0.2M NaOH, 1% SDS |
| SolIII | 5M K acetate, Glacial Acetic Acid |
| Buffer PD | 50mM Tris pH7.5, 150mM NaCl, 20mM $MgCl_2$, 1% NP-40, 0.5% Na Deoxycholate |
| **DG75 Cell culture** | |
| RPMI 1640 Medium | Supplied by LifeTechnologies |
| 100X Penicillin/ streptomycin | |
| PBS | |
| Foetal Bovine serum (FBS) | |
| DG75 cell line | Maintained by Michelle West Laboratory |
| **Purification of RBP-Jκ expressed in insect cells** | |
| Buffer A (lysis) | 50mM Tris pH8.8, 500mM NaCl, 0.5mM TCEP |
| Buffer B (elution) | 50mM Tris pH8.8, 500mM NaCl, 0.5mM TCEP, 1M imidazole |
| Buffer C (low salt buffer) | 20mM Tris pH8.8, 100mM NaCl, 0.5mM TCEP |
| Buffer D (high salt buffer) | 20mM Tris pH8.8, 500mM NaCl, 0.5mM TCEP |
| **Purification of RBP-Jκ expressed in *E.coli*** | |
| Buffer A (lysis) | 50mM Tris pH8.8, 500mM NaCl, 0.5mM TCEP, 10mM imidazole |
| Buffer B (elution) | 50mM Tris pH8.8, 500mM NaCl, 0.5mM TCEP, 1M imidazole |
| Buffer C (low salt buffer) | 20mM Tris pH8.8, 100mM NaCl, 0.5mM TCEP |
| Buffer D (high salt buffer) | 20mM Tris pH8.8, 500mM NaCl, 0.5mM TCEP |
| **Thermodynamic assay buffers** | |
| Dialysis Buffer | 20mM Tris pH8.8, 100mM NaCl, 0.5mM TCEP, 0.5mM EDTA |
| ITC Buffer | 20mM Tris pH8.8, 100mM NaCl, 0.5mM TCEP, 0.5mM EDTA, 2% DMSO |
| FP (fluorescent polarisation assay) Buffer | 20mM Tris pH8.8, 100mM NaCl, 0.5mM TCEP, 0.5mM EDTA, 2% DMSO, 1% IPEGAL |
| SwitchSense Buffer | 20mM Tris pH8.8, 50mM NaCl, 0.5mM TCEP, 0.5mM EDTA |
| **Purification of EBNA3C homology domain expressed in insect cells** | |
| Buffer A (lysis) | 50mM Tris pH8.0, 500mM NaCl, 0.5mM TCEP, 20mM imidazole, 5% glycerol |
| Buffer B (elution) | 50mM Tris pH8.0, 500mM NaCl, 0.5mM TCEP, 1M imidazole, 5% glycerol |

## Appendix 4 : Table of peptides

Peptides were ordered from Peptide Synthetics and arrived purified to 98% purity, in powder form and were stored at -20°C. The peptides were dissolved in DMSO and stocks were flash frozen in liquid nitrogen and stored at -80°C.

| Peptide | WØP | TØGC | Peptide sequence |
|---|---|---|---|
| Notch2.26aa | ✓ | | MAKRKRKHGSL**WLP**EGFTLRRDASNH |
| EBNA2.14aa | ✓ | | HHLPSGPP**WWP**PIS |
| EBNA2.26aa | ✓ | | QQLHHLPSGPP**WWP**PICDPPQPSKTQ |
| EBNA2.28aa.FP | ✓ | | **F-tag-** GGQQLHHLPSGPP**WWP**PICDPPQPSKTQ |
| EBNA3A.14aa | | ✓ | VHLQA**TLGC**TGGRR |
| EBNA3B.14aa | | ✓ | VLVTA**TLGC**DEGTR |
| EBNA3C.14aa | | ✓ | IMLTA**TFGC**QNAAR |
| EBNA3C.Phos.14aa | | ✓ | IMLTA**T(P)FGC**QNAAR |
| EBNA3A.33aa | ~ | ✓ | QA**TLGC**TGGRRCHVTFSAGT**FKL**PRCTPGDRQW |
| EBNA3B.33aa | | ✓ | TA**TLGC**DEGTRHATTYSAGI**VQI**PRISDQNQKI |
| EBNA3C.33aa | ✓ | ✓ | TA**TFGC**QNAARTLNTFSATV**WTP**PHAGPREQER |
| EBNA3C.33aa.mTFGC | ✓ | | TAAAAAQNAARTLNTFSATV**WTP**PHAGPREQER |
| EBNA3C.33aa.mWTP | | ✓ | TA**TFGC**QNAARTLNTFSATVAAAPHAGPREQER |
| EBNA3C.33aa.mTFGC.mWTP | | | TAAAAAQNAARTLNTFSATVAAAPHAGPREQER |